Development of decellularised allogeneic nerve grafts

Georgina Emma Webster

Submitted in accordance with the requirements for the degree of Doctor of Philosophy

The University of Leeds

Institute of Medical and Biological Engineering

School of Mechanical Engineering

Faculty of Engineering

June 2019

The candidate confirms that the work submitted is her own and that appropriate credit has been given where reference has been made to the work of others.

Acknowledgements

Firstly, I would like to thank my supervisors, Professor Eileen Ingham, Professor Paul Rooney, Professor Richard Hall and Dr Stacy-Paul Wilshaw for all their support throughout my PhD. Paul, thank you for all your guidance, and for sponsoring this project and for providing me with some wonderful opportunities. Richard, thank you for all the constructive advice throughout this process, especially during the difficult times. Eileen, I cannot thank you enough for reviewing this thesis. Thank you for carpet-bombing each and every document with comments and advice – I have learned more from this process than I ever thought possible.

I would also like to thank all members of the iMBE laboratories for their contribution to this project. In particular, I would like to thank Dr Daniel Thomas, Dr Hazel Fermor, and Trang Nguyen. Dan, thank you for all the help and for your infinite patience whenever I have spilt, dropped, lost or broken something. Thank you, Hazel, for maintaining my emotional balance and for all your advice and kindness. Trang, thank you for all your help with the hydrogels and DRG dissections. In addition, I would also like to thank Laura Edwards and Fiona Walker, for supporting me professionally and personally throughout this PhD.

I also wish to thank my CDT cohort, for sharing this journey with me and for making this process much more enjoyable. James Holland, thank you for all your help and support through the good, the bad and the downright ugly.

I would also like to thank those closest to me. Dr Kyle Efendi, thank you for your endless love and support each and every day.

Above all, I would like to thank my wonderful family. In particular, I would like to thank my parents, Paul and Marcia Webster, without whom this would never have happened. Thank you for your unconditional love and support in everything I do in life. I feel extraordinarily blessed to have such incredible parents.

Finally, I wish to express my sincerest gratitude to the human tissue donors and their families. The majority of this project would not have been possible without their selfless donations.

To my brother, Robert Webster, without whom life would be unbearable

You are a master of the bodge, a plucky, strong-minded individual, and my favourite lunatic. It is therefore to you that I dedicate this thesis

Abstract

Peripheral nerve injuries affect a large proportion of the population and are often associated with prolonged disability. Current surgical interventions, including autografts and nerve guidance conduits (NGCs), are associated with a number of limitations. Decellularised nerve grafts offer considerable potential for peripheral nerve repair, by providing a non-immunogenic extracellular matrix (ECM) scaffold with biological, biochemical and biomechanical characteristics similar to native nerve.

The aim of this study was to develop a decellularised peripheral nerve allograft with a native ECM histioarchitecture and biochemical composition, able to support viable cell populations. A previously established protocol for the decellularisation of porcine peripheral nerves, utilising a combination of hypotonic buffers, low concentration sodium dodecyl sulphate (SDS) and nuclease enzymes, was further developed to maintain the efficacy of decellularisation whilst minimising structural changes to the ECM. The improved protocol was shown to achieve sufficient cell and DNA removal, and decellularised porcine peripheral nerves were shown to be biocompatible and retain a native ECM histioarchitecture and composition. The protocol was then translated for the decellularisation of human femoral nerves. Following further development, the protocol was shown to achieve sufficient cell and DNA removal, and decellularised human femoral nerves were also found to be biocompatible and retain a native ECM histioarchitecture and composition. Human femoral nerves were then cultured *in vitro* with primary rat dorsal root ganglion (DRG) explants to assess long term biocompatibility and neurite outgrowth. The results presented suggest that decellularised human femoral nerve is a suitable substrate to support cellular infiltration and axon regeneration. Decellularised human femoral nerve was shown to support the long-term cell viability, migration, and neurite outgrowth of DRG explants, for up to 28 days *in vitro*.

In this study, a novel decellularised human femoral nerve graft was developed with clinical potential for use in peripheral nerve repair. Although the results presented in this study are promising, further studies are required prior to clinical translation. A sterilisation process must be developed and evaluated for the decellularised nerve graft, and the biomechanical properties of decellularised and sterilised human femoral nerves must be investigated. The *in vivo* biocompatibility and efficacy of a decellularised and sterilised human femoral nerve graft for peripheral nerve repair must also be evaluated.

Table of Contents

List of Figures

List of Tables

List of Abbreviations

APC	Antigen presenting cell
ASC	Adipose derived multipotential stem cell
ATP	Adenosine triphosphate
BDNF	Brain derived neurotrophic factor
BHK	Baby hamster kidney
BMSC	Bone marrow derived multipotential stem cell
BSA	Bovine serum albumin
CDH19	Cadherin-19
CHAPS	3-[(3-Cholamidopropyl)dimethyl-ammonio]-1-propane sulfonate
CNS	Central nervous system
CPSG	Chondroitin sulphate proteoglycan
CS	Chondroitin sulphate
CTNF	Ciliary derived neurotrophic factor
DAPI	4’,6-diamidino-2-phenylindole
DMB	1,9-dimethylene blue
DMEM	Dulbecco’s minimal essential medium
DMSO	Dimethyl sulfoxide
DRG	Dorsal root ganglion
ECM	Extracellular matrix
EDTA	Ethylene diamine tetra-acetic acid
EngNT	Engineered neural tissue
ESC	Embryonic stem cell
FDA	Food and drug administration
FGF	Fibroblast growth factor
FIJI	FIJI Is Just ImageJ
GABA	γ-amino-butyric acid
GDNF	Glial cell derived neurotrophic factor
GFAP	Glial fibrillary acid protein
GMEM	Glasgow’s minimal essential medium
GS	Glutamine synthetase
H&E	Haematoxylin and eosin
HGF	Hepatocyte growth factor
HTA	Human Tissue Authority

IGF	Insulin like growth factor
IL-1α	Interleukin-1α
IL-1β	Interleukin-1β
IL-6	Interleukin-6
iPSC	Induced pluripotent stem cell
GAG	Glycosaminoglycan
MBP	Myelin basic protein
MEM	Minimal essential medium
MHC	Major histocompatibility complex
MSC	Multipotential stem cell
NBF	Neutral buffered formalin
NCAM-1	Neural cell adhesion molecule-1
NF200	Neurofilament 200
NGC	Nerve guidance conduit
NGF	Nerve growth factor
NHSBT TES	National Health Service Blood and Transplant Tissue and Eye Services
NSC	Neural stem cell
NT	Neurotrophin
OCT	Optimal cutting temperature
PBS	Phosphate buffered saline
PCL	Polycaprolactone
PFA	Paraformaldehyde
PGA	Polyglycolic acid
PLA	Polylactic acid
PLGA	Polylactic-co-glycolic acid
PNS	Peripheral nervous system
Psi	Pounds per square inch
PTE	Polytetrafluoroethylene
SIS	Small intestinal submucosa
SDC	Sodium deoxycholate
SDS	Sodium dodecyl sulphate
SGC	Satellite glial cell
SKP	Skin derived precursor cell
TBS	Tris buffered saline
TNFα	Tumour necrosis factor-α

TPB	Tryptone phosphate broth
TUNEL	Terminal deoxynucleotidyl transferase (TdT) dUTP Nick-End Labelling
VEGF	Vascular endothelial growth factor
α-gal	Galactose-α-1, 3-galactose
3D	Three dimensional

Chapter 1: Introduction

1.1 General Introduction

Peripheral nerve injuries are common and debilitating injuries, with approximately 300,000 cases reported annually in Europe (Bell and Haycock, 2011). The majority of injuries are caused by acute trauma, and are often associated with functional defects, neuropathic pain or paralysis of the affected limb (Kingham *et al.*, 2007). Axons of peripheral nerves are capable of spontaneous regeneration following injury, however axon regeneration is slow (approximately one mm per day), and the ability of axons and Schwann cells to sustain axon regeneration progressively fails over distance and time (Burnett and Zager, 2004; Ruijs *et al.*, 2005).

Severe peripheral nerve injuries, characterised by a gap defect with complete extracellular matrix (ECM) transection, are frequently repaired using autografts or nerve guidance conduits (NGCs) to bridge the gap. However, such techniques have a limited efficacy and axon regeneration is frequently unsuccessful (Grinsell and Keating, 2014). Autografts, the gold standard intervention, require the sacrifice of a functional, minor nerve to repair critical defects and often provide insufficient material for major reconstruction (Colen *et al.*, 2009; Grinsell and Keating, 2014). A number of NGCs have been developed to physically guide regenerating axons, fabricated from both natural and synthetic materials, however relatively few are clinically available and results of clinical trials have only shown a comparable efficacy between autografts and NGCs for small defects, up to 20 mm in length (Kehoe *et al.*, 2012; Naryan *et al.*, 2018).

The limited efficacy of NGCs is thought to be due to the lack of a native ECM architecture and composition (Whitlock *et al.*, 2009; Spivey *et al.*, 2012). The basement membrane is essential for promoting cell-matrix interactions supporting Schwann cell adhesion and axon elongation, and the specific architecture of the endoneurium, the innermost layer of the ECM, provides physical guidance to regenerating axons (Spivey *et al.*, 2012; Szynkaruk *et al.*, 2012). Decellularisation of allogeneic or xenogeneic tissue has the potential to produce a non-immunogenic ECM scaffold with biological, biochemical and biomechanical characteristics similar to native tissue (Crapo *et al.*, 2011; Kawecki *et al.*, 2018). Decellularised peripheral nerve grafts offer considerable potential for peripheral nerve repair by providing a native microenvironment to facilitate axon regeneration with ECM properties that cannot yet be replicated synthetically (Schmidt and Leach, 2003; Whitlock *et al.*,

2009; Szynkaruk *et al.*, 2012). This review will describe the structure and function of peripheral nerves and the pathophysiology of peripheral nerve injury, and will investigate the current interventions for peripheral nerve repair and the clinical need for alternative interventions. This review will then explore experimental therapies for peripheral nerve repair.

1.2 Peripheral nervous system

The nervous system of vertebrates is divided into two parts: the central nervous system (CNS) and peripheral nervous system (PNS). The CNS, consisting of the brain and spinal cord, interprets sensory information from the PNS and coordinates the activity of the body by providing stimuli to the PNS (Kiernan and Rajakumar, 2013). The PNS, consisting of cranial and spinal nerves, is subdivided further into the somatic nervous system (voluntary control of skeletal muscle) and autonomic nervous system (involuntary control of bodily functions, including respiration, digestion, and cardiac regulation). The PNS connects the CNS with the rest of the body, by relaying sensory information from the internal and external environment to the CNS and conducting stimuli from the CNS to muscles and glands (Mai and Paxinos, 2011; Kiernan and Rajakumar, 2013).

There are 31 pairs of spinal nerves, named according to the level of the spinal cord they emerge from (Figure 1.1). Spinal nerves are mixed nerves, comprising motor and sensory neurons that separate into two nerve roots: the ventral root and the dorsal root. Motor neurons, both somatic and autonomic, emerge from the spinal cord as the ventral nerve root, and the cell bodies of motor neurons are located in the ventral horn of the spinal cord (Mai and Paxinos, 2011). Sensory neurons enter the spinal cord as the dorsal nerve root, and on each dorsal root is the DRG, which contains the cell bodies of the sensory neurons (Figure 1.1) (Mai and Paxinos, 2011).

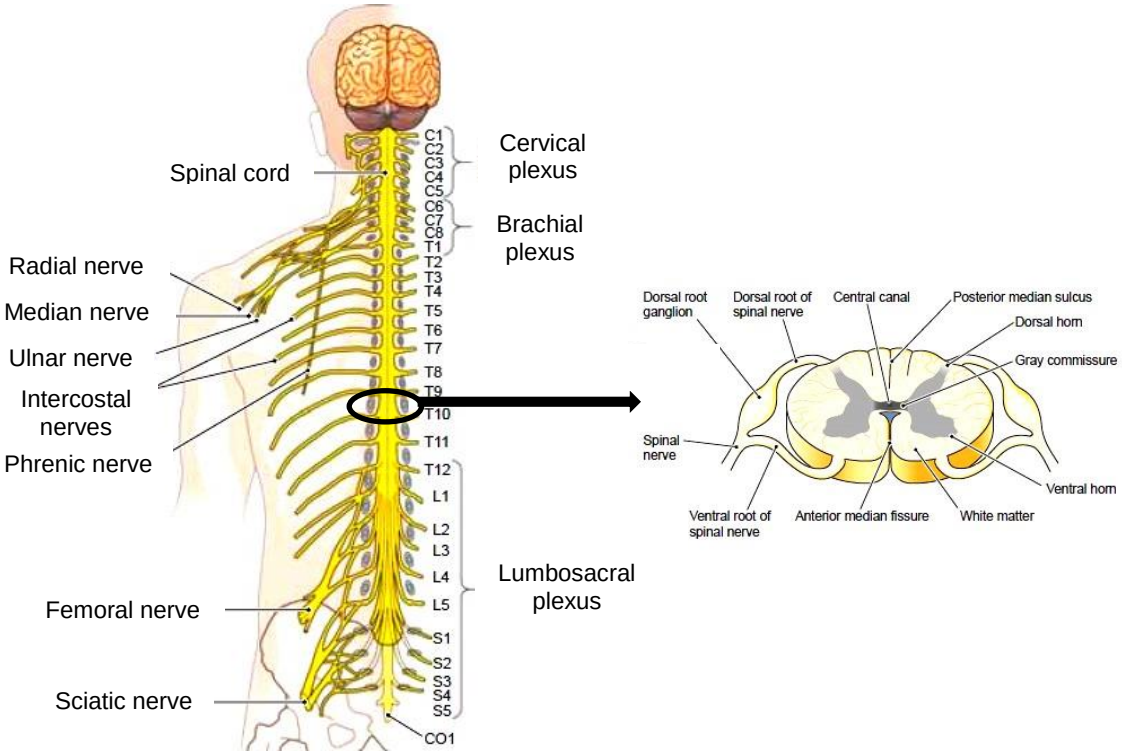

Figure 1.1. Spinal nerves of the human peripheral nervous system. The human peripheral nervous system contains 31 pairs of spinal nerves, each pair numbered according to the level of the spinal cord from which it arises (C = Cervical, T = Thoracic, L = Lumbar S = Sacral and CO = Coccygeal). Each spinal nerve is attached to the spinal cord by two roots: the dorsal and the ventral root. Motor neurons emerge from the spinal cord as the ventral nerve root, with cell bodies of motor neurons located in the ventral horn. Sensory neurons enter the spinal cord as the dorsal nerve root, and each dorsal nerve root contains a swelling of grey matter known as the dorsal root ganglion (DRG), which contains cell bodies of sensory neurons. Adapted from encyclopedia.lubopitko-bg.com

1.3 Peripheral nerve

1.3.1 Structure and function of peripheral nerve

Peripheral nerves are composed of an ECM, a vascular network (vasa nevorum), and both neural and non-neural cells (Kiernan and Rajakumar, 2013). The neural cell types in peripheral nerves are neurons, Schwann cells and perineurial cells, and the non-neural cell types are primarily fibroblasts and adipocytes. In addition, endothelial cells and various cells of the immune system, including macrophages, are also located within the nerve (Kerns, 2008; Grinsell and Keating, 2014). The ECM of peripheral nerves consists of three layers: endoneurium, perineurium and epineurium (Figure 1.2).

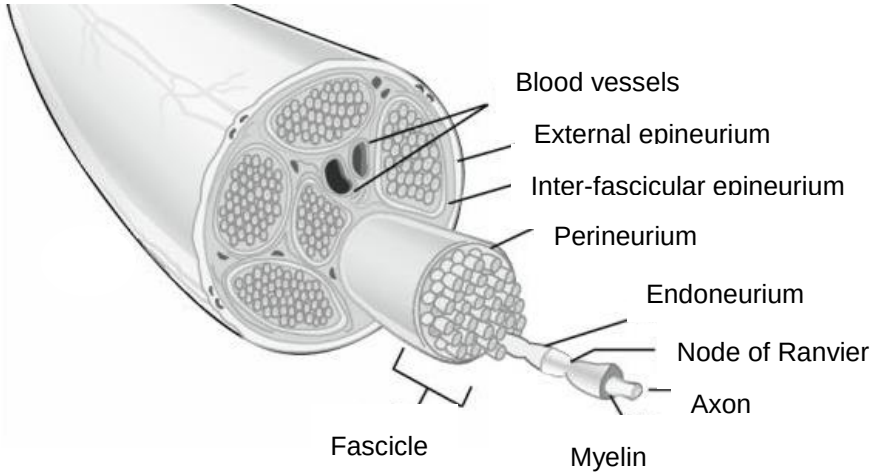

Figure 1.2 Macroscopic structures of peripheral nerve extracellular matrix (ECM). Peripheral nerve ECM consists of three major structures: the epineurium, perineurium and endoneurium. Individual axons are located in endoneurial tubes, which are bundled into fascicles surrounded by the perineurium. Fascicles are separated by inter-fascicular epineurium, which also contains longitudinally aligned blood vessels. The external epineurium forms a sheath surrounding the whole nerve. Figure adapted from Grinsell *et al*. (2014).

The endoneurium is the innermost ECM layer, forming a network of fine tubules surrounding individual myelinated axons (or multiple non-myelinated axons), associated Schwann cells and fibroblasts (Figure 1.2). Individual endoneurial tubes consist primarily of fine collagen type I and type II fibrils, and provide topographic guidance to regenerating axons (Topp and Boyd, 2012). Endoneurial tubes also contain a basement membrane, comprised of collagen type IV, laminin and fibronectin, which is essential for promoting cell-matrix interactions and supporting Schwann cell adhesion and axon elongation (Gabella, 2012). The larger blood vessels of the peripheral nerve vascular network (vasa nevorum) do not directly access the endoneurium, and a fine capillary network connects individual axons with the vasculature (Kerns, 2008).

Multiple axons, individually surrounded by endoneurial tubes, are bundled into nerve fascicles and surrounded by the perineurium (Figure 1.2). The perineurium is a concentric layered lamellar structure, consisting of collagen type I and type II, and each perineurial layer also contains a basement membrane similar to that of the endoneurium (Kerns, 2008; Topp and Boyd, 2012). Squamous perineurial cells, joined by gap junctions, function as a blood-nerve barrier and enable regulation of the intrafascicular microenvironment, including the regulation of pressure and concentration of soluble molecules and ions. Intercellular tight junctions, comprising proteins including occludins and claudins, regulate the transport of molecules to axons in individual endoneurial tubes (Peltonen *et al.*, 2013). The perineurium contributes to the overall biomechanical properties and mechanical strength of the

nerve, and also provides local protection to axons and Schwann cells within individual endoneurial tubes from external mechanical forces, such as compression and tension (Topp and Boyd, 2012; Peltonen *et al.*, 2013).

The epineurium is the outermost layer of the ECM and consists of two regions: the inter-fascicular epineurium and the external epineurium. The inter-fascicular epineurium fills the space between fascicles with an irregular matrix, consisting of collagen types I and III and adipose tissue, and contains the major vessels of the vasa nevorum (Sunderland, 1990; Ishibe *et al.*, 2011). The external epineurium forms a dense, sheath-like structure of collagen type I and type III around the nerve, providing insulation from the external environment (Mason and Phillips, 2011). The external epineurium interfaces with other ECM regions along the nerve path and is tethered at some points, facilitating nerve mobility. In addition to the perineurium, the epineurium also contributes to the overall mechanical strength of the nerve, primarily due a high collagen type I content (Kerns, 2008; Topp and Boyd, 2012).

1.3.2 Extracellular matrix (ECM) components in peripheral nerve

1.3.2.1 Collagens

Collagen is a major component of peripheral nerve ECM, maintaining overall ECM histioarchitecture (tissue architecture) and biomechanical properties (Mason and Phillips, 2011; Gao *et al.*, 2013). Fibrillar collagens (including collagens type I, II, III and V) are structural molecules with a tri-helical conformation, providing mechanical strength to the nerve (Koopmans *et al.*, 2009). Collagen type I, the main collagen in peripheral nerve ECM, is found in all ECM layers. Collagen type I is longitudinally arranged in the endoneurium and perineurium, often in association with collagen type II, and forms an irregular network in the epineurium (Wenger *et al.*, 2007). Collagen type III is located in the epineurium in association with collagen type I, where it forms in an undulated orientation along the nerve to provide tensile strength to protect the inner ECM layers (Wenger *et al.*, 2007; Gao *et al.*, 2013). Collagen type IV is a highly glycosylated network-forming collagen molecule located mainly in the basement membrane of the endoneurium and perineurium (Masand *et al.*, 2012). Collagen type IV provides structure to the basement membrane and provides binding sites for key moieties, including laminins, enabling the cellular processes of Schwann cells and axons (Yurchenco *et al.*, 2002; Yurchenco, 2011; Gao *et al.*, 2013).

1.3.2.2 Laminin

Laminin, along with collagen type IV, fibronectin and various proteoglycans, is a ubiquitous component of the basement membrane, located in both the endoneurium and perineurium (Yurchenco, 2011). Laminin is a heterotrimeric glycoprotein with several cell adhesion motifs (Figure 1.3) (Dalton and Mey, 2009; Nieuwenhuis *et al.*, 2018). Adhesion motifs enable the binding of cellular integrins, enabling cell adhesion and signal transduction from contact with different ligands (Grinsell and Keating, 2014).The RGD sequence has been identified as an adhesion motif for a variety of cell types, including neurons and Schwann cells (Table 1.1), and many studies have investigated the use of RGD functionalised polymers to promote cell adhesion (Hersel *et al.*, 2003). Laminin also contains several other neuron adhesion motifs, including YIGSR, IKVAV, RNIAEIIKDI and RYVVLPR, however YIGSR and IKVAV have both been shown to significantly increase neuronal adhesion and are considered key neuron adhesion motifs (Rao and Winter, 2009). Laminin has extensive functions in regulating Schwann cell adhesion and proliferation, and promoting axonal regeneration (Geuna *et al.*, 2009). Several studies have investigated the axon-growth promoting activity of laminin, providing the adhesive stimulus for successful axon regeneration following injury (Chen *et al.*, 2000; Sun *et al.*, 2009; Suri and Schmidt, 2010).

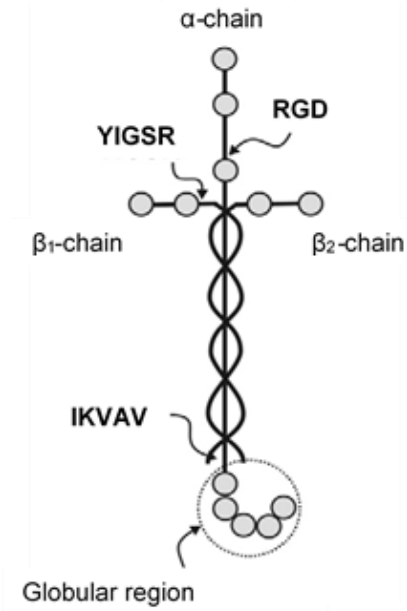

Figure 1.3 Structure of laminin and key cell adhesion motifs. Laminin is a cross-shaped glycoprotein with three polypeptide chains: the α-chain, β1-chain and β2-chain. Laminin contains key cell adhesion motifs that bind with integrin receptors. The YIGSR sequence is located on the β1-chain, and the IKVAV and RGD sequences are on the long and short arm of the α-chain respectively. Figure adapted from Dalton *et al*. (2009).

1.3.2.3 Fibronectin

Fibronectin is a glycoprotein component of the basement membrane synthesised by Schwann cells *in vivo* (Ahmed *et al.*, 2003; Gao *et al.*, 2013). Fibronectin has three types of sequence homology organized into structural domains with interaction sites for binding other ECM molecules, including collagen and fibrin (Gratchev *et al.*, 2001). Fibronectin contains cell adhesion motifs which enable the binding of cellular integrins expressed by Schwann cells (Table 1.1), and has been shown to stimulate Schwann cell proliferation and migration (Ahmed *et al.*, 2003). In addition, fibronectin contains domains for binding neuronal integrins (Table 1.1), including the RGD sequence, and fibronectin has been implicated in axon regeneration and myelination (Gardiner *et al.*, 2007; Han *et al.*, 2010; Gardiner, 2011; Nieuwenhuis *et al.*, 2018).

1.3.2.4 Proteoglycans

Proteoglycans are formed of glycosaminoglycans (GAGs) covalently bound to core proteins. GAGs can be sulphated, such as heparan sulphate and chondroitin sulphate, or non-sulphated (Gandhi and Mancera, 2008). The main GAGs found in peripheral nerve are heparan sulphate and chondroitin sulphate (Gao *et al.*, 2013).

Proteoglycans are located in peripheral nerve ECM, typically associated with the basement membrane in the endoneurium and perineurium, and within blood vessels (Braunewell *et al.*, 1995). Chondroitin sulphate proteoglycans (CPSGs) are proteoglycans comprising a protein core and a chondroitin sulphate side chain. They are the main proteoglycans involved in the regulation of axonal growth, specifically inhibiting the axon growth promoting activity of laminin (Zuo *et al.*, 2002). CPSGs are thought to be inhibitory to axonal regeneration, and several studies have shown that CPSGs bind to and inhibit the axon growth promoting activity of endoneurial laminin and are rapidly upregulated following nerve injury, providing a non-permissive substrate for axonal growth (Krekoski *et al.*, 2001; Zuo *et al.*, 2002; Neubauer *et al.*, 2007). However, as CPSGs are degraded as part of the regeneration process of axons, it has also been suggested that the degradation of CPSGs may represent a mechanism by which the growth-promoting properties of laminin may be restored, thus promoting axonal regeneration (Krekoski *et al.*, 2001; Wang *et al.*, 2012).

1.3.3 Cell types in peripheral nerve

1.3.3.1 Neurons

Neurons are the primary functional cell type of peripheral nerves, responsible for transmitting sensory and motor signals in the form of electrical impulses (Topp and Boyd, 2012). Neurons are a diverse cell type, varying considerably in morphology and electrochemical properties, however a typical neuron consists of a soma (cell body), dendrites, and an axon projecting into the peripheral nervous system (Figure 1.4) (Geuna *et al.*, 2009). The soma is usually compact, and the filamentous dendrites and axon extrude from the soma. The soma can produce multiple dendrites which branch extensively from the soma and become thinner in diameter with increasing distance, but only one axon, either myelinated or unmyelinated, which can extend for great distances (over one metre in an adult human) maintaining a constant diameter (Topp and Boyd, 2012). Although axons of peripheral nerves can be myelinated or non-myelinated, in general axons with a larger diameter become myelinated to facilitate fast conduction of action potentials via saltatory conduction (Sheng and Cai, 2012; Kiernan and Rajakumar, 2013). Saltatory conduction is the propagation of action potentials along myelinated axons between Nodes of Ranvier (breaks in the myelin sheath), which increases the conduction velocity of action potentials (Figure 1.4) (Koenig, 2012; Yuan *et al.*, 2012; Sheng and Cai, 2012).

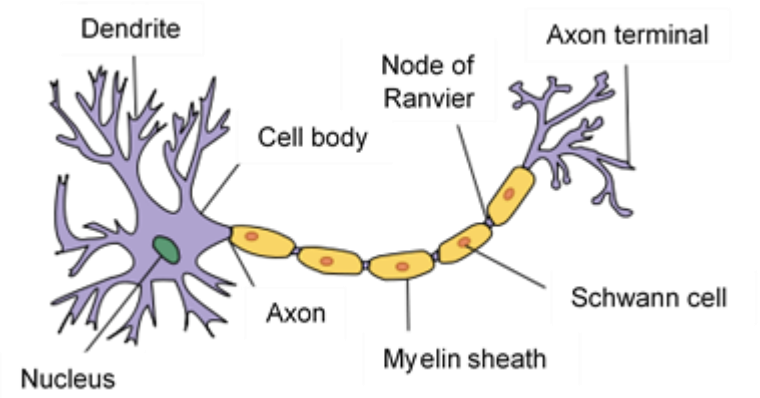

Figure 1.4 Structure of a neuron. A typical neuron consists of a soma (cell body) containing the nucleus, dendrites and an axon. Synaptic signals from other neurons are received by the soma and dendrites, and signals to other neurons are transmitted by the axon, with the axon terminal containing the synapses to communicate with other neurons. Schwann cells form a myelin sheath around myelinated axons with breaks (Nodes of Ranvier) enabling fast conduction of action potentials by propagation from one Node of Ranvier to another. Image adapted from Wikimedia commons.

1.3.3.2 Schwann cells

Schwann cells, a type of glial cell, are an essential component of neural tissue and are required for the survival of both myelinated and non-myelinated axons (Chernousov *et al.*, 2008; Salzer, 2012). The primary function of Schwann cells is to myelinate certain axons to facilitate the fast conduction of impulses (saltatory conduction) by wrapping around them, adopting a flattened morphology to create a membranous, insulating barrier, with each individual Schwann cell covering approximately 100 micrometres of an axon (Pereira *et al.*, 2012; Salzer, 2015). Schwann cells also have important functions in neural development and regeneration (Jessen *et al.*, 2015). In response to injury, Schwann cells rapidly switch phenotype to a “repair Schwann cell” phenotype and assemble into longitudinal bands (termed Bands of Bungner), and the ECM basement membrane essentially serves as a conduit for regeneration (Kim *et al.*, 2013; Jessen and Mirsky, 2016). Schwann cells also produce several growth factors, such as nerve growth factor (NGF) and brain derived neurotrophic factor (BDNF) (Table 1.1) (Gaudet *et al.*, 2011; Jessen and Mirsky, 2016). During homeostasis and post-injury, Schwann cells also adopt immunological functions by serving as phagocytic cells following axon damage, phagocytosing axon and myelin debris, presenting antigens to CD4+ T-lymphocytes, and producing pro-inflammatory cytokines IL-6, TNFα, IL-1α and IL-1β (Burnett and Zager, 2004; Gaudet *et al.*, 2011; Grinsell and Keating, 2014).

1.3.3.3 Perineurial cells

Perineurial cells bundle individual axons, whether myelinated or non-myelinated, into fascicles and are arranged in three zones, in one to 15 concentric layers (Peltonen *et al.*, 2013). The innermost zone consists of a single layer of flat, squamous perineurial cells joined by tight junctions to form a blood-nerve barrier, and the intermediate zone consists of three to 15 layers of perineurial cells (Hirose *et al.*, 2003; Topp and Boyd, 2012). The external zone also consists of layers of perineurial cells, bound with collagen type I and II, and elastin fibres in circumferential arrangements (Kerns, 2008; Bilbao and Schmidt, 2015). The perineurial cells contribute to the biomechanical properties of peripheral nerve, and the number of cell layers increases where nerves cross the articulating joints and at bifurcation points, where nerve strain is increased (Topp and Boyd, 2012). Furthermore, larger nerve fascicles tend to have more perineurial cell layers to modulate tensile and compressive forces, whereas nerves composed of many

fascicles tend to have fewer perineurial cell layers to accommodate shear forces as the fascicles glide during body movement (Topp and Boyd, 2012; Koch *et al.*, 2012).

1.3.3.4 Fibroblasts

Fibroblasts are mainly located in the endoneurium and epineurium, although in the endoneurium fibroblasts are found in close proximity to the basement membrane, in association with collagen type I and II fibres, and in the epineurium fibroblasts are found in a looser arrangement with collagen type I and III fibres and adipose tissue (Gingras *et al.*, 2003; Kim *et al.*, 2013). The primary functions of fibroblasts, both in the endoneurium and epineurium, are to synthesise and maintain the complex ECM, support neurons by cell-cell contacts, and release various growth factors and signalling molecules, including BDNF and vascular endothelial growth factor (VEGF) to promote axon growth (Table 1.1) (Grothe and Nikkhah, 2001; Haastert *et al.*, 2006). Fibroblasts have further roles in axon regeneration, by producing NGF along with Schwann cells, producing inflammatory cytokines including IL-6, and promoting the proliferation and migration of Schwann cells by providing physical guidance and cell-cell contacts (Grothe and Nikkhah, 2001; Gaudet *et al.*, 2011; Wong *et al.*, 2017).

1.3.3.5 Adipocytes

Adipocytes are mainly located in the epineurium, both in the inter-fascicular epineurium and the external epineurium, although their exact functions in peripheral nerves are not well understood (Chernousov *et al.*, 2008; Grinsell and Keating, 2014). Adipocytes are thought to contribute to the biomechanical properties of the epineurium, allowing gliding between nerve fascicles in the inter-fascicular epineurium to reduce shear forces, and supporting the blood vessels passing form the extraneural regions (Kerns, 2008; Topp and Boyd, 2012). Adipocytes are also implicated in fatty acid metabolism by supplying a source of fatty acids, as several metabolic studies have reported that fatty acids have a high turnover rate in the endoneurium (Verheijen *et al.*, 2003). However, several studies, using adult mouse peripheral nerve, have reported high expression of adipokines in the epineurium, including Acrp30 and resistin, and suggest that in addition to supplying fat metabolites the epineurium may regulate the lipid metabolism of Schwann cells and axons using the vascular network (Garbay *et al.*, 2000; Verheijen *et al.*, 2003; Pereira *et al.*, 2012).

Table 1.1 Growth factors and integrins expressed by neurons, Schwann cells and fibroblasts in peripheral nerve. Growth factors produced by Schwann cells and fibroblasts. NGF = Nerve growth factor, BDNF = Brain derived neurotrophic factor, FGF = Fibroblast growth factor, IGF = Insulin like growth factor, CTNF = Ciliary derived neurotrophic factor, GDNF = Glial cell line derived neurotrophic factor, VEGF = Vascular endothelial growth factor, NT-3 = Neurotrophin-3, NT-4/5 = Neurotrophin 4/5. Neurons, Schwann cells and fibroblasts express various integrins including laminin, fibronectin and collagen associated integrins. Data adapted from Jessen et al (2016), Gardiner *et al*. (2011) and Nieuwenhuis *et al*. (2018).

	Neurons	**Schwann cells**	**Fibroblasts**
Growth factors		NGF BDNF FGF IGF CTNF GDNF VEGF NT-3 NT-4/5	BDNF VEGF NGF
Laminin binding integrins	α1β1 α2β1 α3β1 α6β1 α7β1	α1β1 α2β1 α6β1 α6β4	α6β4 α1β1 α2β1
Fibronectin binding integrins	α4β1 α5β1 α8β1 αVβ8	α5β1 αVβ3 αVβ8	
Collagen binding integrins	α1β1 α2β1	α1β1 α2β1	

1.3.4 Peripheral nerve biomechanics

Unlike the nerves of the CNS, peripheral nerves have no physical protection from bone (i.e. from the skull or spine) or biological protection (i.e. from the blood-brain barrier), and are exposed to an array of mechanical forces associated with body movement, including tensile, compressive and shear forces, particularly in the upper extremities (Burnett and Zager, 2004; Topp and Boyd, 2012). Peripheral nerves are able to withstand mechanical forces, particularly across articulating joints, because of the viscoelastic properties of the ECM (Tassler *et al.*, 1994). Viscoelasticity enables the nerve to elongate in response to longitudinal tensile stress during body movements, such as wrist and elbow extension. A study by Topp and Boyd (2006) used cadaveric human limbs to measure increases in nerve strain induced by nerve elongation during certain body movements in the upper extremities. For example, during wrist extension (0 – 60°) with 90° shoulder abduction and 10° elbow flexion, median nerve strain increased by 7.4 % at the elbow and 9.6 % at the wrist and ulnar nerve strain increased by 5.2 % at the elbow and 20.7 % at the wrist.

Peripheral nerves are also able to accommodate longitudinal tensile stress during body movements by excursion. Excursion is the displacement or gliding of the nerve relative to the surrounding nerve bed and may be longitudinal or transverse relative to the nerve tract, however the direction (proximal or distal) and magnitude of excursion varies depending on the joint movement (Verheijen *et al.*, 2003; Grinsell and Keating, 2014). Although it is essential that nerves can glide relative to surrounding tissue during body movement, the gliding of nerves against interfacing non-neural connective tissue can also impose significant shear forces. Nerve excursion follows a consistent pattern - when nerve paths are elongated during body movement, the nerve must slide towards the point of extension and the magnitude of excursion is greatest closest to the moving joint. For example, the median and ulnar nerve paths are elongated during wrist extension, and both the median and ulnar nerves slide towards the point of extension, i.e. the wrist, to accommodate this movement (Figure 1.5 B) (Topp and Boyd, 2012).

It is also essential that peripheral nerves can withstand significant compression from surrounding tissue, as excessive compression disrupts vascular perfusion and can either prevent or cause dysfunctional electrical impulses (Burnett and Zager, 2004; Madura, 2012). Various body movements can impose compressive forces, such as the increase in carpal tunnel pressure resulting from wrist movement (i.e. extension or flexion) and forearm supination (Burnett and Zager, 2004; Grinsell and

Keating, 2014). If the magnitude of any shear, compressive or tensile forces exceeds the capacity of the nerve, either acutely (typically trauma) or cumulatively (typically repeatedly exceeding the upper threshold for vascular perfusion causing a reduction in intra-neural blood flow), injury is likely to occur (Burnett and Zager, 2004; Topp and Boyd, 2012; Madura, 2012).

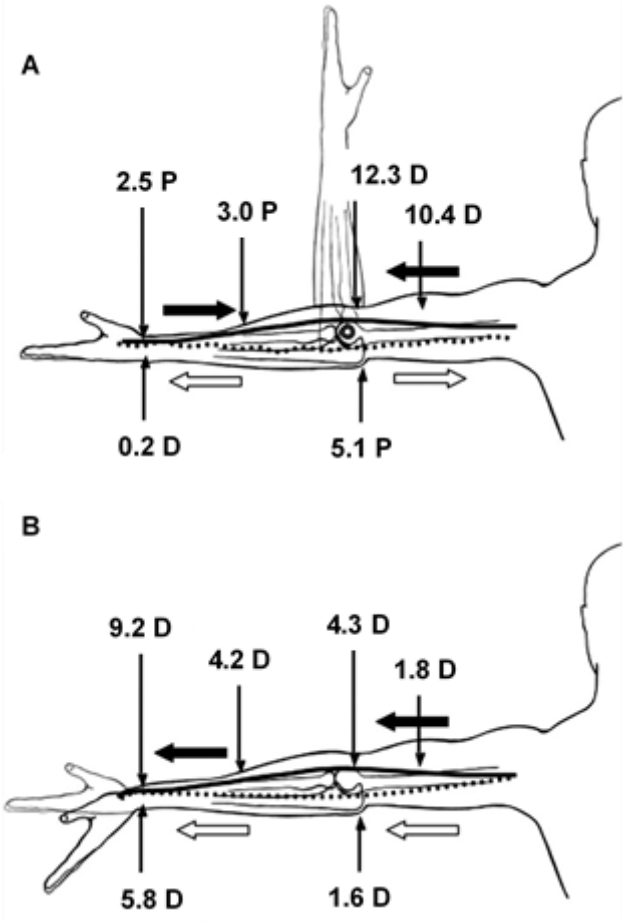

Figure 1.5 Excursion of the median and ulnar nerves during elbow extension and wrist extension. Excursion of the median nerve (solid line) and the ulnar nerve (dotted line) during elbow extension from 90° - 0° (A), followed by wrist extension from 0° - 60° (B). All measurements are reported in millimetres of excursion in the proximal (P) or distal (D) direction. During elbow extension, the median nerve bed lengthens and the median nerve glides towards the elbow (distal), whereas the ulnar nerve shortens and glides away from the elbow (proximal). During wrist extension, both nerve beds lengthen and both nerves glide towards the wrist. Adapted from Topp & Boyd (2006).

1.4 Peripheral nerve injury and regeneration

1.4.1 Peripheral nerve injury

1.4.1.1 Injury mechanisms

Peripheral nerve injuries affect 1 in 1000 of the population in Europe, with the majority of injuries resulting from acute trauma including laceration, traction (excessive stretch induced by longitudinal tensile stress) and compression. Peripheral nerve injuries disproportionately affect young and healthy individuals most at risk of traumatic injury (Kingham *et al.*, 2007; Bell and Haycock, 2011). Severe peripheral nerve injuries, characterised by extensive ECM damage, account for approximately 20% of all peripheral nerve injuries and are often painful, debilitating conditions associated with functional defects, intractable neuropathic pain or complete paralysis of the affected limb (Kingham *et al.*, 2007). Traction injuries are the most common, and although a loss of continuity in the affected nerve can occur, such as in brachial plexus avulsion, continuity is usually retained, for example with traction injuries to the nerve associated with extremity bone fractures (Burnett and Zager, 2004). Lacerations account for up to 30% of peripheral nerve injuries, and although these can result in a complete nerve transection, some degree of continuity is often retained (Jacques and Kline, 2000). Compression injuries do not involve a severance or loss of continuity of the affected nerve and include entrapment neuropathies as well as direct compression, such as radial nerve compression. Although the pathophysiology associated with compression injuries is unclear, it is thought that compression nerve injuries are caused by ischaemia induced by excessive compression, dependent on the magnitude and exposure time (Burnett and Zager, 2004; Madura, 2012).

1.4.1.2 Injury classification

Clinical injury grading systems have been developed that allow correlation of the extent of ECM damage, patient symptomology and likelihood of functional recovery (Figure 1.6). The most widely recognized systems were devised by Seddon (1943) and Sunderland (1951). Seddon assigned nerve injuries to three broad categories: neuropraxia, axonotmesis and neurotmesis (Seddon, 1943). Several years later, Sunderland subsequently subdivided these categories further: type I (neuropraxia), type II (axonotmesis), and type III, IV and V (neurotmesis) to represent the variation in clinical findings and functional recovery in neurotmesis injuries (Sunderland, 1951). Frequently, peripheral nerve injuries comprise multiple types and a type VI

injury, a mixed pattern injury, has been added to the original classification (Mackinnon, 1988).

Neuropraxia, the most common and least severe type of nerve injury, does not affect axon continuity but causes a transient function loss, in which a segment of nerve loses its ability to conduct impulses. This is thought to be due to a local ion-induced conduction block and the segmental demyelination of axons, both of which can be restored as structural continuity is maintained. Mild compression injuries, such as sleeping with pressure on the nerves, are typical examples of neuropraxia and recover within 8 - 12 weeks, without intervention (Seddon, 1943; Burnett and Zager, 2004; Madura, 2012).

Axonotmesis injuries, whereby the axon is severed, result in a complete loss of continuity of the nerve axon and associated myelin, but the surrounding ECM, particularly the perineurium and epineurium, remain intact (Seddon, 1943; Sunderland, 1951; Sunderland, 1990). Distal to the injury site, the axon and surrounding myelin degenerate causing total denervation of the nerve path, although functional recovery is usually achieved without surgical intervention as the remaining ECM provides guidance for subsequent axons to re-innervate the nerve path following the degenerative process (Madura, 2012).

Damage to the ECM of the nerve, in addition to the axon itself, is termed neurotmesis (Sunderland, 1951). As with axonotmesis, degeneration and some subsequent axonal regrowth occurs, except functional recovery is rarely achieved without surgical intervention because of intraneural scarring and the ECM damage, as the loss of the blood-nerve barrier and the necessary structures to direct axon regrowth significantly hampers the regenerative process (Gaudet *et al.*, 2011). The prospect of functional recovery, even with surgical intervention, is difficult to predict as the likelihood is dependent on the location of the injury, time elapsed before intervention and the extent of the ECM damage (corresponding to type III, IV and V of Sunderland's classification) (Sunderland, 1951; Gaudet *et al.*, 2011; Madura, 2012).

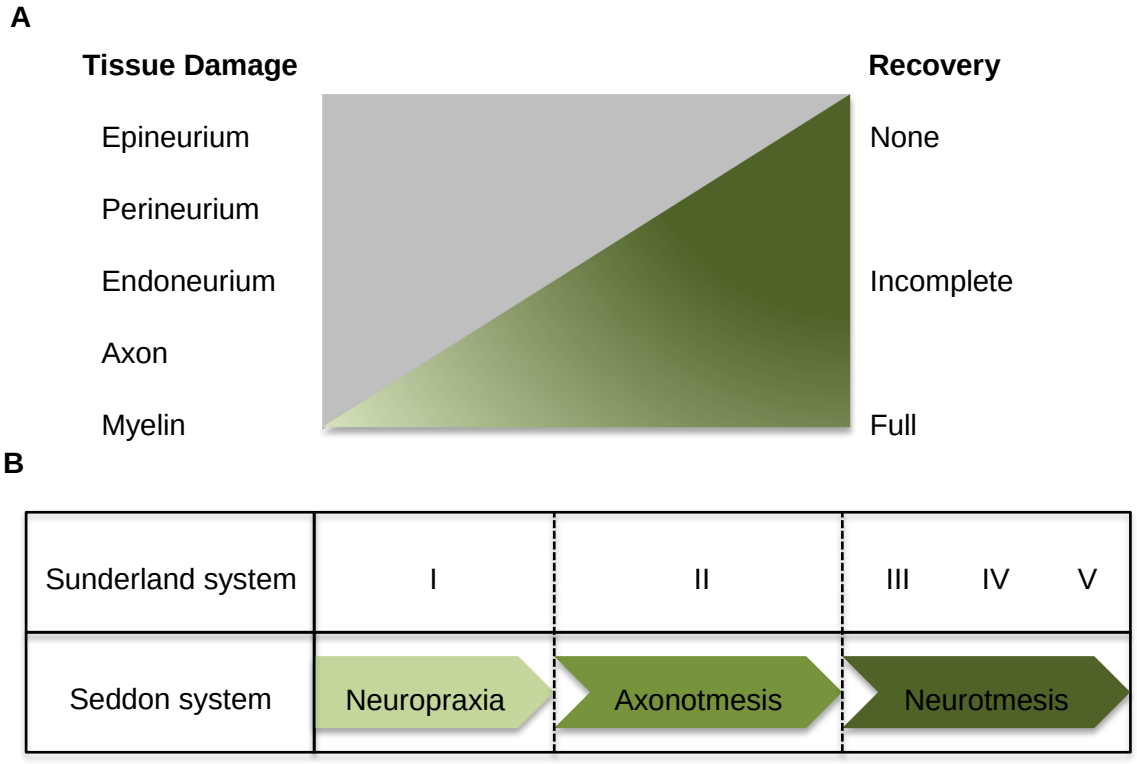

Figure 1.6 Seddon and Sunderland peripheral nerve injury classification systems. (A) Peripheral nerve injury classification systems described by Seddon (1943) and Sunderland (1951) define injury severity by the extent of ECM damage, and correlates the extent of ECM damage with the likelihood of functional recovery. (B) Corresponding injury categories described by the Seddon and Sunderland systems. Neuropraxia (Sunderland type I) is defined by transient loss of axon function, Axonotmesis (Sunderland type II) is defined by axon severance, and neurotmesis (Sunderland types III, IV and IV) is defined by complete transection of axons and ECM structures. Adapted from Burnett et al. (2004)

1.4.2 Peripheral nerve regeneration

For neurotmesis injuries, with extensive ECM damage and a nerve gap, a series of complex and finely regulated degenerative processes must occur prior to regeneration, which often delay or impair the regenerative process (Gaudet *et al.*, 2011). Axon degeneration follows a specific sequence of events, starting within the zone of trauma and extending both proximally and distally to the axotomy (Madura, 2012). The proximal axon segment seals the injured axon to prevent cytoplasm leakage, retracts to the next node of Ranvier and degenerates via chromatolysis, a focal degeneration pathway similar to the degeneration that occurs in other tissues, e.g. muscle, following trauma. The distal axon segment disintegrates via a process known as Wallerian degeneration (Gaudet *et al.*, 2011). Wallerian degeneration occurs in the distal axon segment, beginning with an intracellular calcium influx following axotomy (Burnett and Zager, 2004; Grinsell and Keating, 2014). This

activates axoplasmic proteinases, which break down microtubules and neurofilaments causing axoplasmic granulation, which impedes axonal transport and accelerates degeneration. Responding to a loss of axon contact from the transected axon, Schwann cells switch from a supportive to a reactive phenotype, secreting inflammatory mediators including interleukins IL-1-β and IL-6 instead of secreting myelin and, along with fibroblasts, undergo rapid proliferation (Jessen and Mirsky, 2016). Inflammatory mediators secreted by Schwann cells recruit cells of the immune system, particularly macrophages and T-cells. Macrophages infiltrate the distal axon segment tip and complete the elimination of axons by phagocytosing axon and myelin debris (Jessen *et al.*, 2015; Jessen and Mirsky, 2016).

Before Wallerian degeneration has subsided the proximal axon segment starts to produce regenerative sprouts, as many as 50-100, which mature into a growth cone and elongate responding to neurotrophic signals secreted by Schwann cells (He and Jin, 2016). A fibrin cable forms across the gap between the proximal and distal axon segments, and Schwann cells assemble into bands of Bungner in empty endoneurial tubes (longitudinally aligned columns of laminin-1 and Schwann cells) to physically guide regenerating axons and secrete neurotrophic factors, including NGF, Neurotrophin 3, 4, 5 and 6 as well as BDNF (Madura, 2012; Jessen and Mirsky, 2016). ECM components including laminin and fibronectin also support axon elongation by providing cell-matrix adhesion points (Chernousov *et al.*, 2008). Importantly, this environment can only occur when some of the ECM remains intact, explaining why although neuropraxia and axonotmesis injuries typically successfully regenerate without intervention, neurotmesis injuries do not (Grinsell and Keating, 2014). Axon regeneration is slow (approximately one mm per day), and the ability of neurons and Schwann cells to sustain axon regeneration progressively fails over distance and time (Burnett and Zager, 2004). When regenerating axons reach the injury site they encounter disorganized Schwann cells, fibroblasts, cells of the immune system, collagen fibres and cytoskeletal elements as a result of the degenerative process. Many axons fail to elongate beyond the injury site and form whorls within the tissue, turn back along the proximal segment, innervate inappropriate endoneurial tubes (e.g. sensory as opposed to motor) or take an extra-neural course, significantly hampering regeneration (De Ruiter *et al.*, 2014). Furthermore, if an endoneurial tube is not reached, the regenerative growth cone can develop into a neuroma, manifesting clinically as a painful lump, and empty endoneurial tubes undergo progressive fibrosis with intraneural scarring prohibiting regeneration (Rajput *et al.*, 2012).

1.4.3 Treatment options for peripheral nerve repair

Numerous interventions have been developed to improve functional recovery following severe peripheral nerve injuries (Grinsell and Keating, 2014). The intervention used is typically determined by the severity of the injury (i.e. injury grade), the location of the injury (i.e. proximal or distal) and the importance of the injured nerve, (i.e. a critical motor nerve or a sensory nerve) (Figure 1.7).

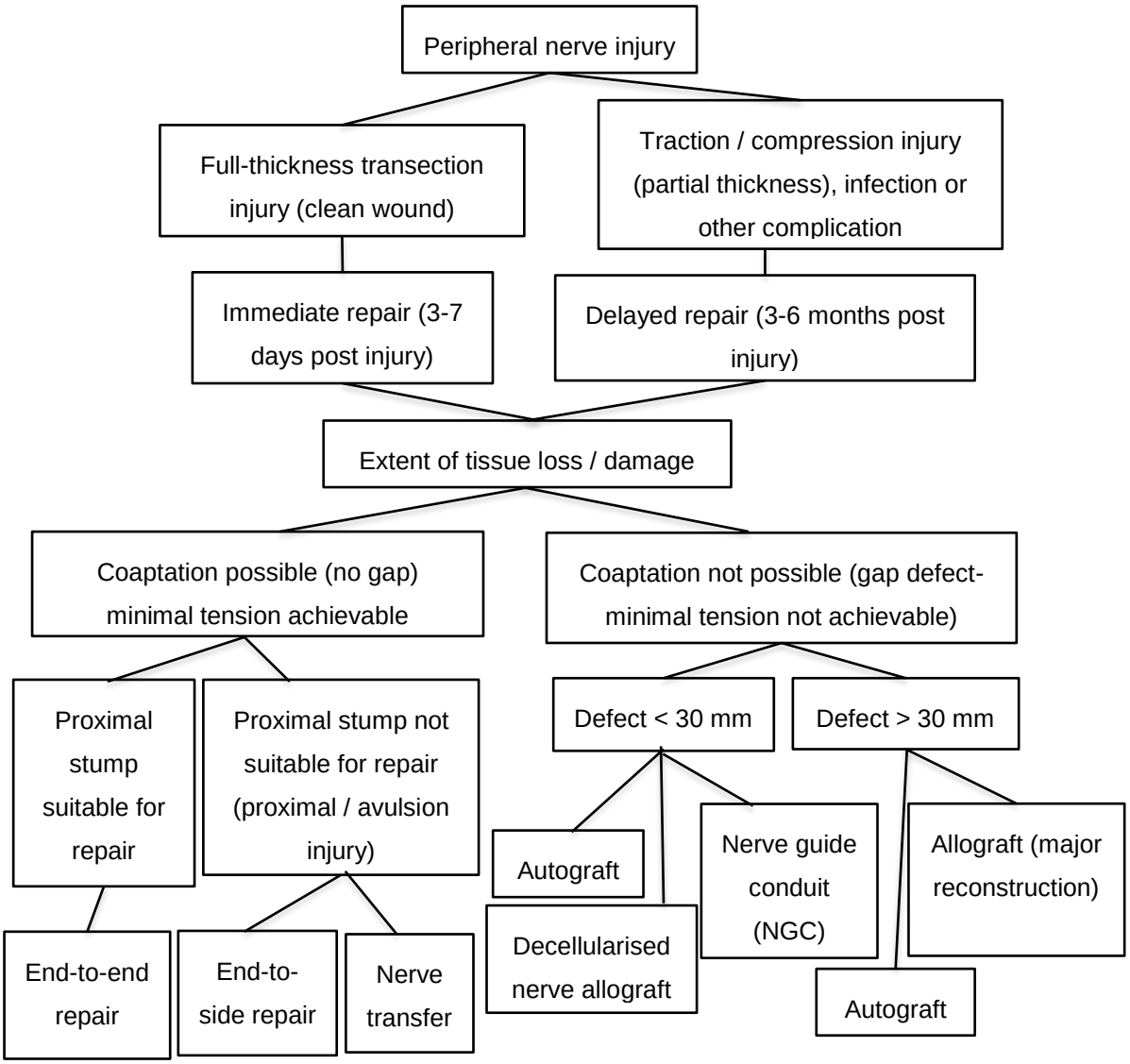

Figure 1.7 Current interventions for peripheral nerve injury. Current interventions for peripheral nerve injury are determined by several factors, including infection and delay in repair, but primarily injury severity. For transection injuries with no gap, where direct coaptation can be achieved, nerve ends are directly repaired, either by end-end or end-side repair, or transfer of an end of an undamaged nerve. For transection injuries with a gap defect, injuries less than 30 mm are repaired using an autograft, decellularised nerve allograft or a nerve guidance conduit (NGC), however gap defects longer than 30 mm are currently repaired using an autograft, or an allograft for severe injuries requiring major reconstruction. Adapted from Grinsell and Keating (2014)

1.4.4 Surgical reconstruction

Small defects, usually up to three mm, are directly sutured together to reunite the proximal and distal segments, providing a tension free coaptation in a well vascularized bed can be achieved (Grinsell and Keating, 2014). Microsutures can be used for gross fascicular matching, using the surface blood vessel patterns as a guide, and although as there is an increased risk of intraneural scarring and devascularisation, epineurial sutures are typically used (Kerns, 2008). Direct repair under excessive tension usually causes devascularisation of the nerve, leading to further atrophy along the nerve path and prohibiting regeneration. As such, nerve defects greater than the few millimeters permissive for suturing either require a graft to bridge the defect, which is most often the case, or an alternative reconstructive option depending on the location of the injury (Szynkaruk *et al.*, 2012).

1.4.5 Autografts

Reversed interposition autologous nerve grafts (autografts) are considered the gold standard for severe nerve gap defects (De Luca *et al.*, 2014). The grafts can be single, cable (multiple small nerve grafts aligned in parallel), trunk (mixed motor and sensory nerve grafts) or vascularized (nerve graft with arterial and venous blood supply intact), depending on the diameter and location of the injured nerve (Colen *et al.*, 2009; Houschyar *et al.*, 2016). Single grafts can be used to bridge the gap of an injured nerve with a smaller diameter, but cable grafts are required to approximate the diameter of larger nerves. Donor graft segments are harvested from more expendable (usually sensory) nerves, typically the sural or medial antebrachial nerve, to repair more critical (usually motor) nerve defects (Grinsell and Keating, 2014).

Following transplantation, the donor autograft undergoes Wallerian degeneration, thus providing physical guidance for regenerating axons in a similar manner to spontaneous regeneration (Bell and Haycock, 2011; Grinsell and Keating, 2014). However, in addition to physical guidance, autografts provide a stimulating, permissive scaffold for regeneration, comprising appropriate ECM composition and architecture, and a basement membrane with adhesion motifs (Gaudet *et al.*, 2011; Madura, 2012). Although autografts are considered the gold standard, approximately only 50 % of patients achieve functional sensory recovery and even less, approximately 40 – 50%, achieve functional motor recovery following nerve autografting (Lee and Wolfe, 2000; Ruijs *et al.*, 2005; Grinsell and Keating, 2014). In addition, autografts are associated with significant limitations, including

sacrificing a functional nerve, donor site morbidity and unavoidable size and fascicle mismatch (Siemionow and Brzezicki, 2009).

1.4.6 Nerve Guidance Conduits (NGCs)

The various limitations of autografts and direct suturing, the most widely used interventions for peripheral nerve repair, has led to the development of NGCs as an alternative (de Ruiter *et al.*, 2009; De Luca *et al.*, 2014). NGCs can be manufactured to any specification, are readily available and easily prepared, and do not require a second site of surgery or sacrifice of a functional nerve (Silva *et al.*, 2017). NGCs are primarily tubular constructs designed to enclose the opposing stumps of the severed axon and provide physical guidance to regenerating axons (Faroni *et al.*, 2015). Following suturing of the severed axon into the NGC, protein rich axoplasmic fluid containing fibrinogen, various growth factors and neurotrophic factors is released into the NGC. A fibrin clot then forms, enabling cellular infiltration of the NGC (Figure 1.8) (Lackington *et al.*, 2017).

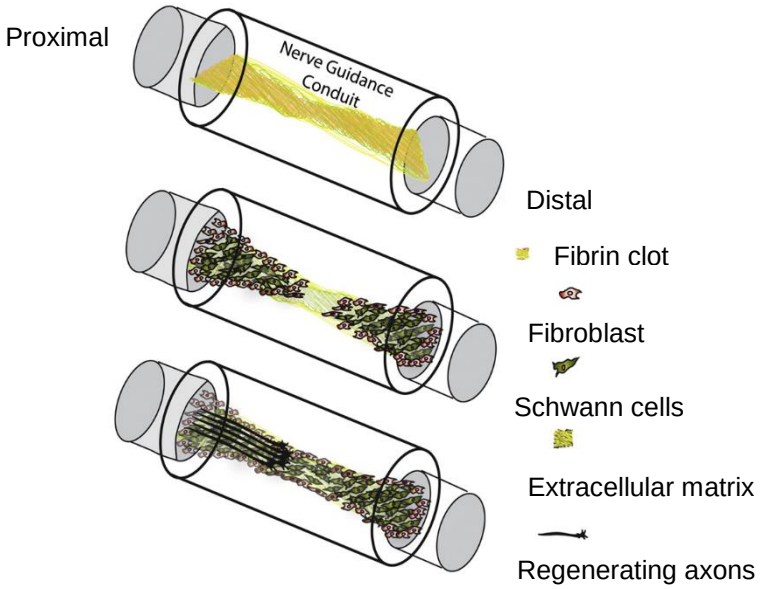

Figure 1.8 Peripheral nerve regeneration through a nerve guidance conduit (NGC). NGCs are used to repair nerve gap defects by suturing at the proximal and distal ends of a severed axon. Protein-rich axoplasmic fluid is released from the nerve stumps, and a fibrin clot then forms. The fibrin clot provides physical guidance to migrating Schwann cells and fibroblasts, enabling ECM remodelling and subsequent elongation of regenerating axons. Adapted from Steed *et al*. (2011)

NGCs can be manufactured from synthetic and natural materials, and there are a number of considerations for clinical application (Dalamagkas *et al.*, 2016). Criteria

for NGCs include biocompatibility, to not induce an adverse host immune response, and biodegradability, enabling tissue remodelling whilst maintaining a mechanically stable environment during the regenerative process (Kehoe *et al.*, 2012; Mobini *et al.*, 2017). In addition, NGCs must have flexibility to enable nerve excursion and movement across articulating joints, and permeability to enable diffusion of nutrients and small molecules (Kehoe *et al.*, 2012).

1.4.6.1 Synthetic materials

A number of different synthetic materials have been used for NGC fabrication, and their physical and chemical properties, including porosity and mechanical strength, can be modified (Wang and Cai, 2010; Bell and Haycock, 2011). Non-degradable polymers have previously been used, including silicone and polytetrafluoroethylene (PTFE). However, non-degradable polymers, such as silicone, have been reported to cause long-term inflammation and chronic nerve compression in clinical studies. For example, a study by Dahlin *et al*. (2001) investigated the use of silicone NGCs for the repair of median and ulnar repair defects, and reported that although promising functional recovery was observed up to 12 months post repair, localised inflammation and discomfort forced the removal of 7 out of 11 implanted conduits (Dahlin *et al.*, 2001). Therefore, as non-degradable NGCs require a second surgery for removal, biodegradable synthetic polymers are preferred, providing that their degradation products are non-cytotoxic (Belkas *et al.*, 2004; Siemionow *et al.*, 2010; Kehoe *et al.*, 2012).

Synthetic biodegradable polymers frequently used for NGCs include polylactic acid (PLA), polyglycolic acid (PGA), and polycaprolactone (PCL) (Wang and Cai, 2010; Daly *et al.*, 2012; Kehoe *et al.*, 2012). However, these polymers are frequently synthesised as co-polymers, such as polylactic-co-glycolic acid (PLGA) or modified, including functionalisation with bioactive molecules, to optimise bioactivity, degradation rate, porosity, rigidity and biocompatibility (De Luca *et al.*, 2014; Dalamagkas *et al.*, 2016). A small number of NGCs manufactured from synthetic materials are commercially available, including resorbable NGCs Neurolac® and Neurotube® (Table 1.2).

Neurotube® is a biodegradable, porous mesh NGC manufactured from PGA with a highly woven tubular structure (Battiston *et al.*, 2007; Kehoe *et al.*, 2012). Clinical studies of Neurotube® have reported comparable efficacy to autografts in defects up to 20 mm in length, however the NGC was found to degrade rapidly *in vivo* (within one – two months) (Mackinnon and Dellon, 1990; Donoghoe *et al.*, 2007;

Bushnell *et al.*, 2008). Furthermore, the high rates of degradation resulted in acidic degradation products (glycolate and pyruvate) (Kehoe *et al.*, 2012).

Neurolac® is a hollow tubular NGC manufactured from the co-polymer poly (D, L-lactide-co-ε-caprolactone) (PCL). Neurolac® has been shown to degrade at a steady rate, without the production of toxic degradation products, and is transparent, enabling easy clinical insertion (Stang *et al.*, 2009; Kehoe *et al.*, 2012). Clinical studies of Neurolac® have demonstrated comparable efficacy to autografts in defects up to 30 mm in length (Bertleff *et al.*, 2005; Meek *et al.*, 2006). However, Neurolac® has also been shown to have high rigidity, and has been shown to induce swelling and fragmentation due to incomplete degradation (Kehoe *et al.*, 2012).

1.4.6.2 Natural materials

Naturally derived polymers, including ECM molecules (e.g. collagens, laminin, fibrin and hyaluronan), other polysaccharides (e.g. chitosan, alginate, agarose) and proteins (silk fibroin, keratin), have been used extensively for manufacturing NGCs and many of the currently commercially available NGCs are manufactured from natural polymers, particularly ECM derived polymers such as collagen (Table 1.2) (Bell and Haycock, 2011; Kehoe *et al.*, 2012; Dalamagkas *et al.*, 2016). The surface chemistry of natural polymers contains adhesion motifs which bind to cellular integrins, enabling cellular adhesion (Hersel *et al.*, 2003; Dalamagkas *et al.*, 2016). For example, collagen type I contains various adhesion motifs, including the RGD amino acid sequence, which bind collagen-associated integrins α1β1 and α2β1 expressed by neurons and Schwann cells, as shown in Table 1.1 (Heino, 2007; Nieuwenhuis *et al.*, 2018).

Although the degradation rate of natural polymers can be modified, for example by chemical cross-linking, natural polymers are associated with poor mechanical properties (Xie *et al.*, 2008; Wang and Cai, 2010; Khaing and Schmidt, 2012). As such, natural polymers are usually used in combination, as co-polymers, with either another biodegradable natural polymer (e.g. collagen-chitosan scaffolds) or with a biodegradable synthetic polymer (e.g. collagen-PGA) (Bell and Haycock, 2011; De Luca *et al.*, 2014).

NeuraGen®, NeuroFlex™ and NeuroMatrix™ are NGCs manufactured from bovine collagen type I, a major component of peripheral nerve ECM (Kehoe *et al.*, 2012). Collagen type I is a commonly used biomaterial due to high biocompatibility, easy

isolation and modification, although there is high batch variation in collagen type I production and therefore reproducibility represents the main limitation of collagen type I NGCs (Stang *et al.*, 2004; Kehoe *et al.*, 2012).

NeuraGen® is a semi permeable, hollow bovine collagen type I construct, and the fibrillar collagen structure is maintained in the fabrication process (Du *et al.*, 2018). Clinical studies of NeuraGen® have shown comparable clinical efficacy to autografts in defects up to 20 mm in length (Farole and Jamal, 2008; Lohmeyer *et al.*, 2009). Furthermore, pre-clinical studies of NeuraGen® have also demonstrated efficacy in defects up to 40 mm in length (Archibald *et al.*, 1991).

NeuroFlex™ and NeuroMatrix™ are crimped, semi-permeable, hollow bovine collagen type I constructs, however NeuroFlex™ is also flexible and kink-resistant up to 140° of flexion. Interestingly, there are currently no published studies on the clinical efficacy of NeuroFlex™ or NeuroMatrix™, however both conduits are not recommended for the repair of defects exceeding 25 mm (Kehoe *et al.*, 2012; Lackington *et al.*, 2017). However, whereas the degradation time of NeuroFlex™ and NeuroMatrix™ is 4 – 8 months, NeuraGen® has a degradation time of approximately 4 years, which may lead to long-term chronic nerve compression and require further surgery for the removal of the conduit. Clinical studies of NeuraGen® have only included follow up of a maximum of two years, so the long-term outcomes are currently unknown (Dahlin *et al.*, 2001; Kehoe *et al.*, 2012; Du *et al.*, 2018).

Table 1.2 Current FDA approved absorbable nerve guidance conduits (NGCs). Current FDA approved absorbable NGCs for use in peripheral nerve repair. Non-resorbable conduits, cuffs and wraps are not included in the table. Adapted from Kehoe *et al*. (2012) and Lackington *et al*. (2017).

	Company	Biomaterial	Composition	Diameter	Length	Degradation	Clinical studies	
							Clinical study	Outcome
NeuroTube®	Polyglycolic acid (PGA) Synovis Micro Companies Alliance Inc.	Polyglycolic acid (PGA)	Hollow tubular construct	2.3–8 mm	2–4 cm	3 months	4 repairs, median nerve <30 mm, unspecified follow up – (Donoghoe et al., 2007)	Good recovery of motor and sensory function
							136 repairs, digital nerve, < 4 mm gap, follow up 8 – 10 months (Bushnell et al., 2000)	Good recovery, however no statistical significance between conduit and control group
NeuraGen®	Integra Life Sciences Corp.	Bovine collagen type I	Hollow tubular construct	1.5–7 mm	2–3 cm	36-48 months	12 repairs digital nerve < 20 mm, 12-22 months follow up (Farole et al., 2008)	4/9 excellent 4/9 good 1/9 fair
							15 repairs digital nerve, < 20 mm gap, 12 months follow up – Lohmeyer et al., 2009)	4/12 excellent sensibility 5/12 good 1/12 poor 2/12 no recovery
Neurolac®	Polyganics Inc.	Poly(DL-lactide-ε-caprolactone); PCL	Hollow tubular construct	1.5–10 mm	3 cm	16 months	34 repairs, digital nerve, < 20 mm, follow up 12 months (Bertleff et al., 2005)	Good recovery, however no statistical significance between conduit and control group
NeuraGen® 3D	Integra Life Sciences Corp.	Bovine collagen type I and glycosaminoglycan (chondroitin-6-sulfate)	Tubular collagen conduit with porous inner hydrogel matrix of collagen and chondroitin-6-sulfate	1.5 – 7 mm	Up to 6.5 cm	Unknown	Clinical data not yet available in the published literature	
NeuroMatrix™	Collagen Matrix Inc.	Bovine collagen type I	Hollow tubular construct	2–6 mm	2.5 cm	4-8 months	Clinical data not yet available in the published literature	
NeuroFlex™	Collagen Matrix Inc.	Bovine collagen type I	Hollow tubular construct	2–6 mm	2.5 cm	4-8 months	Clinical data not yet available in the published literature	
NerBridge®	Toyobo Co., Ltd	Polyglycolic acid (PGA) with porcine collagen type I and III	Tubular construct with outer and inner surfaces coated with collagen	0.5 – 4 mm	3 – 5 cm	Unknown	Clinical data not yet available in the published literature	

1.4.6.3 Recent advances in NGC fabrication

Recent developments in NGC fabrication have included architectural modifications at the macro, micro and nanoscale level, designed to provide different topographical cues to promote axon regeneration (Lackington *et al.*, 2017). Macroscale modifications include the development of single lumen, multi-lumen, rolled and hydrogel based luminal fillers (Ansselin *et al.*, 1997; Stang *et al.*, 2005; Chang *et al.*, 2007; Jenkins *et al.*, 2015). Microscale modifications include the development of highly axially aligned channels, microgrooves, microfilaments and fibres, and microporous scaffolds to provide intraluminal surface topography to support cellular attachment and alignment (Cai *et al.*, 2005; Lin *et al.*, 2008; Lee *et al.*, 2012; Gnavi *et al.*, 2018). Various techniques are used for these modifications, including direct moulding to shape multi-lumen NGCs and controlled crosslinking, freeze drying and electrospinning to generate pores and fibres (Sill and von Recum, 2008; Haugh *et al.*, 2010; Gnavi *et al.*, 2018).

Another advance in NGC fabrication is surface modification of constructs with ECM proteins, including basement membrane proteins to enhance cell attachment and axon regeneration (Gao *et al.*, 2013; Lackington *et al.*, 2017). ECM molecules, including laminin and fibronectin, have been added to the surface of NGCs and incorporated into luminal fillers to stimulate cell adhesion, migration and axon regeneration (Gao *et al.*, 2013; De Luca *et al.*, 2014). The incorporation of laminin has been shown to promote Schwann cell proliferation and stimulate neurite extension *in vitro* and *in vivo* (Matsumoto *et al.*, 2000; Suri and Schmidt, 2010; Cao *et al.*, 2011). Fibronectin has been shown to act synergistically with laminin, and requires controlled deposition as excess debris prevents completion of regeneration (Chen *et al.*, 2000; Ahmed *et al.*, 2003; Mosahebi *et al.*, 2003; Han *et al.*, 2010). In addition to ECM molecules themselves, research has focused on incorporating selective cell-binding motifs derived from ECM proteins, as these motifs can be incorporated at a higher density and can convey specific cell-material interactions (Gao *et al.*, 2013). Several motifs, including the RGD, IKVAV and YIGSR amino acid sequences have been shown to promote Schwann cell and neuron adhesion (Hersel *et al.*, 2003; Wei *et al.*, 2007). However, there are few studies investigating functionalized NGCs *in vivo,* aside from NGCs functionalised with the RGD motif which has been shown to successfully promote axon regeneration in a 10 mm rat sciatic defect model up to three months post-injury (Ahmed and Jayakumar, 2003).

1.4.6.4 Limitations of NGCs

Relatively few NGCs are commercially available, confined to those manufactured from a limited number of biodegradable materials such as collagen I, PGA and PCL (Table 1.2) (Kehoe *et al.*, 2012). Clinical studies of the currently available NGCs have reported a comparable efficacy between autografts and NGCs for small defects, typically up to 20 mm in length, however clinical studies have yet to demonstrate superior efficacy to autografts (Kehoe *et al.*, 2012; Gerth *et al.*, 2015). In addition, outcomes from clinical studies are highly variable, and variations in nerve type, cause of injury, and outcome measures limit comparisons between NGCs (Gerth *et al.*, 2015).

The majority of NGCs currently available are hollow tubular conduits, and NeuraGen® is the only NGC containing a collagen-glycosaminoglycan hydrogel luminal filler (Faroni *et al.*, 2015). It is thought that the limited efficacy of NGCs, particularly for the repair of longer defects, is due to the lack of a native ECM architecture and biochemical composition necessary to provide physical guidance to regenerating axons, and support the attachment and proliferation of Schwann cells (Whitlock *et al.*, 2009; Faroni *et al.*, 2015). Although, as discussed previously, recent advances in NGC development have focused on architectural modifications and the addition of ECM components to NGCs, the majority of this research is still experimental and is yet unable to replicate the complex properties of the natural ECM (Mobini *et al.*, 2017; Lackington *et al.*, 2017).

1.4.7 Allografts

Human cadaveric allografts are rarely used, except in a limited number of cases when there is insufficient autograft material available for major nerve reconstruction following extensive injury (Grinsell and Keating, 2014). In contrast to autografts, there are no donor supply or donor site morbidity limitations associated with the use of allografts, although there are several other complications (Schmidt and Leach, 2003; Siemionow and Brzezicki, 2009).

Allografts contain donor cells, displaying major histocompatibility complex (MHC) molecules (Ayala-García *et al.*, 2012). The role of MHC molecules is to present foreign antigens, such as epitopes from cytoplasmic or internalised pathogens, inducing a specific cell-mediated immune response. However, as MHC molecules are specific to each individual, MHC molecules displayed on allogeneic cells are recognised as foreign by the host immune system, and induce a T-cell mediated

immune response, ultimately causing rejection of the graft. Initial acute rejection of transplants can be caused by direct or indirect recognition of allogeneic MHC class II proteins presented by antigen presenting cells, or by indirect recognition of MHC molecules shed by allogeneic cells (Ayala-García *et al.*, 2012; Lakkis and Lechler, 2013). Consequently, nerve allograft recipient patients require systemic immunosuppression (typically for up to two years) until the graft has been repopulated with recipient cells, and are exposed to associated risks of infection and malignancy (Grinsell and Keating, 2014). As a result, it is widely stated that allografts should be reserved for patients with injuries irreparable by autograft which, without an allograft, would result in limb paralysis (Moore *et al.*, 2009; Grinsell and Keating, 2014).

1.4.8 Decellularised tissue grafts

Decellularisation of allogeneic or xenogeneic tissue has the potential to produce a non-immunogenic ECM scaffold with biological, biochemical and biomechanical characteristics similar to native tissue (Badylak *et al.*, 2009; Crapo *et al.*, 2011; Kawecki *et al.*, 2018). Decellularisation processes have been designed to remove cells and nucleic acids from tissue, thus minimising the potential for an adverse immunological response by removing the major immunogenic components (Gilbert *et al.*, 2006; Nagata *et al.*, 2010). Xenogeneic ECM proteins, such as collagens, can also elicit an adverse immune response (Wong and Griffiths, 2014; Aamodt and Grainger, 2016). However, ECM proteins are highly conserved within higher mammals, including humans and pigs, and therefore porcine ECM proteins are also non-immunogenic (Badylak, 2004; Bayrak *et al.*, 2010).

The decellularised tissue retains overall ECM histioarchitecture and biochemical composition, and contains appropriate regenerative cues, including topographical and biological cues necessary for forming cell-cell and cell-matrix contacts, providing a three-dimensional, native scaffold for regeneration (Gilbert *et al.*, 2006; Badylak, 2014). As such, decellularised tissues have great potential as scaffolds for uses in tissue engineering applications, and a number of allogeneic and xenogeneic decellularised tissue products are commercially available (Table 1.3) (Crapo *et al.*, 2011; Chen and Liu, 2016; Parmaksiz *et al.*, 2016; Boccafoschi *et al.*, 2019).

Table 1.3 Commercially available decellularised tissue products.
Examples of commercially available allogeneic and xenogeneic decellularised tissue products for the repair of various tissues. NHSBT TES = NHS Blood and Transplant Tissue and Eye Services, BDM = Demineralised Bone Matrix, AV = Arteriovenous. Adapted from Chen and Liu (2016), Parmaksiz *et al*. (2016) and Boccafoschi *et al*. (2019).

Product	Manufacturer	ECM source	Application
AlloDerm®	LifeCell Corp., USA	Human dermis	Skin and soft tissue repair
AlloMatrix®	Wright Medical Inc., USA	Human bone (DBM with calcium sulphate)	Bone repair (cavitary bone deficiency, augmentation of segmental bone loss)
AlloPatch®	Musculoskeletal transplant foundation, USA	Human fascia lata	Rotator cuff augmentation
AlloPatch HD™	Musculoskeletal transplant foundation, USA	Human dermis	Tendon reconstruction
Artegraft®	Artegraft Inc., USA	Bovine carotid artery	AV access
CorMatrix ECM™	CorMatrix Cardiovascular Inc., USA	Porcine small intestine	Cardiovascular repair
CryoArtery®	CryoLife Inc., USA	Human femoral artery	Peripheral revascularization, AV access
dCELL® Human Dermis	NHSBT TES, UK	Human dermis	Skin and soft tissue repair
dCELL® DBM	NHSBT TES, UK	Human bone (DBM combined with glycerol)	Bone void filler
DermaMatrix™	Depuy Synthes Inc., UK	Human dermis	Soft tissue repair
Epic™	SJM Biocor®, St. Jude Medical Inc., USA	Porcine heart valve	Cardiovascular repair
Grafton®	Osteotech Inc., USA	Bone (BDM combined with glycerol)	Bone repair (cavitary bone deficiency)
GraftJacket®	Wright Medical Inc., USA	Human dermis	Augmentation of rotator cuff, tendon repairs
Hancock® II, Mosaic®, and Freestyle®	Medtronic Inc., USA	Porcine heart valve	Valve replacement
NeoForm™	Mentor Worldwide LLC, USA	Human dermis	Breast augmentation
Optefil®, Opteform® and Optecure®	Exactech Inc., USA	Human bone (DBM ready to be hydrated in gelatin carrier	Bone repair (cavitary bone deficiency, augmentation of segmental bone loss)
Perimount®	Edwards Lifesciences LLC, USA	Bovine pericardium	Valve replacement
Prima™ Plus	Edwards Lifesciences LLC, USA	Porcine heart valve	Valve replacement
Restore™	DuPuy, West Chester, PA, USA	Porcine small intestine	Soft tissue repair
Surgisis®, Durasis® and Stratasis®	Cook Biotech, USA	Porcine small intestine	Soft tissue repair
Strattice™	LifeCell Corp., USA	Porcine dermis	Skin and soft tissue repair
Viagraf®	Smith & Nephew Inc., USA	Human bone (DBM combined with glycerol)	Bone void filler

1.4.8.1 Decellularisation criteria

Decellularisation processes should remove sufficient immunogenic material from the tissue to minimise the potential for an adverse immunological response (Gilbert *et al.*, 2006; Nagata *et al.*, 2010; Crapo *et al.*, 2011). Whilst there are no existing national or international standards for defining tissue decellularisation, the widely used criteria for the successful removal of immunogenic material are based upon data presented by Crapo *et al*. (2011). The criteria proposed include a total of less than 50 ng of double stranded DNA (dsDNA) per mg of tissue (dry weight), no fragments of DNA greater than 200 base pairs in length, and no nucleic acids visible when decellularised tissue sections are stained with haematoxylin and eosin (H & E) (Crapo *et al.*, 2011). These criteria proposed by Crapo *et al*. (2011) are considered as guidelines, and are based on evidence suggesting that the amount of double stranded DNA in a decellularised tissue scaffold is proportional to the host immune response upon implantation (Gilbert *et al.*, 2009; Crapo *et al.*, 2011; Kawecki *et al.*, 2018). Residual fragments of double stranded DNA are recognised by intracellular sensor proteins of cells of the innate immune system, such as macrophages and dendritic cells (Paludan and Bowie, 2013). Binding of double stranded DNA activates signalling pathways which initiate an inflammatory response, characterised by the induction of the M1 phenotype in activated macrophages, and enhanced secretion of pro-inflammatory cytokines including IL-1β and IL-6 (Erdag and Morgan, 2004; Paludan and Bowie, 2013; Jønsson *et al.*, 2017).

However, several studies have reported no adverse immune responses from decellularised tissues containing trace amounts of DNA, and many clinically available decellularised tissue products have been found to contain residual quantities of DNA, including the Oasis™ and Restore™ products, processed from porcine small intestinal submucosa (Gilbert *et al.*, 2009; Gilpin and Yang, 2017; Kawecki *et al.*, 2018). Gilbert *et al.* (2009) reported quantifiable DNA levels in eight commercially available decellularised tissues, however each scaffold demonstrated clinical efficacy and no adverse immune response (Gilbert *et al.*, 2009). Furthermore, it has been suggested that residual DNA in isolation may only induce localised calcification (Booth *et al.*, 2002; Kawecki *et al.*, 2018).

It has also been suggested that the host immune response to decellularised tissue scaffolds may primarily be due to cellular remnants, including membrane phospholipids and associated proteins (Wong and Griffiths, 2014; Badylak, 2014;

Morris *et al.*, 2017; Gilpin and Yang, 2017). A study by Londono *et al*., (2017) supplemented Puracol^{TM} Plus collagen scaffolds with differing concentrations of xenogeneic cellular remnants that may be present in decellularised ECM scaffolds, including calf thymus DNA, mitochrondia isolated from L929 fibroblasts, and cell membranes isolated from porcine red blood cells. The supplemented scaffolds were then cultured *in vitro* with primary murine macrophages for 18 hours, or implanted *in vivo* in a rat abdominal wall defect model for 14 days. The study reported that murine macrophages showed an increase in pro-inflammatory marker inducible nitric oxide synthase (iNOS), and no expression of pro-remodelling marker Fizz1, regardless of concentration of cellular remnants when cultured *in vitro* with collagen scaffolds supplemented with cellular remnants. However, immunolabelling of rat macrophages following implantation of collagen scaffolds supplemented with cellular remnants *in vivo* showed a dose dependent pro-inflammatory response to differing concentrations of cellular remnants (Londono *et al.*, 2017). Although the quantities of cellular remnants required to elicit an adverse host immune response upon implantation have yet to be established, these results reinforce the importance of the removal of cellular remnants from decellularised tissues. Therefore, it has recently been proposed that in addition to the criteria proposed by Crapo *et al.* (2011), decellularisation criteria should include the removal of cell membrane debris, including intracellular membrane compartments such as mitochondrial membranes (Kawecki *et al.*, 2018).

1.4.8.2 Immune response to xenografts

Although both allogeneic and xenogeneic cells are recognised as foreign and can elicit immune rejection, as discussed previously, there are further risks associated with the presence of xenoantigens (Badylak, 2004). Xenogeneic cells of mammalian origin, with the exception of humans, apes and old world monkeys, possess a cell surface sugar, galactose α1-3 galactose (α-gal) (Galili *et al.*, 1987). Humans have an abundance of anti-α-gal antibodies due to constant antigenic stimulation from bacteria in the gut, which rapidly bind to the α-gal epitope upon transplantation of xenogeneic cells, initiating hyper-acute rejection of xenografts (Erdag and Morgan, 2004). However, decellularisation of xenogeneic tissues removes immunogenic material, including whole cells, membranes and cytoplasmic proteins, and although small quantities of α-gal have been shown to be present in some decellularised scaffolds, such as porcine small intestinal submucosa (SIS), several studies have shown that this does not induce graft rejection (McPherson *et al.*, 2000). A study in which α1,3 galactosyltransferase knockout mice were

implanted with decellularised porcine SIS containing high levels of α-gal found that the presence of α-gal increased the duration of inflammation and delayed tissue remodelling, but that the graft ultimately remodelled (Raeder *et al.*, 2002). Another study by Daly *et al*. (2009) investigated decellularised porcine SIS containing α-gal in a primate model, and reported that the presence of α-gal elicited a serum antibody response, but had no adverse effect upon tissue remodelling (Daly *et al.*, 2009). Furthermore, several studies have shown that non-cell associated α-gal can, in fact, enhance wound healing, by the rapid recruitment and activation of macrophages to the injury site (Wigglesworth *et al.*, 2011; Hurwitz *et al.*, 2012).

1.4.8.3 Methods of decellularisation

Numerous methods have been developed for tissue decellularisation. Methods used in decellularisation processes can be broadly classified as physical, chemical, or enzymatic methods, and are often used in combination in decellularisation protocols to achieve sufficient removal of immunogenic material (Gilbert *et al.*, 2006; Crapo *et al.*, 2011; Gilpin and Yang, 2017). However, although effective in removing immunogenic material, many decellularisation methods disrupt the structure and composition of the ECM, potentially compromising the biological and mechanical integrity of the resulting decellularised biological scaffold (White *et al.*, 2017). Consequently, decellularisation protocols are developed using a number of different methods to optimise the removal of immunogenic material whilst minimising alterations to ECM properties, preserving the integrity and regenerative capacity of the ECM scaffold (Gilbert *et al.*, 2006; Kawecki *et al.*, 2018).

1.4.8.3.1 Chemical methods

1.4.8.3.1.1 Detergents

Detergents are surfactants, with a hydrophilic head region and a hydrophobic tail. Detergents are amphipathic molecules, and are able to solubilise hydrophobic molecules, such as membrane proteins in water (Seddon *et al.*, 2004; White *et al.*, 2017). Detergents disrupt the cell membrane by integrating into the phospholipid bilayer, interacting with the hydrophobic portion of the bilayer and replacing the lipids. At concentrations above the critical micelle concentration, the detergent molecules form micelles containing lipids from the phospholipid bilayer and encapsulating solubilised membrane proteins, ultimately causing cell membrane disintegration into mixed micelles with detergent molecules which can then be washed from the tissue (Seddon *et al.*, 2004; Gilbert *et al.*, 2006).

1.4.8.3.1.2 Ionic detergents

Ionic detergents have a hydrophilic head group with either a negative or a positive net charge. Ionic detergents are highly effective for the solubilisation of both nuclear and cytoplasmic membranes, acting by disrupting non-covalent protein-protein, protein-lipid and lipid-lipid interactions (Seddon *et al.*, 2004). However, ionic detergents can cause significant ECM protein denaturation (White *et al.*, 2017).

Ionic detergents, such as sodium dodecyl sulphate (SDS) and sodium deoxycholate (SDC) are widely used and have been shown to be much more effective than non-ionic or zwitterionic detergents for decellularisation (Seddon *et al.*, 2004). SDS, an anionic detergent, is highly effective in disrupting cell membranes and facilitating the removal of both phospholipid and protein components, but has also been shown to disrupt matrix components, with decellularised tissues showing collagen damage and a reduction in GAG content when SDS is used at high concentrations for prolonged periods of time (Bhuyan, 2010; Faulk *et al.*, 2014a). Using low SDS concentrations (0.1 % w/v; 0.5 % w/v) has been shown to minimise the disruption of ECM proteins, with improved retention of collagen structure and GAGs reported in decellularised tissues (Paniagua Gutierrez *et al.*, 2014). Incorporating protease inhibitors, such as aprotinin, has also been shown to further minimise ECM disruption, by inhibiting the activity of matrix metalloproteinases released during cell membrane disintegration and cell lysis and preventing enzymatic ECM degradation (Wilshaw *et al.*, 2012).

1.4.8.3.1.3 Non-ionic detergents

Non-ionic detergents have an uncharged hydrophilic head region and do not disrupt protein-protein interactions, and therefore have minimal effects on ECM proteins. Triton X-100 is one of the most widely used non-ionic detergents for decellularisation (Seddon *et al.*, 2004; White *et al.*, 2017). Decellularisation using Triton X-100 has shown mixed results, in terms of efficacy and the effects on the ECM, dependent on tissue type, concentration and exposure time (Gilbert *et al.*, 2006; Crapo *et al.*, 2011). A study by Dahl *et al.* (2003) comparing decellularisation of porcine carotid arteries with Triton X-100 and SDS reported that decellularisation with Triton X-100, even at high concentrations (5 % v/v or 10 % v/v), had a lower efficacy in terms of cell nuclei and DNA removal compared to decellularisation with 1.8 mM SDS (Dahl *et al.*, 2003)

1.4.8.3.1.4 Zwitterionic detergents

Zwitterionic detergents have a net neutral charge, possessing both a positive and a negative charge at different regions of the molecule, and as such exhibit properties of both ionic and non-ionic detergents and disrupt protein-protein interactions more effectively than non-ionic detergents. One of most commonly used zwitterionic detergents is 3-[(3-cholamidopropyl)dimethylammonio]-1-propanesulfonate (CHAPS) (Seddon *et al.*, 2004; Crapo *et al.*, 2011). CHAPS has been used to successfully decellularise human and porcine lung tissue, and the use of 8 mM CHAPS was shown to preserve tissue architecture and biomechanical properties better than 1.8 mM SDS (O'Neill *et al.*, 2013). However, other studies have reported incomplete decellularisation using CHAPS. Booth *et al*. (2002) reported incomplete decellularisation of porcine aortic heart valve tissue with CHAPS (0.5 % w/v), although no deleterious effects on ECM architecture or biochemical composition were observed (Booth *et al.*, 2002). Ferng *et al*. (2017) reported incomplete decellularisation of whole porcine hearts with CHAPS, and showed that whole cell nuclei were still present in the tissue (Ferng *et al.*, 2017).

1.4.8.3.1.5 Hypotonic and hypertonic buffers

Hypotonic buffers induce cell swelling and cell lysis by osmosis, and hypertonic buffers dissociate DNA-protein complexes within cells (Crapo *et al.*, 2011). These solutions are also used to aid the removal of cellular debris from tissue, however it is often necessary to use these solutions in combination with other chemical or enzymatic treatments, e.g. detergents, to increase efficacy and fully remove DNA and cellular material (Gilbert *et al.*, 2006).

1.4.8.3.1.6 Other chemical agents

Acids and bases hydrolyse biomolecules, enabling solubilisation and removal of cell membrane components and intracellular nucleic acids (Crapo *et al.*, 2011). Peracetic acid is an effective decellularisation agent and also a sterilant, with a high level of oxidative activity inducing the denaturation of intracellular and membrane-associated microbial proteins (Dai *et al.*, 2016). Low concentrations of peracetic acid (0.1 % v/v in 4 % v/v ethanol) have been used to successfully decellularise several thin tissues, such as intestinal submucosa and bladder, with minimal effects on ECM structure (Rosario *et al.*, 2008; Syed *et al.*, 2014). However, such treatments have also been shown to disrupt ECM collagen. Analysis of murine lung tissue treated with peracetic acid showed denaturation of collagens type I, IV and VI and laminin, most likely caused by oxidative damage (Bonenfant *et al.*, 2013).

Porcine small intestinal submucosa decellularised using a 12 hour incubation in 0.1 % (v/v) peracetic acid showed significant increases in Young's modulus and yield stress, and a significant reduction in failure strain (Syed *et al.*, 2014). Peracetic acid has also been used in combination with other reagents to facilitate decellularisation. Porcine bladder has been successfully decellularised using a combination of 0.1 % (v/v) SDS and 0.1 % (v/v) peracetic acid, with minimal effects on ECM structure or biomechanical properties (Rosario *et al.*, 2008).

Chelating agents such as ethylene diamine tetra-acetic acid (EDTA) are often incorporated into decellularisation processes to facilitate the removal of cells from the ECM (Crapo *et al.*, 2011). Chelating agents disrupt the interactions between cell adhesion molecules and the ECM by chelating metal ions (e.g. $Mg^{2+,}$ Ca^{2+}) that are necessary for adhesions through attachment molecules such as integrins (Yamniuk and Vogel, 2005; Faulk *et al.*, 2014a). Furthermore, the chelation of metal ions inhibits the activity of matrix metalloproteinases released during cell lysis (Gilbert *et al.*, 2006). Booth *et al.* (2002) used SDS (0.1 % w/v) for the decellularisation of porcine aortic valves, and included EDTA (0.1 %; w/v) in combination with aprotinin (10 $KIU.mL^{-1}$), a serine proteinase inhibitor, in the decellularisation process to inhibit all proteinases that may be present within the tissue (Booth *et al.*, 2002).

1.4.8.3.2 Enzymatic methods

Enzymes, such as nucleases, proteinases and lipases are often used as part of decellularisation processes to mediate highly specific removal of certain components (Gilbert *et al.*, 2006).

Proteinases, such as trypsin, have been considered for use in isolation for decellularisation (Crapo *et al.*, 2011). However, the relatively high enzyme concentration and long exposure times required to complete decellularisation have been shown to cause significant damage to various ECM components, including collagen fibres and elastin (Kasimir *et al.*, 2003; Zou and Zhang, 2012). Lower concentrations of trypsin have been successfully used as an initial decellularisation step, to mediate the detachment of cells and enhance the diffusion of reagents in tissues with a relatively dense ECM (Rana *et al.*, 2017). The use of trypsin in combination with other reagents, such as EDTA, SDS or Triton X-100 has been shown to increase the efficacy of decellularisation of various tissues, including human articular cartilage, porcine articular cartilage, and porcine trachea (Rahman *et al.*, 2018).

Nucleases are used to cleave nucleic acids, and are essential for the removal of DNA and nucleic acids which remain in the tissue following cell lysis induced by physical or chemical treatments (Gilpin and Yang, 2017; Philips *et al.*, 2018; Kawecki *et al.*, 2018). Nucleases have been shown to reduce the DNA content of several tissues, including heart valves, tendon, and osteochondral tissues following detergent treatment (Crapo *et al.*, 2011; Philips *et al.*, 2018; Kawecki *et al.*, 2018). Endonucleases, such as Benzonase, are advantageous in that they are able to cleave nucleotide sequences from within, as opposed to exonucleases which remove nucleotides from the ends of the sequence (Gilpin and Yang, 2017).

1.4.8.3.3 Physical methods

A number of physical methods can be used as part of decellularisation procedures, with freeze-thaw cycles, sonication and agitation often incorporated (Crapo *et al.*, 2011). Repetitive freeze-thaw cycles are commonly used, and have been included in decellularisation processes for various tissues including cartilage, liver and lung (Venkatasubramanian *et al.*, 2006; Poornejad *et al.*, 2015). Freezing produces ice crystals, which induce cell lysis but also increase tissue permeability, enhancing diffusion of solutions. However, the formation of ice crystals can also damage ECM proteins and adversely affect ECM microstructure, therefore it is important to optimise the freezing rate and temperature to control ice crystal size and formation (Keane *et al.*, 2015).

Agitation and sonication are commonly employed in decellularisation protocols to enhance the permeation of chemical and enzymatic solutions and aid the wash out of cellular debris. Sonication is often used to increase the permeability of dense tissues and agitation, provided by using orbital shakers, magnetic stirrers or rollers, is used to enhance diffusion of reagents and has been shown to increase DNA wash out from tissues (Montoya and McFetridge, 2009a; Azhim *et al.*, 2014). However, excessive agitation speed or sonication frequency can lead to the disruption of ECM structure, so these processes must be optimised for each tissue type, size and density (Keane *et al.*, 2015; Gilpin and Yang, 2017).

1.4.8.4 Decellularised peripheral nerve grafts

Decellularised peripheral nerve grafts offer considerable potential for peripheral nerve repair, overcoming the limitations associated with the immunogenicity of allografts and providing a native microenvironment to facilitate axon regeneration with ECM properties that cannot yet be recapitulated using current NGC fabrication

techniques (Schmidt and Leach, 2003; Whitlock *et al.*, 2009; Szynkaruk *et al.*, 2012). It has been hypothesised that a decellularised nerve graft will promote axon elongation and facilitate regeneration through the provision of a native microenvironment, particularly intact endoneurial tubes and a basement membrane (Whitlock *et al.*, 2009; Karabekmez *et al.*, 2009; Moore *et al.*, 2011). A number of methods have been documented for the decellularisation of allogeneic and xenogeneic peripheral nerve, including physical, chemical or enzymatic methods (Hiles, 1972; Sondell *et al.*, 1998; Hudson *et al.*, 2004a; Wang *et al.*, 2016; Zilic *et al.*, 2016).

1.4.8.4.1 Avance® nerve graft

The Avance® nerve graft is currently the only commercially available decellularised peripheral nerve graft, a decellularised human allograft with lengths ranging between 15 and 70 mm marketed for clinical use in the USA since 2007 (AxoGen Inc. Alachua, FL). A chemical decellularisation process developed by Hudson *et al*. (2004), using Triton X-200 (0.14 % v/v) in combination with zwitterionic detergents sulfobetaine-10 (125 mM) and sulfobetaine-16 (0.6 mM) to decellularise rat sciatic nerve, has been licenced by Axogen® Inc. to produce the Avance® graft (Hudson *et al.*, 2004a). The decellularisation process used to produce the Avance® graft has been further developed for human nerves, with the addition of enzymatic digestion of CSPG, a known inhibitor of axon regeneration (Zuo *et al.*, 2002). The Avance® nerve graft has been shown to achieve positive results in several clinical case studies, demonstrating performance superior to NGCs for small defects (up to approximately 30 mm), and often equivalent performance to autografts (Karabekmez *et al.*, 2009; Moore *et al.*, 2011; Johnson *et al.*, 2011). Early clinical studies have shown that the Avance® graft is safe and effective in sensory nerve defects up to 30 mm in length. The Mayo clinic reported on ten nerve injuries within the hand and fingers, and found that all ten subjects recovered two-point discrimination of 6 mm or better (Karabekmez *et al.*, 2009).

A comprehensive, multi-centre clinical study between 2007 and 2012 investigated the efficacy of Avance® grafts in sensory, mixed and motor nerve injuries with a mean graft length of 22 ± 11 (5 – 50) mm (Brooks *et al.*, 2012). The study involved 132 individual nerve injuries, with the majority of injuries in the digital nerves in the hand (60 %), followed by upper extremity nerves (32 %), head/neck regions (5 %) and lower extremities (3 %). Sufficient data for efficacy analyses was reported for 76 injuries (49 sensory, 18 mixed, and 9 motor nerves). The graft was found to be safe, as no graft related adverse events were reported, and a 5 % revision rate was

reported. Meaningful recovery was observed in 87 % of the repairs, and subgroup analysis to determine the effects of factors known to influence outcome, including but not limited to nerve type, patient age, gap length, and mechanism of injury, found no significant differences with regard to recovery outcomes between the groups, demonstrating consistency. However, although not significant, several of the factors identified in the subgroup analysis did affect recovery, including nerve type (88.6 %, 85.7 % and 77 % meaningful recovery for sensory, motor and mixed nerves respectively), and defect length (100 %, 90.0% and 76.2 % for defects 5-14 mm, 30-50 mm and 15-29 mm respectively). Overall, the Avance® graft was found to be safe and effective in sensory, mixed and motor nerve defects between 5 and 50 mm. In comparison to similar studies, the results compared favourably to autografts, and were superior to those reported for NGCs (Brooks *et al.*, 2012).

However, the study by Brooks *et al*. (2012) has various limitations, such as an increased risk of heterogeneity in the datasets, variability between subjects, injuries and data sources, and that observational studies could not be performed in a prospective, randomised manner. Furthermore, there are no obvious conclusions with respect to the relationship between outcome and influencing factors including gap length, patient age, and nerve type, in contrast to other literature reporting statistically significant relationships between these factors and outcomes. These findings could be attributed to the variation in the number of subjects in each group, the distribution of covariates across the groups, the impact of the graft on regeneration or differences in surgical approach (Brooks *et al.*, 2012).

1.4.8.4.2 Limitations of decellularised nerve grafts

Although the Avance® graft has demonstrated superior clinical efficacy to NGCs when used to treat a range of nerve defect sizes, clinical studies using the Avance® graft have not yet demonstrated consistently superior outcomes in comparison to autografts, even in small defects (up to 30 mm) (Whitlock *et al.*, 2009; Karabekmez *et al.*, 2009; Moore *et al.*, 2011; Szynkaruk *et al.*, 2012). A functional model of a rat sciatic nerve defect showed that for defects of 14 and 28 mm, the Avance® graft facilitated the growth of a 20 fold greater population of myelinated axons in comparison to NeuraGen®, an NGC manufactured from type 1 bovine collagen, and contained significantly more nerve fibres at all time points (Whitlock *et al.*, 2009). However, the study also reported that the Avance® nerve graft contained only approximately 30 % of the number of nerve fibres found in autografts. A potential explanation for this could be that the decellularised nerve graft had diminished regenerative capacity as a consequence of ECM disruption (Whitlock *et*

al., 2009). It has been hypothesised that inadequate preservation of the linear architecture of endoneurial tubes and specific basement membrane components, including laminin and collagen type IV, impairs axon regeneration and cellular infiltration in a decellularised nerve graft (Whitlock *et al.*, 2009; Lovati *et al.*, 2018).

1.4.9 Experimental strategies for peripheral nerve regeneration

Autografts remain the gold standard intervention for the repair of longer nerve gap defects (over 30 mm) (Siemionow and Brzezicki, 2009; Faroni *et al.*, 2015; Lackington *et al.*, 2017). Currently available NGCs are limited to the repair of shorter distances, typically 20 – 30 mm, and clinical studies have only demonstrated efficacy equivalent to autografts for the repair of defects up to 20 mm (Kehoe *et al.*, 2012; Gerth *et al.*, 2015). Although the Avance® graft has demonstrated superior clinical efficacy to NGCs for the repair of defects up to 30 mm, clinical studies using the Avance® graft have shown limited efficacy over longer distances (up to 60 mm) (Moore *et al.*, 2011).

It is hypothesised that the efficacy of decellularised nerve grafts and NGCs is limited to shorter distances due to insufficient host Schwann cell migration to sustain axon regeneration (Szynkaruk *et al.*, 2012; Gerth *et al.*, 2015; Busuttil *et al.*, 2017). As discussed previously, Schwann cells are intrinsic for axonal survival and function, and serve a pivotal role in orchestrating peripheral nerve repair (Jessen *et al.*, 2015; Jessen and Mirsky, 2016; López-Leal and Diaz, 2018). In addition to providing physical guidance to regenerating axons, Schwann cells produce various neurotrophic factors and cytokines and express cell adhesion molecules, as shown in Table 1.1 (Jessen and Mirsky, 2016). A study by Poppler *et al*. (2016) used rat decellularised nerve grafts for the repair of 30 mm and 60 mm defects in a rat sciatic nerve injury model, and although the study reported successful axon regeneration across the 30 mm defect, axonal elongation and regeneration was arrested across the 60 mm defects (Poppler *et al.*, 2016). The study reported a higher stromal cell presence in the 60 mm grafts and found higher levels of Schwann cell senescence markers, including p16, concluding that longer nerve defects induce Schwann cell senescence and that host Schwann cell migration is insufficient to promote axon regeneration across longer defects (Poppler *et al.*, 2016).

Recent experimental strategies for enhancing peripheral nerve regeneration have focused on the supplementation of NGCs and decellularised nerve grafts with exogenous factors to provide trophic support, stimulating axon regeneration and

delaying cell senescence (Figure 1.9). There have been two primary experimental approaches to supplementing NGCs and decellularised nerve grafts with exogenous factors: cellular therapies and pharmacotherapy (Faroni *et al.*, 2015; Mobini *et al.*, 2017; Lackington *et al.*, 2017). Cellular therapies have included repopulation with Schwann cells and various stem cells including adult multipotential stem cells (MSCs), and pharmacotherapies have included delivery of the various neurotrophic factors produced by Schwann cells during axon regeneration.

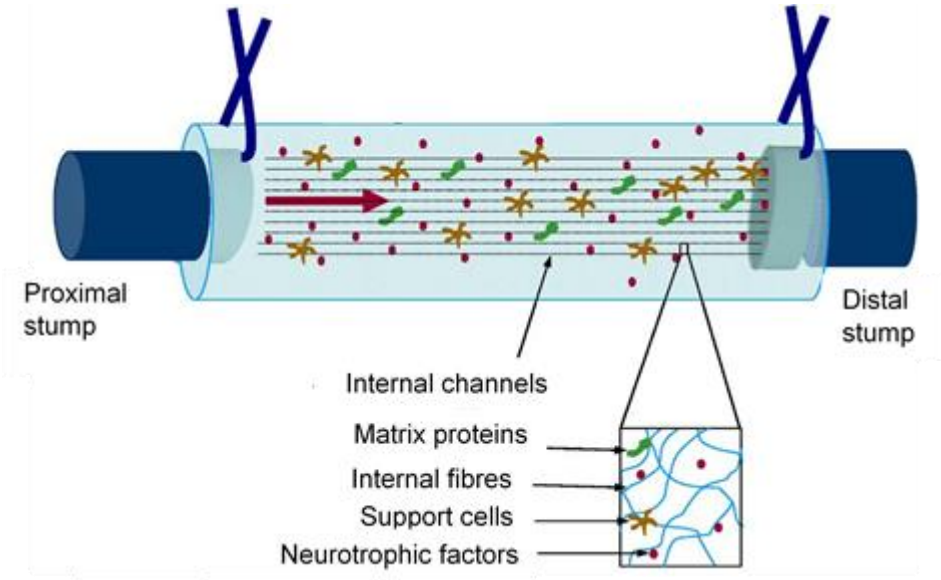

Figure 1.9 Supplementation of nerve guidance conduits (NGCs) with exogenous factors. Recent experimental advances in NGC fabrication have included the incorporation of axially aligned channels, microfibers and pores to provide physical guidance to regenerating axons. NGCs have also been supplemented with exogenous factors such as ECM proteins, support cells such as Schwann cells and various stem cells, and neurotrophic factors. Adapted from Bellamkonda *et al*. (2006)

1.4.10 Cellular therapies

1.4.10.1 Autologous Schwann cells

An extensive number of studies have focussed on supplementing NGCs with Schwann cells, and have demonstrated improved regenerative outcomes *in vivo* in rat sciatic nerve defect models for varying distances (8 – 20 mm) (Zack-Williams *et al.*, 2015; Lackington *et al.*, 2017; Jiang *et al.*, 2017). Several different methods have been used to introduce Schwann cells into NGCs, including direct injection, suspension within an intraluminal hydrogel, or release from the luminal wall (Faroni

et al., 2015; Fathi and Zaminy, 2017). Hydrogels, including alginate/fibronectin, gelatin, collagen, and Matrigel™, have been commonly used as substrates to incorporate Schwann cells into the lumen of NGCs (Faroni *et al.*, 2015; Houschyar *et al.*, 2016; Jiang *et al.*, 2017). Autologous Schwann cells seeded into collagen type I NGCs have been shown to increase axon regeneration distance and improve functional recovery when used to treat 18 mm and 20 mm defects in a rat sciatic nerve injury model (Ansselin *et al.*, 1997; Stang *et al.*, 2005). A study by Georgiou *et al*., (2013) describes the development of an engineered neural tissue (EngNT) as a method to introduce Schwann cells. Self-alignment of primary Schwann cells within a tethered collagen hydrogel, followed by the removal of interstitial fluid, was shown to produce an aligned sheet of cellular collagen hydrogel. The sheets were then rolled up and delivered within a NeuraGen® conduit for the repair of a 15 mm rat sciatic nerve defect model. The study reported that, at 8 weeks post-implantation, the constructs had facilitated axon regeneration across the defect (Georgiou *et al.*, 2013).

A number of studies have also focussed on supplementing human and rat decellularised nerve grafts with Schwann cells (Pedrini *et al.*, 2018). Studies of *in vivo* rat sciatic nerve defects of 10-12 mm have demonstrated minimal improvement in axon regeneration with the inclusion of Schwann cells, however several studies of longer nerve gap defects have shown enhanced axon regeneration with the inclusion of Schwann cells (Guenard *et al.*, 1992; Frerichs *et al.*, 2002; Jesuraj *et al.*, 2011; Szynkaruk *et al.*, 2012). It has been hypothesised that this is due to the fact that host Schwann cells are able to traverse shorter distances, and that supplementation with Schwann cells may be most beneficial for the repair of longer defects in which endogenous Schwann cell infiltration is insufficient to support axon regeneration (Szynkaruk *et al.*, 2012; Pedrini *et al.*, 2018).

Minimally manipulated autologous Schwann cells are currently the only clinically viable source of Schwann cells for supplementation of NGCs or decellularised nerve grafts, however they are associated with numerous limitations (Lackington *et al.*, 2017). Schwann cell isolation requires an invasive nerve biopsy, consequently sacrificing a healthy, donor nerve, and several weeks of expensive, labour intensive culture expansion is required to obtain a sufficient number of viable cells (typically 1-2 x 10^6 cells) (Jiang *et al.*, 2010; Muheremu and Ao, 2015). In addition, culture expanded Schwann cells may display an abnormal phenotype following extensive manipulation as Schwann cell culture requires a highly specific medium, often with the addition of exogenous mitogens to induce proliferation (e.g. heregulin, or

forskolin) (Casella *et al.*, 1996; Rodríguez *et al.*, 2000; Komiyama *et al.*, 2003; Dahlin *et al.*, 2007). Due to these limitations, research has shifted towards stem cells and alternative cell sources to provide more accessible sources of Schwann cells for clinical application (Dahlin *et al.*, 2007; Gu *et al.*, 2011).

1.4.10.2 Stem cells

Embryonic stem cells (ESC), neural stem cells (NSC), and induced pluripotent stem cells (iPSC) have been considered for use in peripheral nerve repair (Zack-Williams *et al.*, 2015; Jiang *et al.*, 2017; Fathi and Zaminy, 2017). Mouse ESC-derived neural progenitor cells have been shown to promote nerve repair in immunocompromised rats in a 10 mm sciatic nerve defect model, and histological, molecular and electrophysiological studies demonstrated functional axon regeneration (Cui *et al.*, 2008). Furthermore, Schwann cell-like cells have been generated from human ESCs, and have been shown to promote axon regeneration *in vitro* and express myelin protein (Ziegler *et al.*, 2011). Rat NSCs seeded in NGCs manufactured from chitosan have demonstrated comparable results to autografts when used to repair a 10 mm rat sciatic nerve defect (Murakami *et al.*, 2003). In addition, NSCs can be induced to overexpress trophic factors involved in axon regeneration, including glial-cell derived neurotrophic factor (GDNF) or NT-3 (Lackington *et al.*, 2017; Busuttil *et al.*, 2017). Functional neural crest cells have been generated from rat iPSCs, and have been shown to support axon regeneration in a 10 mm rat sciatic nerve defect model when incorporated into PLA-PCL conduits using FGF-enriched gelatin microspheres (Ikeda *et al.*, 2014). However, human ESCs and NSCs are not clinically viable cell sources, and due to ethical considerations and the risk of teratoma formation or undesired cell differentiation, alternative adult stem cell types, mainly multipotential stem cells (MSCs), have received more interest (Jiang *et al.*, 2017; Busuttil *et al.*, 2017; Lackington *et al.*, 2017).

Bone marrow-derived MSCs (BMSCs), harvested by aspiration of bone marrow from the long bones or iliac crest, have been extensively researched due to their accessibility, rapid culture expansion and inherent plasticity (Jiang *et al.*, 2010; Zack-Williams *et al.*, 2015; Jiang *et al.*, 2017). Human and rat BMSCs have demonstrated promising results both *in vitro* and *in vivo*, and have been shown to differentiate into a Schwann cell-like phenotype and express glial markers such as glial fibrillary acid (GFAP) and S100 (Safford *et al.*, 2004; Franco Lambert *et al.*, 2009). Chen *et al.* (2007) used rat BMSCs incorporated in silicone NGCs and reported increased numbers of regenerating axons and reduced muscle atrophy

when used to repair a rat sciatic nerve defect (Chen *et al.*, 2007). A study by Fan *et al.* (2014) demonstrated improved functional recovery with the incorporation of rat BMSCs, differentiated into Schwann cells, into a decellularised nerve allograft used to repair a rat sciatic defect model, with similar outcomes reported to autografts (Fan *et al.*, 2014). However, BMSCs also present several limitations, including the painful surgical procedure required to harvest bone marrow aspirates, and the relatively low cellular yield (Faroni *et al.*, 2014; Fathi and Zaminy, 2017; Jiang *et al.*, 2017).

Adipose-derived MSCs (ASCs) have been considered as a viable alternative to BMSCs as a source of multipotent stem cells (Zack-Williams *et al.*, 2015). ASCs are easier to harvest, requiring a less invasive liposuction procedure and subsequent isolation of ASCs from the stromal vascular fraction, and have a 500-600 fold greater yield and faster culture expansion than BMSCs (Zack-Williams *et al.*, 2015; Jiang *et al.*, 2017). Several studies have demonstrated that human and rat ASCs can be induced to express glial cell markers, including S100, GFAP and P75 neurotrophin receptor *in vitro* (Kingham *et al.*, 2007). Oliveira *et al*. (2010) used rat ASCs incorporated in PCL conduits and demonstrated improved functional regeneration and myelination in a rat sciatic nerve defect model in comparison to PCL conduits in isolation (Oliveira *et al.*, 2010). Similar to these findings, another study by Orbay *et al.* (2012) demonstrated functional improvement comparable to autografts when using a collagen conduit with rat ASCs incorporated into a collagen gel luminal filler (Orbay *et al.*, 2012). Rat ASCs have also been used to supplement decellularised nerve grafts, and ASCs were shown to improve functional recovery and support an increased number of myelinated fibres when used to repair a rat sciatic nerve defect model (Sowa *et al.*, 2016).

Recent research has also focused on the use of skin derived precursor cells, (SKPs), and human and rat SKPs have been shown to differentiate into Schwann cell-like cells expressing S100, myelin basic protein (MBP), and GFAP (Biernaskie *et al.*, 2006; McKenzie *et al.*, 2006). Schwann cell-like cells differentiated from rat SKPs have been incorporated into rat decellularised nerve grafts, and were shown to improve functional recovery with electrophysiological outcomes similar to those observed for autografts (Walsh *et al.*, 2009). Recently, adult human skin fibroblasts have been transdifferentiated into mature Schwann cells (Kitada *et al.*, 2019). Genome-wide expression analysis suggested the conversion of fibroblasts to a Schwann cell lineage, and the Schwann cells were shown to improve axon

regeneration in a sciatic nerve defect model using immunosuppressed rats (Kitada *et al.*, 2019).

CTX0E03 is a clinical grade, clonal human neural stem cell line derived originally from the foetal cortex. CTX0E03 cells are multipotent, and are able to differentiate into neurons, astrocytes, and oligodendrocytes both *in vitro* and *in vivo* (Hicks *et al.*, 2013). CTX0E03 cells have been shown to be a suitable option for allogeneic implantation in humans without immunosuppression, and have been recently used in a Phase II clinical trial for patients with stroke disability (PISCES trial, NCT02117635), and a Phase I clinical trial for patients with lower limb ischaemia (NCT01916369). Recently, O'Rourke *et al*. (2018) used differentiated CTX0E03 cells combined with collagen to form EngNT (EngNT-CTX). The EngNT-CTX constructs were then delivered within a NeuraGen® conduit to repair a 12 mm sciatic nerve defect model in athymic nude rats. The study reported no adverse events, and that the EngNT-CTX constructs supported neurite outgrowth and vascular growth through the injury site and facilitated the reinnervation of the target muscle (O'Rourke *et al.*, 2018). However, although these results suggest that EngNT-CTX constructs could have clinical potential, differentiated CTX0E03 cells represent a source of extensively manipulated stem cells and are associated with a number of limitations (O'Rourke *et al*., 2018).

Despite promising experimental results and the advantages to using stem cells as support cells, particularly the relative ease of harvest and rapid culture expansion in comparison to autologous Schwann cells, there remain several obstacles preventing their clinical use (Szynkaruk *et al.*, 2012; Jiang *et al.*, 2017; Lackington *et al.*, 2017). The molecular mechanisms by which stem cells, including BMSCs and ASCs, enhance regeneration are not well understood, and further research is required prior to clinical translation (Zack-Williams *et al.*, 2015; Jiang *et al.*, 2017). For example, it has been suggested that implanted MSCs may enhance regeneration by synthesising ECM components or producing neurotrophic molecules, delaying cell death and stimulating regeneration (Chen *et al.*, 2007; Wang *et al.*, 2009). Furthermore, recent research has also suggested that the immunomodulatory properties of MSCs may also influence regeneration via indirect modulation of Schwann cell behaviour and / or establishing a favourable microenvironment for regeneration (Wang *et al.*, 2009; Jiang *et al.*, 2017). Further concerns regarding the use of stem cells include de-differentiation of Schwann cell-like cells and the long term behaviour of the implanted cells, as this has not been established in detail, and the potential for teratoma formation or other malignancies

associated with extensively manipulated stem cells (Szynkaruk *et al.*, 2012; Lackington *et al.*, 2017).

1.4.11 Pharmacotherapy

Currently, there are no clinically available pharmacological treatments for peripheral nerve injury (Faroni *et al.*, 2015; Lackington *et al.*, 2017). However, several peptides, hormones, growth factors and other small molecules have been suggested as therapeutic agents (Faroni *et al.*, 2015). Several hormones, including progesterone or allopreganolone, have been suggested as therapeutic targets as neuroactive steroids, modulating Schwann cell myelination (Melcangi *et al.*, 2005; Faroni and Magnaghi, 2011). Several neurotransmitters have also been considered, including γ-aminobutiric acid (GABA), adenosine triphosphate (ATP), glutamate and acetylcholine, involved in neuron-glial interactions and neuron metabolism (Magnaghi *et al.*, 2009). However, research has mainly focused on neurotrophic factors and other growth factors as potential therapeutic targets (Faroni *et al.*, 2015; Mobini *et al.*, 2017).

Schwann cells provide trophic support to regenerating axons, releasing various neurotrophic molecules, cytokines and growth factors including NGF, brain-derived BDNF, and IGF (Jessen and Mirsky, 2016). Although the mechanisms by which MSCs promote axon regeneration are not well understood, it is thought that it is due to the provision of trophic support similar to Schwann cells (Jiang *et al.*, 2017; Fathi and Zaminy, 2017). Several studies of rat sciatic nerve defect models have observed enhanced axon regeneration rates upon transplantation of undifferentiated ASCs seeded in poly-3-hydroxybutyrate and PCL NGCs, and did not observe any cell differentiation *in situ*, therefore concluding axon regeneration was likely enhanced by neurotrophin expression (Santiago *et al.*, 2009; Erba *et al.*, 2010).

NGF has been shown to support axon regeneration when administered both systemically and locally following peripheral nerve injury in rat sciatic nerve defect models (Wang *et al.*, 2014; Emin Önger *et al.*, 2016). Similarly, BDNF and ciliary derived neurotrophic factor (CTNF) have also been shown to improve axon regeneration and re-myelination (Sahenk *et al.*, 1994; Lewin *et al.*, 1997; Fine *et al.*, 2002). Neurotrophic molecules and other growth factors have been researched extensively as part of NGC development, and supplementation of collagen type I conduits with NGF has been shown to enhance axon regeneration across a 20 mm defect in a rat sciatic nerve injury model (Bellamkonda, 2006; Dodla and

Bellamkonda, 2008). Several studies have also demonstrated enhanced axon regeneration in decellularised nerve grafts used to repair 10-20 mm rat sciatic nerve defect models when supplemented with NGF, hepatocyte growth factor (HGF) and VEGF (Rovak *et al.*, 2004; Li *et al.*, 2008; Hu *et al.*, 2009).

Clinical application of growth factors is associated with significant limitations, including the timing and dosage of the growth factor, the method of administration, release and interactions with other growth factors and potent side effects (Szynkaruk *et al.*, 2012; Faroni *et al.*, 2015; Lackington *et al.*, 2017). For example, mistimed or excessive concentrations of BDNF have been shown to inhibit axonal growth or induce neuronal death (Boyd and Gordon, 2002). In addition, several neurotrophins, including NGF and CTNF have half-lives of approximately 10 minutes (Poduslo and Curran, 1996). As continuous infusion of growth factors is not a clinically viable delivery method, alternative methods for local delivery must be explored (Magnaghi *et al.*, 2009; Szynkaruk *et al.*, 2012). Therefore, current research has focused on exogenous modulation of endogenous growth factors, controlled growth factor release systems, or genetic modification of Schwann cells, BMSCs and ASCs to induce expression of desired growth factors (Busuttil *et al.*, 2017; Sun *et al.*, 2019; Manoukian *et al.*, 2019).

1.5 Rationale for the study

Current interventions for peripheral nerve repair are limited and variable in efficacy, and are associated with a number of limitations (Siemionow and Brzezicki, 2009; Grinsell and Keating, 2014). Direct surgical repair is limited to defects of up to three mm, where a tension free coaptation can be achieved, and autografts, the gold standard intervention, require the sacrifice of a functional, minor nerve and often provide insufficient material for major reconstruction (Lee and Wolfe, 2000; Schmidt and Leach, 2003). Cadaveric fresh-frozen allografts can provide a native ECM to support axon regeneration in a similar manner to autografts, but the potential immunogenicity and risks associated with recipient immunosuppression present a significant limitation (Lee and Wolfe, 2000; Gao *et al.*, 2013).

Despite the development of a diverse array of NGCs relatively few are clinically available, confined to a limited number of biodegradable materials (Gu *et al.*, 2014; De Luca *et al.*, 2014). Furthermore, clinical studies of currently available NGCs have only demonstrated efficacy equivalent to autografts for the repair of defects up to 20 mm (Kehoe *et al.*, 2012; Naryan *et al.*, 2018). Clinical studies of the Avance® nerve graft, currently the only commercially available decellularised nerve allograft, have reported equivalent efficacy to autografts for the repair of defects up to 30 mm, and have demonstrated superior clinical efficacy to NGCs when used to treat a range of nerve defect sizes (Karabekmez *et al.*, 2009; Johnson *et al.*, 2011).

The limited efficacy of NGCs is thought to be due to the lack of a native ECM architecture and composition, at both a macrostructural and microstructural level (Whitlock *et al.*, 2009; Faroni *et al.*, 2015). The basement membrane, comprised of collagen type IV, laminin and fibronectin is essential for promoting cell-matrix interactions and supporting Schwann cell adhesion and axon elongation and maturation (Yurchenco *et al.*, 2002; Yurchenco, 2011). Furthermore, the topography of endoneurial tubes is critical for guiding regenerating axons and avoiding axon deviation to restore function (Gao *et al.*, 2013). However, clinical studies of the Avance® graft have not yet demonstrated consistently superior clinical outcomes to autografts, even in small defects (Karabekmez *et al.*, 2009; Faroni *et al.*, 2015). A potential explanation for this could be that the decellularised nerve graft has diminished regenerative capacity as a consequence of ECM disruption caused by the decellularisation process. Therefore, it has been hypothesised that a decellularised nerve allograft, with intact endoneurial tubes and a basement membrane, will promote axon regeneration and support Schwann cell infiltration (Whitlock *et al.*, 2009).

Currently, autografts remain the gold standard intervention for the repair of longer nerve gap defects (over 30 mm) (Siemionow and Brzezicki, 2009; Lackington *et al.*, 2017). Clinically available NGCs are limited to the repair of shorter distances, typically 20 – 30 mm, and clinical studies using the Avance® graft have shown limited efficacy over longer distances (up to 60 mm) (Moore *et al.*, 2011; Gerth *et al.*, 2015). As discussed previously, Schwann cells have a pivotal role in axon regeneration and peripheral nerve repair, and it is hypothesised that the efficacy of decellularised nerve grafts and NGCs is limited to shorter distances due to insufficient host Schwann cell migration (Szynkaruk *et al.*, 2012; Gerth *et al.*, 2015; Busuttil *et al.*, 2017). It is therefore essential for decellularised nerve grafts and NGCs to support viable Schwann cell populations and promote cellular adhesion, migration and proliferation (Lackington *et al.*, 2017; Mobini *et al.*, 2017).

Recently, a collaborative partnership between the University of Leeds and the University of Sheffield resulted in the development of a decellularisation process for porcine peripheral nerve (Zilic *et al.*, 2016). This process was adapted from the proprietary University of Leeds decellularisation process, which has been adapted for the decellularisation of various tissues, including porcine (Luo *et al.*, 2014) and human (Vafaee *et al.*, 2018) heart valves, porcine dermis (Helliwell *et al.*, 2017), porcine tendon (Jones *et al.*, 2017) and cartilage (Kheir *et al.*, 2011). The decellularisation process utilises low concentration SDS (0.1 %; w/v) plus protease inhibitors, in combination with hypotonic and hypertonic buffers and nuclease treatment. The process was shown to sufficiently remove cellular and nuclear material from porcine peripheral nerves and preserve several key basement membrane components including laminin and collagen type IV (Zilic *et al.*, 2016). However, the decellularisation process resulted in structural changes to ECM histioarchitecture, and changes in the distribution of laminin and fibronectin (Zilic *et al.*, 2016). Therefore, the decellularisation process could be developed further to maintain the efficacy of decellularisation, but minimise structural changes to nerve histioarchitecture.

1.6 Hypothesis

It is hypothesised that a biocompatible decellularised peripheral nerve graft, with a native ECM histioarchitecture and basement membrane, can be developed for use in peripheral nerve repair.

1.7 Aims and objectives

1.7.1.1 Aim

The aim of this project is to develop a decellularised peripheral nerve allograft with a native ECM histioarchitecture and biochemical composition, able to support viable cell populations, for use in peripheral nerve repair.

1.7.1.2 Objectives

I. To further develop the decellularisation process previously developed for porcine peripheral nerves, maintaining the efficacy of decellularisation in terms of sufficient cell removal and DNA content reduction, whilst ensuring the preservation of overall histioarchitecture and major ECM structures.
II. To characterise the biological and biochemical properties of native and decellularised porcine peripheral nerve by histological, immunohistochemical and biochemical analyses
III. To develop a process for the decellularisation of human femoral nerves by translating the decellularisation process developed for porcine peripheral nerve
IV. To characterise the biological and biochemical properties of native and decellularised human femoral nerve by histological, immunohistochemical and biochemical analyses
V. To assess the *in vitro* recellularisation capacity of decellularised human femoral nerve and investigate the importance of endoneurial structure by culture with primary dorsal root ganglion (DRG) explants

Chapter 2: Materials and Methods

2.1 Materials

2.1.1 Equipment

The equipment used and equipment suppliers are listed in Appendix A, Table I.

2.1.2 Consumables

The consumables and plastic ware used and suppliers are listed in Appendix A, Table II.

2.1.3 Chemicals and reagents

The chemicals and reagents used and suppliers are listed in Appendix A, Table III.

2.1.4 Glassware

Glassware (beakers and bottles [100 mL, 1,000 mL and 2,000 mL]) were cleaned by immersion in a 1 % (v/v) detergent solution (Neutracon®, Decon Laboratories Ltd) overnight. Glassware were then rinsed in tap water followed by distilled water to remove residual detergent. Items were then dried and sterilised as described in Section 2.2.1.3.

2.1.5 Cell lines

The cell lines used in this study and suppliers are listed in Table 2.1

Table 2.1 Cell lines used throughout the study

Cells	Type	Species	Supplier
Baby Hamster Kidney (BHK	Epithelial	Hamster	Health Protection Agency
L929	Fibroblast	Mouse	Health Protection Agency

2.1.6 Antibodies

The primary, secondary and isotype control antibodies used and suppliers are listed in Table 2.2.

Table 2.2 Primary, secondary and isotype control antibodies used throughout the study

Antibody type	Antigen	Isotype	Supplier	Code
Primary	Laminin	Monoclonal mouse IgG1	Sigma Aldrich	L8271
Primary	Fibronectin	Polyclonal rabbit IgG	Dako	A0245
Primary	Collagen type IV	Monoclonal mouse IgG1	Dako	M0785
Primary	Chondroitin sulphate	Monoclonal mouse IgM	Sigma Aldrich	C8035
Primary	Sox2	Monoclonal mouse IgG1	Abcam	Ab79351
Primary	Glutamine synthetase (GS)	Polyclonal rabbit IgG	Abcam	Ab49873
Primary	Myelin basic protein (MBP)	Polyclonal rabbit IgG	Abcam	Ab40390
Primary	Neural cell adhesion molecule-1 (NCAM-1)	Monoclonal mouse IgG1	Abcam	Ab9272
Primary	Neurofilament-200 (NF-200)	Polyclonal rabbit IgG	Sigma Aldrich	N4142
Isotype control	Mouse monoclonal IgG1	-	Dako	X0931
Isotype control	Rabbit polyclonal IgG	-	Genetex	GTX35035
Isotype control	Mouse monoclonal IgM	-	Dako	X0942
Secondary	Goat anti-mouse IgG AlexaFluor 488	-	Invitrogen	A11001
Secondary	Goat anti-rabbit IgG AlexaFluor 488	-	Invitrogen	A11070
Secondary	Goat anti-mouse IgG AlexaFluor 647	-	Abcam	Ab150115
Secondary	Goat anti-mouse IgM AlexaFluor 647	-	Abcam	Ab150123

2.1.7 General chemical stock solutions

2.1.7.1 Phosphate buffered saline (PBS)

Ten PBS tablets were dissolved in 1 L distilled water, and the pH adjusted to 7.2 – 7.4 as described in Section 2.2.1.1. The solution was autoclaved as described in Section 2.2.1.2 and stored at room temperature for up to one month.

2.1.7.2 Sodium hydroxide solution (NaOH), 6M

NaOH pellets (120 g) were dissolved into 500 mL distilled water. The solution was stored at room temperature for up to six months.

2.1.7.3 Ethanol (70 %; v/v)

Distilled water (300 mL) was added to 100 % (v/v) ethanol (700 mL) to make up 1 L of 70 % (v/v) ethanol.

2.1.7.4 Virkon solution (1 %; w/v)

Virkon powder (50 g) was added to 5 L distilled water to make Virkon solution (1 %; w/v).

2.1.8 Decellularisation solutions

2.1.8.1 Antibiotic solution (0.05 $mg.mL^{-1}$ vancomycin, 0.5 $mg.mL^{-1}$ gentamicin, 0.2 $mg.mL^{-1}$ polymyxin B)

Vancomycin hydrochloride (50 mg), gentamicin sulphate (500 mg) and polymyxin B (200 mg) were added to PBS (100 mL). The pH was adjusted to 7.2 – 7.4 as described in Section 2.2.1.1, and made up to 1L with PBS. The solution was used within one hour of production.

2.1.8.2 EDTA solution (200 mM)

EDTA (74.4 g) was added to 1 L distilled water. The pH was adjusted to 7.2 – 7.4 as described in Section 2.2.1.1, and the solution was autoclaved as described in Section 2.2.1.3. The solution was stored for up to one month at room temperature.

2.1.8.3 Hypotonic buffer (10 mM Tris, 2.7 mM EDTA, 10 KIU. mL^{-1} aprotinin)

Trizma base (1.21 g) and EDTA (1 g) were added to 900 mL distilled water. The pH was adjusted to 8.0 – 8.2 as described in Section 2.2.1.1, and the solution was autoclaved as described in Section 2.2.1.3. The solution was stored for up to one month at room temperature. Immediately before use, 1 mL of aprotinin (10,000 KIU. mL^{-1}) was added aseptically using a needle and syringe.

2.1.8.4 SDS hypotonic buffer (0.1 % (w/v) SDS, 10 mM Tris, 2.7 mM EDTA, 10 KIU. mL^{-1} aprotinin)

Sodium dodecyl sulphate (SDS) solution (10 mL; 10 %(w/v)) was added to 990 mL of autoclaved hypotonic buffer aseptically. Immediately before use, 1 mL of aprotinin (10 KIU.mL^{-1}) was added aseptically using a needle and syringe.

2.1.8.5 PBS EDTA solution (2.7 mM EDTA, 10 KIU. mL^{-1} aprotinin)

Ten PBS tablets and EDTA (1 g) were dissolved in 1 L distilled water. The pH was adjusted to 7.2 – 7.4 as described in Section 2.2.1.1, and the solution was autoclaved as described in Section 2.2.1.3. The solution was stored for up to one month at room temperature. Immediately before use, 1 mL aprotinin (10 KIU.mL^{-1}) was added aseptically using a needle and syringe.

2.1.8.6 Nuclease solution (50 mM Tris, 1 mM $MgCl_2.6H_2O$, 1 U.mL^{-1} Benzonase)

Trizma base (6.1 g) and magnesium chloride (0.203 g) were added to 100 mL distilled water. The pH was adjusted to 7.5 – 7.7 as described in Section 2.2.1.1, and the solution was autoclaved as described in Section 2.2.1.3. The solution was stored for up to one month at room temperature. Immediately before use, 4 µL of Benzonase (250 U.μL^{-1}) was added aseptically.

2.1.8.7 Hypertonic solution (50 mM Tris, 1.5 M NaCl)

Sodium chloride (87.66 g) and Trizma base (6.06 g) were added to 900 mL distilled water. The pH was adjusted to 7.5 – 7.7 as described in in Section 2.2.1.1, and the solution was autoclaved as described in Section 2.2.1.3. The solution was stored for up to one month at room temperature.

2.2 Methods

2.2.1 General methods

2.2.1.1 Measurement of pH

The pH of solutions was measured using a Jenway 3020 pH meter. Prior to use, the pH meter was calibrated using solutions of pH 4, pH 7 and pH 10, with a temperature probe. Drop-wise addition of either 6 M hydrochloric acid or 6 M sodium hydroxide was used to adjust the pH of solutions.

2.2.1.2 Microscopy

Bright field (Köhler), circularly polarised light and fluorescent microscopy were performed using an Axio Imager M2 microscope (Zeiss). An AxioCam MCr5 digital camera (Zeiss) and Zen Pro software (Zeiss blue edition version 2.3) were used to capture digital images. A fluorescent illuminator, in conjunction with appropriate filters, was used for fluorescent microscopy. Phase contrast microscopy was performed using a BX51 inverted microscope (Olympus), and an XC-50 Camera (Olympus) and Cell B software (Olympus version 3.2) were used to capture digital images.

2.2.1.3 Sterilisation

Solutions and equipment were sterilised using dry heat, moist heat or filtration:

- Dry heat sterilisation: items for dry heat sterilisation were placed in a hot oven for four hours at 180 °C.
- Moist heat sterilisation: items not suitable for dry heat sterilisation were autoclaved for 20 minutes at 121 °C, at a pressure of 103 kPa.
- Filter sterilisation: solutions not suitable for heat sterilisation were filtered using 0.2 µm pore sized filters with a disposable 10 mL syringe in a Class II safety cabinet.

2.2.2 Acquisition of porcine peripheral nerves

2.2.2.1 Porcine hind leg procurement

Porcine hind legs (from Large White Yorkshire pigs, between 24 and 26 weeks of age) were obtained from a local abattoir (J. Penny, Leeds, United Kingdom). Hind legs were received up to three days following slaughter.

2.2.2.2 Porcine peripheral nerve dissection

Peripheral nerves were dissected from the posterior and lateral sections of the posterior compartment of the hind leg respectively, to isolate the sciatic, peroneal and tibial nerves (Figure 2.1). Excess fat was removed by blunt dissection, and each nerve was washed for ten minutes three times using sterile PBS to remove excess blood and tissue fluid, at 4 °C and agitated at 50 rpm. Tissues were then stored at -70 °C on PBS moistened filter paper for future use.

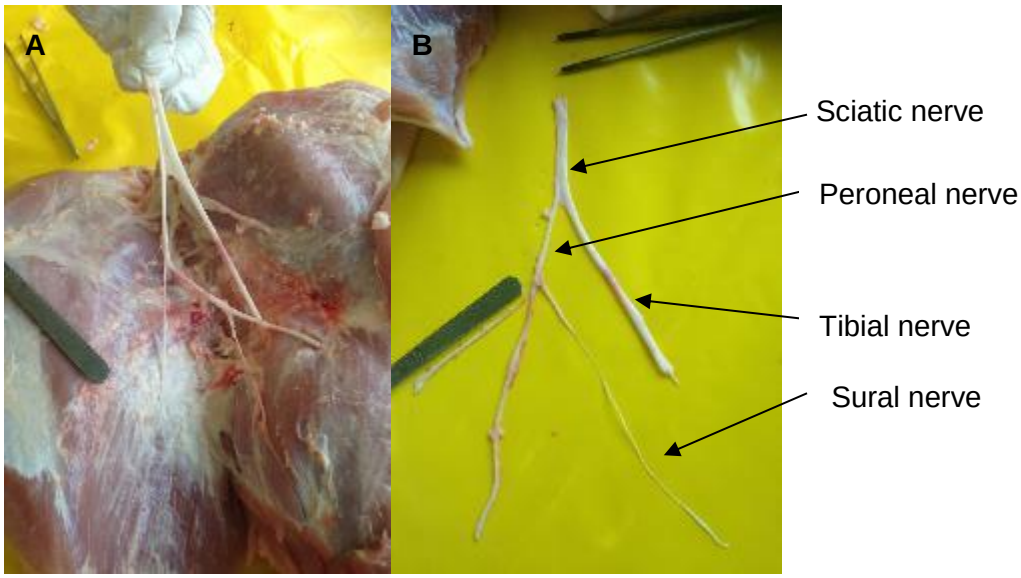

Figure 2.1 Dissection of porcine peripheral nerves from hind legs. (A) Porcine peripheral nerves were dissected from the posterior and lateral sections of the posterior compartment of each porcine hind leg. (B) The whole peripheral nerve plexus was dissected to isolate the sciatic, peroneal, tibial and sural nerves.

2.2.3 Acquisition of human femoral nerves

2.2.3.1 Human tissue procurement

Following ethical approval (North East Health Research Authority and Tyne and Wear South NHS Research Ethics Committee ref 15/NE/0082, IRAS project ID 199203), human femoral bundles were procured from NHS Blood and Transplant Tissue and Eye Services (NHSBT TES). Full written consent for the use of femoral bundles for research and development purposes was obtained from donors or donor families by the NHSBT National Referral Centre. Femoral bundles were obtained from cadaveric donors by NHSBT TES Tissue Retrieval personnel, and anonymised and assigned a tissue reference number. Femoral bundles were stored at -80 ºC prior to release to the University of Leeds. Human femoral bundles were

transported from NHSBT TES to the University of Leeds in 48 hour dry ice storage boxes. Upon receipt, femoral bundles were stored at -80 ºC until use.

2.2.3.2 Human tissue handling

Human tissue storage, dissection, processing and disposal was carried out in accordance with the Human Tissue Act (2004). All tissue samples were assigned unique identification codes and tracked using an electronic tracking system (Achiever Medical, Version 1712.4, Interactive Software Ltd, Birmingham, UK). Storage locations for all samples were recorded using this system.

2.2.3.3 Human femoral nerve dissection

Prior to dissection, human femoral bundles were thawed for approximately three hours in a 37 °C incubator or until fully thawed. Femoral nerves were dissected from each femoral bundle aseptically using a Class II safety cabinet. Femoral nerves were located in close proximity to the femoral artery, and excess tissue and fascia were cut away to isolate the femoral nerve (Figure 2.2). Excess fat was removed by blunt dissection, and each nerve was washed for ten minutes three times using sterile PBS to remove excess blood and tissue fluid, at 4 °C and agitated at 50 rpm. Each nerve was then processed for decellularisation, histological analysis (Section 2.2.4), DNA quantification (Section 2.2.8) or biochemical analysis (Section 2.2.9) immediately.

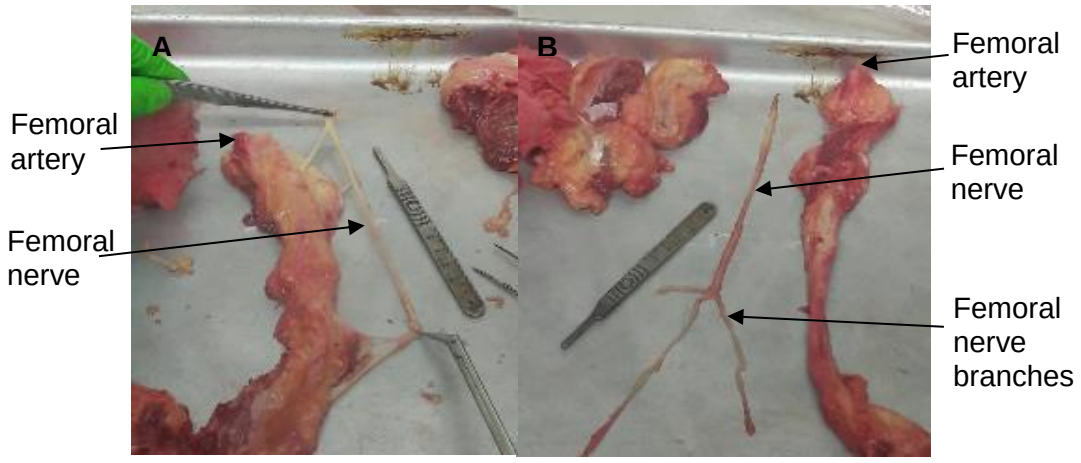

Figure 2.2 Dissection of human femoral nerves from femoral bundles. (A) Femoral nerves were dissected from each femoral bundle. Femoral nerves were located in close proximity to the femoral artery. (B) The femoral nerve and associated branches were isolated from each femoral bundle, and branches were cut away and discarded.

2.2.4 Basic histological techniques

2.2.4.1 Fixation, processing and paraffin wax embedding

Tissue samples (10 mm) of native or decellularised peripheral nerve were placed into pencil labelled plastic histology cassettes. All tissue samples were fixed and processed using a Leica TP1020 automatic tissue processor using a predetermined protocol (Table 2.3). Tissue samples were then oriented in metal wax block moulds using heated forceps, covered in molten paraffin wax and left to set overnight at room temperature.

Table 2.3 Automatic tissue processing protocol

Station	Solution	Duration (hours)
1	10 % (w/v) neutral buffered formalin	1
2	70 % (v/v) ethanol	1
3	90 % (v/v) ethanol	1
4	100 % (v/v) ethanol	0.5
5	100 % (v/v) ethanol	1
6	100 % (v/v) ethanol	1
7	100 % (v/v) ethanol	1
8	Xylene	1
9	Xylene	1
10	Xylene	1
11	Molten wax	1
12	Molten wax	1

2.2.4.2 Sectioning and slide preparation

Paraffin wax embedded samples were cooled using ice and sectioned at a thickness of 5 μm using a microtome (Leica RM2255). Sections were floated onto Superfrost plus slides (Thermo Scientific) using a water bath at 30 °C. All sections were allowed to air dry at room temperature overnight.

2.2.4.3 Dewaxing and rehydration

Sections were dewaxed using two successive changes of xylene (100 %; v/v) for ten minutes each. Sections were then rehydrated in three successive changes of ethanol (100 %; v/v) for three minutes, two minutes and two minutes respectively, followed by immersion in ethanol (70 %; v/v) for two minutes. Sections were then immersed in running tap water for three minutes to rehydrate.

2.2.4.4 Dehydration and mounting

Stained sections were dehydrated by immersion in ethanol (70 %; v/v) for five seconds, followed by successive immersion in ethanol (100 %; v/v) for one minute, two minutes and three minutes respectively. Sections were then immersed twice in xylene, for ten minutes each, before covering with DPX mountant and a glass coverslip. Slides were left to air dry in a fume cupboard for a minimum of four hours before viewing.

2.2.5 Histological staining

2.2.5.1 Haematoxylin and Eosin (H&E) staining

H&E staining was used to visualise cell nuclei and tissue histioarchitecture. Following dewaxing and rehydration (Section 2.2.4.3.), tissue sections were immersed in haematoxylin (Mayer's) for one minute, rinsed in running tap water for three minutes and immersed in Scott's tap water substitute for three minutes. Sections were then rinsed again in running tap water for three minutes and immersed in eosin for three minutes, followed by dehydration and mounting (Section 2.2.4.4.). Stained slides were viewed using normal Köhler illumination (Section 2.2.1.2).

2.2.5.2 DAPI staining

Reagents:

- DAPI stock solution (1 mg.mL^{-1}) — 10 mg DAPI; 10 mL nuclease free water
- DAPI working solution (0.1 µg.mL^{-1}) — 10 µL DAPI stock solution; 100 mL PBS

Method:

Fluorescent visualisation of whole cell nuclei and nuclear remnants was performed using 4',6-diamidino-2-phenylindole (DAPI), a fluorescent nucleic acid stain. Following dewaxing and rehydration (Section 2.2.4.3.), each section was immersed in DAPI working solution for ten minutes in the dark. Sections were then immersed in three changes of PBS in the dark, for ten minutes each, and mounted using fluorescent mounting medium. Slides were viewed under fluorescence illumination with a DAPI filter (460 nm) and images captured digitally (Section 2.2.1.2).

2.2.5.3 Sirius Red / Miller's staining

Reagents:

- Potassium permanganate (5 %; w/v)
  - 15 g potassium permanganate
  - 100 mL distilled water
- Oxalic acid (1 %; w/v)
  - 1 g oxalic acid
  - 100 mL distilled water
- Weigert's haematoxylin
  - 1 part solution A
  - 1 part solution B
- Sirius red (0.1 %; w/v)
  - 0.1 g Sirius red
  - 100 mL saturated picric acid solution
  - 50 mL distilled water

Method:

Sirius red was used to stain collagen, Miller's stain was used to stain elastin fibres, and Weigert's haematoxylin was used to stain cell nuclei. Using circularly polarised light to view sections stained with Sirius red, collagen fibre diameter can be deduced based on the birefringence of the fibres, with thicker fibrils appearing as yellow/red, and smaller fibrils appearing as green. Following dewaxing and rehydration (Section 2.2.3.3.), sections were immersed in potassium permanganate (5 %; w/v) for five minutes, and rinsed using distilled water. Sections were then

immersed in oxalic acid solution (1 %; w/v) for two minutes, followed by distilled water for one minute then four minutes. Sections were dehydrated in ethanol (70 %; v/v) for one minute and ethanol (95 %; v/v) for one minute before immersion in Miller's stain for one hour. Sections were rinsed in ethanol (70 % v/v), immersed in ethanol (95 %; v/v) for one minute and rinsed in running tap water for two minutes. Sections were then immersed in Weigert's haematoxylin for ten minutes, rinsed using running tap water for one minute, and immersed in distilled water for 30 seconds. Sections were then immersed in Sirius red (0.1 %; w/v) for one hour followed by rinsing with distilled water prior to dehydration and mounting (Section 2.2.3.4.). Slides were viewed and imaged using both Köhler illumination and circularly polarized light, and images captured digitally (Section 2.2.1.2).

2.2.5.4 Sirius Red, Luxol Fast Blue and Haematoxylin staining

Reagents:

- Luxol fast blue (0.1 %; w/v)
  - 0.1 g Luxol fast blue
  - 0.5 mL glacial acetic acid
  - 100 mL 95 % (v/v) ethanol
- Lithium carbonate solution (0.05 %; w/v)
  - 0.05 g Lithium carbonate
  - 100 mL distilled water
- Sirius red (0.1 %; w/v)
  - 0.1 g Sirius red
  - 100 mL saturated picric acid solution
  - 50 mL distilled water
- Weigert's haematoxylin
  - 1 part solution A
  - 1 part solution B

Method:

Sirius red was used to stain collagen, Luxol fast blue was used to stain myelin, and Weigert's haematoxylin was used to stain cell nuclei. Following dewaxing and rehydration (Section 2.2.3.3.), sections were immersed in Luxol fast blue (0.1 %;

w/v) in a coplin jar, and placed in a 56 °C water bath overnight (approximately 14 – 16 hours). The coplin jar was sealed with Parafilm before placing in the water bath. Sections were rinsed with 95 % (v/v) ethanol, and rinsed with distilled water to remove excess stain. Sections were then differentiated using lithium carbonate solution (0.05 %; w/v) for approximately 20 seconds. Sections were rinsed twice with 70 % (v/v) ethanol, and rinsed with distilled water. Sections were then immersed in Sirius red (0.1 %; w/v) for 30 minutes. Sections were rinsed twice in distilled water, and immersed in Weigert's haematoxylin for ten minutes. Sections were then dewaxed and rehydrated (Section 2.2.3.4.). Slides were viewed and imaged using both Köhler illumination and circularly polarized light, and images captured digitally (Section 2.2.1.2).

2.2.5.5 Masson's Trichrome staining

Reagents:

• Ponceau fuschin (Masson) working solution	30 mL Ponceau fuschin (Masson) 10 X concentrate 270 mL distilled water
• Weigert's haematoxylin	1 part solution A 1 part solution B
• Acid alcohol (0.5 %; v/v)	2.5 mL hydrochloric acid 37 % (v/v) 497 mL 70 % (v/v) ethanol
• Acetic acid (1 % v/v)	5 mL glacial acetic acid 495 mL distilled water

Method:

Masson's trichrome staining was used to visualise collagen (light green), nuclei (dark brown) and cytoplasm (red). Following dewaxing and rehydration (Section 2.2.3.3.), sections were immersed in Bouin's fixative for 24 hours. Sections were then rinsed in running tap water for four minutes, followed by distilled water for one minute. Sections were immersed in Weigert's haematoxylin for 25 minutes and

rinsed in running tap water to remove excess stain. Sections were differentiated in acid alcohol (0.5 %; v/v), and rinsed in running tap water for one and three minutes respectively. Sections were then immersed in Ponceau Fuschin (Masson) working solution for five minutes, and rinsed in running tap water to remove excess stain. Sections were immersed in distilled water for one minute followed by phosphotungstic acid (1 %; w/v) twice for eight minutes each. Sections were immersed in light green Masson solution for 15 minutes, and rinsed in running tap water. Sections were immersed in distilled water for one minute, immersed in phosphotungstic acid (1 %; w/v) for five minutes, immersed in acetic acid (1 %; v/v) for five minutes and rinsed in running tap water for three minutes. Sections were dehydrated and mounted (Section 2.2.3.4.). Sections were viewed using normal Köhler illumination, and images captured digitally (Section 2.2.1.2).

2.2.6 Immunofluorescent labelling of tissue sections

2.2.6.1 Antigen retrieval methods

2.2.6.1.1 Proteinase K

Sections were covered with Proteinase K solution and incubated for 20 minutes at room temperature. Sections were rinsed with TBS for five minutes.

2.2.6.1.2 Proteinase K and Trypsin / EDTA

Sections were covered with Proteinase K solution and incubated for 20 minutes. Sections were covered with Trypsin/EDTA solution and incubated for 30 seconds at room temperature, and rinsed with TBS for five minutes.

2.2.6.1.3 Citric acid buffer (pH 6)

2.2.6.1.4 Reagents

2.2.6.1.4.1 Citric acid buffer (10 mM)

- Citric acid buffer (10 mM, pH 6) — 2.1 g citric acid (monohydrous)
  1 L distilled water

2.2.6.1.5 Method

Sections were immersed in citric acid buffer (10 mM, pH 6) for one hour at room temperature. Sections were rinsed with TBS for five minutes.

2.2.6.2 Immunofluorescent labelling of tissue sections with primary antibodies and fluorescently tagged secondary antibodies:

2.2.6.2.1 Reagents

• Sodium chloride solution (3 M)	175.32 g sodium chloride 1 L distilled water
• Tris solution (2 M, pH7.6)	242.26 g Trizma base Made up to 1 L with distilled water
• Tris buffered saline (TBS) (20 mM tris, 150 mM NaCl, pH 7.6)	25 mL tris solution (2 M) 50 mL sodium chloride solution (3 M) Made up to 1 L with distilled water
• TBS-Tween (0.05 % (w/v) Tween-20, pH 7.6)	500 µL Tween-20 1 L TBS
• Goat serum blocking solution (TBS, 10 % (w/v) goat serum, 0.1 % (w/v) Triton X-100)	1 mL goat serum 10 µL Triton X-100 Made up to 10 mL with TBS
• Bovine serum albumin (BSA) solution (5 %; w/v)	2.5 g BSA 50 mL PBS
• Antibody diluent (TBS, 0.1 % (w/v) BSA, 0.1 % (w/v) sodium azide, pH 6)	300 µL BSA solution 6 mL sodium azide solution (1 %; w/v) Made up to 60 mL with TBS

2.2.6.2.2 Method

Specific primary, isotype and secondary antibodies, antibody dilutions, and antigen retrieval methods used for immunofluorescent labelling of tissue sections are specified within individual chapters. Cryosections for immunofluorescent labelling of specific antigens were thawed for 30 minutes, and rinsed in running tap water for three minutes. Wax sections were dewaxed and rehydrated as described in Section 2.2.4.3. If required, antigen retrieval was carried out as described in Section 2.2.6.1. Following antigen retrieval, sections were washed twice with TBS, for five minutes each with gentle agitation. Sections were circled using a hydrophobic marker (ImmEdge barrier pen). Sections were incubated with goat serum blocking solution for one hour at room temperature. Primary antibodies or isotype control antibodies (diluted to appropriate concentration in antibody diluent) or antibody diluent were added to test, isotype control or negative control sections respectively, and incubated in a humidified chamber for 1 hour at room temperature. Sections were washed for five minutes twice with TBS-Tween and washed twice for five minutes with TBS with gentle agitation. Secondary antibodies (diluted to appropriate concentration in antibody diluent) were added to each section, and incubated in a humidified chamber in the dark for 30 minutes at room temperature. Sections were washed for five minutes twice with TBS-Tween and washed for five minutes twice with TBS with gentle agitation. Sections were then immersed in DAPI working solution for ten minutes in the dark. Sections were immersed in three changes of PBS in the dark, for ten minutes each, and mounted using fluorescent mounting medium. Slides were viewed under fluorescence illumination using appropriate filters and images captured digitally (Section 2.2.1.2).

2.2.7 DNA quantification

2.2.7.1 Lyophilisation

Tissue samples were macerated and placed in sterile Eppendorf tubes. Samples were weighed three times to calculate a mean wet weight. Samples were placed in a freeze dryer (Thermo, Savant ModulyoD) at -50 °C, 0.15 – 0.2 mbar, and the weight measured every 24 hours until constant (48 - 72 hours).

2.2.7.2 DNA extraction

Tissue samples were lyophilised to a constant weight as described in Section 2.2.7.1. DNA was extracted from tissue samples using the DNeasy Blood and Tissue kit (Qiagen) according to the manufacturer’s instructions. Following

lyophilisation, 360 µL Buffer ATL and 40 µL Proteinase K were added to each sample. Samples were vortexed for 15 seconds, and incubated at for three hours at 56 °C, with vortexing for 15 seconds every 30 minutes. Samples were vortexed for 15 seconds, and 400 µL Buffer AL and 400 µL ethanol (100 %; v/v) were added to each sample. Each sample (600 µL) was added to a DNeasy spin column and centrifuged at 6000 x g for one minute. The flow-through was discarded. This step was repeated until all of the original solution had been filtered through the spin column. The spin columns were transferred to fresh collection tubes, and 500 µL Buffer AW1 was added. The spin columns were centrifuged at 6000 x g for one minute and the collection tube was discarded. The spin columns were transferred to fresh collection tubes and 500 µL Buffer AW2 was added, before centrifugation at 16,000 x g for five minutes. The spin columns were transferred to fresh sterile Eppendorf tubes, and 200 µL Buffer AE was added to the membrane at the base of the columns. The columns were incubated at room temperature for one minute and then centrifuged at 6000 x g for one minute. The eluted DNA contained was stored at - 20 °C until quantification.

2.2.7.3 Spectrophotometric DNA quantification

Reagents:

- Digestion buffer (5 mM L-cysteine hydrochloride, 5 mM Na_2EDTA, pH 6.0)
  - 0.788 g L-cysteine hydrochloride
  - 1.8612 g Na_2EDTA
  - 1 L PBS
- Calf thymus DNA stock solution (1 $mg.mL^{-1}$)
  - 5 mg calf thymus DNA
  - 5 mL nuclease free water

Method:

Calf thymus DNA stock solution was diluted in digestion buffer to produce calf thymus DNA standards of known concentration (ranging from 0 to 50 $ng.mg^{-1}$). Calf thymus DNA standards were used to create a standard curve to assess the accuracy of the spectrophotometer. The total DNA content of samples and standards (2 µL) was quantified by measuring absorbance (at 260 nm) using a NanoDrop spectrophotometer. Each sample was blanked against Buffer AE, and measured in triplicate. DNA content ($ng.mg^{-1}$) of tissues was calculated by normalising for dilution volume and dry tissue weight.

2.2.7.4 Quantification of double stranded DNA

The double stranded DNA content of DNA samples extracted from tissues was determined using the PicoGreen™ detection kit. TE buffer was produced by diluting TE buffer stock solution (20 X) in nuclease free water. PicoGreen working solution was produced by diluting PicoGreen stock solution (200 X) in TE buffer, and this was kept in the dark until use. Lambda DNA (1 $mg.mL^{-1}$) was diluted in TE buffer to produce lambda DNA standards of known concentration (1, 10, 100, 1000, 1500 and 2000 $ng.mL^{-1}$). Lambda DNA standards (100 µL) were added to individual wells of a 96-well black walled plate, in triplicate. DNA samples were diluted 1:10 by adding 30 µL of each DNA sample to 270 µL TE buffer. Diluted DNA samples (100 µL) were also added to individual wells of the 96-well black walled plate, in triplicate. PicoGreen working solution (100 µL) was added to each well, and the plate was incubated for five minutes at room temperature in the dark. The luminescence of each well (excitation at 480 nm and emission at 520 nm) was then determined using a microplate spectrophotometer, measured in arbitrary fluorescent units. Lambda DNA values were used to create a standard curve to interpolate unknown values of test samples. DNA content ($ng.mg^{-1}$) was calculated by normalising for dilution volume and dry tissue weight.

2.2.8 Biochemical analyses

2.2.8.1 Acid hydrolysis

Tissue samples were lyophilised as described in Section 2.2.7.1. Lyophilised samples were then placed in vented glass test tubes and 5 mL of HCl (6 M) was added to each tube. Samples were then autoclaved in a bench top autoclave for 121 °C for four hours at a pressure of 103 kPa to hydrolyse the tissue samples. Samples were then neutralized by the addition of NaOH (6 M). The volume of the hydrolysed samples was recorded for final calculations.

2.2.8.2 Quantification of hydroxyproline content

The amino acid hydroxyproline is a major constituent of collagen in vertebrates. Hydroxyproline occurs at a known frequency in the amino acid sequence of collagen, and therefore quantification of hydroxyproline within a tissue sample can be used to estimate collagen content. Hydroxyproline content was quantified using a colourimetric assay based on the method described by Edwards and O'Brien (1980). Pyrroles formed by oxidation of hydroxyproline react with p-

dimethylaminobenzaldehyde to produce a red chromophore, which can then be measured spectrophotometrically.

Reagents:

- Hydroxyproline buffer (pH 6.2)
  - 13.3 g citric acid
  - 32 g sodium acetate 3 hydrate
  - 9.1 g sodium hydroxide
  - 3.2 mL glacial acetic acid
  - 80 mL propan-1-ol
  - Made up to 400 mL with distilled water
- Chloramine T solution
  - 1.41 g Chloramine T
  - 100 mL distilled water
- Ehrlich's reagent
  - 7.5 g p-dimethylbenzaldehyde
  - 13 mL perchloric acid (62 %; v/v)
  - 30 mL propan-1-ol
  - Made up to 50 mL with distilled water

Method:

Samples were lyophilized and hydrolysed as described in Sections 2.2.7.1 and 2.2.8.1 respectively. Trans-4-hydroxy-L-proline was diluted in hydroxyproline buffer to produce hydroxyproline standards of known concentration (0, 2, 4, 6, 8, 10, 15, 20, 25 and 30 $\mu g.mL^{-1}$). Test samples were diluted 1:20 in hydroxyproline buffer. Test samples and standards (50 µL) were added to a clear flat-bottomed 96-well plate, in triplicate. Chloramine T solution was added to each well (100 µL), and the plate incubated for five minutes at room temperature with gentle agitation. Ehrlich's reagent (100 µL) was then added to each well, and the plate was incubated at 60 °C for 45 minutes. The optical density of each well was then measured at 570 nm using a microplate spectrophotometer. Hydroxyproline standard values were then used to create a standard curve of absorbance vs concentration to interpolate

unknown test values. Hydroxyproline content of test samples (µg.mg^{-1}) was calculated by normalising for dilution volume and dry tissue weight.

2.2.8.3 Quantification of denatured collagen content

Reagents:

- Digestion buffer (pH 7.8) — 1.21 g Trizma base; 0.15 g calcium chloride; 100 mL distilled water
- α-chymotrypsin digestion solution (5 mg.mL^{-1}) — 100 mg α-chymotrypsin (≥40 units.mg^{-1}); 20 mL digestion buffer

Method:

Samples were lyophilized as described in Section 2.2.7.1. α-Chymotrypsin working solution (5 mL) was added to each sample, and the samples were incubated in a water bath for 24 hours at 30 °C. The digested samples were centrifuged at 600 g for ten minutes, and the supernatant (4 mL) was transferred to vented glass test tubes. Supernatants were then hydrolysed and neutralized as described in Section 2.2.8.1. The hydroxyproline content of each hydrolysed sample was then determined using a hydroxyproline assay, as described in Section 2.2.8.2. The hydrolysed samples were not diluted prior to hydroxyproline assay.

2.2.8.4 Quantification of GAG content

The GAG content (sulphated GAGs) of tissues samples was determined using a colourimetric assay based on the method described by Farndale et al (1982). The cationic dye 1,9-dimethylene blue (DMB) reacts with sulphate groups of GAGs under acidic conditions, which can then be measured spectrophotometrically.

Reagents:

• Papain digest buffer (pH 6.0)	0.788 g L-cysteine hydrochloride 1.8612 g Na_2EDTA 1 L distilled water
• Papain digestion solution	1250 U papain 25 mL digestion buffer
• Sodium di-hydrogen orthophosphate solution (0.1 M)	3.45 g sodium di-hydrogen orthophosphate 250 mL distilled water
• Di-sodium hydrogen orthophosphate solution (0.1 M)	3.55 g di-sodium hydrogen orthophosphate 250 mL distilled water
• Assay buffer (pH 6.0)	137 mL sodium di-hydrate orthophosphate solution 63 mL di-sodium hydrogen orthophosphate solution
• DMB dye (pH 3.0)	16 mg DMB 2 mL formic acid 5 mL ethanol (100 %; v/v) sodium formate 2 g sodium formate Made up to 1 L with distilled water

Method:

Tissue samples were lyophilised to a constant weight as described in Section 2.2.7.1. Papain digestion solution (5 mL) was added to each sample, and the

samples were were incubated at 60 °C for 36 hours. Chondroitin sulphate B was diluted in assay buffer to produce chondroitin sulphate B standards of known concentration (0, 3.125, 6.25, 12.5, 25, 50, 100, 150, 200 $\mu g.mL^{-1}$). Test samples were assayed without dilution. Test samples and standards (40 µL) were added to a clear flat-bottomed 96-well plate, in triplicate. DMB dye (250 µL) was added to each well, and the plate was incubated at room temperature for two minutes with gentle agitation. The optical density of each well was then measured at 525 nm using a micro plate spectrophotometer. Chondroitin sulphate B standard values were used to create a standard curve of absorbance vs concentration to interpolate unknown test values. GAG content of test samples ($\mu g.mg^{-1}$) was calculated by normalising for dilution volume and dry tissue weight.

2.2.8.5 Quantification of fat content

The fat content of tissue samples was determined using a colourimetric assay based on the method developed by Stern and Shapiro (1953). Hydroxamic acids are formed by a reaction between hydroxylamine and esters of fatty acids in solution. The colourimetric change formed by the reaction between hydroxamic acids and iron (III) chloride can then be measured spectrophotometrically.

Reagents:

- Sodium hydroxide solution (3.5 M)
  - 14 g sodium hydroxide
  - 100 mL distilled water
- Hydrochloric acid solution (4 M)
  - 60 mL hydrochloric acid (6 M)
  - 30 mL distilled water
- Hydroxylamine hydrochloride solution (2 M)
  - 1.39 g hydroxylamine hydrochloride
  - 10 mL distilled water
- Iron (III) chloride solution
  - 500 mg iron (III) chloride (hexahydrate)
  - 3.75 g trichloroacetic acid
  - 5 mL distilled water

Method:

Tissue samples were lyophilised to a constant weight as described in Section 2.2.7.1 in rubber-sealed Eppendorf tubes. Ethanol (100 %; v/v, 600 µL) was added to each sample, and samples were incubated at 42 °C for 4 hours, with gentle agitation. Lard was diluted in ethanol (100 %; w/v) to produce fat standards of known concentration (0, 39, 78, 156, 312.5, 625, 1250, 2500 $\mu g.mL^{-1}$). Fat standards (600 µL) were added to rubber-sealed Eppendorf tubes. Hydroxylamine hydrochloride solution (100 µL) and sodium hydroxide solution (100 µL) were added to each test sample and standard. The test samples and standards were incubated for 20 minutes at room temperature, before adding hydrochloric acid solution (100 µL) and iron (III) chloride solution (100 µL) to each. The samples and standards (250 µL) were then added to individual wells of a clear flat-bottomed 96-well plate, in triplicate. The optical density of each well was measured at 540 nm using a microplate spectrophotometer. Fat standard values were then used to create a standard curve of absorbance vs concentration to interpolate unknown test values. The fat content of test samples ($\mu g.mg^{-1}$) was calculated by normalising for dilution volume and dry tissue weight.

2.2.9 Cell culture

All cell culture work was performed aseptically in a Class II safety cabinet. Cells were cultured in cell culture medium, as described in Section 2.2.9.1. All cells were incubated at 37 °C in 5 % CO_2 (v/v) in air. Before use, all cell culture medium and appropriate additives were equilibrated to 37 °C in a water bath.

2.2.9.1 BHK and L929 cell culture media

2.2.9.1.1 Tryptone phosphate broth (TPB) stock solution (29.5 $g.L^{-1}$)

Tryptone phosphate broth stock (7.98 g) was added to 250 mL distilled water. The solution was filter sterilised as described in Section 2.2.1.3, and stored at -25 °C for up to six months.

2.2.9.1.2 BHK cell culture medium (5 % (v/v) FBS, 10 % (v/v) TPB, 2 mM L-glutamine, penicillin/ streptomycin 100 U / 100 $\mu g.mL^{-1}$)

To make up BHK cell culture medium, 5 mL foetal bovine serum (FBS), 10 mL TPB stock solution, 1 mL L-glutamine (200 mM) and 2 mL penicillin/ streptomycin (penicillin 5000 U.mL-1; streptomycin 5 mg.mL-1) was added to 82 mL Glasgow's

minimal essential medium (GMEM). The medium was stored at 4 °C for up to one week.

2.2.9.1.3 L929 cell culture medium (10 % (v/v) FBS, 2 mM L-glutamine, penicillin/ streptomycin 100 U / 100 µg.mL^{-1})

To make up L929 cell culture medium, 10 mL foetal bovine serum (FBS), 1 mL L-glutamine (200 mM) and 2 mL penicillin/ streptomycin (penicillin 5000 U.mL-1; streptomycin 5 mg.mL^{-1}) was added to 87 mL Dulbecco's minimal essential medium (DMEM). The medium was stored at 4 °C for up to one week.

2.2.9.2 Resurrection and maintenance of cells

L929 and BHK cells were stored in appropriate culture medium containing dimethyl sulfoxide (DMSO; 20 %; v/v) in the vapour phase of liquid nitrogen. Following removal from storage, cell stocks (1 mL) were thawed rapidly at 37 °C in a water bath, and appropriate cell culture medium (10 mL) was added dropwise. To remove the DMSO, the cell suspension was centrifuged at 150 g for ten minutes. The supernatant was aspirated, and cells were re-suspended in 10 mL fresh cell culture medium and transferred to a T75 tissue culture flask. Cell culture medium was replaced every 48 hours until cells had reached approximately 80 - 90 % confluency and could be passaged.

2.2.9.3 Cell passaging

Cell culture medium was aspirated and the cell monolayer gently washed twice with 10 mL PBS (without Ca^{2+} or Mg^{2+}). Adherent cells were detached from the tissue culture plastic by adding trypsin/ EDTA solution (2 mL) and incubating the flask for five minutes. Flasks were then gently tapped to ensure cell detachment, and appropriate cell culture medium (10 mL) was added to inactivate the trypsin. The cell suspension was then centrifuged at 150 g for ten minutes. The cell pellet was re-suspended in 1 mL appropriate culture medium, and cells were counted using a haemocytometer as described in Section 2.2.9.4. The cell suspension was then adjusted to the appropriate cell density, and transferred to a T175 tissue culture flask with 20 mL fresh culture medium. Cell culture medium was replaced every 48 hours until cells had reached approximately 80 - 90 % confluency and could be passaged again.

2.2.9.4 Cell counting and determination of cell viability

In order to determine the viability of cells, trypan blue was added to cell suspensions prior to counting. Trypan blue is able to traverse the membranes of dead cells due to a loss of membrane potential, therefore dead cells microscopically appear blue while live cells appear transparent, enabling dead cells to be excluded from cell counts. To perform a cell count, cell suspension was diluted 1:10 mL in cell culture medium, and 20 µL cell suspension was added to 20 µL trypan blue (0.4 %; w/v), and added to an Improved Neubauer haemocytometer. Viable cells were counted in 1 mm^2 grids, which resulted in a typical cell count of between 100 – 300 cells. The total number of cells.mL^{-1} suspension was calculated as follows:

$$Number\ of\ viable\ cells.mL^{-1} = \frac{number\ of\ viable\ cells}{n} x\ 10^4\ x\ Dilution\ factor$$

n = number of 1 mm^2 grids used in cell count
dilution factor = dilution of cells in Trypan blue (in this case dilution factor = 2)

2.2.9.5 Cell cryopreservation

Cells were harvested from flasks and a cell count performed as described in Section 2.2.9.3 and Section 2.2.9.4. Cells were re-suspended at a density of 1 x 10^6.mL^{-1} in cryopreservation medium (appropriate cell culture medium containing 10% (v/v) DMSO. Cell aliquots (1 mL) were transferred to cryovials, placed in cryofreezing chambers containing isopropanol, and frozen at -80 °C overnight. Cell cryovials were then transferred to liquid nitrogen for long term storage.

2.2.10 Contact cytotoxicity testing

Tissue samples (5 mm^2) were attached to the centre of three wells of a six-well tissue culture plate using wound closure strips (SteriStrips). Cyanoacrylate contact adhesive and SteriStrips were used as positive and negative control wells respectively. Each well was washed three times with PBS (without Ca^{2+} or Mg^{2+}) for ten minutes without agitation. L929 cells or BHK cells were adjusted to a concentration of 250,000 cells.mL^{-1} as described in Section 2.2.9.4 , and 2 mL cell suspension was added to each well. Plates were then incubated for 48 hours. Following incubation, the plates were examined microscopically using phase contrast microscopy. Cell culture medium was then aspirated, and the cell

monolayer washed gently with 2 mL PBS (without Ca^{2+} or Mg^{2+}). Cells were then fixed by adding 2 mL 10% (v/v) NBF to each well, and incubating for 10 minutes at room temperature. NBF was then aspirated from each well, Giemsa stain (a differential cellular stain) was added to each well (enough to cover the cell monolayer), and plates were incubated for five minutes. Each well was then washed with running tap water until clear, before air-drying. Images of the wells were captured using an inverted Olympus IX71 microscope and Olympus XC50 digital camera, under normal Köhler illumination.

2.2.11 Statistical analysis

2.2.11.1.1 Confidence limits

Numerical data were analysed using Excel (Version 2013, Microsoft Incorporated Ltd) and presented as mean (n ≥ 3) ± 95 % confidence limits. The 95 % confidence limits were calculated using the descriptive statistics package in Excel.

$$mean = \frac{\Sigma x}{n}$$

$$Standard\ Deviation = \sqrt{\frac{\Sigma x^2}{n-1}}$$

$$Standard\ Error\ mean = \frac{St\ Dev}{\sqrt{n}}$$

$$95\ \%\ Confidence\ limits = mean\ \pm t\ x\ SE$$

x = individual value
n = sample number
t = critical value
Σ = Sum of

2.2.11.1.2 Comparison of means

Group means were analysed using GraphPad prism 7. A student's t-test was used for the comparison of two means, and one or two-way analysis of variance (ANOVA) was used to compare the means of more than two groups. The individual differences between means were identified by calculating the minimum significant

difference (MSD) at p = 0.05. For two-way ANOVA analyses, Tukey's post hoc testing was used to identify the location of significant differences.

$$MSD = Q\ (a[k, v])x\ SE$$

Q = critical value
α = p = 0.05
k = number of groups
v = degrees of freedom (n – 1)

2.2.11.1.3 Linear regression analysis

GraphPad prism 7 was used for linear regression analyses of standard curves. The coefficient of determination (r^2) value is the ratio of explained variation to total variation, and denotes the strength of the linear relationship between *x* and *y,* such that $0 < r^2 < 1$. This represents how accurately the regression line explains variation in the data (with 0 = no relationship and 1 = perfect relationship) and thus the accuracy with which unknown values could be interpolated from the regression.

Chapter 3: Decellularisation and characterisation of porcine peripheral nerves

3.1 Introduction

A number of methods have been documented for the decellularisation of allogeneic and xenogeneic peripheral nerve, including physical, chemical or enzymatic methods (Hiles, 1972; Sondell *et al.*, 1998; Hudson *et al.*, 2004a; Wang *et al.*, 2016; Zilic *et al.*, 2016). Physical methods that have been used in isolation to decellularise peripheral nerve include repetitive freeze-thaw cycles (Gulati, 1988; Ide *et al.*, 1998), and radiation (Hiles, 1972). Repetitive freeze thaw cycles, used to lyse cells within tissue, have been shown to result in insufficient removal of cellular debris and a fractured basement membrane in endoneurial tubes surrounding myelinated and unmyelinated axons in rat sciatic nerve (Zalewski and Gulati, 1982). Furthermore, when implanted *in vivo* in a rat sciatic nerve defect model these “decellularised” nerves induced an inflammatory response and consequently graft rejection. Similarly, the use of radiation to decellularise rat peripheral nerve also resulted in inadequate removal of cellular debris, and the treated nerve induced an inflammatory response upon implantation in a rat sciatic nerve defect model (Hiles, 1972; Pollard and Fitzpatrick, 1973).

Although physical methods are effective in lysing and detaching cells from the ECM and freeze-thaw cycles are often incorporated in peripheral nerve decellularisation processes, such methods are insufficient when applied in isolation due to the disruptive effects of repetitive freeze-thaw cycles on ECM structure and inadequate removal of cellular debris (Hudson *et al.*, 2004a). Chemical decellularisation methods can overcome these limitations and are widely employed. Chemical decellularisation methods are often combined with physical and enzymatic methods to achieve sufficient decellularisation (Gilbert *et al.*, 2006).

Detergents are the predominant chemical method used for the decellularisation of peripheral nerve, and various protocols including ionic detergents, non-ionic and zwitterionic detergents have been developed (Sondell *et al.*, 1998; Hudson *et al.*, 2004b; Zilic *et al.*, 2016). Common ionic detergents that have been used include sodium dodecyl sulphate (SDS), and sodium deoxycholate (White *et al.*, 2017). The non-ionic detergent Triton X-100 and zwitterionic detergent sulfobetaine have also been widely used (Hudson *et al.*, 2004a; Gilbert *et al.*, 2006).

Non-ionic detergents such as Triton X-100 have been used for the decellularisation of peripheral nerve due to their mild effects upon ECM architecture, and have been used in combination with ionic detergents to increase decellularisation efficacy (Hudson *et al.*, 2004a; Seddon *et al.*, 2004). Using a combination of 3 % (v/v) Triton X-100 and 4 % (v/v) sodium deoxycholate, Sondell *et al*. (1998) produced a decellularised rat nerve graft which was shown to support axon regeneration *in vivo* in a rat sciatic nerve defect model (Sondell *et al.*, 1998). Analysis of the implanted graft after 10 days showed regenerating axons within endoneurial tubes and migration of recipient Schwann cells, which repopulated empty endoneurial tubes without excessive inflammation. However, the graft was unable to match the performance of autografts, even when pre-seeded with Schwann cells (Sondell *et al.*, 1998; Frerichs *et al.*, 2002). It was hypothesised that this was due to inadequate preservation of the basement membrane. Other studies that have used 3 % (v/v) Triton X-100 to decellularise peripheral nerves have reported a decrease in basement membrane proteins, including laminin and fibronectin (Hudson *et al.*, 2004b). A more recent study by Wang et al (2016) used 1 % (v/v) Triton X-100 alone and in combination with 1 % (v/v) sodium deoxycholate to decellularise rat peripheral nerve, and reported preservation of laminin, fibronectin, collagen type I and collagen type IV (Wang *et al.*, 2016). However, some structural irregularity of endoneurial tubes was observed, and axon density and maturity were significantly less than observed for autografts up to 24 weeks post implantation *in vivo* in a rat sciatic nerve defect model (Wang *et al.*, 2016).

A chemical decellularisation process developed by Hudson et al (2004) used Triton X-200 (0.14 % v/v) in combination with zwitterionic detergents sulfobetaine-10 (125 mM) and sulfobetaine-16 (0.6 mM) to decellularise rat sciatic nerve (Hudson *et al.*, 2004a). This process was shown to achieve sufficient decellularisation, and demonstrated superior preservation of the ECM in comparison to the method developed by Sondell *et al.* (1998). Furthermore, analysis of the graft 28 days post implantation in a rat sciatic nerve defect model showed that axon density at the midpoint was not significantly different from isograft controls, and significantly higher than in the grafts produced using the method developed by Sondell *et al.* (1998) and in a decellularised graft produced using a repetitive freeze-thaw cycle process developed by Gulati *et al*. (1988). The graft was not subject to an adverse immune response *in vivo*, however macrophage infiltration into the graft was slightly higher than in the isograft controls (Hudson *et al.*, 2004b). One potential explanation for this was that increased ECM porosity and open endoneurial tubes enabled greater macrophage infiltration.

The decellularisation process developed by Hudson *et al*. (2004) has been licenced by Axogen® Inc. to produce the Avance® graft, developed for human nerves with the addition of enzymatic digestion of chondroitin sulphate proteoglycan (CSPG), a known inhibitor of axon regeneration (Zuo *et al.*, 2002). The Avance® graft has demonstrated superior clinical efficacy to NGCs when used to treat a range of nerve defect sizes (Karabekmez *et al.*, 2009; Johnson *et al.*, 2011). However, the Avance® graft has not yet demonstrated consistently superior clinical outcomes compared to autografts, even in small defects. A potential explanation for this could be that the decellularised nerve graft has diminished regenerative capacity as a consequence of ECM disruption (Whitlock *et al.*, 2009).

As discussed previously, the collagenous ECM of peripheral nerve is crucial to supporting the function of axons travelling within the nerve, maintaining an optimal microenvironment and providing protection from mechanical stress (Bell and Haycock, 2011; Topp and Boyd, 2012). ECM structures, including endoneurial tubes, provide topographic guidance and support to elongating axons and infiltrating cells, and determine the mechanical properties of the nerve. Furthermore, various basement membrane components in the endoneurium and perineurium, including collagen type IV, laminin and fibronectin have been shown to be critical for enabling the attachment and migration of perineurial cells, Schwann cells and neurons (De Luca *et al.*, 2014). It has been hypothesised that inadequate preservation of ECM microstructures, such as endoneurial tubes and the basement membrane, impairs cellular infiltration and proliferation in a decellularised nerve graft (Bellamkonda, 2006; Whitlock *et al.*, 2009).

In comparison to other detergents, including Triton X-100, studies using SDS have demonstrated superior efficacy for the removal of cellular material, nuclear remnants and cytoplasmic proteins from a wide array of tissues, such as rat aortic valves, porcine aortic valves and porcine carotid arteries (Booth *et al.*, 2002; Grauss *et al.*, 2003; Dahl *et al.*, 2003). SDS has previously been used for the decellularisation of peripheral nerve in combination with other detergents. A study by Wakimura et al (2015) used a combination of 1% (w/v) SDS and 1 % (v/v) Triton X-100 to decellularise rat peripheral nerve, and reported sufficient cell removal with the preservation of the overall ECM structure. Furthermore, *in vivo* analysis in a rat sciatic nerve defect model showed an abundance of axons and Schwann cells migrating through the implanted graft (Wakimura *et al.*, 2015).

The use of ionic detergents such as SDS at high concentrations is known to denature ECM proteins, including collagen fibrils, through the disruption of protein-protein interactions, affecting tissue architecture and mechanical strength (Faulk *et al.*, 2014b; Ferng *et al.*, 2017). At high concentrations, SDS has been shown to induce significant denaturation of ECM proteins; a study of decellularised porcine aorta reported extensive collagen disruption and increased ECM porosity when treated with 2 % (w/v) SDS, whereas minimal alterations were observed when treated with 0.1 % (w/v) SDS (Azhim *et al.*, 2014). However, low concentration SDS (0.1 %; w/v) in combination with protease inhibitors to inhibit the activity of endogenous matrix metalloproteases, followed by the use of nuclease enzymes, has been shown to sufficiently remove cellular and nuclear material from several tissues, with minimal alterations to the ECM (Booth *et al.*, 2002; Wilshaw *et al.*, 2012; Azhim *et al.*, 2014).

As discussed in Chapter 1, a collaborative partnership between the University of Leeds and the University of Sheffield resulted in the development of a decellularisation process for porcine peripheral nerve (Zilic *et al.*, 2016). The process was adapted from the proprietary University of Leeds decellularisation process, and utilised low concentration SDS (0.1 %; w/v) plus protease inhibitors in combination with hypotonic and hypertonic buffers and nuclease treatment. The developed process was shown to achieve sufficient DNA content reduction and preserve several key basement membrane components including laminin and collagen type IV (Zilic *et al.*, 2016). However, the decellularisation process resulted in structural changes to the perineurium and endoneurial tubes, and changes in the distribution of collagen fibrils, laminin and fibronectin (Zilic *et al.*, 2016). Therefore, in this chapter the decellularisation process was further developed to maintain the efficacy of decellularisation whilst minimising structural changes to nerve histioarchitecture.

3.2 Aims and objectives

3.2.1 Aims:

I. To further develop the decellularisation process previously developed for porcine peripheral nerves, maintaining the efficacy in terms of sufficient cell removal and DNA reduction, whilst improving the preservation of overall histioarchitecture and the major ECM structures responsible for maintaining axonal function and directing axon growth, including the endoneurium.

II. To characterise the properties of native and decellularised porcine peripheral nerve, and assess the effects of decellularisation on biochemical composition and specific ECM components, including basement membrane components crucial for cell adhesion, survival and migration.

3.2.2 Objectives:

I. To determine the efficacy of various iterations of the Zilic *et al.* (2016) decellularisation protocol for porcine peripheral nerves using DAPI staining of tissue sections to assess cell removal, and to determine the effects of the various protocols on the histioarchitecture and major ECM structures using histology.

II. To select an improved decellularisation process for porcine peripheral nerves based upon the results of Objective I.

III. To investigate the efficacy of the improved decellularisation protocol by quantifying total and double stranded DNA content of the tissue.

IV. To determine the biocompatibility of nerves decellularised using the improved protocol by contact culture using two distinct cell types, BHK and L929 cells.

V. To determine the effects of the improved decellularisation protocol on specific ECM components and macroscopic structures, including the structure and distribution of collagens and elastin, by histological analyses.

VI. To determine the effects of the improved decellularisation protocol on key basement membrane components, including collagen type IV, laminin, fibronectin and chondroitin sulphate using immunohistochemical analyses.

VII. To determine the effects of the improved decellularisation protocol on the biochemical composition of porcine peripheral nerves, by quantification of collagen, denatured collagen, GAG and fat content.

3.3 Methods and experimental approach

3.3.1 Experimental approach

Various iterations of the original decellularisation protocol developed by Zilic *et al*. (2016) were applied to porcine peripheral nerves. The process was developed with the purpose of establishing a decellularisation protocol that would maintain the efficacy of decellularisation, with sufficient cell removal and reduction in DNA content, whilst ensuring the preservation of overall nerve histioarchitecture and important ECM structures, such as the endoneurium. Once an improved process had been developed, nerves that had been decellularised using the improved process were compared with native porcine peripheral nerves using various histological, immunohistochemical and biochemical analyses.

3.3.2 Methods

3.3.2.1 Development of the decellularisation process

3.3.2.1.1 Decellularisation protocols

The peripheral nerve plexus was dissected from the hind legs of 6 large white pigs, cut into 30 mm segments (approximately n = 30 segments per hind leg) and stored on PBS-moistened filter paper at -80 °C as described in Chapter 2 (Section 2.2.2.2). A total of 24 nerve segments randomly selected from each hind leg were subject to each decellularisation protocol, described below. The decellularisation process was carried out aseptically, using aseptic technique in a class II safety cabinet. All decellularisation solutions were autoclaved prior to use, as described in Chapter 2 (Section 2.2.1.3). Following decellularisation, nerve segments were stored aseptically in PBS at 4 °C for up to one month.

The original decellularisation process for porcine peripheral nerve segments developed by Zilic *et al.* (2016) is shown in Table 3.1. The decellularisation solutions used are described in Chapter 2 (Section 2.1.8).

The original decellularisation protocol and four modified decellularisation protocols, utilising either one, or two, incubations in hypotonic buffer and / or SDS hypotonic buffer were applied to the porcine peripheral nerve segments (Table 3.2).

Table 3.1 Decellularisation process for porcine peripheral nerve segments. Decellularisation process developed for porcine peripheral nerve by Zilic *et al.* (2016). Each step is shown in chronological order. For details of each solution, see Chapter 2 (Section 2.2.7). Each step was carried out in a 150 mL sterile pot, with 100 mL of each solution added, with horizontal agitation. Three 30 mm nerve segments were added to each pot.

Process step	Time	Temperature	Agitation
Thaw	30 minutes	37 °C	
Antibiotic solution (0.05 mg.mL^{-1} vancomycin, 0.5 mg.mL^{-1} gentamicin, 0.2 mg.mL^{-1} polymyxin B), pH 7.2 – 7.4	30 minutes	37 °C	240 rpm
EDTA solution (200 mM EDTA), pH 7.2 - 7.4	24 hours	4 °C	240 rpm
Hypotonic buffer *(10 mM tris, 2.7 mM EDTA, 10 10000 KIU.mL^{-1} aprotinin),* pH 8.0 – 8.2	24 hours	42 °C	240 rpm
SDS hypotonic buffer *(0.1 % w/v SDS, 10 mM tris, 2.7 mM EDTA, 10 10000 KIU.mL^{-1} aprotinin),* pH 8.0 - 8.2	24 hours	42 °C	240 rpm
Hypotonic buffer *(10 mM tris, 2.7 mM EDTA, 10000 KIU.mL^{-1} aprotinin),* pH 8.0 – 8.2	24 hours	42 °C	240 rpm
PBS EDTA solution *containing aprotinin (2.7 mM EDTA, 10 10000 KIU.mL^{-1} aprotinin),* pH 7.2 - 7.4	48-56 hours	4 °C	50 rpm
Hypotonic buffer *(10 mM tris, 2.7 mM EDTA, 10 10000 KIU.mL^{-1} aprotinin),* pH 8.0 – 8.2	24 hours	42 °C	240 rpm
PBS, pH 7.2 – 7.4	24 hours	42 °C	240 rpm
Nuclease solution *(50 mM Tris, 1 mM $MgCl_2.6H_20$, 1 U.mL^{-1} benzonase),* pH 7.5 – 7.7, x 2	3 hours	37 °C	50 rpm
PBS, pH 7.2 – 7.4, (x 3)	30 minutes	42 °C	240 rpm
Hypertonic buffer *(50 mM tris, 1.5 M NaCl),* pH 7.5 - 7.7	24 hours	42 °C	240 rpm
PBS, pH 7.2 – 7.4, (x 3)	30 minutes	42 °C	240 rpm
Storage in PBS		4 °C	

Table 3.2 Decellularisation protocols applied to porcine peripheral nerve segments. Number of hypotonic and SDS hypotonic buffer incubations used as part of the original and four modified decellularisation protocols applied to porcine peripheral nerve segments. Each incubation was for 24 hours at 42 °C, with agitation at 240 rpm, as described in Table 3.1.

Protocol	Number of hypotonic buffer incubations	Number of SDS hypotonic buffer incubations
Original	3	1
1	1	1
2	1	2
3	2	1
4	2	2

3.3.2.1.2 Histological analysis

Porcine peripheral nerve segments decellularised using each protocol (n = 3) were evaluated and compared to native nerve segments (n = 3) using histology to assess the efficacy and reproducibility of each protocol. Decellularised nerve segments were cut into three 10 mm samples, in order to analyse both the middle and end areas of the nerve segment. Samples of native and decellularised tissue were fixed in 10 % (w/v) NBF, processed and embedded in paraffin wax as described in Chapter 2 (2.2.4.1). Wax blocks of native (n = 3), and middle (n = 3) and end (n= 3) regions of decellularised nerve were sectioned (5 µm thickness) as described in Chapter 2 (Section 2.2.4.2). Sections were then stained using H&E (n = 6) or DAPI (n = 6) as described in Chapter 2 (Sections 2.2.5.1 and 2.2.5.2 respectively). H&E staining was used to assess overall histioarchitecture and the preservation of major ECM structures, and DAPI staining was used to assess cell removal by visualising whole cell nuclei or nuclear remnants. Following histological analysis of nerve segments decellularised using the different protocols, Protocol (1), with a reduced agitation speed of 120 rpm, was identified as the improved process. Images presented are of the middle regions of native and decellularised nerve segments.

Nerve segments (30 mm, n = 24) were decellularised using Protocol (1) with a reduced agitation speed of 120 rpm. These segments were used for further detailed analyses as described below.

3.3.2.1.3 DNA content of native and decellularised porcine peripheral nerve segments

The efficacy and reproducibility of decellularisation, in terms of sufficient reduction in DNA content, was determined in nerve samples decellularised using Protocol (1) with a reduced agitation speed of 120 rpm. Whole 30 mm segments of native (n = 6) and decellularised (n = 6) nerve were lyophilised to a constant weight prior to DNA extraction and spectrophotometric quantification as described in Chapter 2 (Sections 2.2.7.1 – 2.2.7.3). The double stranded DNA (dsDNA) content of the same DNA samples was also determined using the PicoGreen assay, as described in Chapter 2 (Section 2.2.7.4).

3.3.2.1.4 Biocompatibility of decellularised porcine peripheral nerve

The biocompatibility of porcine peripheral nerve tissue decellularised using Protocol (1) with a reduced agitation speed of 120 rpm was determined using a contact cytotoxicity assay, as described in Chapter 2 (Section 2.2.10), using BHK cells (n = 3) and L929 cells (n = 3). Cyanoacrylate contact adhesive was used as a positive control for cytotoxicity, and surgical closure strips (SteriStrips) were used as a negative control. Biocompatibility was assessed by examining cell growth up to and in contact with the samples after 48 hours in culture.

3.3.2.2 Characterisation of native and decellularised porcine peripheral nerve segments

Various histological, immunohistochemical and biochemical analyses were used to characterise the properties of native (n = 6) and decellularised (n = 6) porcine peripheral nerve segments, and assess the effects of decellularisation Protocol (1) with a reduced agitation speed of 120 rpm on nerve histioarchitecture and specific ECM components.

3.3.2.2.1 Histological analysis

Native (n = 6) and decellularised (n = 6) nerve samples were cut into three 10 mm segments, fixed in 10 % (w/v) NBF, processed and embedded in paraffin wax as described in Chapter 2 (Section 2.2.4.1). Wax blocks were sectioned (5 µm thickness) as described in Chapter 2 (Section 2.2.4.2), and processed for histological analysis, or analysis by immunofluorescent labelling. Images presented are of the middle regions of native and decellularised nerve segments.

3.3.2.2.2 Histological stains

Sections were stained using Sirius red / Miller's elastin and Sirius red / Luxol fast blue, as described in Chapter 2 (Sections 2.2.5.3 and 2.2.5.4 respectively). Sirius red staining was used to assess overall collagen structure, and imaged under circularly polarised light to examine collagen fibril configuration and distribution. Miller's stain was used to stain elastin, and Luxol fast blue was used to stain myelin.

3.3.2.2.3 Immunofluorescent labelling of specific ECM components

For immunofluorescent labelling, sections of native and decellularised nerve were labelled with primary antibodies specific for collagen IV, laminin, fibronectin and chondroitin sulphate, as described in Chapter 2 (Section 2.2.6), and counterstained with DAPI (Table 3.3). Sections of native and decellularised nerve were incubated with isotype control antibodies, and sections of native porcine artery or cartilage were used as positive controls. Omission of primary antibodies served as negative controls.

Table 3.3 Specific antibodies and solutions for immunofluorescent labelling of laminin, fibronectin, collagen type IV and chondroitin sulphate. Specific antibodies, antigen retrieval methods and blocking steps used for immunofluorescent labelling. For details of each antibody, see Chapter 2 (Section 2.1.6). Isotype control antibodies were applied at the same protein concentration as the primary antibody.

	Laminin	Fibronectin	Collagen type IV	Chondroitin sulphate (CS)
Primary antibody	Monoclonal mouse anti-laminin (1 $mg.mL^{-1}$); 1:500 dilution	Polyclonal rabbit anti-fibronectin (4.9 $g.L^{-1}$); 1:200 dilution	Monoclonal mouse anti-collagen IV (50 $mg.mL^{-1}$); 1:400 dilution	Monoclonal mouse anti-CS (35.6 $mg.mL^{-1}$); 1:200 dilution
Secondary antibody	Goat anti-mouse IgG AF488 (2 $mg.mL^{-1}$); 1:200 dilution	Goat anti-rabbit IgG AF488 (2 $mg.mL^{-1}$); 1:200 dilution	Goat anti-mouse IgG AF488 (2 $mg.mL^{-1}$); 1:200 dilution	Goat anti-mouse IgG AF488 (2 $mg.mL^{-1}$); 1:200 dilution
Isotype antibody	Mouse IgG1	Rabbit polyclonal IgG	Mouse IgG1	Mouse IgM
Antigen retrieval	Proteinase K 20 minutes	Proteinase K 20 minutes, Trypsin / EDTA 30 seconds	Proteinase K 20 minutes	None
Blocking buffer	None	None	None	Goat serum (10 %; w/v in TBS) 1 hour

3.3.2.2.4 Biochemical analysis

The biochemical composition of native (n = 6) and decellularised (n = 6) nerve segments was determined using assays to quantify collagen, denatured collagen, fat and GAG content as described in Chapter 2 (Section 2.8).

3.4 Results

3.4.1 Development of the decellularisation process

3.4.1.1 Decellularisation protocols and histological analysis

A number of different decellularisation protocols were applied to porcine peripheral nerve segments (Table 3.1). These included the original protocol, including one incubation in SDS hypotonic buffer and three incubations in hypotonic buffer, and four modified protocols. Protocols (1) and (2) included one and two incubations in hypotonic buffer respectively, and one incubation in SDS hypotonic buffer. Protocols (3) and (4) included one and two incubations in hypotonic buffer respectively, and two incubations in SDS hypotonic buffer. H&E staining of tissue sections was used to assess overall histioarchitecture and cell removal. DAPI staining of tissue sections was used to assess cell removal by visualising whole cell nuclei or nuclear remnants.

Sections of native nerve stained with H&E and DAPI are shown in Figure 3.1 (A & G). Observations of the stained sections revealed regular shaped and sized endoneurial tubes, although the size and shape of fascicles varied. The perineurium surrounding each fascicle appeared as a discrete, concentric band, with little variation between fascicles. The inter-fascicular epineurium appeared loose and disorganised in comparison to the perineurium, forming irregular networks (Figure 3.1 A). The endoneurium and perineurium appeared to have dense cell populations, forming aligned, flattened configurations around endoneurial tubes and along the perineurial border (Figure 3.1 A & G). The blood vessels in the inter-fascicular epineurium, the vasa nervorum, also contained dense cell populations, whereas cells in the inter-fascicular region were sporadically distributed (Figure 3.1 A & G).

Observations of DAPI stained sections revealed that no whole nuclei were present following any of the decellularisation protocols (Figure 3.1 G & H). However, observations of H&E stained sections indicated differences in the histoarchitecture of decellularised nerve in comparison to native nerve. For nerves decellularised using any of the protocols, the endoneurium and epineurium appeared less dense, with irregular organisation compared to native nerve, and the perineurium appeared thinner but remained as an intact barrier between the fascicles and epineurium (Figure 3.1 A-F).

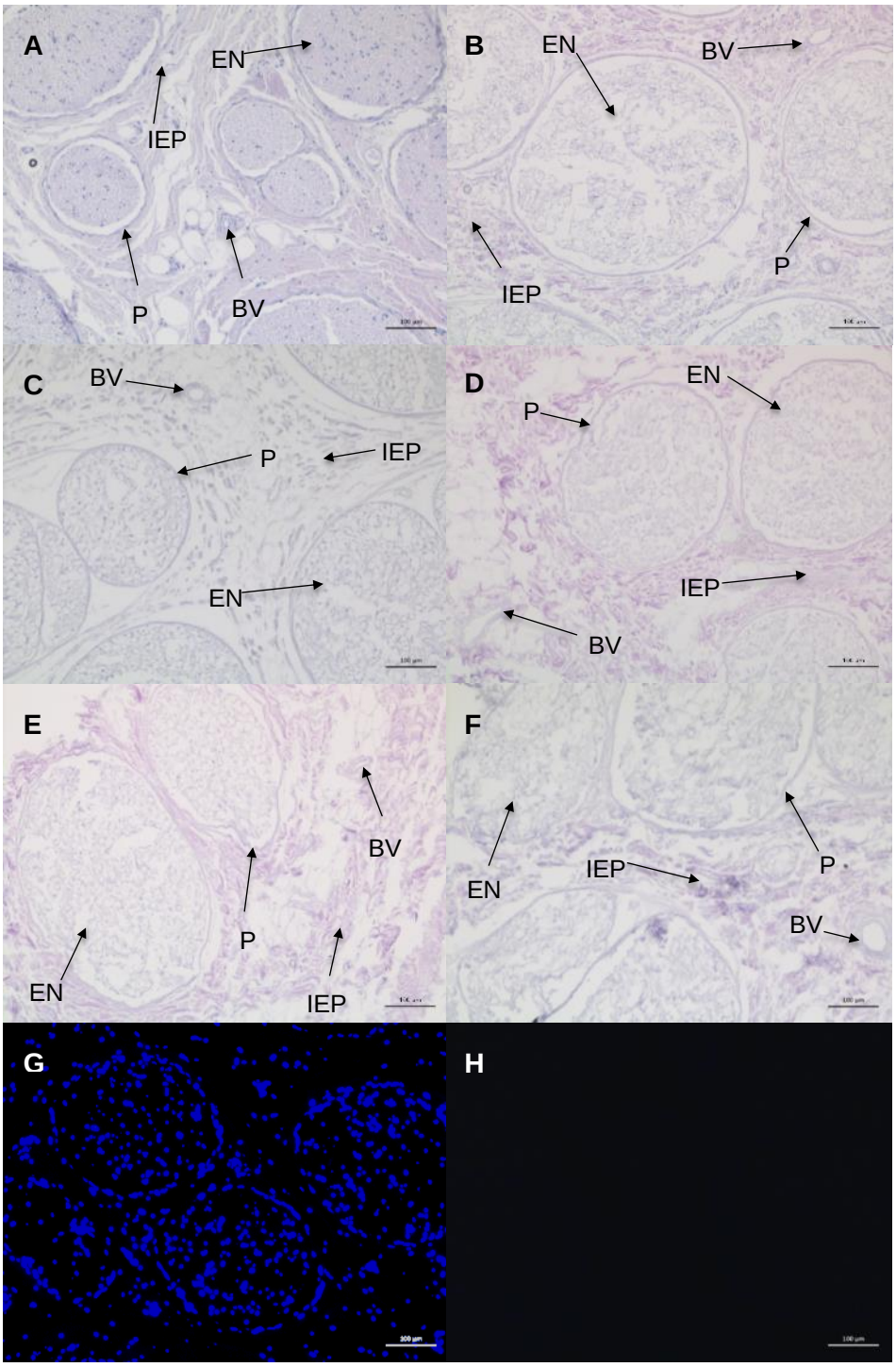

Figure 3.1 Images of sections of porcine peripheral nerve stained with H&E and DAPI before and after different decellularisation protocols.
Representative images of native porcine peripheral nerve (A & G) and decellularised porcine peripheral nerve segments produced using the original decellularisation protocol (B) and Protocols 1 (C & H), 2 (D) 3 (E) and 4 (F). Sections stained with H&E (A – F) and DAPI (G & H). Labels added to H&E images to identify ECM structures, EN = endoneurium, IEP = inter-fascicular epineurium, P = perineurium, BV = blood vessels. Major ECM structures were well preserved following decellularisation, although greater ECM degradation corresponded with increased cycles of hypotonic and / or SDS hypotonic buffer. Images acquired under Köhler illumination using a x10 objective. Scale bars = 100 µm.

Observations of H&E stained sections showed that increased numbers of incubations in hypotonic and / or SDS hypotonic buffer appeared to correspond to greater ECM degradation, with an increasing loss of definition of the major ECM structures (Figure 3.1 B-F). In particular, Protocols (3) (Figure 3.1E) and (4) (Figure 3.1 F), incorporating two incubations in SDS hypotonic buffer and the original protocol, incorporating three incubations in hypotonic buffer (Figure 3.1 B), led to severe disruption to the major ECM structures, especially the endoneurium (Figure 3.1 B, E & F).

Protocol (1), the minimal protocol with one incubation in hypotonic buffer and one incubation in SDS hypotonic buffer, appeared to be an improved protocol. Sections of porcine peripheral nerve segments decellularised using Protocol (1) retained clear definition of the major ECM structures, although some structural damage was observed, particularly to the endoneurium (Figure 3.1 C). However, since observations of DAPI stained sections showed that no whole nuclei were present following any of the decellularisation protocols, the agitation speed used during incubations was reduced from 240 rpm to 120 rpm in an attempt to further minimise structural damage to the nerve (Figure 3.2).

Two further groups of porcine peripheral nerve segments (n = 12 each) were decellularised using Protocol (1); one group using the original agitation speed of 240 rpm and one group with a reduced agitation speed of 120 rpm. Both versions of Protocol (1) appeared to successfully remove cells from the nerve (Figure 3.2 B & D). However, reducing the agitation speed to 120 rpm appeared to enable better retention of ECM structures, particularly the endoneurium, and individual endoneurial tubes could be identified (Figure 3.2 A & C). Therefore, Protocol (1), incorporating one incubation in hypotonic buffer and SDS hypotonic buffer, with a reduced agitation speed of 120 rpm, was used to produce decellularised porcine peripheral nerve segments for subsequent analyses.

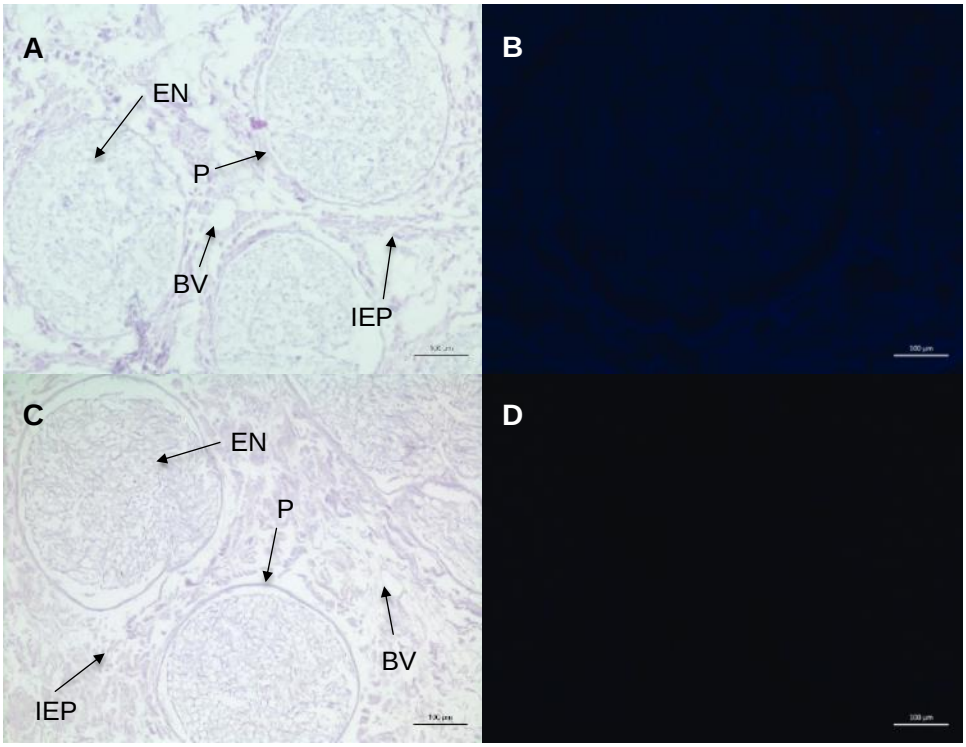

Figure 3.2 Images of sections of native porcine peripheral nerve and nerve segments decellularised using Protocol (1) with agitation speeds of 120 and 240 rpm stained with H&E and DAPI. Representative images of sections of decellularised porcine peripheral nerve produced using Protocol 1, with an agitation speed of 240 rpm (A & B), and Protocol 1 with a reduced agitation speed of 120 rpm (C & D). Sections stained with H&E (A & C) and DAPI (C & D). Cell nuclei were removed from the tissue using both agitation speeds, whilst a reduced agitation speed enabled better preservation of ECM structures, particularly the endoneurium. Labels added to H&E images to identify ECM structures, EN = endoneurium, IEP = inter-fascicular epineurium, P = perineurium, BV = blood vessels. Images acquired under Köhler illumination using a x10 objective. Scale bars = 100 µm.

3.4.1.2 DNA content of native and decellularised porcine peripheral nerve

The DNA content of native and decellularised porcine peripheral nerve was determined to assess the efficacy and reproducibility of Protocol (1) with a reduced agitation speed of 120 rpm. Following DNA extraction from the tissues, total DNA content was quantified using spectrophotometry, and double stranded DNA content quantified using a PicoGreen assay (Table 3.4). Calf thymus DNA was used to create a standard curve to assess the accuracy of the spectrophotometer (Figure 3.3 A), and lambda DNA was used to create a standard curve to interpolate unknown values to quantify double stranded DNA (Figure 3.3 B).

Using a Student's t- test for each comparison, a significant difference was found between the total DNA content of native and decellularised nerves ($p < 0.0001$), and the double stranded DNA content of native and decellularised nerve ($p < 0.0001$).

Table 3.4 Quantification of the DNA content of native and decellularised nerve. Average total DNA content ($ng.mg^{-1}$) and average double stranded DNA (dsDNA) content ($ng.mg^{-1}$) of native (n = 6) and decellularised (n = 6) nerve samples.

	Average total DNA content ($ng.mg^{-1}$)	**Average dsDNA content ($ng.mg^{-1}$)**
Native nerve	379 ± 62	298 ± 75
Decellularised nerve	15 ± 7	3 ± 1

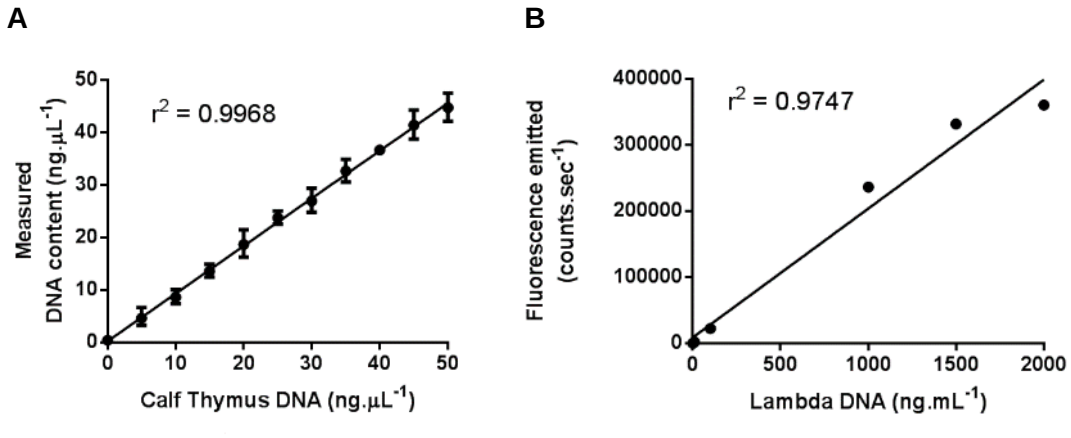

Figure 3.3 DNA content of calf thymus and lambda DNA standards. (A) Linear relationship between calf thymus DNA concentration and measured DNA content of calf thymus DNA standards. Data represented as mean (n = 3) ± 95 % confidence limits (B) Standard curve of lambda DNA concentration against fluorescence emitted. Data represented as mean (n = 3) ± 95 % confidence limits.

3.4.1.3 Biocompatibility of decellularised porcine peripheral nerve

The biocompatibility of decellularised porcine peripheral nerve was assessed using a contact cytotoxicity assay using two distinct cell lines, BHK and L929 (Figure 3.4). Cells cultured with cyanoacrylate, the positive control, were sparsely distributed, displayed a rounded morphology and were not adhered, indicating cell death (Figure 3.4 A & B). Both cell types cultured with SteriStrips, the negative control, and samples of decellularised nerve grew up to and in contact with the samples, and displayed normal morphological characteristics. L929 cells displayed an elongated, spindle morphology and BHK cells displayed a more rounded morphology and a denser population (Figure 3.4 C-F).

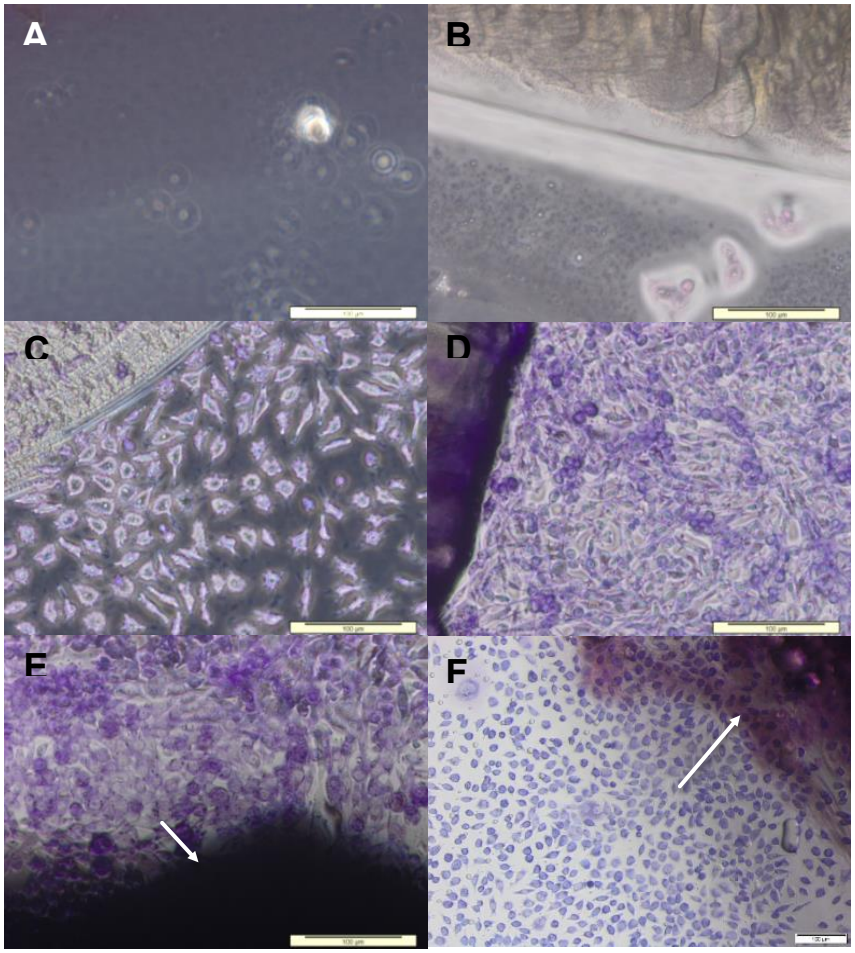

Figure 3.4 Contact cytotoxicity assay of decellularised porcine peripheral nerve. BHK cells (A, C & E), and L929 cells (B, D, & F) were cultured with either cyanoacrylate adhesive (A & B) to serve as a positive control, SteriStrips (C & D) to serve as a negative control, or 5 mm^2 segments of decellularised porcine peripheral nerve (n = 3) (E & F). White arrows indicate position of decellularised nerve (E & F). Both cell types grew up to and in contact with the tissue, and displayed normal morphological characteristics. Images acquired under brightfield illumination using a x10 objective. Scale bars 100 µm.

3.4.2 Characterisation of native and decellularised porcine peripheral nerve

3.4.2.1 Histological analysis

Picro-Sirius red was used to stain collagen fibres within sections of native and decellularised nerve, whilst Miller's solution was used to stain elastin fibres (Figure 3.5 A-D). The specific configuration and distribution of the collagen fibres was visualised using circularly polarized light microscopy, as collagen fibre diameter can be deduced based on the birefringence of the fibres under polarised light, with thicker fibrils appearing as yellow/red, and smaller fibrils appearing as green (Figure 3.5 C & D) (Junqueira *et al.*, 1979). Visualisation under normal Köhler illumination revealed fine collagen fibres forming the endoneurial tubes of native nerve, and slightly thicker, discrete bands forming the perineurium. The collagen appeared to form evenly interspersed networks between fascicles in the inter-fascicular epineurium, and a dense, thick layer in the external epineurium with crimped regions (Figure 3.5 A). In comparison to sections of native nerve, the collagen in the epineurium of sections of decellularised nerve appeared sparse and lacking network configurations. In addition, the collagen also appeared significantly thinner in the perineurium of decellularised nerve sections, and less defined within the endoneurium (Figure 3.5 B). Under circularly polarized light, the collagen fibres in native nerve sections appeared to form tightly aligned configurations of red/yellow fibres along the perineurial borders and in the external epineurium, irregular networks of red/yellow fibrils in the inter-fascicular epineurium, and fine networks of green fibrils surrounding individual endoneurial tubes (Figure 3.5 D). Visualisation of decellularised nerve sections under circularly polarised light indicated the retention of these fine collagen fibril networks, and a similar distribution of red, yellow and green collagen fibres between native and decellularised nerve (Figure 3.5 C & D). No elastin fibres were revealed within the native nerve sections, except within the blood vessels located in the inter-fascicular epineurium, the vasa nervorum, and these elastin fibres were retained in decellularised nerve sections (Figure 3.5 A & B).

Luxol fast blue was used to stain the myelin in native and decellularised peripheral nerve sections, although staining was improved when used in conjunction with another stain to visualise myelin in the context of other ECM components. Picro-Sirius red was used, as collagen is a ubiquitous component of peripheral nerve ECM, and haematoxylin was used as a counterstain to visualise cell nuclei (Figure

3.5 E & F). Myelin was only observed within the endoneurium of native nerve sections; however the myelin staining appeared fragmented and patchy within individual endoneurial tubes (Figure 3.5 E). Myelin was not observed in decellularised nerve sections, indicating that the decellularisation process may have removed the myelin from porcine peripheral nerves (Figure 3.5 F).

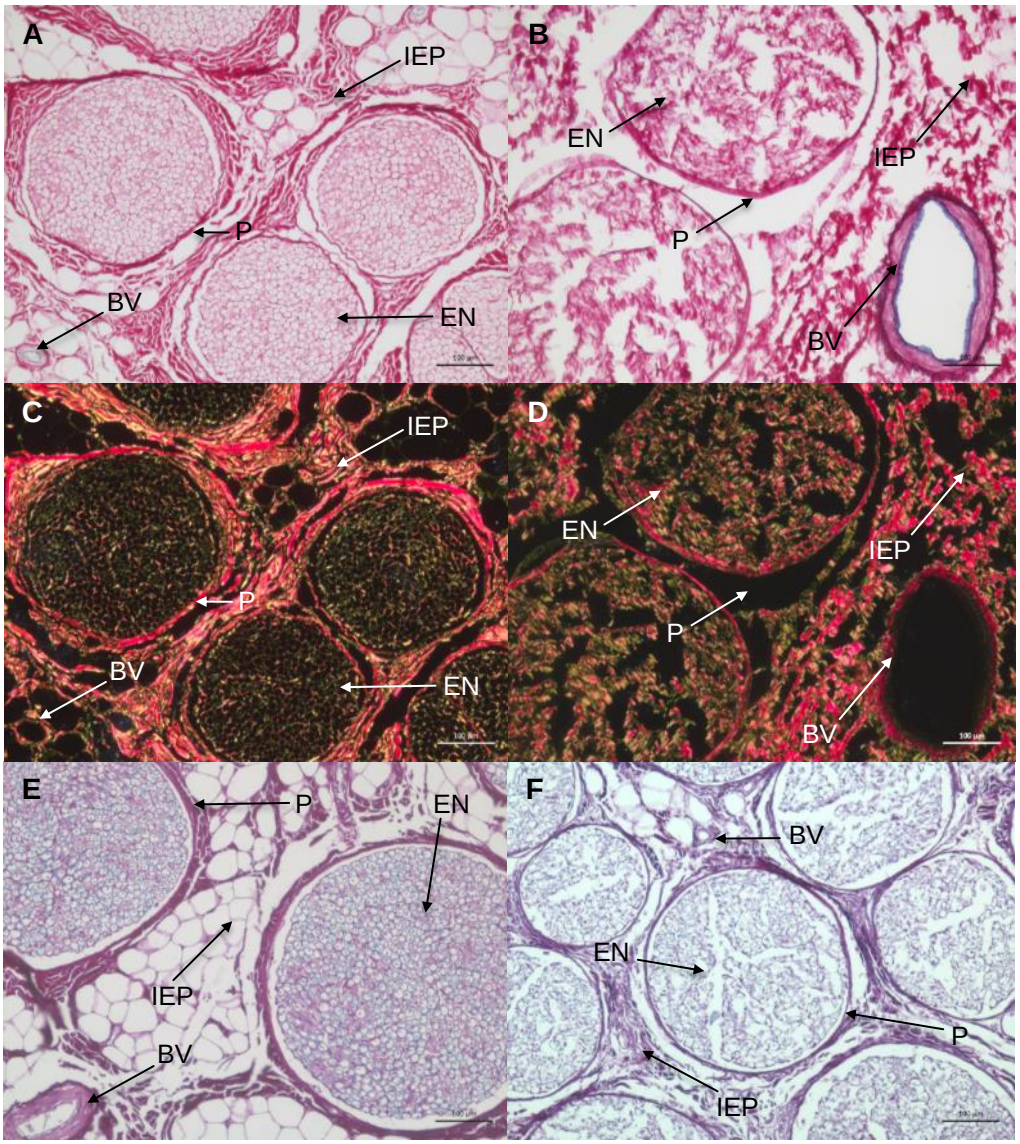

Figure 3.5 Images of sections of native and decellularised porcine peripheral nerve stained with Sirius red / Miller's elastin and Sirius red / Luxol Fast blue. Representative images of native (A, C & E) and decellularised (B, D & F) porcine peripheral nerve sections stained with Sirius red / Miller's elastin (A – D) or Sirius red, Luxol Fast blue and haematoxylin (E & F). Sirius red imaged using normal Köhler illumination (A & B) or circularly polarised light (C & D). The structure and distribution of collagen appeared to be well preserved following decellularisation, and the decellularisation process appeared to remove myelin from the nerve. Labels added to H&E images to identify ECM structures, EN = endoneurium, IEP = inter-fascicular epineurium, P = perineurium, BV = blood vessels. Images taken using a x 10 objective. Scale bars 100 μm.

3.4.2.2 Immunofluorescent labelling of specific ECM components

3.4.2.2.1 Immunofluorescent labelling of collagen type IV

Sections of native and decellularised peripheral nerve were labelled with a primary monoclonal antibody against collagen type IV and a goat anti-mouse IgG secondary antibody (Figure 3.6). Collagen type IV was present within fascicles, located in both the endoneurium and perineurium, and in inter-fascicular blood vessels. In the endoneurium, collagen IV appeared to form discrete bands around individual endoneurial tubes, and in the perineurium collagen type IV appeared to form a thick layer surrounding each fascicle (Figure 3.6 C & D). Although labelling intensity was reduced following decellularisation, collagen type IV was still located in the endoneurium, perineurium and blood vessels of decellularised nerve (Fig 3.6 D). Intense labelling was observed in the smooth muscle and luminal regions of sections of porcine femoral artery, the positive control (Figure 3.6 A), and no labelling was observed in sections of native porcine peripheral nerve incubated with the isotype control antibody (Figure 3.6 B).

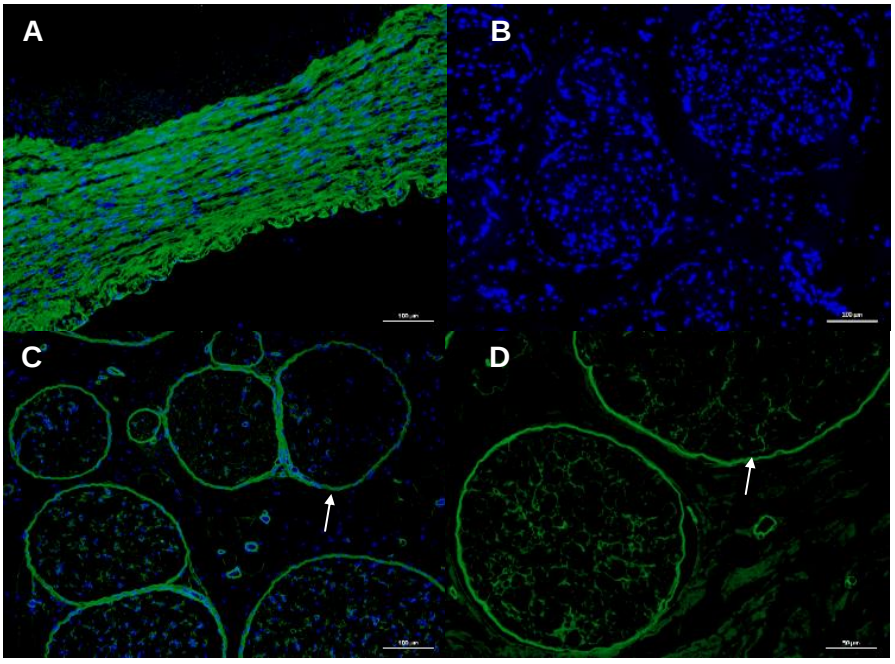

Figure 3.6 Immunofluorescent labelling of collagen type IV in sections of porcine peripheral nerve. Representative images of sections of native porcine artery labelled with a primary monoclonal antibody to collagen IV (A), native nerve sections incubated with an isotype control antibody (B) and native (C) and decellularised (D) porcine peripheral nerve sections labelled with a primary monoclonal antibody to collagen type IV, and counterstained with DAPI. Collagen type IV was present following decellularisation and labelling was most intense in the perineurium, as indicated by white arrows. Images taken using a x 10 and x 20 objective using a DAPI and FITC filter. Scale bars 100 µm (A-C) and 50 µm (D).

3.4.2.2.2 Immunofluorescent labelling of laminin

Sections of native and decellularised porcine peripheral nerve were labelled with a primary monoclonal antibody against laminin and a goat anti-mouse IgG secondary antibody (Figure 3.7). Labelling of native nerve sections revealed laminin in the endoneurium and perineurium. Within the endoneurium, where labelling was most prominent, there appeared to be discrete, fine bands of laminin forming each endoneurial tube, although some sporadic staining was observed within nerve fascicles (Figure 3.7 C & D). Laminin appeared visible in faint, thin bands along the perineurium, although labelling was not as intense as in the endoneurium. Labelling of decellularised peripheral nerve sections showed similar observations, indicating that laminin was present following decellularisation, but labelling appeared more dispersed when compared to native nerve sections (Figure 3.7 C & D). Labelling was observed throughout the smooth muscle region of the porcine femoral artery positive control, with sporadic intense labelling located along the luminal region (Figure 3.7 A). No labelling was observed in sections of native porcine peripheral nerve incubated with the isotype control antibody (Figure 3.7 B).

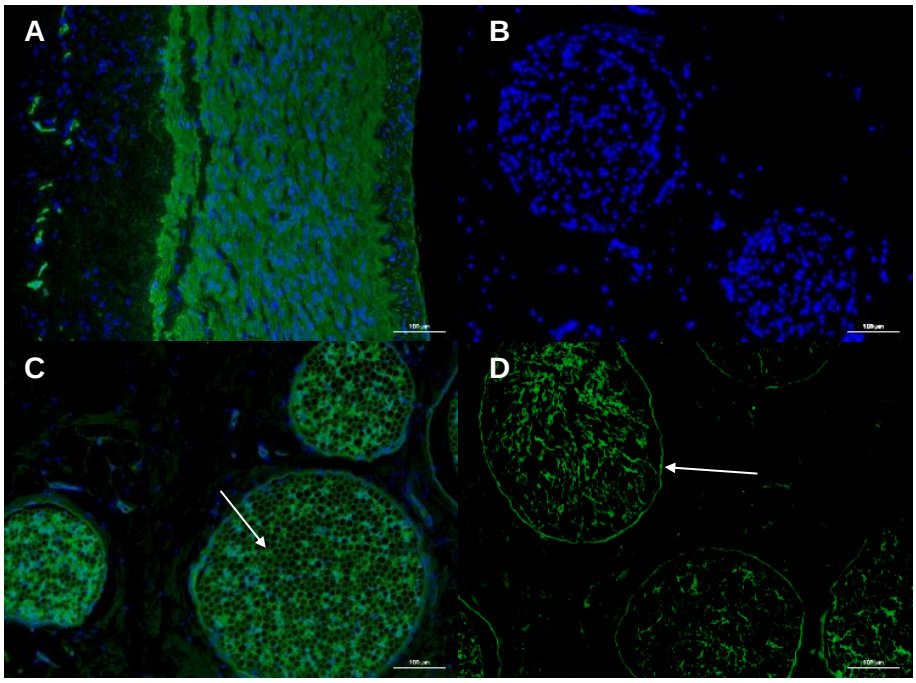

Figure 3.7 Immunofluorescent labelling of laminin in sections of porcine peripheral nerve. Representative images of native porcine artery sections labelled with a primary monoclonal antibody to laminin (A), native nerve sections incubated with an isotype control antibody (B), and native (C) and decellularised (D) porcine peripheral nerve sections labelled with a primary monoclonal antibody to laminin, and counterstained with DAPI. Laminin was present following decellularisation and labelling was most intense in the endoneurium, as indicated by white arrows. Images taken using a x 10 objective using a DAPI and FITC filter. Scale bars 100 µm.

3.4.2.2.3 Immunofluorescent labelling of fibronectin

Sections of native and decellularised porcine peripheral nerve were labelled with a primary antibody against fibronectin and a goat anti-rabbit IgG secondary antibody (Figure 3.8). Similarly to collagen type IV, fibronectin was located in both the endoneurium and perineurium, but labelling was most prevalent in the perineurium, appearing as a distinct band surrounding each fascicle (Figure 3.8 C & D). However, fibronectin labelling in the endoneurium was not as ubiquitous as collagen type IV, and fine bands of fibronectin were sporadically located around endoneurial tubes (Figure 3.8 C & D). Labelling of decellularised nerve sections revealed similar observations, with only a slight reduction in staining intensity, indicating that fibronectin was present following decellularisation (Figure 3.8 D). Labelling was observed ubiquitously along the smooth muscle region of the porcine femoral artery positive control, with intense labelling in the luminal region (Figure 3.8 A). No labelling was observed in sections of native porcine peripheral nerve incubated with the isotype control antibody (Figure 3.8 D).

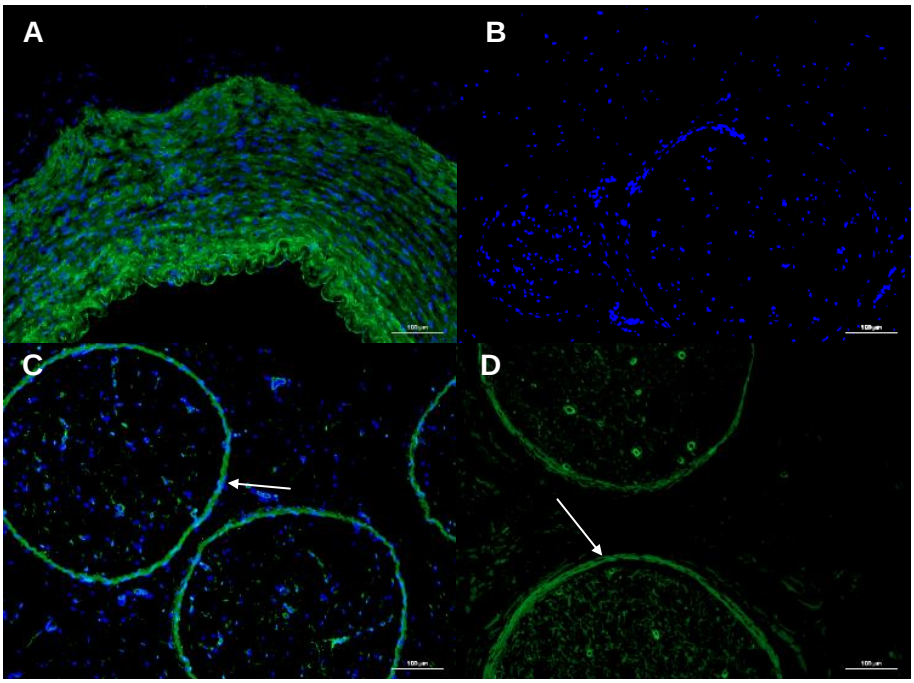

Figure 3.8 Immunofluorescent labelling of fibronectin in sections of porcine peripheral nerve. Representative images of native porcine artery sections labelled with a primary antibody to fibronectin (A), native nerve sections incubated with an isotype control antibody (B), and native (C) and decellularised (D) porcine peripheral nerve sections labelled with a primary antibody to fibronectin, and counterstained with DAPI. Fibronectin was present following decellularisation and labelling was most intense in the perineurium, as indicated by white arrows. Images taken using a x 10 objective using a DAPI and FITC filter. Scale bars 100 µm.

3.4.2.2.4 Immunofluorescent labelling of chondroitin sulphate

Sections of native and decellularised porcine peripheral nerve were labelled with a primary monoclonal antibody against chondroitin sulphate and a rabbit anti-mouse IgG secondary antibody (Figure 3.9). Labelling of native nerve sections revealed chondroitin sulphate in the endoneurium and inter-fascicular blood vessels (Figure 3.9 C). However, whereas intense labelling was observed within blood vessels, chondroitin sulphate was only located sporadically in the endoneurium (Figure 3.9 C). Labelling of decellularised nerve sections only revealed chondroitin sulphate in the endoneurium, and labelling intensity was reduced compared to native tissue, indicating the decellularisation process may have reduced chondroitin sulphate and / or affected its localisation (Figure 3.9 D). A characteristic zonal distribution of chondroitin sulphate was observed in sections of porcine cartilage labelled with the primary antibody (positive control), with intense labelling in the ECM of the deep region and cellular expression in the middle regions of the cartilage (Figure 3.9 A). No labelling was observed in sections of native porcine peripheral nerve incubated with the isotype control antibody (Figure 3.9 B).

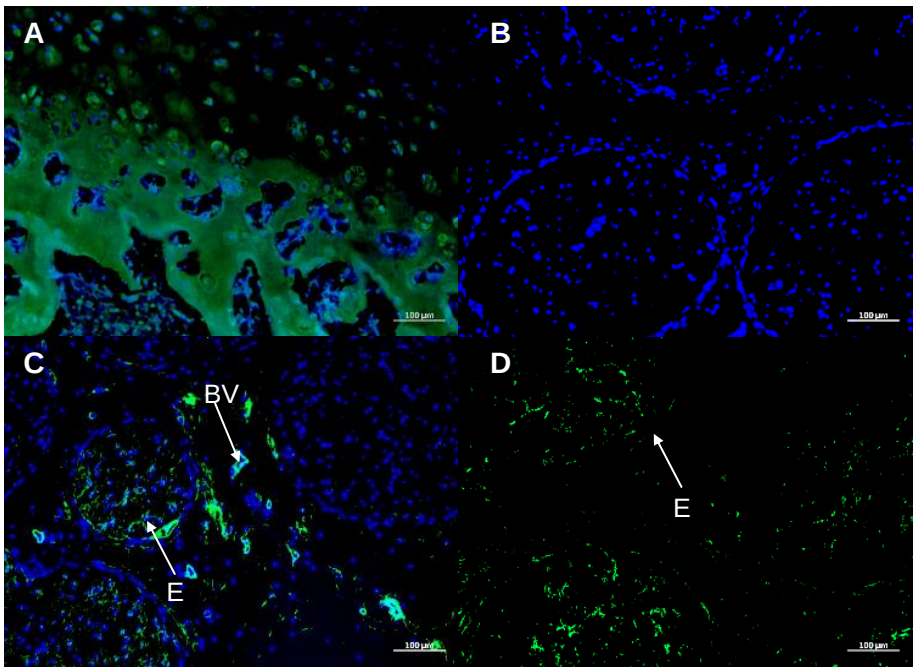

Figure 3.9 Immunofluorescent labelling of chondroitin sulphate in sections of porcine peripheral nerve. Representative images of native porcine cartilage labelled with a primary monoclonal antibody to chondroitin sulphate (A), native porcine nerve incubated with an isotype control antibody (B), and native (C) and decellularised (D) porcine peripheral nerve labelled with a primary monoclonal antibody to chondroitin sulphate and counterstained with DAPI. Chondroitin sulphate was still present following decellularisationLabels added to identify ECM structures, EN = endoneurium and BV = blood vessels. Images taken using a x 10 objective using DAPI and FITC filters. Scale bars 100 μm.

3.4.2.3 Biochemical analysis

3.4.2.3.1 Quantification of collagen content

The collagen content of native and decellularised porcine peripheral nerve samples was determined following tissue hydrolysis and hydroxyproline assay. Hydroxyproline content of hydrolysed samples was quantified using a linear regression of a trans-4-hydroxy-L-proline standard curve (Figure 3.10 A). The hydroxyproline content of native and decellularised nerve was 36.10 ± 5.89 and 39.05 ± 11.43 µg.mg^{-1} dry weight respectively (Figure 3.10 B). These values were converted to estimate collagen content, using a previously determined conversion factor of 7.52. The collagen content of native and decellularised nerve was 271.45 ± 44.29 µg.mg^{-1} and 293.68 ± 85.98 µg.mg^{-1} respectively. No significant difference was found between the collagen content of native and decellularised peripheral nerve (Student`s t-test; p> 0.05).

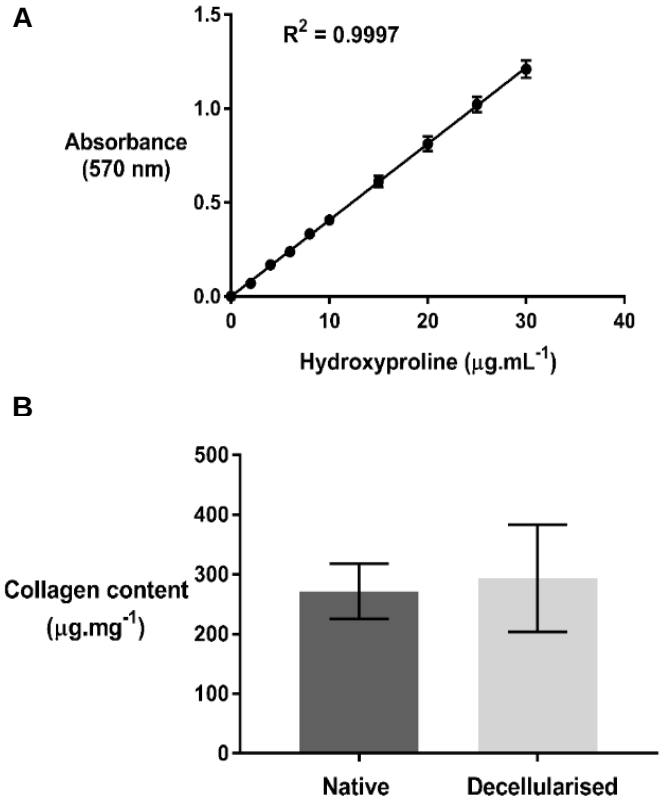

Figure 3.10 Collagen content of native and decellularised porcine peripheral nerve. (A) Standard curve of hydroxyproline concentration against absorbance at 570 nm. Data represented as mean (n = 3) ± 95 % confidence limits. (B) Estimated collagen content of native and decellularised porcine peripheral nerve. Data represented as mean (n = 6) ± 95 % confidence limits.

3.4.2.3.2 Quantification of denatured collagen content

The denatured collagen content of native and decellularised porcine peripheral nerve samples was determined by selectively digesting denatured collagen with α-chymotrypsin enzyme and collecting the supernatant for quantification using a hydroxyproline assay. Hydroxyproline content of the supernatants was quantified using a linear regression of a trans-4-hydroxy-L-proline standard curve (Figure 3.11 A). The hydroxyproline content of the denatured collagen in native and decellularised peripheral nerve was 0.65 ± 0.24 and 0.93 ± 0.31 $\mu g.mg^{-1}$ dry weight respectively, and these values were used to calculate the denatured content by using a conversion factor of 7.52 as described previously. The denatured collagen content of native and decellularised nerve was 4.96 ± 1.81 and 6.97 ± 2.37 $\mu g.mg^{-1}$ respectively (Figure 3.11 B). No significant difference was found between the denatured collagen content of native and decellularised peripheral nerve (Student` t-test; $p>0.05$).

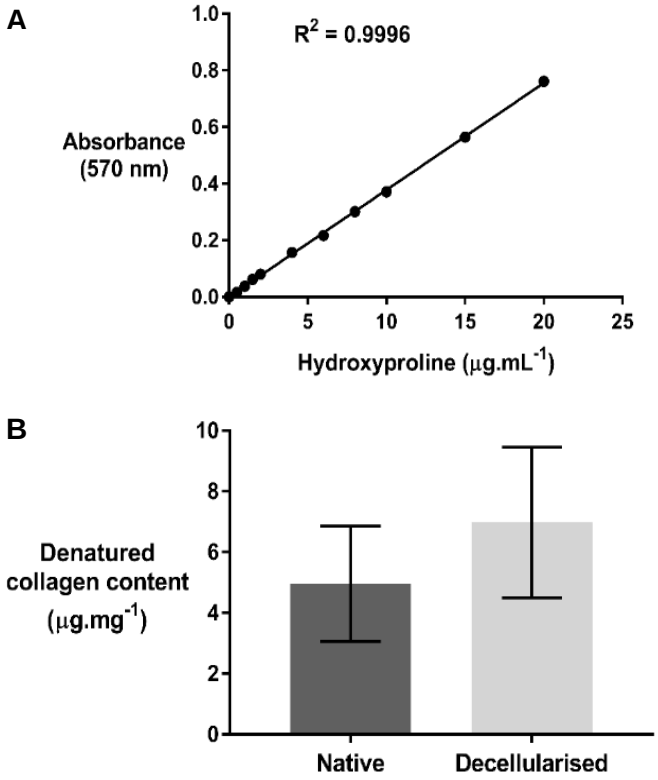

Figure 3.11 Denatured collagen content of native and decellularised porcine peripheral nerve. (A) Standard curve of hydroxyproline concentration against absorbance at 570 nm. Data represented as mean (n = 3) ± 95 % confidence limits. (B) Estimated denatured collagen content of native and decellularised porcine peripheral nerve. Data represented as mean (n = 6) ± 95 % confidence limits.

3.4.2.3.3 Quantification of fat content

The fat content of native and decellularised nerve was determined by the extraction of fat in a known volume of ethanol. The concentration of fat in the extracts was used to determine the fat content of the nerve samples, using a linear regression of a standard curve of known fat concentrations (Figure 3.12 A). The fat content of native and decellularised nerve was 639.13 ± 40.72 and 667.68 ± 58.02 µg.mg^{-1} dry weight respectively (Figure 3.12 B). No significant difference was found between the fat content of native and decellularised peripheral nerve (Student`s t-test $p>0.05$).

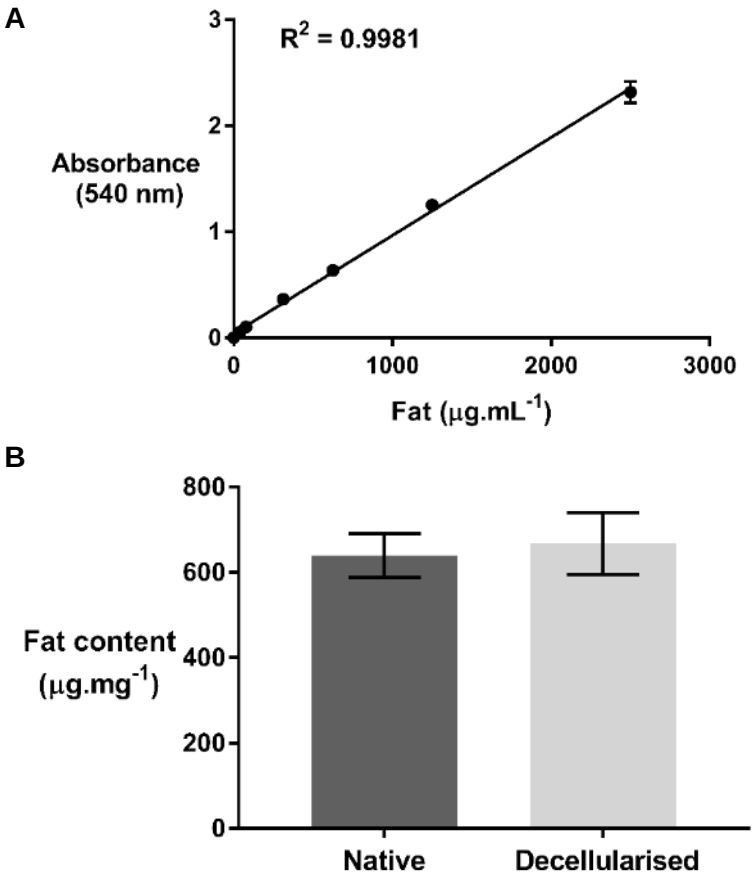

Figure 3.12 Fat content of native and decellularised porcine peripheral nerve. (A) Standard curve of fat concentration against absorbance at 540 nm. Data represented as mean (n = 3) ± 95 % confidence limits. (B) Estimated fat content of native and decellularised porcine peripheral nerve. Data represented as mean (n = 6) ± 95 % confidence limits.

3.4.2.3.4 Quantification of GAG content

The GAG content of native and decellularised nerve was determined by digestion of samples with papain and collection of the supernatant containing GAGs, followed by quantification using the dimethylene blue (DMMB) assay. The GAG content of the supernatants was quantified using a linear regression of a standard curve of chondroitin sulphate B (Figure 3.13 A). The GAG content of native and decellularised nerve was 10.16 ± 6.43 and 8.47 ± 6.27 µg.mg^{-1} dry weight respectively (Figure 3.13 B). No significant difference was found between the GAG content of native and decellularised peripheral nerve (Student`s t-test; p>0.05).

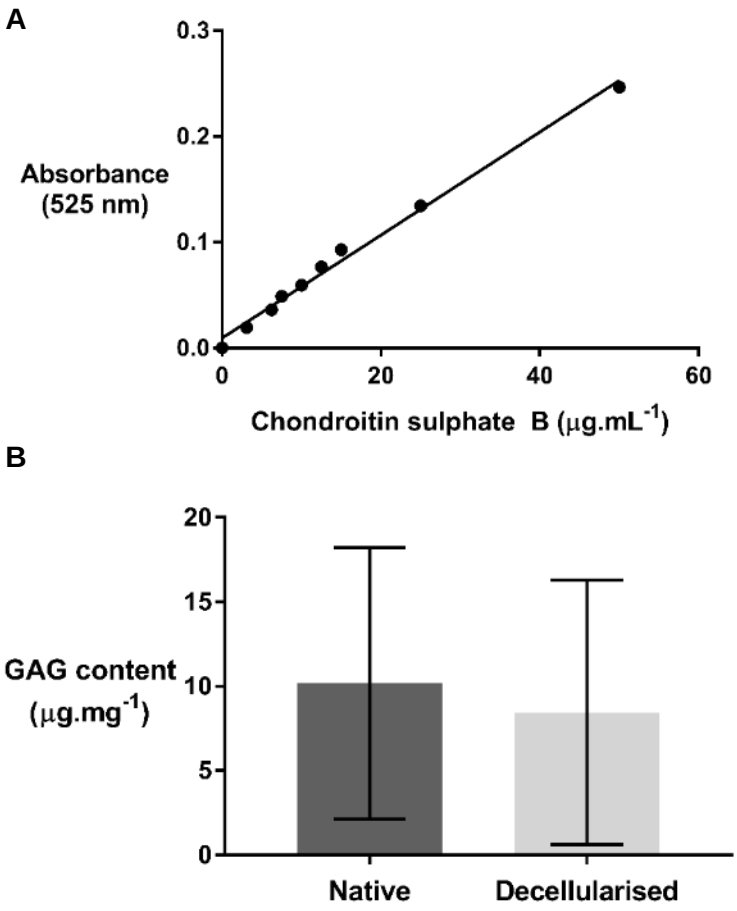

Figure 3.13 GAG content of native and decellularised porcine peripheral nerve. (A) Standard curve of chondroitin B sulphate concentration against absorbance at 570 nm. Data represented as mean (n = 3) ± 95 % confidence limits. (B) Estimated GAG content of native and decellularised porcine peripheral nerve. Data represented as mean (n = 6) ± 95 % confidence limits.

3.5 Discussion

Porcine peripheral nerves were decellularised using a combination of low concentration SDS (0.1 %; w/v), hypertonic and hypotonic buffers, Benzonase nuclease and protease inhibitors. The decellularisation protocol, described by Zilic *et al*. (2016) for porcine peripheral nerve decellularisation, was shown to sufficiently remove cellular and nuclear material and preserve key basement membrane components, however the decellularisation process resulted in structural damage to the endoneurium and perineurium. Therefore, the decellularisation process was further developed to minimise structural changes by varying the number of SDS hypotonic buffer and hypotonic buffer cycles and minimising the agitation speed during incubations.

H&E and DAPI staining of sections of porcine peripheral nerve before and after decellularisation indicated that one cycle each of hypotonic buffer and SDS hypotonic buffer was sufficient to achieve decellularisation, as no whole cell nuclei or cellular remnants were observed. However, the decellularisation process was developed for 30 mm nerve segments, and the process may need further development for the decellularisation of longer segments for large grafts. Although overall ECM architecture was preserved, some structural damage was observed in comparison to native nerve. High agitation speeds used during tissue decellularisation protocols have been reported to disrupt ECM structure (Montoya and McFetridge, 2009b), with particularly damaging effects to soft tissues, and are typically used to enhance the perfusion of decellularisation solutions rather than as a primary decellularisation mechanism (Gilbert *et al.*, 2006; Azhim *et al.*, 2014). Therefore to minimise structural damage, the agitation speed was reduced from 240 rpm to 120 rpm. H&E and DAPI staining of sections of tissues decellularised using the improved protocol at lower agitation speed indicated successful decellularisation and showed improved preservation of individual ECM structures; the epineurium, perineurium and endoneurial tubes. However, some structural differences were observed in the endoneurium in comparison to native nerve, with less definition of individual endoneurial tubes and a more irregular appearance.

The implications of these structural alterations are unclear as the topography of endoneurial tubes, which provide physical guidance to elongating axons, is one of the key advantages of decellularised nerve grafts compared to NGCs and it has been hypothesised that the inability of decellularised nerve grafts to consistently match the regeneration rates of autografts *in vivo* is due to inadequate preservation

of these structures (Whitlock *et al.*, 2009; Karabekmez *et al.*, 2009; Szynkaruk *et al.*, 2012). However, porcine peripheral nerve decellularised using the protocol described by Zilic *et al*. (2016) has been shown to support axon regeneration *in vivo* in a rat sciatic nerve defect model, and the histological results shown here demonstrate improved preservation of ECM structures following development of the decellularisation process. Furthermore, the structural changes were similar to those observed in other decellularised peripheral nerve grafts, including the Avance® graft (Inc, 2013). Chemical detergents, including SDS and Triton X-100 can disrupt ECM proteins, affecting histioarchitecture and biomechanical properties (White *et al.*, 2017). Low concentration SDS was chosen here rather than Triton X-100, the principal detergent used to produce the Avance® graft, due to superior efficacy in the removal of cellular material, and low concentration SDS has previously been shown to cause less alteration to the biomechanical properties of soft tissues than Triton X-100 (Grauss *et al.*, 2003; Liao *et al.*, 2008).

Following development of the decellularisation process, the DNA content of the decellularised nerve was quantified to further evaluate the efficacy of the process. Criteria for successful decellularisation previously proposed by Crapo *et al.* (2011) are widely employed and stipulate an upper threshold of 50 ng double stranded DNA per mg (dry weight) of decellularised tissue (Crapo *et al.*, 2011). Other studies have used different criteria to determine decelularisation, including a reduction of greater than 90 % (w/v) of the native DNA content, which was used in a study of small diameter blood vessels (Fercana *et al.*, 2014). Studies have reported no adverse immune responses to decellularised tissues containing trace amounts of DNA, and many clinically available decellularised tissue products have been found to contain small residual quantities of DNA, including the Oasis™ and Restore™ products, processed from porcine small intestine submucosa (Gilbert *et al.*, 2009; Badylak, 2014). Based on these criteria, the decellularisation process developed here achieved acceptable levels of residual DNA content in the decellularised porcine peripheral nerve segments.

In addition to ensuring sufficient DNA content reduction, the decellularisation process must result in a scaffold which is biocompatible, as residual traces of detergent, EDTA and aprotinin have shown cytotoxic effects (Booth *et al.*, 2002; Phillips *et al.*, 2004; Wilshaw *et al.*, 2012). SDS has been shown to have cytotoxic effects when not sufficiently removed from decellularised tissues, and can impart a negative charge and denature proteins, which may inhibit cell attachment and viability (Rieder *et al.*, 2004; Seddon *et al.*, 2004). The decellularised nerves

developed here appeared to be biocompatible, with a contact cytotoxicity assay using BHK and L929 cells showing no changes in cell morphology and growth when cultured with the decellularised nerve.

Further characterisation of the decellularised porcine peripheral nerve showed that the ECM histioarchitecture, specific ECM components and biochemical composition were well preserved in comparison to native tissue.

Biochemical analysis showed that porcine peripheral nerve ECM is comprised of approximately 64 % (w/w) fat, 27 % (w/w) collagen, and 1 % (w/w) GAGs, with cell content also contributing to the residual weight. Quantification of fat content showed that fat is the main component of peripheral nerve ECM, and that the decellularisation process did not significantly alter the fat content. Although there has been little research into the function of adipose tissue in peripheral nerve ECM, it is thought that its primary function is to provide inter-fascicular protection from mechanical compression during movement (Topp and Boyd, 2012; Grinsell and Keating, 2014). Along with fat, collagens are the main components of peripheral nerve ECM, forming the overall architecture, defining the epineurium, perineurium and endoneurium, and providing mechanical strength to the nerve, protecting the axons from external stress and enabling the nerve to stretch under tension during movement (Topp and Boyd, 2012). Disruption to collagen structure and configuration can be caused by physical and / or chemical treatments, particularly the use of detergents which may denature collagen fibrils, and the removal of cells from tissue causes the ECM to loosen (Gilbert *et al.*, 2006; White *et al.*, 2017). Biochemical analysis revealed that approximately 30 % of the dry weight of native nerve was collagen, and that the decellularisation process did not significantly alter the collagen content. Furthermore, the denatured collagen content of decellularised peripheral nerve was not significantly different from native nerve.

Histological evaluation of the decellularised porcine peripheral nerve sections did, however, reveal some alterations to collagen structures. In comparison to native nerve sections, the network configuration of collagen in the inter-fascicular epineurium appeared looser and more sporadic, similar to the results described by Zilic *et al.* (2016), although in contrast to the results reported by Zilic *et al.* (2016) the structural disruption of collagen appeared to be confined to the epineurium, with a clearly defined, tightly aligned perineurium and a less fragmented endoneurium (Zilic *et al.*, 2015; Zilic *et al.*, 2016). Furthermore, decellularisation did not appear to

affect the distribution of fine and thicker collagen fibril networks across the ECM layers.

Depending on tissue type, a degree of structural disruption is often necessary to ensure sufficient cell removal during decellularisation, and the enhanced porosity of a loosened ECM may facilitate cellular infiltration and graft integration (Colen *et al.*, 2009; Faulk *et al.*, 2014b; Koch *et al.*, 2015). Although increased porosity in the epineurium of porcine peripheral nerve may be well tolerated upon implantation, the presence of individual endoneurial tubes confining myelinated and unmyelinated axons would ensure appropriate target innervation, and avoid axon deviation which can form whorls within the nerve and cause painful neuromas (Burnett and Zager, 2004). As such, the development of NGCs often focuses on stimulating directional axon growth by optimising scaffold porosity and utilising patterning techniques within the conduit (Siemionow and Brzezicki, 2009; De Luca *et al.*, 2014). However, similar to studies investigating recellularisation of the Avance® graft, which also reported alterations to the collagen structure, Zilic *et al.* (2016) demonstrated that the decellularised porcine peripheral nerve graft was able to support the attachment and migration of Schwann cells both *in vitro* and *in vivo* (Whitlock *et al.*, 2009; Johnson *et al.*, 2011).

The basement membrane, located in the endoneurium and perineurium, facilitates cell-matrix interactions, enabling Schwann cell adhesion and promoting axon elongation and maturation in the endoneurium (Kerns, 2008). In addition, it has been shown that the basement membrane is required for Schwann cells to form Bands of Bungner, which rapidly switch phenotype and assemble into longitudinal bands following injury, serving as a conduit to guide regenerating axons (Gaudet *et al.*, 2011; Allodi *et al.*, 2012). Immunofluorescent labelling showed that the specific basement membrane components laminin, fibronectin and collagen type IV were preserved following decellularisation, however antibody labelling intensity was reduced in comparison to native nerve.

Many of the methods used to decellularise peripheral nerve, including chemical and thermal decellularisation processes, have been shown to induce significant damage to the basement membrane (Sondell *et al.*, 1998; Evans *et al.*, 1998; Krekoski *et al.*, 2001). The decellularisation process developed by Sondell *et al*. (1998), which utilised 3 % (v/v) Triton X-100, has been shown to cause a reduction in the laminin and fibronectin content, whereas the milder detergent method developed by Hudson *et al*. (2004), licenced for the production of the Avance® graft, using

sulfobeteine 10 (125 mM) and sulfobetaine 16 (0.6 mM) in combination with 0.14 % (v/v) Triton X-200 has demonstrated superior preservation of the basement membrane (Sondell *et al.*, 1998; Hudson *et al.*, 2004a). A comparative study of these decellularisation processes showed superior axon regeneration using the Hudson method, with significantly higher axon densities, and this was attributed to the presence of an intact basement membrane (Hudson *et al.*, 2004b). In addition, another study comparing nerve decellularised using the Hudson method and NeuraGen®, a clinically available collagen type I NGC, demonstrated a significantly greater axon regeneration rate using the decellularised nerve graft (Hudson *et al.*, 2004a; Karabekmez *et al.*, 2009). As such, it is hypothesised that decellularised nerve grafts support axon regeneration through the provision of endoneurial tubes with an intact basement membrane. One of the main limitations to the currently available NGCs is the lack of ECM architecture and specific basement membrane components, and the development of NGCs often focuses on supplementation with basement membrane factors, such as the incorporation of laminin (Bellamkonda, 2006; de Ruiter *et al.*, 2009).

The reduction in antibody labelling intensity for collagen IV, laminin and fibronectin following decellularisation may be explained by the alterations to the collagenous structure, through the disruption of collagenous basement membrane components. Similar alterations to the basement membrane have also been shown for various other tissues decellularised using the low concentration (0.1 %; w/v) SDS protocol patented by the University of Leeds (Wilshaw *et al.*, 2012; Zilic *et al.*, 2016; Helliwell *et al.*, 2017; Jones *et al.*, 2017). Studies of porcine pulmonary heart valves, dermis and human pulmonary and aortic valves have reported a reduction in labelling intensity for laminin and collagen type IV, however decellularised porcine aortic roots demonstrated functional biocompatibility and cellular repopulation *in vivo* in a sheep model (Paniagua Gutierrez *et al.*, 2014).

Glycosaminoglycans (GAGs) have various functions in peripheral nerve ECM, implicated in the maintenance of other ECM molecules, structural integrity and the regulation of cellular growth, and are located in the basement membrane (Krekoski *et al.*, 2001; Zuo *et al.*, 2002; Neubauer *et al.*, 2007). The quantity and distribution of GAGs in peripheral nerve has not been characterised in detail, and biochemical analysis revealed only a small quantity of GAGs in native porcine peripheral nerve ECM and a reduction, although not significant, in GAG content following decellularisation. Immunofluorescent labelling of chondroitin sulphate, one of the main GAGs present in peripheral nerve, also showed a reduction in GAG content. A

reduction in GAG content is consistent with the findings of other studies of tissues decellularised using SDS. It is hypothesised that this is due to the ionic disruption of link protein interaction with hyaluronan, leading to the disaggregation of aggrecan and hyaluronan and thus increasing GAG mobility (Kheir *et al.*, 2011). Chondroitin sulphate proteoglycans are the main proteoglycans involved in the inhibition of axonal growth, and are thought to be inhibitory to the regenerative process (Krekoski *et al.*, 2001; Gao *et al.*, 2013). Therefore, a reduction in GAG content may not be detrimental to the regenerative potential of the decellularised nerve graft, and many peripheral nerve decellularisation processes, including the method used to produce Avance®, include chondroitinase ABC to remove residual chondroitin sulphate (Zuo *et al.*, 2002; Hudson *et al.*, 2004a; Wang *et al.*, 2012).

Histological analysis indicated that myelin was removed from the nerve following decellularisation. In addition to chondroitin sulphate, myelin is thought to be inhibitory to the regenerative process (Burnett and Zager, 2004). Following peripheral nerve injury, the distal segment of the severed axon degenerates following a defined pathway, termed Wallerian degeneration. This involves the breakdown of axons and associated myelin, the recruitment of macrophages to the lesion and the subsequent phagocytosis of axon and myelin debris before axon regeneration can commence (Gaudet *et al.*, 2011). Residual axon and myelin debris have been shown to inhibit axonal growth by prolonging the degenerative process, and evidence suggests axon regeneration is impaired by delayed Wallerian degeneration (Burnett and Zager, 2004). Therefore, the presence of myelin in a decellularised nerve graft may adversely affect axon regeneration, and several studies using other methods of decellularisation have shown incomplete removal of myelin. Peripheral nerve decellularised using thermal techniques, including repetitive freeze thaw and cold preservation have shown incomplete removal of cellular remnants, including myelin, and Wang et al (2016) reported residual traces of myelin sheath when rat sciatic nerve was decellularised using 1 % (v/v) Triton-X 100 and 1 % (v/v) sodium deoxycholate both in isolation and in combination (Gulati, 1988; Evans *et al.*, 1998; Wang *et al.*, 2016).

3.6 Conclusions

The porcine peripheral nerve decellularisation protocol described by Zilic *et al*. (2016) was further developed to minimise alterations to ECM architecture and composition. The developed protocol, using one cycle each of hypotonic and SDS hypotonic buffer, showed improved preservation of ECM architecture whilst meeting the criteria required for decellularisation. The decellularised peripheral nerve was biocompatible and retained the basement membrane components thought to be essential for supporting regeneration, providing a substrate to support cellular infiltration and growth. The decellularisation protocol developed here offers potential for translation to human peripheral nerves, and the development of a decellularisation process for human peripheral nerve is discussed in Chapter 4.

Chapter 4: Decellularisation and characterisation of human femoral nerves

4.1 Introduction

Decellularised peripheral nerve grafts have been produced from both allogeneic tissue, and xenogeneic tissue from a range of species, including rat, pig and rabbit (Wood *et al.*, 2014; Zilic *et al.*, 2016; Wang *et al.*, 2016). The use of porcine tissue as a source material offers considerable clinical potential as the ECM molecules, including collagens, are generally conserved from pig to human, and the use of porcine tissue ensures a consistent supply of high quality tissue (Badylak *et al.*, 2009; Badylak, 2014). However, preclinical and clinical evidence of axon regeneration only exists for decellularised allogeneic peripheral nerve grafts such as the Avance® graft, as discussed in Chapter 3 (Karabekmez *et al.*, 2009; Szynkaruk *et al.*, 2012). The use of xenogeneic tissue for decellularised tissue grafts also has several limitations, which have been discussed in Chapter 1.

Although the Avance® graft has demonstrated superior clinical efficacy to NGCs when used to treat a range of defect sizes, clinical studies using the Avance® graft have not yet demonstrated consistently superior outcomes in comparison to autografts, even in small defects (up to 30 mm) (Karabekmez *et al.*, 2009; Szynkaruk *et al.*, 2012). As discussed in Chapter 3, a potential explanation for this could be that the decellularised nerve graft has diminished regenerative capacity as a consequence of ECM disruption resulting from the decellularisation process. It has been hypothesised that inadequate preservation of ECM structures, such as endoneurial tubes, and specific ECM components including laminin and collagen type IV, impairs cellular infiltration and proliferation in a decellularised nerve graft (Whitlock *et al.*, 2009).

The porcine peripheral nerve decellularisation process developed in Chapter 3 achieved sufficient decellularisation, in terms of cell removal and DNA content reduction, and the decellularised tissue retained a native histioarchitecture, biochemical composition, and specific ECM components including collagen type IV, laminin and fibronectin. Therefore, in this chapter, the porcine peripheral nerve decellularisation protocol was translated to establish a decellularisation process for human femoral nerve.

4.2 Aims and objectives

4.2.1 Aims:

I. To develop a process for the decellularisation of human femoral nerve by translating the decellularisation process developed for porcine peripheral nerve, maintaining the efficacy of decellularisation in terms of sufficient cell removal and DNA reduction, whilst ensuring the preservation of overall histioarchitecture and major ECM structures.

II. To characterise the properties of native and decellularised human femoral nerve, and assess the effects of decellularisation on the biochemical composition and specific ECM components, including basement membrane components crucial for cell adhesion, survival and migration.

4.2.2 Objectives:

I. To apply and develop the porcine peripheral nerve decellularisation protocol to human femoral nerve segments.

II. To determine the efficacy of decellularisation of human femoral nerve segments using total DNA quantification and DAPI staining of tissue sections to assess cell removal, and determine the effects of decellularisation on histioarchitecture using H&E staining of tissue sections.

III. To determine the biocompatibility of decellularised human femoral nerve segments by contact culture using two distinct cell types, BHK and L929 cells.

IV. To determine the effects of decellularisation on specific ECM components and macroscopic structures of human femoral nerve segments, including the structure and distribution of collagens, by histological analyses.

V. To determine the effects of decellularisation on biochemical composition, by quantification of collagen, denatured collagen, fat and GAG content of native and decellularised human femoral nerve segments.

4.3 Methods and experimental approach

4.3.1 Experimental approach

The decellularisation protocol developed for porcine peripheral nerves described in Chapter 3 was initially applied to human femoral nerves (Protocol 1H). The process was further developed (Protocol 2H and 3H) to ensure sufficient decellularisation in terms of cell removal and DNA content reduction, and the preservation of overall nerve histioarchitecture and important ECM structures, such as the endoneurium. Once an improved process (Protocol 3H) had been developed, the decellularised tissue was compared with native human femoral nerve using various histological, immunohistochemical and biochemical analyses.

4.3.2 Methods

4.3.2.1 Development of a decellularisation protocol for human femoral nerve

Human femoral nerves were acquired from the NHSBT TES with appropriate ethical approval and stored as described in Chapter 2 (2.2.3.1). All human tissues were stored, tracked and disposed of in accordance with the Human Tissue Act (2004) and HTA regulations as described in Chapter 2 (Section 2.2.3.2)

4.3.2.1.1 Application of porcine peripheral nerve decellularisation protocol to human femoral nerve segments (Protocol 1H)

Human femoral nerves were dissected from three femoral bundles, cut into 60 mm segments and stored on PBS moistened filter paper at -80 °C as described in Chapter 2 (Section 2.2.3.3). Human femoral nerve segments (n = 12) were subject to the decellularisation protocol developed for porcine peripheral nerve segments in Chapter 3, using the decellularisation solutions described in Chapter 2 (Section 2.1.8), with the modification of using Cambridge antibiotic solution in place of the disinfection solution (Table 4.1) The decellularisation process was carried out aseptically, using aseptic technique throughout in a class II safety cabinet. All decellularisation solutions were autoclaved prior to use, as described in Chapter 2 (Section 2.2.1.3). Following decellularisation, nerve segments were stored aseptically in PBS at 4 °C for up to one month.

Table 4.1 Decellularisation Protocol 1H applied to human femoral nerve segments. Each step is shown in chronological order. For details of each solution, see Chapter 2 (Section 2.2.7). Each step was carried out in a 150 mL sterile pot with 100 mL of each solution added, with horizontal agitation, and each human femoral nerve segment (60 mm) was processed in an individual pot.

Process step	Time	Temperature	Agitation
Antibiotic solution (Cambridge antibiotics)	1 hour	37 °C	120 rpm
EDTA solution (200 mM EDTA), pH 7.2 – 7.4	24 hours	4 °C	120 rpm
Hypotonic buffer *(10 mM tris, 2.7 mM EDTA, 10 10000 KIU.mL^{-1} aprotinin),* pH 8.0 – 8.2	24 hours	42 °C	120 rpm
SDS hypotonic buffer *(0.1 % w/v SDS, 10 mM tris, 2.7 mM EDTA, 10 10000 KIU.mL^{-1} aprotinin),* pH 8.0 – 8.2	24 hours	42 °C	120 rpm
PBS, pH 7.2 – 7.4 (x 3)	30 minutes	42 °C	120 rpm
PBS EDTA solution *containing aprotinin (2.7 mM EDTA, 10 10000 KIU.mL^{-1} aprotinin),* pH 7.2 – 7.4	48-56 hours	4 °C	50 rpm
PBS pH 7.2 – 7.4	30 minutes	42 °C	120 rpm
Nuclease solution *(50 mM Tris, 1 mM $MgCl_2.6H_20$, 1 U.mL^{-1} benzonase),* pH 7.5 – 7.7, (x 2)	3 hours	37 °C	50 rpm
PBS, pH 7.2 – 7.4 (x 3)	30 minutes	42 °C	120 rpm
Hypertonic buffer *(50 mM tris, 1.5 M NaCl) (pH 7.5 – 7.7)*	24	42 °C	120 rpm
PBS pH 7.2 – 7.4 (x 3)	30 minutes	42 °C	120 rpm
Storage in PBS, pH 7.2 – 7.4		4 °C	

4.3.2.1.2 Further development of the decellularisation process for human femoral nerve segments

Following histological analysis and total DNA quantification of human femoral nerve segments decellularised using Protocol 1H it was apparent that the process required further development. Two modified versions of the decellularisation protocol were therefore applied to human femoral nerve segments (n = 12 for each protocol, dissected from six femoral bundles as described previously). Protocol 2H included an additional nuclease solution incubation following the existing two nuclease solution incubations, and Protocol 3H included an additional hypertonic buffer incubation following the existing hypertonic buffer incubation (Table 4.2). Following histological analysis and DNA quantification, Protocol 3H, including an additional hypertonic buffer incubation, was identified as the improved process. Human femoral nerve segments (n = 48, dissected from 12 femoral bundles as described above), were decellularised using Protocol 3H, and subject to histological analysis, DNA quantification, immunohistochemical and biochemical evaluation.

Table 4.2 Decellularisation protocols applied to human femoral nerve segments. Number of nuclease solution incubations and hypertonic buffer incubations used as part of decellularisation protocols 1H, 2H and 3H applied to human femoral nerve segments. Each nuclease solution incubation was for 3 hours at 37 °C, with agitation at 50 rpm, and each hypertonic buffer incubation was for 24 hours at 42 °C, with agitation at 240 rpm, as described in Table 4.1.

Protocol	Number of nuclease solution incubations	Number of hypertonic buffer incubations
Protocol 1H	2	1
Protocol 2H	3	1
Protocol 3H	2	2

4.3.2.1.3 Histological analysis

Decellularised human femoral nerve segments subjected to each decellularisation protocol (n = 3) were evaluated and compared to native nerve (n = 3) using histology to assess the efficacy and reproducibility of the decellularisation protocol. Decellularised nerve segments were cut into three (20 mm) segments, in order to analyse both the middle and end areas of the nerve. Samples of native and decellularised nerve were fixed in 10 % (w/v) NBF, processed and embedded in paraffin wax as described in Chapter 2 (Section 2.2.4.1). Wax blocks of native (n = 3), and middle (n = 3) and end (n = 3) regions of decellularised nerve were

sectioned (5 µm thickness) as described in Chapter 2 (Section 2.2.4.2). Sections were stained using H&E (n = 3) or DAPI (n = 3) as described in Chapter 2 (Sections 2.2.5.1 and 2.2.5.2 respectively). H&E staining was used to assess overall histioarchitecture and the preservation of major ECM structures, and DAPI staining to assess cell removal by visualising whole cell nuclei or cell remnants. Images presented are of the middle regions of native and decellularised nerve segments.

4.3.2.1.4 DNA content of native and decellularised human femoral nerve segments

The efficacy and reproducibility of decellularisation, in terms of sufficient reduction in DNA content, was determined by DNA extraction and quantification. Whole segments of native (n = 6) and decellularised (n = 6) nerve were lyophilised to a constant weight prior to DNA extraction and spectrophotometric quantification as described in Chapter 2 (Sections 2.2.7.1 – 2.2.7.3). The double stranded DNA (dsDNA) content the same DNA samples was also determined using the PicoGreen assay, as described in Chapter 2 (Section 2.2.8.4).

4.3.2.1.5 Biocompatibility of decellularised human femoral nerve segments

The biocompatibility of human femoral nerve segments decellularised using Protocol 3H was investigated using the contact cytotoxicity assay, as described in Chapter 2 (Section 2.2.10), using BHK cells (n = 3) and L929 cells (n = 3). Cyanoacrylate contact adhesive was used as a positive control for cytotoxicity, and surgical closure strips (SteriStrips) were used as a negative control. Biocompatibility was assessed by examining cell growth up to and in contact with the samples after 48 hours in culture.

4.3.2.2 Characterisation of native and decellularised human femoral nerve segments

Various histological, immunohistochemical and biochemical analyses were used to characterise the properties of native (n = 6) and decellularised (n = 6) human femoral nerve segments, and assess the effects of decellularisation Protocol 3H on the ECM histioarchitecture and specific ECM components.

4.3.2.2.1 Histological analysis

Native (n = 3) and decellularised (n = 3) nerve segments were cut into three 20 mm segments as described previously, and fixed in 10 % (w/v) NBF, processed and embedded in paraffin wax as described in Chapter 2 (Section 2.2.4.1). Wax blocks were sectioned (5 µm thickness) as described in Chapter 2 (Section 2.2.4.2), and processed for histological analysis, or analysis by immunofluorescent labelling. Images presented are of the middle regions of native and decellularised nerve segments.

4.3.2.2.2 Histological stains

Sections were stained using Sirius red / Miller's elastin and Sirius red / Luxol fast blue, as described in Chapter 2 (Sections 2.2.5.3 and 2.2.5.4 respectively). Sirius red staining was used to assess overall collagen structure, and imaged under circularly polarised light to examine collagen fibril configuration and distribution. Miller's stain was used to stain elastin, and Luxol fast blue was used to stain myelin.

4.3.2.2.3 Immunofluorescent labelling of specific ECM components

For immunofluorescent labelling, sections of native and decellularised nerve were labelled with primary antibodies specific for collagen IV, laminin, fibronectin and chondroitin sulphate, as described in Chapter 2 (Section 2.2.6), and Chapter 3 (Table 3.3). Sections of native and decellularised nerve were also incubated with isotype control antibodies, and sections of native human femoral artery were used as positive controls. Omission of primary antibodies served as negative controls.

4.3.2.2.4 Biochemical analysis

The biochemical composition of native (n = 6) and decellularised (n = 6) nerve segments was determined using assays to quantify collagen, denatured collagen, fat and GAG content as described in Chapter 2 (Section 2.2.8).

4.4 Results

4.4.1 Development of a decellularisation protocol for human femoral nerve

4.4.1.1 Application of Protocol 1H

The decellularisation process developed for porcine peripheral nerve in Chapter 3, with one modification (use of Cambridge antibiotic solution; Table 4.1) was applied to human femoral nerve segments. H&E staining of native and decellularised tissue sections was used to assess overall histioarchitectue and cell removal. DAPI staining of native and decellularised tissue sections was used to assess cell removal by visualising whole cell nuclei or nuclear remnants.

Sections of native human femoral nerve stained with H&E and DAPI are shown in Figure 4.1. Observations of the H&E stained sections revealed regular shaped and sized endoneurial tubes, although the size and shape of fascicles varied greatly (Figure 4.1 B). The perineurium surrounding each fascicle appeared as dense, concentric bands with little variation. The inter-fascicular epineurium appeared loose and disorganised, containing inter-fascicular blood vessels (vasa nevorum). The endoneurium, perineurium and inter-fascicular blood vessels contained dense, evenly distributed cell populations, whereas cells in the inter-fascicular epineurium were sporadically distributed (Figure 4.1 B). Observations of DAPI stained tissue sections showed that no whole nuclei were present following decellularisation (Figure 4.1 A & C). However, observations of H&E stained sections indicated differences in the decellularised nerve in comparison to native nerve (Figure 4.1 B & D). The endoneurium appeared less dense, with a more irregular structure compared to native nerve, however individual endoneurial tubes could still be observed. The perineurium of decellularised nerve appeared thinner, but remained as a discrete, intact barrier between the fascicles and epineurium.

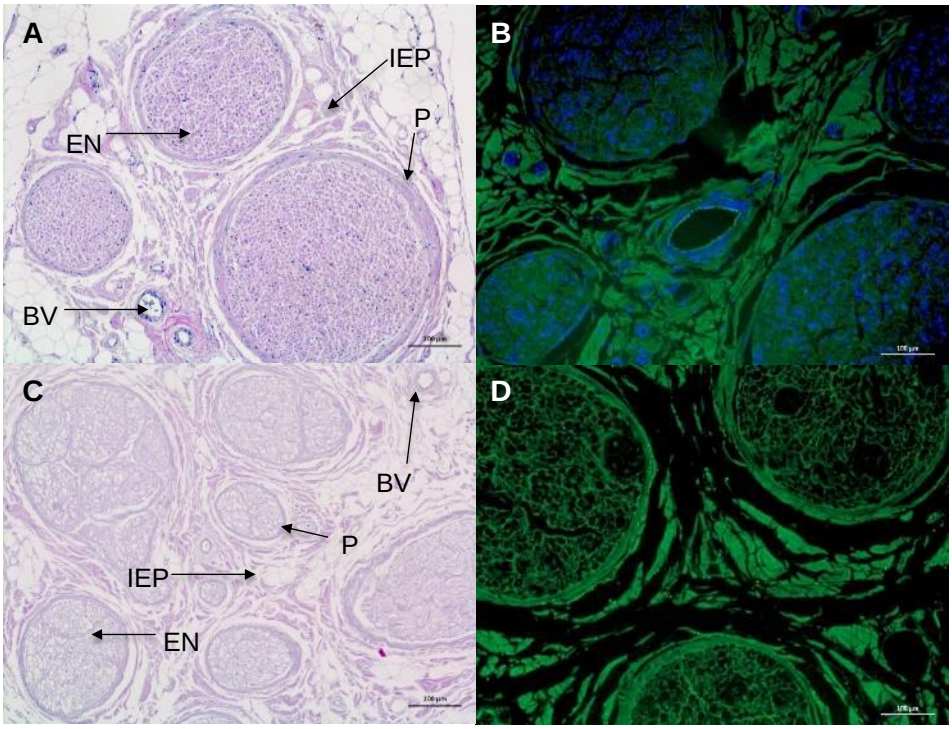

Figure 4.1 Images of sections of human femoral nerve stained with H&E and DAPI before and after decellularisation with protocol 1H.
Representative images of sections of native human femoral nerve (A & B) and human femoral nerve decellularised using Protocol 1H (C & D). Sections stained with H&E (A & C) and DAPI (B & D). Labels added to H&E images to identify ECM structures, EN = endoneurium, IEP = inter-fascicular epineurium, P = perineurium, BV = blood vessels. Major ECM structures were well preserved following decellularisation, and no whole cell nuclei were observed. H&E images acquired under Köhler illumination using a x10 objective, and DAPI images acquired using DAPI & GFP filters using a x10 objective. Scale bars = 100 µm.

4.4.1.1.1 DNA content of native and decellularised human femoral nerve

The DNA content of native and decellularised human femoral nerve was determined to assess the efficacy and reproducibility of decellularisation Protocol 1H . Following extraction, total DNA content was quantified using spectrophotometry.

The total DNA content of native and decellularised nerve was 346 ± 53 and 62 ± 45 $ng.mg^{-1}$ respectively. Since the total DNA content of the decellularised nerves was high and inconsistent, ranging from 17 - 107 $ng.mg^{-1}$, the decellularisation process was developed further.

4.4.1.2 Further development of the decellularisation protocol

Two modified versions of the decellularisation process were also applied to human femoral nerves; Protocol 2H and Protocol 3H. Protocol 2H included an additional nuclease solution incubation following the existing two nuclease solution incubations, and Protocol 3H included an additional hypertonic buffer incubation following the existing hypertonic buffer incubation.

Sections of human femoral nerves decellularised using Protocol 2H or 3H were assessed using H&E and DAPI staining (Figure 4.2). Observations of H&E stained sections showed that nerve decellularised using either Protocol 2H or 3H retained overall histioarchitecture and major ECM structures (Figure 4.3), with similar observations to nerve decellularised using Protocol 1H (Figure 4.1).

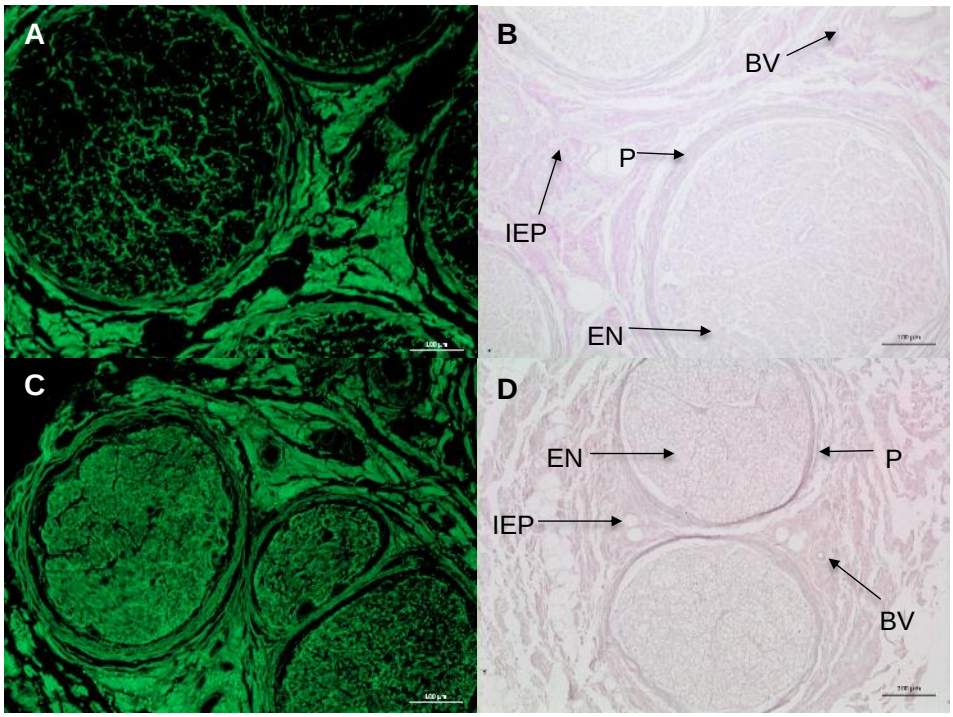

Figure 4.2 Images of sections of human femoral nerve decellularised using Protocols 2H and 3H stained with H&E and DAPI. Representative images of sections of decellularised human femoral nerve produced using Protocol 2H (A & B) and Protocol 3H (C & D). Sections stained with H&E (B & D) and DAPI (A & C). Labels added to H&E images to identify ECM structures, EN = endoneurium, IEP = inter-fascicular epineurium, P = perineurium, BV = blood vessels. Major ECM structures were well preserved following decellularisation, and no whole cell nuclei were observed. Images acquired under Köhler illumination using a x10 objective. Scale bars = 100 µm.

The total DNA content and double stranded DNA content of native nerve and nerve decellularised using Protocols 1H, 2H and 3H was quantified. The results are presented in Table 4.3. Calf thymus DNA was used to create a standard curve to assess the accuracy of the spectrophotometer (Figure 4.3 A), and lambda DNA was used to create a standard curve to interpolate unknown values to quantify double stranded DNA (Figure 4.3 B).

Statistical analysis of total DNA content by one-way ANOVA with Tukey's post hoc test showed that there were significant differences between the mean total DNA content of native nerve and nerve decellularised using protocols 1H, 2H and 3H ($p < 0.0001$). However, there were no significant differences between the mean total DNA content of nerve decellularised using protocols 1H, 2H and 3H ($p > 0.05$).

Statistical analysis of average double stranded DNA content by one-way ANOVA showed that there was a significant difference between the average double stranded DNA content of native nerve and nerve decellularised using protocol 2H ($p < 0.0001$) and between the average double stranded DNA content of native nerve and nerve decellularised using protocol 3H ($p < 0.0001$). However, there was no significant difference between the average double stranded DNA content of nerve decellularised using protocol 2H or 3H ($p > 0.05$).

Human femoral nerve segments decellularised using Protocol 3H were found to have a lower total and double stranded DNA content than nerve decellularised using Protocols 1H or 2H with less variability (Table 4.3). Therefore, Protocol 3H was identified as the improved process, and human femoral nerve segments decellularised using Protocol 3H were subject to further analysis.

Table 4.3 Quantification of the DNA content of native and decellularised nerve. Mean total DNA content (ng.mg^{-1}) and mean double stranded DNA (dsDNA) content (ng.mg^{-1}) of native nerve (n = 6) and nerve decellularised using Protocol 1H, 2H or 3H (n = 6 each). Data is presented as the mean ± 95% confidence limits. Statistical analysis content was by one-way ANOVA with Tukey's post hoc test ($p < 0.05$).

	Average total DNA content (ng.mg^{-1})	**Average dsDNA content (ng.mg^{-1})**
Native nerve	357 ± 58	244 ± 33
Protocol 1H	69 ± 37	*
Protocol 2H	43 ± 16	3 ± 1
Protocol 3H	26 ± 5	2 ± 1

* Mean dsDNA content of nerve decellularised using Protocol 1H was not quantified as the total DNA content was high and inconsistent

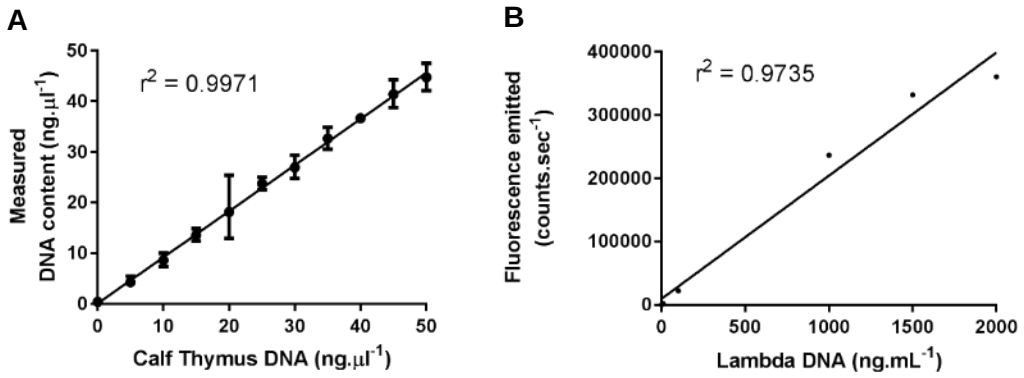

Figure 4.3 DNA content of calf thymus and lambda DNA standards. Linear relationship between calf thymus DNA concentration and measured DNA content of calf thymus DNA standards. (B) Standard curve of lambda DNA concentration against fluorescence emitted. Data represented as mean (n = 3) ± 95 % confidence limits.

4.4.1.3 Biocompatibility of decellularised human femoral nerve

The biocompatibility of human femoral nerve decellularised using Protocol 3H was assessed using a contact cytotoxicity assay with two distinct cell lines, BHK and L929 (Figure 4.4). Cells cultured with cyanoacrylate adhesive, the positive control, were sparsely distributed and most cell were not adhered, indicating cell death (Figure 4.4 A & B). Both BHK and L929 cells cultured with SteriStrips, the negative control, and samples of decellularised nerve grew up to and in contact with the samples, and displayed normal morphological characteristics. L929 cells displayed an elongated, spindle morphology and BHK cells displayed a more rounded morphology and a denser population (Figure 4.4 C-F).

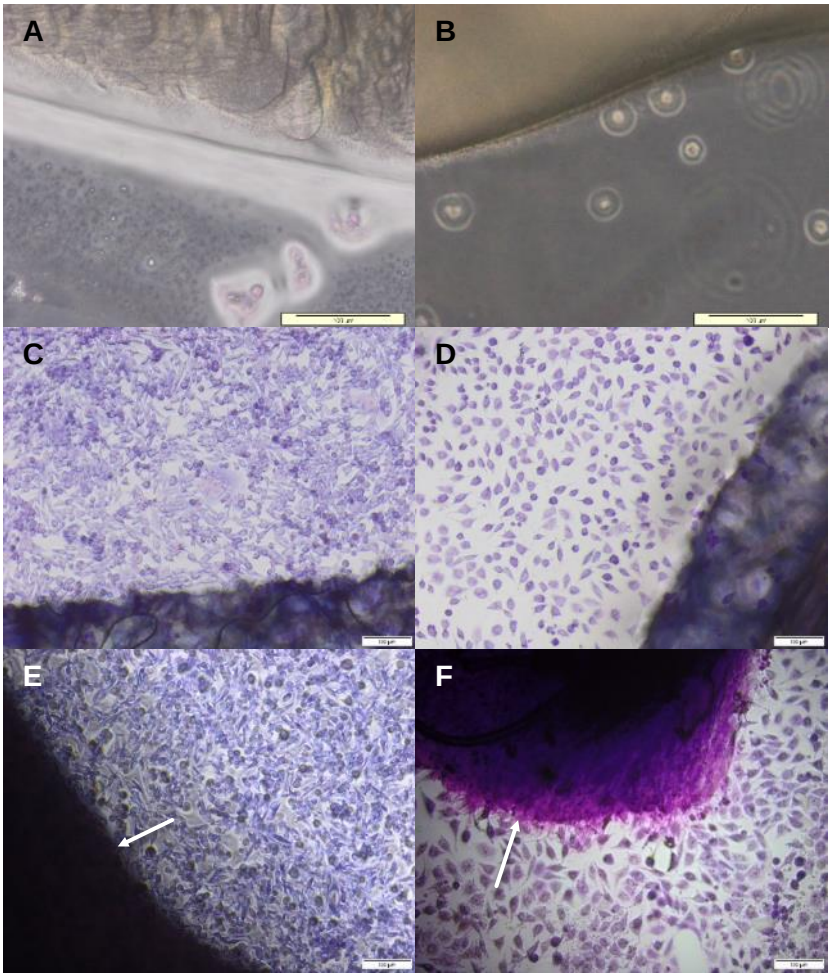

Figure 4.4 Contact cytotoxicity assay of decellularised human femoral nerve. BHK cells (A, C & E), and L929 cells (B, D, & F) were cultured with either cyanoacrylate adhesive (A & B) to serve as a positive control, SteriStrips (C & D) to serve as a negative control, or 5 mm^2 segments of decellularised human femoral nerve (n = 3) (E & F). White arrows indicate position of decellularised nerve (E & F). Both cell types grew up to and in contact with the tissue, and displayed normal morphological characteristics. Images acquired under brightfield illumination using a x10 objective. Scale bars 100 µm.

4.4.2 Characterisation of native and decellularised human femoral nerve

4.4.2.1 Histological analysis

Picro-sirius red was used to stain collagen fibres within sections of native and decellularised nerve, whilst Miller's solution was used to stain elastin fibres (Figure 4.5 A – D). Visualisation under normal Kohler illumination revealed fine collagen fibres forming the endoneurial tubes of native nerve, and thicker, discrete bands forming the perineurium (Figure 4.5 A). The collagen appeared to form dense, regular networks in the inter-fascicular epineurium.

In comparison to native nerve, the collagen in the inter-fascicular epineurium of the native nerve appeared more disorganised and fragmented, and the collagen forming the perineurium appeared thinner, although remaining as a discrete band surrounding the fascicle (Figure 4.5 B). The collagen in endoneurial tubes appeared thinner and slightly less defined, although individual endoneurial tubes were still observed. Visualisation of decellularised nerve under circularly polarised light indicated the retention of fine collagen fibril networks in the endoneurium, and a similar distribution of red, yellow and green collagen fibres between native and decellularised nerve (Figure 4.5 A & B). No elastin fibres were revealed within the native nerve, except within the blood vessels located in the inter-fascicular epineurium, and these elastin fibres were retained in decellularised nerve (Figure 4.5 A & B).

Luxol fast blue was used to stain the myelin in native and decellularised nerve, in conjunction with Picro-sirius red to stain collagen and haematoxylin to visualise cell nuclei (Figure 4.5 E & F). Myelin was only observed in the endoneurium of native nerve, within most individual endoneurial tubes (Figure 4.5 E). Myelin was not observed in decellularised nerve, indicating that the decellularisation process may have removed the myelin from human femoral nerve (Figure 4.5 F).

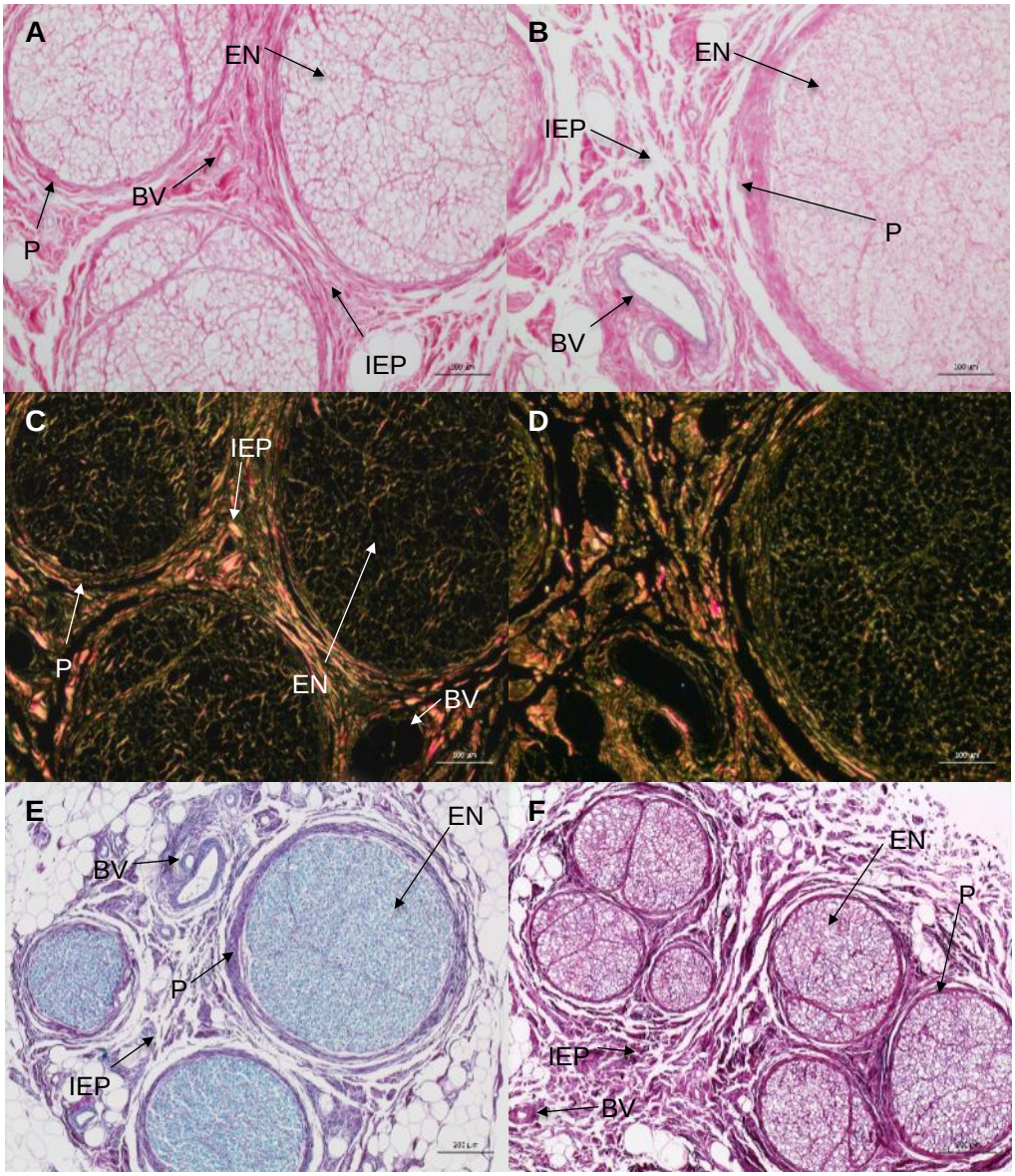

Figure 4.5 Images of sections of native and decellularised human femoral nerve stained with Sirius red / Miller's elastin and Sirius red / Luxol fast blue. Representative images of sections of native (A, C & E) and decellularised (B, D & F) nerve stained with Sirius red / Miller's elastin (A – D) or Sirius red, Luxol fast blue and haematoxylin (E & F). Sirius red imaged using normal Köhler illumination (A & B) or circularly polarised light (C & D). The structure and distribution of collagen appeared to be well preserved following decellularisation, and the decellularisation process appeared to remove myelin from the nerve. Labels added to H&E images to identify ECM structures, EN = endoneurium, IEP = inter-fascicular epineurium, P = perineurium, BV = blood vessels. Images taken using a x 10 objective. Scale bars 100 μm.

4.4.2.2 Immunofluorescent labelling of specific ECM components

4.4.2.2.1 Immunofluorescent labelling of collagen type IV

Sections of native and decellularised human femoral nerve were labelled with a primary monoclonal antibody against collagen type IV and a goat anti-mouse IgG secondary antibody (Figure 4.6). Collagen type IV was located within the endoneurium, perineurium and blood vessels of native nerve. Collagen type IV appeared to form fine, discrete bands around individual endoneurial tubes, and dense layers in the perineurium surrounding each fascicle (Figure 4.6 C). Collagen type IV was still located in the endoneurium, perineurium and blood vessels of decellularised nerve, although labelling intensity appeared slightly reduced (Figure 4.6 D). Intense labelling was observed in the smooth muscle region of the human femoral artery positive control (Figure 4.6 A), and no labelling was observed in sections of native human femoral nerve labelled with the isotype control antibody (Figure 4.6 B).

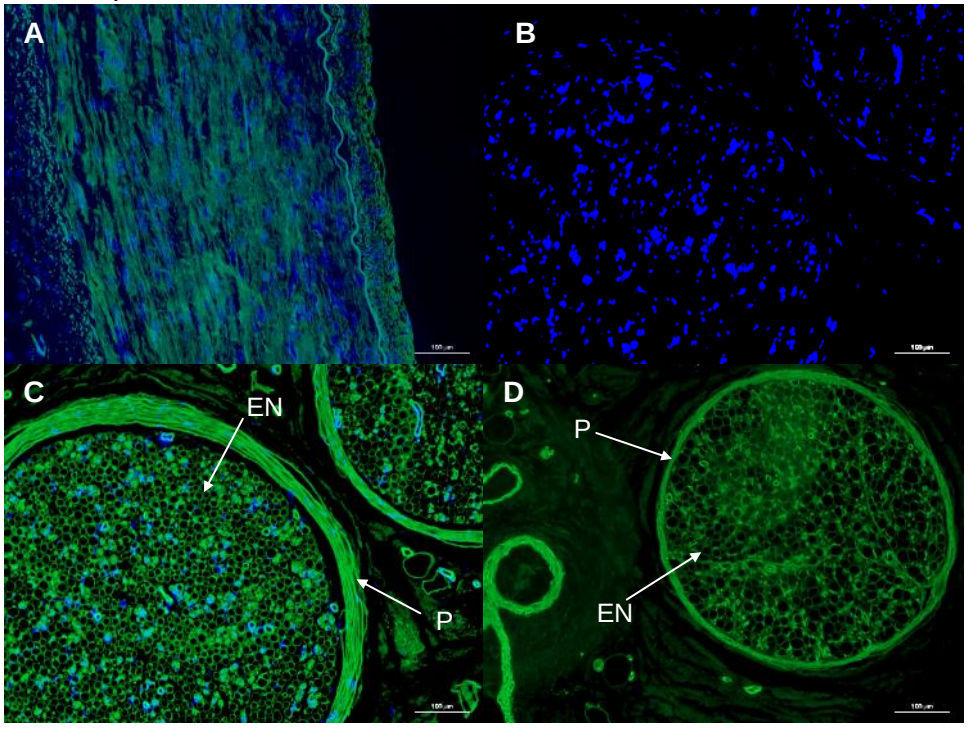

Figure 4.6 Immunofluorescent labelling of collagen type IV in sections of native and decellularised human femoral nerve. Representative images of sections of native human artery (A), native human femoral nerve incubated with an isotype control antibody (B), and native (C) and decellularised (D) human femoral nerve labelled with a primary monoclonal antibody against collagen type IV and counterstained with DAPI. Collagen type IV was still present following decellularisation and labelling was most intense in the endoneurium and perineurium. Labels added to identify ECM structures, EN = endoneurium and P = perineurium. Images taken using a x 10 objective using DAPI and FITC filters. Scale bars 100 µm

4.4.2.2.2 Immunofluorescent labelling of laminin

Sections of native and decellularised human femoral nerve were labelled with a primary monoclonal antibody against laminin, and a goat anti-mouse IgG secondary antibody (Figure 4.7). Similarly to collagen type IV, laminin was located in the endoneurium, perineurium and blood vessels of native nerve, although labelling was most intense in the endoneurium (Figure 4.7 C). Laminin appeared to form fine, discrete bands surrounding individual endoneurial tubes, although some dense, sporadic staining was also observed in the endoneurium. In the perineurium, laminin appeared as faint, thin bands surrounding fascicles. Laminin was still located in the endoneurium, perineurium and blood vessels of decellularised nerve, with clear definition of endoneurial tubes, and labelling intensity did not appear to be reduced in comparison to native nerve (Figure 4.7 D). Laminin was observed in the smooth muscle and luminal regions of the human femoral artery positive control (Figure 4.7 A), and no labelling was observed in sections of native human femoral nerve labelled with the isotype control antibody (Figure 4.7 B).

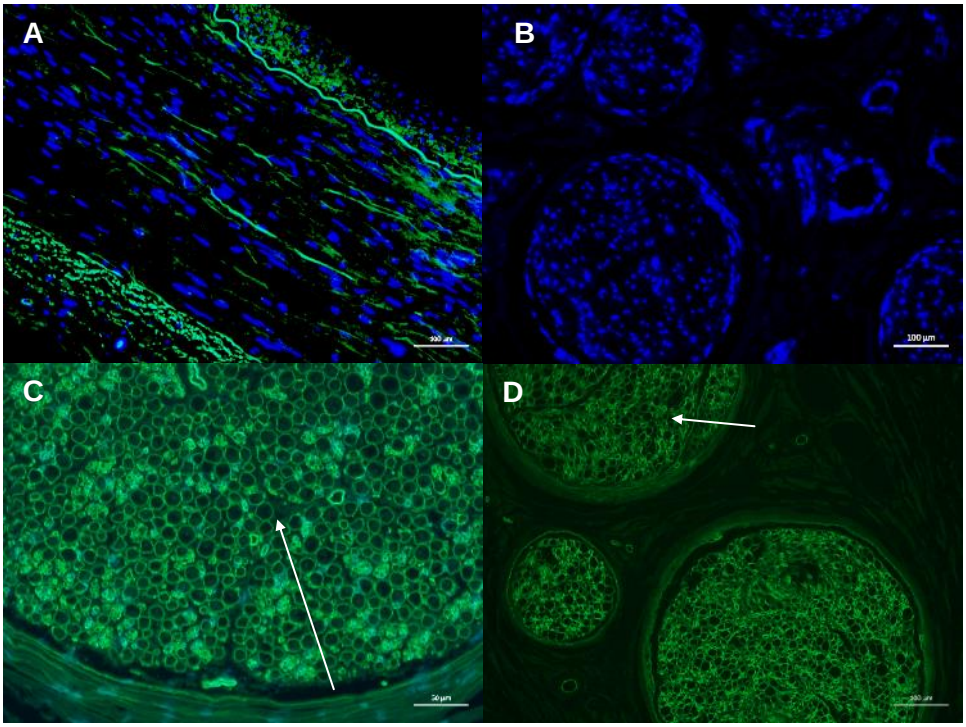

Figure 4.7 Immunofluorescent labelling of laminin in sections of native and decellularised human femoral nerve. Representative images of sections of native porcine artery sections (A), native nerve sections incubated with an isotype control antibody (B), and native (C) and decellularised (D) porcine peripheral nerve sections labelled with a primary monoclonal antibody against laminin, and counterstained with DAPI. Fibronectin was still present following decellularisation and labelling was most intense in the endoneurium, as indicated by white arrows. Images taken using a x 10 objective using a DAPI and FITC filter. Scale bars 100 µm.

4.4.2.2.3 Immunofluorescent labelling of fibronectin

Sections of native and decellularised human femoral nerve were labelled with a primary antibody against fibronectin and a goat anti-rabbit IgG secondary antibody (Figure 4.8). Fibronectin was located in the endoneurium, perineurium and blood vessels of native nerve, although labelling was most intense in the perineurium. Fibronectin appeared as a dense, discrete band in the perineurium surrounding each fascicle, whereas in the endoneurium fibronectin was sporadically located (Figure 4.8 C). Labelling of decellularised nerve showed similar observations, with fibronectin still located in the endoneurium, perineurium and blood vessels (Figure 4.8 D). Labelling was observed ubiquitiously along the smooth muscle region of the human femoral artery positive control, with sporadic labelling in the luminal region (Figure 4.8 A). No labelling was observed in sections of native human femoral nerve labelled with the isotype control antibody (Figure 4.8 B)

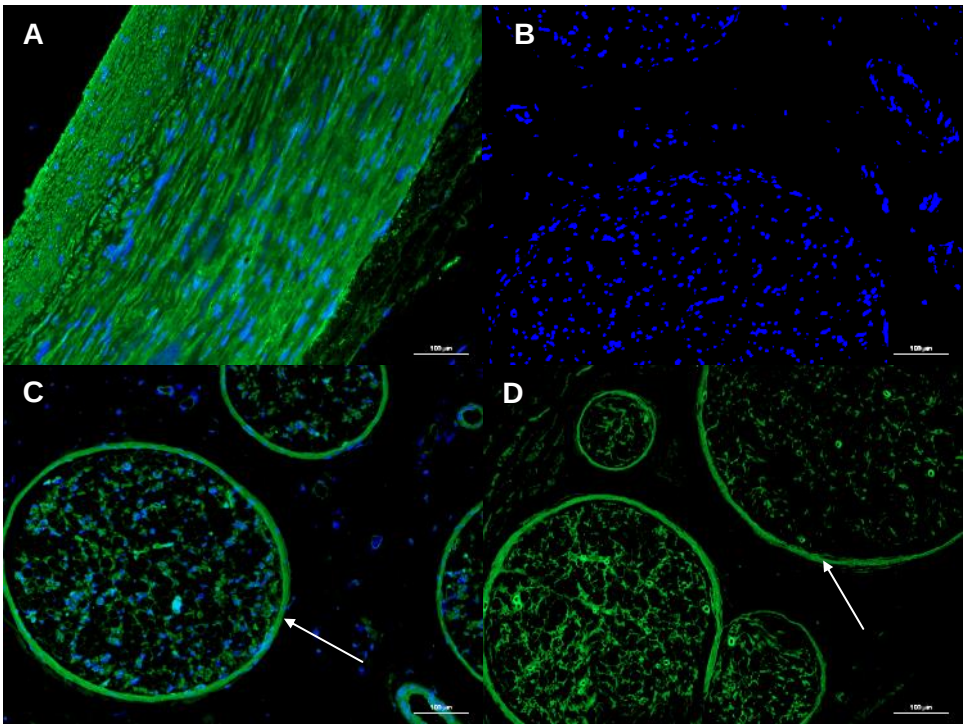

Figure 4.8 Immunofluorescent labelling of fibronectin in sections of native and decellularised human femoral nerve. Representative images of sections of native human artery (A), native human femoral nerve incubated with an isotype control antibody (B), and native (C) and decellularised (D) human femoral nerve labelled with a primary antibody against fibronectin and counterstained with DAPI. Fibronectin was still present following decellularisation and labelling was most intense in the perineurium, indicated by white arrows. Images taken using a x 10 objective using DAPI and FITC filters. Scale bars 100 μm

4.4.2.2.4 Immunofluorescent labelling of chondroitin sulphate

Sections of native and decellularised human femoral nerve were labelled with a primary monoclonal antibody against chondroitin sulphate and a rabbit anti-mouse IgG secondary antibody (Figure 4.9). Chondroitin sulphate was observed in the endoneurium and blood vessels of native nerve, although labelling was most intense in the blood vessels. Intense labelling was observed within the lumen of blood vessels of native nerve, whereas labelling was faint and sporadically located in the endoneurium (Figure 4.9 C). Chondroitin sulphate was still observed in the endoneurium and blood vessels of decellularised nerve, although labelling intensity was reduced in comparison to native nerve (Figure 4.9 D). Chondroitin sulphate was observed in both the smooth muscle and luminal regions of the human femoral artery positive control (Figure 4.9 A), and no labelling was observed in sections of native human femoral nerve labelled with the isotype control antibody (Figure 4.9 B).

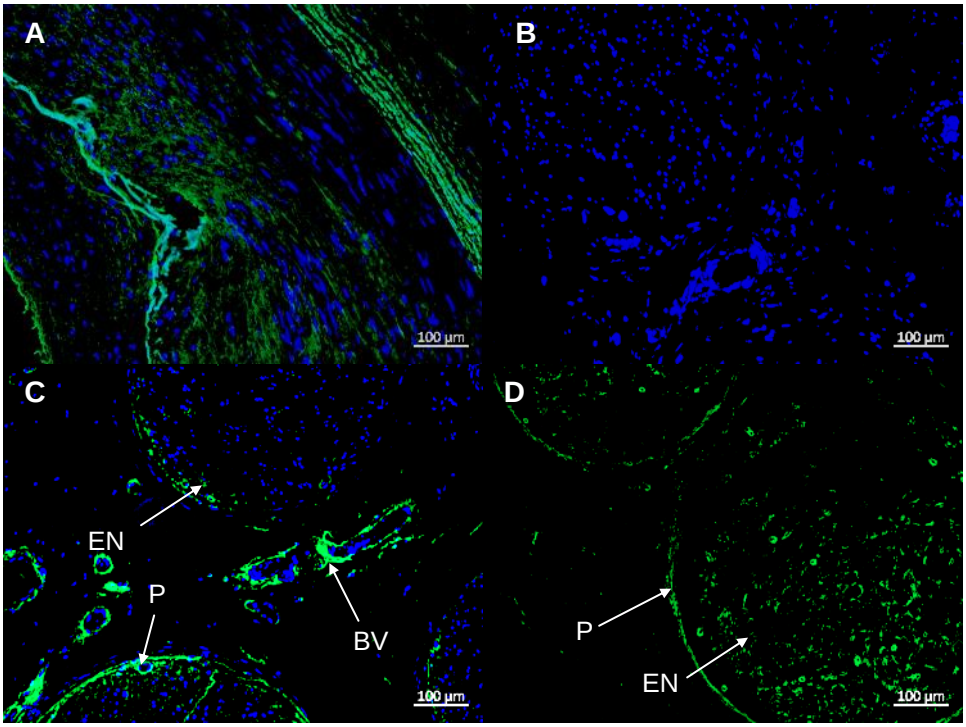

Figure 4.9 Immunofluorescent labelling of chondroitin sulphate in sections of native and decellularised human femoral nerve. Representative images of sections of native human artery (A), native human femoral nerve incubated with an isotype control antibody (B), and native (C) and decellularised (D) human femoral nerve labelled with a primary monoclonal antibody against chondroitin sulphate and counterstained with DAPI. Chondroitin sulphate was still present following decellularisation and labelling was most intense in the endoneurium, perineurium and blood vessels. Labels added to identify ECM structures, EN = endoneurium, P = perineurium and BV = blood vessels. Images taken using a x 10 objective using DAPI and FITC filters. Scale bars 100 µm

4.4.2.3 Biochemical analysis

4.4.2.3.1 Quantification of collagen content

The collagen content of native and decellularised human femoral nerve was determined following tissue hydrolysis and hydroxyproline assay. Hydroxyproline content was quantified using a linear regression of a trans-4-hydroxy-L-proline standard curve (Figure 4.10 A). The hydroxyproline content of native and decellularised nerve was 36.11 ± 2.75 and 38.12 ± 1.64 µg.mg^{-1} dry weight respectively. These values were converted to estimate collagen content, using a previously determined conversion factor of 7.52. The collagen content of native and decellularised nerve was 271.48 ± 20.75 and 286.53 ± 12.29 µg.mg^{-1} dry weight respectively (Figure 4.10 B). No significant difference was found between the collagen content of native and decellularised nerve (Student's t-test; p> 0.05).

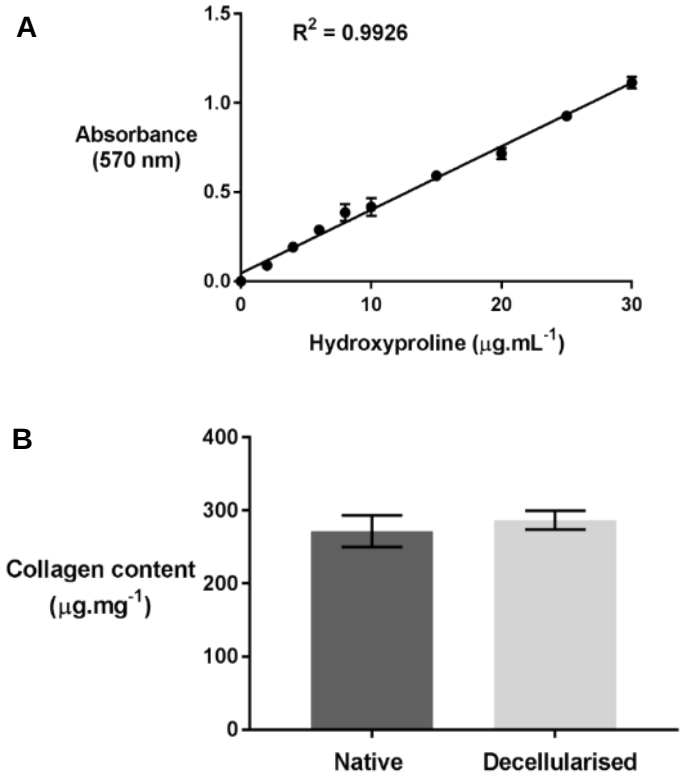

Figure 4.10 Collagen content of native and decellularised human femoral nerve. (A) Standard curve of hydroxyproline concentration against absorbance at 570 nm. Data represented as mean (n = 3) ± 95 % confidence limits. (B) Estimated collagen content of native and decellularised human femoral nerve. Data represented as mean (n = 6) ± 95 % confidence limits.

4.4.2.3.2 Quantification of denatured collagen content

The denatured collagen content of native and decellularised human femoral nerve nerve was determined by selectively digesting denatured collagen with α-chymotrypsin enzyme and collecting the supernatant containing denatured collagen prior to quantification using a hydroxyproline assay. Hydroxyproline content was quantified using a linear regression of a trans-4-hydroxy-L-proline standard curve (Figure 4.11 A). The hydroxyproline content of the denatured collagen in native and decellularised nerve was 0.51 ± 0.16 and 0.48 ± 0.15 μg.mg^{-1} dry weight respectively, and these values were used to calculate the denatured content by using a conversion factor of 7.52 as described previously. The denatured collagen content of native and decellularised nerve was 3.84 ± 1.22 and 3.66 ± 1.15 μg.mg^{-1} dry weight respectively (Figure 4.11 B). No significant difference was found between the denatured collagen content of native and decellularised nerve (Student's t-test; $p>0.05$).

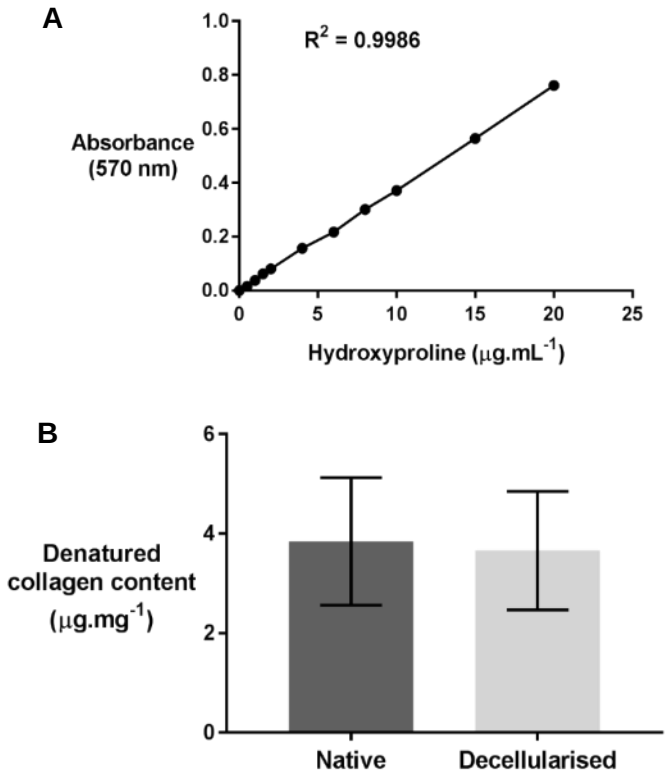

Figure 4.11 Denatured collagen content of native and decellularised human femoral nerve. (A) Standard curve of hydroxyproline concentration against absorbance at 570 nm. Data represented as mean (n = 3) ± 95 % confidence limits. (B) Estimated denatured collagen content of native and decellularised human femoral nerve. Data represented as mean (n = 6) ± 95 % confidence limits.

4.4.2.3.3 Quantification of fat content

The fat content of native and decellularised human femoral nerve was determined by the extraction of fat in a known volume of ethanol. The concentration of fat in the extracts was used to determine the fat content of the nerve samples, using a linear regression of a standard curve of known fat concentrations (Figure 4.12 A). The fat content of native and decellularised nerve was 529.71 ± 19.85 and 567.82 ± 39.84 µg.mg^{-1} dry weight respectively (Figure 4.12 B). No significant difference was found between the fat content of native and decellularised nerve (Student`s t-test $p>0.05$).

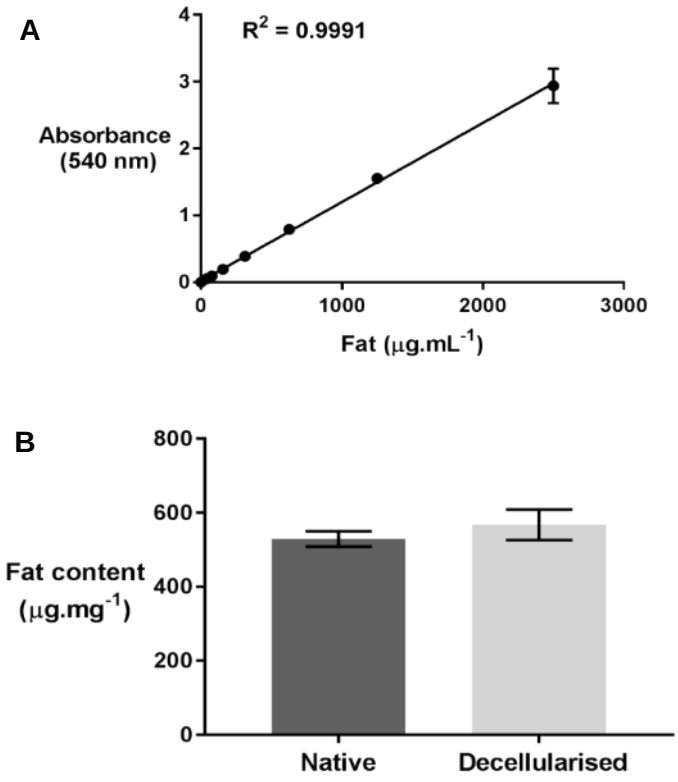

Figure 4.12 Fat content of native and decellularised human femoral nerve. (A) Standard curve of fat concentration against absorbance at 540 nm. Data represented as mean (n = 3) ± 95 % confidence limits. (B) Estimated fat content of native and decellularised human femoral nerve. Data represented as mean (n = 6) ± 95 % confidence limits.

4.4.2.3.4 Quantification of GAG content

The GAG content of native and decellularised human femoral nerve was determined by digestion of samples with papain and collection of the supernatant containing GAGs, followed by quantification using the dimethylene blue (DMMB) assay. The GAG content was quantified using a linear regression of a standard curve of chondroitin sulphate B (Figure 4.13 A). The GAG content of native and decellularised nerve was 2.25 ± 0.38 and 0.69 ± 0.43 µg.mg^{-1} dry weight respectively (Figure 4.13 B). Statistical analysis revealed a significant difference between the GAG content of native and decellularised nerve (Student's t-test, $p<0.0001$)

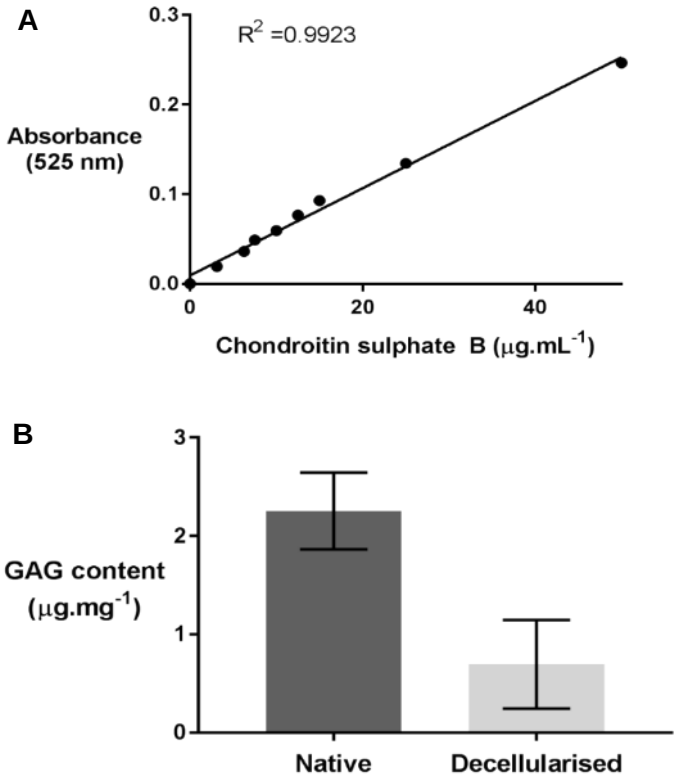

Figure 4.13 GAG content of native and decellularised human femoral nerve. (A) Standard curve of chondroitin B sulphate concentration against absorbance at 570 nm. Data represented as mean (n = 3) ± 95 % confidence limits. (B) Estimated GAG content of native and decellularised human femoral nerve. Data represented as mean (n = 6) ± 95 % confidence limits.

4.5 Discussion

The decellularisation protocol developed using 30 mm segments of porcine peripheral nerve in Chapter 3 was applied to 60 mm segments of human femoral nerve (Protocol 1H). Although 30 mm segments of decellularised nerve are generally used for both *in vitro* and *in vivo* studies of axon regeneration, 30 mm segments were considered inappropriate for human femoral nerves with the potential to be used in the clinic (Zilic *et al.*, 2016; Lovati *et al.*, 2018). Therefore, based on advice from collaborators within NHSBT TES, 60 mm segments of human femoral nerve were decellularised. The only other change to the protocol was the use of Cambridge antibiotic solution instead of disinfection solution, in order to comply with Good Manufacturing Practice (GMP) standards for human tissue processing.

H&E and DAPI staining of sections of human femoral nerve before and after decellularisation indicated that Protocol 1H achieved sufficient decellularisation, as no whole cell nuclei or cellular remnants were observed. However, the DNA content of decellularised nerve was found to be high, with a high degree of variability, indicating that the decellularisation process was not consistently removing the majority of the DNA from the tissue. This was likely due to the increase in nerve segment size, from 30 mm to 60 mm, reducing the efficacy of the decellularisation process. As H&E and DAPI staining of sections of decellularised nerve did not show any whole cell nuclei or cell remnants, the high DNA content of the decellularised nerve produced using Protocol 1H was thought to be due to insufficient removal of residual DNA fragments from the tissue. Therefore, the decellularisation process was developed further to facilitate the removal of DNA fragments from the tissue, and ensure consistent DNA content reduction. Two modified versions of the decellularisation protocols were developed, including (1) an additional nuclease treatment to digest fragments of residual DNA (Protocol 2H), and (2) an additional hypertonic buffer incubation to dissociate DNA-protein complexes within the tissue (Protocol 3H) (Gilbert *et al.*, 2006). Statistical analysis showed that there were no significant differences between the total and double stranded DNA content of decellularised nerve produced using Protocols 1H, 2H or 3H. However, the mean total and double stranded DNA content of nerve decellularised using Protocol 3H was the lowest (26 $ng.mg^{-1}$) and importantly showed very little variability between the replicates, and was therefore identified as a more robust decellularisation process.

The biocompatibility of decellularised human femoral nerve was assessed, as residual traces of detergent, EDTA and aprotinin have been shown to have cytotoxic effects, as discussed in Chapter 3 (Rieder *et al.*, 2004; Seddon *et al.*, 2004). The decellularised human femoral nerves developed here were biocompatible, with the contact cytotoxicity assay using BHK and L929 cells showing no changes in cell morphology and growth when cultured with the decellularised human femoral nerve.

Histological analysis of decellularised human femoral nerve showed that overall the ECM histioarchitecture and major ECM structures were preserved, although some structural differences were observed in comparison to native nerve. The endoneurium of decellularised nerve appeared more irregular in comparison to native nerve, with less definition of individual endoneurial tubes. The implications of these structural alterations are unclear, as the presence of a native ECM microenvironment is one of the key advantages of decellularised nerve grafts compared to NGCs (Bellamkonda, 2006; Karabekmez *et al.*, 2009; Szynkaruk *et al.*, 2012; Spivey *et al.*, 2012). The Avance® nerve graft has demonstrated consistently superior clinical outcomes to NGCs, and this is thought to be due to the provision of a native microenvironment, particularly endoneurial tubes, and it has been hypothesised that the inability of decellularised nerve grafts to consistently match the regeneration rates of autografts *in vivo* is due to inadequate preservation of endoneurial tubes (Whitlock *et al.*, 2009; Moore *et al.*, 2011; Johnson *et al.*, 2011). However, although some structural differences were observed in the endoneurium of the decellularised human femoral nerve compared to the native tissue, individual endoneurial tubes could still be identified. Furthermore, based on the histological results presented in this chapter, the endoneurial structure of the decellularised human femoral nerve may be better preserved than the endoneurial structure of the Avance® graft, with more regular, clearly defined endoneurial tubes.

Another key advantage of decellularised nerve grafts in comparison to NGCs is the provision of specific basement membrane components, as discussed in Chapter 3 (Burnett and Zager, 2004; de Ruiter *et al.*, 2009; Gaudet *et al.*, 2011). Laminin is a major component of the basement membrane, with axon-growth promoting activity and providing the adhesive stimulus for axon regeneration (Chen *et al.*, 2000; De Luca *et al.*, 2014). Immunofluorescent labelling of laminin in decellularised human femoral nerve showed that laminin was preserved following decellularisation, primarily located in the endoneurium. Similar to results demonstrated here, studies of the Avance® decellularised nerve graft have shown that laminin is preserved

following decellularisation, and a study by Yang et al. (2011) demonstrated the preservation of laminin in human peripheral nerves decellularised using Triton X-100 (46 mM) and sodium deoxycholate (96 mM) (Yang *et al.*, 2011; Wood *et al.*, 2014). Immunofluorescent labelling of native and decellularised human femoral nerve showed that basement membrane components collagen type IV and fibronectin were also preserved following decellularisation, located in the endoneurium and perineurium. Collagen type IV is a highly glycosylated collagen in the basement membrane, providing binding sites for key moieties, including laminins, enabling the cellular processes of Schwann cells and axons (Chernousov *et al.*, 2008; Yurchenco, 2011). Fibronectin is a glycoprotein component of the basement membrane, enabling the binding of cell surface proteins, such as integrins, and has been shown to stimulate Schwann cell proliferation and migration (Ahmed *et al.*, 2003; Mosahebi *et al.*, 2003). However, studies of the Avance® decellularised nerve graft, and the decellularised nerve graft produced by Yang *et al.* (2011) discussed previously, have not assessed the effect of decellularisation on collagen type IV or fibronectin (Yang *et al.*, 2011; Wood *et al.*, 2014).

Biochemical analysis showed that native human femoral nerve ECM was comprised of approximately 55 % (w/w) fat, 30 % (w/w) collagen, and 0.2 % (w/w) GAGs, similar to the biochemical composition of native porcine peripheral nerve as described in Chapter 3. However, porcine peripheral nerve contained approximately 10 % (w/w) more fat, likely due to the young age of porcine tissue in comparison to human tissue, and that pigs are commercially reared for rapid weight gain. Biochemical analysis also showed that the decellularisation process did not significantly alter the fat or collagen content of human femoral nerve. Furthermore, the denatured collagen content of decellularised human femoral nerve was not significantly different from native nerve. However, histological analysis of decellularised human femoral nerve showed some differences in collagen structure. In comparison to native nerve, the collagen in the inter-fascicular epineurium appeared more disorganised and fragmented, and the collagen forming the perineurium appeared thinner following decellularisation. The alterations to collagen structure were similar to those observed in decellularised porcine peripheral nerve, described in Chapter 3, and the results described by Zilic *et al.* (2016), although in contrast to the results reported by Zilic *et al.* (2016) the collagen disruption appeared to be confined to the epineurium and perineurium (Zilic *et al.*, 2016). As the alterations to the collagen structure of decellularised human nerve were confined to the epineurium and perineurium, this may not necessarily impair the

directional regeneration of axons in individual endoneurial tubes (Colen *et al.*, 2009; Koch *et al.*, 2015; White *et al.*, 2017).

Quantification of GAG content showed that there was a significant difference between the GAG content of native and decellularised human femoral nerve. Immunofluorescent labelling of chondroitin sulphate, one of the main GAGs present in human peripheral nerve, showed a reduction in staining intensity in sections of decellularised human femoral nerve compared to native nerve. However, as discussed in Chapter 3, no significant difference was found between the GAG content of native and decellularised porcine peripheral nerve. A reduction in GAG content is consistent with the findings of other studies of tissues decellularised using SDS, as discussed in Chapter 3. It is hypothesised that this is due to the ionic disruption of link protein interaction with hyaluronan, leading to the disaggregation of aggrecan and hyaluronan and thus increasing GAG mobility. Hypertonic buffer dissociates negatively charged DNA from proteins, and as GAGs are also negatively charged, hypertonic buffer may facilitate the removal of mobile GAGs from tissue. Therefore, as Protocol 3H included an additional hypertonic buffer incubation, this may explain the significant reduction in GAG content in decellularised human femoral nerve compared to native tissue.

Chondroitin sulphate proteoglycans (CPSGs) are the main GAGs involved in the inhibition of axonal growth, as discussed in Chapter 3 (Krekoski *et al.*, 2001). Several studies have shown that CPSGs bind to and inhibit the growth promoting activity of endoneurial laminin, and are rapidly upregulated following nerve injury, providing a non-permissive substrate for axonal growth (Zuo *et al.*, 2002; Neubauer *et al.*, 2007). However, during the degenerative process, CPSGs are subsequently degraded. As such, it has also been suggested that the degradation of CPSGs may represent a mechanism by which the growth-promoting properties of laminin may be restored, thus promoting axonal regeneration (Krekoski *et al.*, 2001; Wang *et al.*, 2012). The decellularistion process used to produce the Avance® graft includes treatment with chondroitinase ABC, a bacterial enzyme that degrades the disaccharide side-chains of CPSGs, and it has been shown that chondroitinase ABC does not affect the basement membrane or displace laminin (Braunewell *et al.*, 1995). Furthermore, it has been shown that degradation of CPSGs enhances axon regeneration in decellularised rat nerve grafts in a rat sciatic injury model, and the regeneration of axons following transection repair in a rat sciatic nerve (Krekoski *et al.*, 2001; Zuo *et al.*, 2002). Therefore, the significant reduction in GAG

content in decellularised human femoral nerve may be beneficial to promoting axonal regeneration.

Following nerve injury, Schwann cells become activated, dissociate myelin and migrate extensively. The myelin sheath fragments and associated debris are removed by phagocytosis, and residual myelin debris has been shown to inhibit axonal growth by delaying the degenerative process, as discussed in Chapter 3 (Gaudet *et al.*, 2011; Salzer, 2012). Similar to decellularised porcine peripheral nerve, the decellularisation process was shown to remove myelin from human femoral nerves, which may promote axonal regeneration (Burnett and Zager, 2004). However, other studies of decellularised human nerves, including the Avance® graft and the study of Yang *et al.* (2011), have not assessed the removal of myelin (Neubauer *et al.*, 2010; Wolford and Rodrigues, 2011; Yang *et al.*, 2011; Wood *et al.*, 2014).

4.6 Conclusions

The porcine peripheral nerve decellularisation protocol developed in Chapter 3 was further developed for human femoral nerves. The improved process was shown to achieve sufficient decellularisation, in terms of cell removal and DNA content reduction, and preserve ECM histioarchitecture. The decellularised nerve was biocompatible and retained the basement membrane components essential for supporting axon regeneration, providing a substrate to support cellular infiltration and migration. The ability of the decellularised nerve to support cellular infiltration, migration and neurite outgrowth *in vitro* is discussed in Chapter 5.

Chapter 5: Dorsal Root Ganglion (DRG) cell interaction with decellularised human femoral nerve

5.1 Introduction

The provision of a native microenvironment to support axon elongation and Schwann cell infiltration is believed to be one of the key advantages of decellularised nerve grafts in comparison to NGCs (Whitlock *et al.*, 2009; Khaing and Schmidt, 2012; Faroni *et al.*, 2015). Despite the development of a diverse array of NGCs aiming to replicate complex ECM properties, such as endoneurial topography, the majority of currently available NGCs are simple conduits with either a hollow or homogenous structure, and these NGCs have not demonstrated equivalent performance to autografts, even for the repair of small defects (up to 30 mm) (Kehoe *et al.*, 2012; Faroni *et al.*, 2015; Silva *et al.*, 2017). Recent experimental advances in the design of NGCs have included the development of highly aligned, porous scaffolds, intraluminal fillers with axially aligned channels, and the inclusion of ECM components, adhesion molecules and neurotrophic factors to provide a permissive environment for Schwann cell infiltration and axon regeneration (Gerth *et al.*, 2015; Dalamagkas *et al.*, 2016; Mobini *et al.*, 2017). NeuraGen® was the first FDA approved NGC to incorporate a luminal filler to provide three-dimensional guidance to regenerating axons and Schwann cells (Dalamagkas *et al.*, 2016). NeuraGen® is a type I collagen conduit with a luminal filler of collagen type I and axially aligned porosity to provide topographic guidance to migrating cells (Kehoe *et al.*, 2012; Dalamagkas *et al.*, 2016). However, a comparative study using both the Avance® graft and NeuraGen® for the repair of 14 mm and 28 mm rat sciatic nerve defects reported a significantly greater axon regeneration rate using the decellularised nerve graft (Whitlock *et al.*, 2009).

Currently, autografts remain the gold standard intervention, particularly for the repair of longer nerve gap defects (over 30 mm) (Whitlock *et al.*, 2009; Mobini *et al.*, 2017). It is hypothesised that this is due to the presence of Schwann cells, and that the efficacy of decellularised nerve grafts and NGCs is limited to shorter distances (up to 30 mm) due to insufficient host Schwann cell migration to sustain axon regeneration (Szynkaruk *et al.*, 2012; Gerth *et al.*, 2015; Busuttil *et al.*, 2017). As discussed in Chapter 1, Schwann cells are essential for axonal survival and function, and serve a pivotal role in orchestrating peripheral nerve repair (Jessen *et al.*, 2015; Jessen and Mirsky, 2016; López-Leal and Diaz, 2018). Following peripheral nerve injury, distal myelinating and non-myelinating Schwann cells

undergo large scale changes in gene expression and rapidly switch to a transient repair (Bungner) phenotype to support the survival of injured neurons and axonal regeneration (Jessen and Mirsky, 2016; Poplawski *et al.*, 2018; Wagstaff, 2018). The repair Schwann cells have several functions, including the up-regulation of a number of neurotrophic factors and surface proteins to promote axon survival, and pro-inflammatory cytokines to recruit macrophages to the site of injury (Jessen and Mirsky, 2016; Wagstaff, 2018). In addition, the repair Schwann cells adopt an elongated morphology, rapidly migrate and align in columns (bands of Bungner) inside endoneurial tubes, providing essential substrate and guidance cues to enable the elongation of regenerating axons towards the distal stump (Jessen and Mirsky, 2016; Ronchi and Raimondo, 2017; Wong *et al.*, 2017). However, the ability of Schwann cells and neurons to sustain axon regeneration is influenced by distance, and progressively fails over time if axon contact is not re-established due to deterioration of the distal nerve stump. This involves a decrease in Schwann cell numbers and the trophic factors initially upregulated by Schwann cells following injury (Ronchi and Raimondo, 2017; Wagstaff, 2018).

Currently, there is no *in vitro* model of peripheral nerve, and peripheral nerve regeneration cannot be replicated *in vitro*. The majority of *in vitro* studies of axonal regeneration and Schwann cell survival, migration and interaction with decellularised nerve grafts or NGCs have been performed using short-term cultures of dissociated rat primary cells, either in isolation or in co-cultures (Geuna *et al.*, 2016; Mobini *et al.*, 2017). Sensory neurons dissociated from rat dorsal root ganglion (DRG) explants are most commonly used, as they are easily isolated and sprout neurites *in vitro*. Sensory neurons can be co-cultured with primary Schwann cells to represent an *in vitro* model of peripheral nerve regeneration (De Luca *et al.*, 2015; Geuna *et al.*, 2016; Neto *et al.*, 2017). However, primary neuron cultures do not survive for a prolonged period of time in the absence of a permissive environment, which consists of a heterogeneous population of cells, including glial cells and fibroblasts (De Luca *et al.*, 2015; Geuna *et al.*, 2016).

Rat DRG explant organotypic cultures have also been used for *in vitro* studies of peripheral nerve regeneration, as rat DRGs can be easily isolated and inserted into scaffolds, and enable quantification of neurite outgrowth from the body of the DRG explant. DRG explants are also considered to be more physiologically relevant for studies of neuron interactions, because the *in vivo* three-dimensional architecture, ECM organisation, and the complex niche involving a heterogeneous population of neurons, mature Schwann cells and glial cells is preserved (Morano *et al.*, 2014;

Geuna *et al.*, 2016; Neto *et al.*, 2017). Furthermore, the appropriate spatial arrangement, connectivity and cell-cell communication between neurons, Schwann cells and glial cells is not disrupted in rat DRG explant cultures (Neto *et al.*, 2017). Although many studies of peripheral nerve regeneration have used embryonic DRG explants, extrapolation from embryonic to adult DRGs is limited since embryonic neurons differ from adult neurons in terms of axonal survival, outgrowth and gene expression (Allodi *et al.*, 2011; Neto *et al.*, 2017). Therefore, adult DRG explant cultures may better represent an *in vitro* model for the regeneration of mature axons (Fornaro *et al.*, 2008; Allodi *et al.*, 2011; Neto *et al.*, 2017).

DRG explants also contain satellite glial cells (SGCs) that form sheaths around the neuronal cell body. SGCs are thought to participate in peripheral nerve repair, however, the interaction between SGCs and decellularised nerve grafts or NGCs has not been studied (Geuna *et al.*, 2016; Kastriti and Adameyko, 2017; George *et al.*, 2018). SGCs have been described as being similar to astrocytes in the central nervous system, since they modulate neuronal activity through recycling glutamate, a neurotransmitter also involved in neuron metabolism, by converting glutamate to glutamine (Hanani, 2005; Costa and Moreira Neto, 2015; Kastriti and Adameyko, 2017). Glutamine synthetase (GS), an enzyme involved in the glutamate recycling, has previously been described as a unique marker for rat SGCs (George *et al.*, 2018). Rat SGCs have also been shown to exhibit an activated state and undergo enhanced proliferation in response to injury (George *et al.*, 2018; Dubový *et al.*, 2019). Rat SGCs have been shown to be highly plastic and can differentiate into a range of cell types including oligodendrocytes and Schwann cells, and it has been proposed that SGCs may be a population of multipotent cells that could differentiate to replace neurons in the DRG (Svenningsen *et al.*, 2004; Hanani, 2005; Weider *et al.*, 2015). Furthermore, the notion that SGCs may not be fully differentiated cells is supported by the expression of the transcription factor, Sox2 in the nuclei of SGCs, which has been described as a stem cell marker (Koike *et al.*, 2015; Weider *et al.*, 2015).

It is hypothesised that SGCs represent a population of developmentally arrested Schwann cells (George *et al.*, 2018). SGCs have been shown to express a number of markers associated with Schwann cell precursors, including adhesion molecule cadherin-19 (CDH19), which has previously been described as a unique marker for Schwann cell precursors, even in adult DRGs (George *et al.*, 2018). SGCs have been shown to differentiate into Schwann cell-like cells, transcriptionally and morphologically similar to Schwann cells, when cultured independently *in vitro*, and

are also capable of migrating and myelinating embryonic axons *in vitro* (George *et al.*, 2018). Therefore, it is thought that SGCs are a population of cells within the Schwann cell lineage whose further differentiation appears to be arrested by contact with the DRG neuronal soma, and are capable of differentiating into multiple cell types, including Schwann cell-like cells in response to injury (Weider *et al.*, 2015; Koike *et al.*, 2015; George *et al.*, 2018).

In order to investigate the ability of human decellularised nerve to support axon regeneration *in vitro*, primary adult rat DRG explants were cultured in segments of decellularised human nerve. The effects of decellularised human nerve on DRG cell viability and migration up to 28 days in culture was assessed, and neurite growth was assessed using the neuron marker neurofilament-200 (NF-200). SGCs within the DRG were also investigated by assessing changes in the expression of Sox2 and GS over 28 days in culture. In addition, Schwann cells within the DRG were also studied by assessing changes in the expression of the mature myelinating Schwann cell marker myelin basic protein (MBP) and the non-myelinating Schwann cell marker neural cell adhesion molecule-1 (NCAM-1).

As discussed previously, the linear microarchitecture of endoneurial tubes is believed to be one of the key advantages of decellularised nerve grafts in comparison to NGCs (Khaing and Schmidt, 2012; Faroni *et al.*, 2015). Previous research investigating sterilisation strategies for decellularised porcine peripheral nerve grafts (JDR Holland, unpublished data) showed that lyophilisation of porcine peripheral nerve resulted in physical damage to endoneurial structure, whilst preserving the basement membrane components laminin and collagen type IV. Therefore, lyophilised decellularised human nerve was investigated as a potential variable to assess the importance of endoneurial architecture, and DRG explants were also cultured in segments of lyophilised decellularised human nerve. In addition, DRG explants were also cultured with rat tail type I collagen hydrogels to represent a non-aligned control scaffold, and compared to DRG explants cultured in decellularised human nerve and lyophilised decellularised human nerve.

5.2 Aims and objectives

5.2.1 Aims:

I. To culture primary adult rat DRG explants in decellularised human femoral nerve *in vitro*, and determine the effects of decellularised nerve on cell viability, cell migration, neurite outgrowth and the expression of SGC and Schwann cell markers

II. To investigate the importance of endoneurial structure by culturing primary rat DRG explants in lyophilised decellularised human femoral nerve, and compare the effects on cell viability, cell migration, neurite outgrowth and the expression of SGC and Schwann cell markers with decellularised human femoral nerve.

III. To culture primary rat DRG explants in collagen type 1 hydrogels, to represent a non-aligned control, and compare the effects on cell viability, cell migration, neurite outgrowth and the expression of SGC and Schwann cell markers with decellularised and lyophilised decellularised human femoral nerve

5.2.2 Objectives:

I. To lyophilise decellularised human femoral nerve and determine the effects on nerve histioarchitecture and the specific basement membrane components collagen type IV and laminin by histological and immunofluorescent analyses.

II. To establish a culture system for primary rat DRG explants with decellularised nerve segments *in vitro.*

III. To establish a culture system for primary rat DRG explants in collagen type 1 hydrogels *in vitro*

IV. To determine cell viability at various time points in the culture systems developed in Objectives II and III using the ATP lite™ assay and TUNEL staining to detect apoptotic cells

V. To investigate cell migration and neurite outgrowth at various time points in the culture systems developed in Objectives II and III by immunofluorescent labelling of Neurofilament-200 (NF-200)

VI. To investigate the expression of satellite glial cell markers Sox2 and GS, and Schwann cell markers NCAM-1 and MBP at various time points in the culture systems developed in Objective II using immunofluorescent labelling.

5.3 Methods and experimental approach

5.3.1 Experimental approach

Decellularised human femoral nerves were lyophilised and rehydrated to structurally damage the endoneurium, in order to assess the importance of endoneurial structure on cell viability and migration when they were used to culture primary rat DRG explants. The histioarchitecture and specific basement components laminin and collagen type IV of lyophilised decellularised nerve were analysed by histology and immunofluorescent labelling. Decellularised human femoral nerve segments and lyophilised decellularised human femoral nerve segments were then cultured with primary rat DRG explants for 1, 7, 14, 21 or 28 days. Primary rat DRG explants were also cultured in collagen hydrogels to represent non-aligned scaffold controls, for 1, 7, 14, 21 or 28 days in order to compare cell viability and migration with DRGs cultured in decellularised and lyophilised decellularised nerve. At each time point in culture, cell viability was assessed using the ATP lite™ assay, and apoptosis was assessed using the terminal deoxynucleotidyl transferase (TdT) dUTP Nick-End Labelling (TUNEL) assay. Immunofluorescent labelling was also used to assess cell migration and determine the expression of Neurofilament-200, Sox2, GS, MBP and NCAM-1 at each time point in culture. At each time point in culture, DRGs cultured with decellularised nerve and DRGs cultured with lyophilised decellularised nerve were analysed by histology to visualise migrating cells.

5.3.2 Methods

5.3.2.1 Decellularisation of human femoral nerves

Human femoral nerves were dissected from 16 femoral bundles, cut into 60 mm segments and stored on PBS moistened filter paper at -80 °C as described in Chapter 2 (Section 2.2.3). Human femoral nerve segments (n = 72) were decellularised using decellularisation Protocol 3H developed for human femoral nerves, as described in Chapter 4. The decellularisation process was carried out aseptically, using aseptic technique in a class II safety cabinet. All decellularisation solutions were autoclaved prior to use, as described in Chapter 2 (Section 2.2.1.3). Following decellularisation, nerve segments were stored aseptically in PBS at 4 °C for up to one month.

5.3.2.2 Lyophilisation and rehydration of decellularised human femoral nerves

Decellularised human femoral nerve segments (n = 36) were weighed three times and a mean wet weight calculated. Samples were placed in a freeze dryer at -50 °C, 0.15 – 0.2 mbar, and the weight measured every 24 hours until constant (48 -72 hours). Once samples were lyophilised to a constant weight, samples were immersed in PBS at 4 °C until rehydrated to the initial wet weight calculated for each sample (24 – 48 hours). Samples were then were stored aseptically in PBS at 4 °C for up to one month.

5.3.2.3 Histological analysis of lyophilised decellularised human femoral nerve

Native (n = 3), decellularised and lyophilised decellularised (n = 3) human femoral nerve segments were cut into three 20 mm samples as described previously, and fixed in 10 % (w/v) NBF, processed and embedded in paraffin wax as described in Chapter 2 (Section 2.2.4.1). Wax blocks were sectioned (5 µm thickness) as described in Chapter 2 (Section 2.2.4.2) and processed for histological analysis, or analysis by immunofluorescent labelling.

5.3.2.3.1 Histological stains

Sections of native, decellularised and lyophilised decellularised human femoral nerve were stained using Sirius red / Miller's elastin, as described in Chapter 2 (Section 2.2.5.3). Sirius red staining was used to assess overall collagen structure, and stained sections were imaged under circularly polarised light to examine collagen fibril configuration and distribution. Miller's stain was used to stain elastin.

5.3.2.3.2 Immunofluorescent labelling of collagen type IV and laminin

For immunofluorescent labelling, sections of native, decellularised and lyophilised decellularised human femoral nerve were labelled with primary antibodies specific for collagen IV and laminin, as described in Chapter 2 (Section 2.2.6), and counterstained with DAPI. Specific antibodies and concentrations are detailed in Chapter 3 (Table 3.3). Sections of native and lyophilised decellularised nerve were also incubated with isotype control antibodies, and sections of native human femoral artery were used as positive controls. Omission of primary antibodies served as negative controls.

5.3.2.4 Isolation of primary rat DRG explants

All procedures involving animals were performed in accordance with the UK Home Office Animals (Scientific Procedures) Act 1986. Adult Wistar rats (approximately 45 days, male and female) were sacrificed by Schedule 1 asphyxiation in a rising concentration of CO_2 (to 100%; v/v) for 5 minutes. Following asphyxiation, rats were exsanguinated by incision through the carotid artery to confirm death.

DRG explants were isolated aseptically. The rat body was sprayed with 70 % (v/v) ethanol, and scissors were used to cut through the skin horizontally at the base of the back of the neck and then vertically along the length of the spine. Connective tissues and muscles either side of the spine were removed, and the spine was excised from the body by cutting through the spinal column at the cervical and lumbar ends, removing the ribs, remaining muscle and fascia. The spinal column was cut into three segments using scissors, and stored in cold Hanks balanced salt solution (HBSS) in a 50 mL Falcon tube on ice prior to dissection. Using small scissors, the spinal column segment was dissected in half along the sagittal plane, and the spinal cord was exposed. Using fine tweezers, the spinal cord was gently peeled away from the spinal column to reveal the nerve roots, which could be traced to locate the DRG of each vertebrae (Figure 5.1). Individual DRGs were removed by pulling the axon bundles either side of the DRG with fine tweezers. Each DRG was placed in a petri dish containing cold naked DMEM on ice, and the meninges were removed using 3 mm spring-back scissors under a dissection microscope. DRGs were then cut in half, and stored in petri dishes containing cold DMEM on ice until all DRGs were dissected.

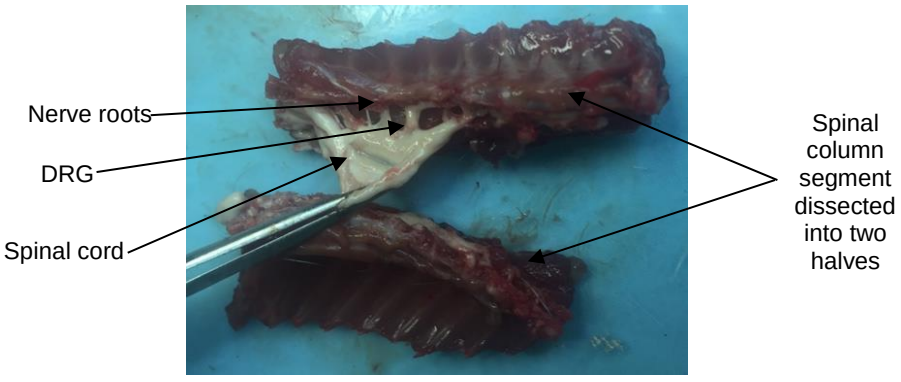

Figure 5.1 Dissection of Dorsal Root Ganglion (DRG) explants from adult rat spinal column. The rat spinal column segment is dissected into two halves by cutting along the dorsal and ventral sides of the vertebral column. The spinal cord is peeled away to reveal the DRGs located in small cavities along the column attached to nerve roots.

5.3.2.5 Cryo-embedding freshly isolated primary rat DRG explants

Freshly isolated DRGs (n = 3) were placed into individual plastic histology cassettes with an inner mesh cage. Samples were fixed by immersion in 50 mL 4 % (v/v) paraformaldehyde (PFA) solution in sterile 100 mL pots for one hour. Following fixation, samples were immersed in 100 mL PBS for 10 minutes, then immersed in 50 mL 15 % (w/v) sucrose in PBS for 24 hours at 4 °C. Samples were then immersed in 50 mL 30 % (w/v) sucrose in PBS for 24 hours at 4 °C, and transferred to small plastic cryo-moulds. Optimal cutting temperature (OCT) compound was added to each mould to cover the sample, and allowed to equilibrate for three hours at room temperature. Samples were then transferred to fresh plastic cryo-moulds, covered in OCT compound and cryo-embedded by placing in a metal tray filled with dry ice and 100 % (v/v) ethanol. Once samples were frozen, they were stored at -80 °C in an air tight container until use.

5.3.2.6 Development of a culture method for primary rat DRG explants with decellularised and lyophilised decellularised human femoral nerve

5.3.2.6.1 Solutions

5.3.2.6.1.1 Agarose (4 %; w/v)

Agarose (4 g) was added to 100 mL distilled water. The solution was autoclaved, as described in Chapter 2 (Section 2.2.1.3), and stored at room temperature for up to one month. Prior to use, the solution was heated in a microwave until re-melted.

5.3.2.6.1.2 NGF stock solution (1 mg.mL^{-1} NGF)

HBSS (1 mL) was added to a 1 mg vial of nerve growth factor (NGF) to reconstitute. The stock solution was stored in 50 µL aliquots in sterile Eppendorf tubes at -20 °C for up to two years.

5.3.2.6.1.3 DRG culture medium (10 % v/v FBS, 2 mM L-glutamine, penicillin/ streptomycin 100 U / 100 µg.mL^{-1}, 0.1 µg.mL^{-1} NGF)

To make up the DRG culture medium, 20 mL foetal bovine serum (FBS), 2 mL L-glutamine (200 mM), and 4 mL penicillin/ streptomycin (penicillin 5000 U.mL^{-1}; streptomycin 5 mg.mL^{-1}) was added to 87 mL Hams F12 and 87 mL DMEM. The medium was stored at 4 °C for up to one week. Immediately before use, 20 µL NGF

stock solution (1 mg.mL^{-1}) was added, and the medium was pre-warmed to 37 °C in a water bath.

5.3.2.6.2 Culture method

Culture plates were prepared aseptically by coating the base of each well of a 6-well tissue culture plate with 4 mL melted 4 % (w/v) agarose solution in a class II safety cabinet. Once the agarose solution had set at room temperature, each plate was wrapped in Parafilm and stored at 4 °C for up to one week. Prior to use, the plates were allowed to equilibrate to room temperature.

Decellularised (n = 30) or lyophilised decellularised (n = 30) nerve segments (20 mm) were adhered to the base of agarose coated plates by pinning each end into the agarose using 3 mm sterile stainless steel pins (Figure 5.2). A small incision was made in the top of each segment, and one half of a primary rat DRG was inserted into the cavity of each segment. DRG culture medium (4 mL) was added to each well, and the plates were cultured at 37 °C in 5 % CO_2 (v/v) in air, for up to 28 days. DRG culture medium was aspirated and replaced with 4 mL fresh culture medium every 48 hours. DRGs were cultured for either 1, 7, 14, 21 or 28 days.

At each time point (days 1, 7, 14, 21 and 28), six segments were removed from culture and processed for ATP lite™ assay (n = 3), as described in Section 5.3.2.12 below, or processed for cryoembedding (n =3), as described in Section 5.3.2.8 below.

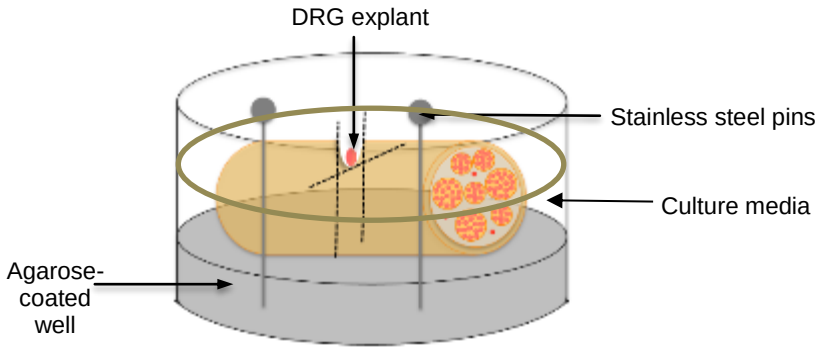

Figure 5.2 Culture design for culturing primary rat DRGs in decellularised and lyophilised decellularised human femoral nerve segments. Individual wells of 6 – well culture plates were coated with agarose (4 % w/v) and segments of decellularised or lyophilised decellularised nerve (20 mm) were pinned into position using stainless steel pins (11 x 3 mm). DRG explants were halved, and one half was inserted into each segment in a small cavity snipped in the top. DRG culture medium (4 mL) was added to each well.

5.3.2.7 Culture of primary rat DRG explants in collagen type I hydrogels

5.3.2.7.1 Solutions

5.3.2.7.1.1 Sodium hydroxide (1.94 M NaOH)

NaOH pellets (7.76g) were dissolved in 100 mL distilled water using a magnetic stirrer and stirrer bar. The solution was stored for up to six months at room temperature.

5.3.2.7.2 Culture method

Collagen hydrogels (n = 30) were made according to the following composition: 80 % (v/v) rat tail type I collagen (2.06 $mg.mL^{-1}$ stock solution), 10 % (v/v) 10 X minimal essential medium (MEM), 5.8 % (v/v) NaOH solution, and 4.2 % (v/v) DRG culture medium. All reagents were kept on ice to slow down the gelation process, and all work was performed aseptically in a class II safety cabinet.

Rat tail type I collagen (80 % v/v of final volume, final concentration 1.65 $mg.mL^{-1}$) and MEM solution (10 % v/v of final volume) were added to a sterile 30 mL universal tube. The solution was neutralised by the addition of NaOH solution dropwise, until the colour of the solution changed from yellow to rose pink, indicating neutralisation. Following neutralisation, DRG cell culture medium (4.2 % v/v of final volume) was added, and the gel solution was pipetted into individual wells of a 48-well culture plate (300 µL per well). Prior to complete gelation, one half of a primary rat DRG was added to each well to suspend the half DRG within the gel. Once gelation was complete, gels were transferred to individual wells of 6-well culture plates, 4 mL DRG culture medium was added to each well, and the gels were cultured at 37 °C in 5 % CO_2 (v/v) in air, for up to 28 days. DRG culture medium was aspirated and replaced with 4 mL fresh culture medium every 48 hours. DRGs were cultured for either 1, 7, 14, 21 or 28 days.

At each time point (days 1, 7, 14, 21 and 28), six gels were removed from culture and processed for ATP lite™ assay (n = 3), as described in Section 5.3.2.12 below, or processed for cryoembedding (n = 3), as described in Section 5.3.2.9 below.

5.3.2.8 Cryo-embedding cultured decellularised human femoral nerve segments

Decellularised nerve segments (n = 3) and lyophilised decellularised nerve segments (n = 3) were removed from culture at each time point, and transferred to plastic histology cassettes. Samples were fixed by immersion in 50 mL 4 % (v/v) paraformaldehyde (PFA) solution in sterile 100 mL pots for one hour. Following fixation, samples were immersed in 100 mL PBS for 10 minutes, then immersed in 50 mL 15 % (w/v) sucrose in PBS for 24 hours at 4 °C. Samples were then immersed in 50 mL 30 % (w/v) sucrose in PBS for 24 hours at 4 °C, and transferred to large plastic cryo-moulds. OCT compound was added to each mould to cover the sample, and allowed to equilibrate for three hours at room temperature. Samples were then transferred to fresh large plastic cryo-moulds, covered in OCT compound and cryo-embedded by placing in a metal tray filled with dry ice and 100 % (v/v) ethanol. Once samples were frozen, they were stored at -80 °C in an air tight container until use.

5.3.2.9 Cryo-embedding primary rat half DRGs in collagen hydrogels

DRG culture medium was aspirated from each gel (n = 3 per time point), and gels were fixed by adding 1 mL 4 % (v/v) PFA solution to each well and incubating at room temperature for one hour. Following fixation, the PFA solution was aspirated from each well, and 1 mL PBS was added to each well and incubated for 10 minutes. PBS was aspirated from the wells, then 1 mL 15 % (w/v) sucrose in PBS was added to each well and incubated for 24 hours at 4 °C. Gels were then immersed in 1 mL 30 % (w/v) sucrose solution in PBS and incubated for 24 hours at 4 °C. Gels were then transferred to large plastic cryo moulds, covered in OCT compound and cryo-embedded by placing in a metal tray filled with dry ice and 100 % (v/v) ethanol. Once samples were frozen, they were stored at -80 °C in an air tight container until use.

5.3.2.10 Cryo-sectioning and slide preparation

Freshly isolated DRGs (n = 3), cryo-embedded decellularised nerve segments and lyophilised decellularised nerve segments cultured with DRGs from each time point (n = 3 per time point) and DRGs cultured in collagen gels from each time point (n = 3 per time point) were sectioned using a cryotome at a temperature of -30 °C. Each block was serially sectioned, with sections cut at a thickness of 10 µm. The sections were transferred to Superfrost Plus slides, and each slide was numbered and left to dry at room temperature for 30 minutes. Slides were stored in plastic slide storage

boxes at -20 °C until staining. Prior to staining, slides were thawed at room temperature for 30 minutes.

Numbered slides from each block of DRGs cultured with decellularised nerve segments were systematically separated for TUNEL assay (n = 3 slides, numbers 1, 6 and 11), immunofluorescent labelling with Sox2 and GS (n = 3 slides, numbers 2, 7 and 12) MBP and NCAM-1 (n = 3 slides, numbers 3, 8 and 13), and NF-200 (n = 3 slides, numbers 4, 9 and 14) and Masson's trichrome staining (n = 3 slides, numbers 5, 10 and 15). This process was repeated for the numbered slides from each block of DRGs cultured with lyophilised decellularised nerve segments.

Numbered slides from each block of collagen hydrogels cultured with DRGs were systematically separated for TUNEL assay (n = 3 slides, numbers 1, 6 and 11), immunofluorescent labelling with Sox2 and GS (n = 3 slides, numbers 2, 7 and 12) MBP and NCAM-1 (n = 3 slides, numbers 3, 8 and 13), and NF-200 (n = 3 slides, numbers 4, 9 and 14). Sections of collagen hydrogels cultured with DRGs were not stained with Masson's Trichrome as it was not found to be technically possible, as sections would not adhere to slides during staining.

5.3.2.11 Histological analysis

5.3.2.11.1 Masson's trichrome staining

Cryosections of DRGs cultured with decellularised nerve (n = 3 per time point) and DRGs cultured with lyophilised decellularised nerve (n = 3 per time point) were stained with Masson's trichrome as described in Chapter 2 (Section 2.2.5.5). Masson's trichrome staining was used to visualise collagen (light green), nuclei (dark brown) and cytoplasm (red), assess the positioning of the DRGs and visualise migrating cells in the decellularised nerve or lyophilised decellularised nerve

5.3.2.11.2 TUNEL staining

Cryosections of freshly isolated DRGs (n = 3), DRGs cultured with decellularised nerve (n = 3 per time point), DRGs cultured with lyophilised decellularised nerve (n = 3 per time point) and DRGs cultured in collagen hydrogels (n = 3 per time point) were subject to a TUNEL assay to detect apoptotic cells.

5.3.2.11.2.1 Reagents

- DeadEnd™ Fluorometric TUNEL system

- Sodium chloride solution (0.85 %; w/v NaCl)
  - 0.85 g NaCl
  - 100 mL distilled water

- Methanol free formaldehyde solution (4 %; w/v in PBS)
  - 20 mL 16 % methanol free formaldehyde
  - 60 mL PBS

- Proteinase K buffer solution *(100 mM Tris-HCl, 50 mM EDTA),* pH 8.0
  - 788 mg Tris-HCl
  - 930.5 mg EDTA
  - 50 mL distilled water

- Proteinase K stock solution (10 $mg.mL^{-1}$)
  - 10 mg Proteinase K
  - 1 mL proteinase K buffer solution

- Proteinase K working solution (20 $\mu g.mL^{-1}$)
  - 2 µL Proteinase K stock solution
  - 998 µL PBS

- Benzonase solution (1 $U.mL^{-1}$)
  - 1 µL Benzonase (250 $U.\mu L^{-1}$)
  - 250 mL Nuclease solution (see Chapter 2 Section 2.1.8.6)

- Terminal deoxynucelotidyl transferease (recombinant) (rTdT) reaction mix
  - 44 µL Equilibration buffer
  - 5 µL nucleotide mix
  - 1 µL rTdT enzyme

- rTdT-free negative control mix
  44 µL Equilibration buffer
  5 µL Nucleotide mix
  1 µL sterile nuclease free water

- 2X SSC solution
  4 mL 20 x SSC solution
  36 mL distilled water

5.3.2.11.2.2 Method

Cryo-sections were thawed for 30 minutes, then immersed in running tap water for 3 minutes. Sections were then immersed in sodium chloride solution for 5 minutes, followed by PBS for 5 minutes. Sections were then fixed by immersion in methanol free formaldehyde solution for 15 minutes at room temperature. Sections were immersed twice in PBS for 5 minutes each at room temperature. Each section was circled with a hydrophobic marker, washed for 3 minutes with PBS, and incubated with 100 µL Proteinase K working solution for 10 minutes at room temperature. Sections were washed twice with PBS, for 3 minutes each. Sections were fixed again by immersion in methanol free formaldehyde solution for 5 minutes at room temperature. Sections were washed twice with PBS for 3 minutes each. Positive control sections were incubated with 100 µL Benzonase solution for 5 minutes at 37 °C, and washed twice in PBS for 2 minutes each. Sections were incubated in 50 µL equilibration buffer for 10 minutes at room temperature. Test sections and positive control sections were incubated in 50 µL rTdT reaction mix, and negative control sections were incubated in 50 µL negative control mix for one hour at 37 °C in a humidified chamber in the dark. Plastic coverslips were added to each slide to prevent sections drying. Plastic coverslips were then removed, and sections were immersed in 2 X SCC solution for 15 minutes at room temperature in the dark. Sections were washed three times in PBS in the dark, for 5 minutes each. Sections were immersed in DAPI working solution (Chapter 2 Section 2.2.5.2) for 10 minutes at room temperature in the dark. Sections were washed three times in PBS for 5 minutes each in the dark, and mounted using a glass coverslip and fluorescent mounting medium. Sections were kept in the dark 4°C for a maximum of 24 hours until visualised using an upright fluorescent microscope and a DAPI filter (460 nm) and fluorescein filter (520 nm ± 20 nm).

5.3.2.11.3 Immunofluorescent labelling

For immunofluorescent labelling, cryosections of freshly isolated DRGs (n = 3), DRGs cultured with decellularised nerve (n = 3 per time point), DRGs cultured with lyophilised decellularised nerve (n = 3 per time point) and DRGs cultured in collagen hydrogels (n = 3 per time point) were labelled with primary antibodies specific for neurofilament-200 (NF-200), Sox2, GS, MBP and NCAM-1 as described in Chapter 2 (Section 2.2.6) and Table 5.1 below. Sections were also incubated with isotype control antibodies, and omission of primary antibodies served as negative controls.

Table 5.1 Specific antibodies and solutions for immunofluorescent labelling of NF-200, Sox2, GS, MBP and NCAM-1. Specific antibodies, antigen retrieval methods and block steps used for immunofluorescent labelling. For details of each antibody, see Chapter 2 (Section 2.1.6). Isotype control antibodies were applied at the same concentration as the primary antibody. GS = Glutamine Synthetase, MBP = Myelin Basic Protein, NCAM-1 = Neural Cell Adhesion Molecule-1, NF-200 = Neurofilament-200, RT = Room temperature, TBS = Tris buffered Saline.

	Sox2	**GS**	**MBP**	**NCAM-1**	**NF-200**
Primary antibody	Monoclonal mouse anti-Sox2 (1 $mg.mL^{-1}$); 1:100 dilution	Polyclonal rabbit anti-GS (6.9 $mg.mL^{-1)}$; 1:500 dilution	Polyclonal rabbit anti-MBP (1 $mg.mL^{-1}$); 1:100 dilution	Monoclonal mouse anti-NCAM-1 (1 $mg.mL^{-1}$); 1:500 dilution	Polyclonal rabbit anti-NF-200 (8 $mg.mL^{-1}$); 1:200 dilution
Secondary antibody	Goat anti-mouse IgG AF647 (2 $mg.mL^{-1}$); 1:200 dilution	Goat anti-rabbit IgG AF488 (2 $mg.mL^{-1}$); 1:200 dilution	Goat anti-rabbit IgG AF488 (2 $mg.mL^{-1}$); 1:200 dilution	Goat anti-mouse IgG AF647 (2 $mg.mL^{-1}$); 1:200 dilution	Goat anti-rabbit IgG AF488 (2 $mg.mL^{-1}$); 1:200 dilution
Isotype antibody	Mouse IgG1	Rabbit polyclonal IgG	Rabbit polyclonal IgG	Mouse IgG1	Rabbit polyclonal IgG
Antigen retrieval	Citrate buffer, pH 6, 1 hour at RT	Citrate buffer, pH 6, 1 hour at RT	Citrate buffer, pH 6, 1 hour at RT	Citrate buffer, pH 6, 1 hour at RT	Proteinase K, 20 mins at RT
Blocking buffer	Goat serum (10 %; w/v serum, 0.1 %; w/v Triton X-100 in TBS) for 1 hour	Goat serum (10 %; w/v serum, 0.1 %; w/v Triton X-100 in TBS) for 1 hour	Goat serum (10 %; w/v serum, 0.1 %; w/v Triton X-100 in TBS) for 1 hour	Goat serum (10 %; w/v serum, 0.1 %; w/v Triton X-100 in TBS) for 1 hour	Goat serum (10 %; w/v serum, 0.1 %; w/v Triton X-100 in TBS) for 1 hour

5.3.2.11.4 Image capture

Sections of DRGs cultured in decellularised nerve, lyophilised decellularised nerve and collagen hydrogels subject to TUNEL assay or labelled with NF-200, Sox2, GS, MBP or NCAM-1 were visualised using an upright fluorescent microscope and appropriate filters, as described in Chapter 2 (Section 2.2.1.2). Images acquired for analysis were taken using x 10 magnification, and the whole DRG was captured within the field of view.

5.3.2.11.5 Image analysis

5.3.2.11.5.1 Quantification of TUNEL staining

Images of sections of DRGs cultured in decellularised nerve, lyophilised decellularised nerve and collagen hydrogels subject to TUNEL assay (n = 3 per time point) were analysed using FIJI Is Just ImageJ (FIJI) software program to quantify the number of apoptotic cells in each image.

Each fluorescent multi-channel image was separated into single channel images of TUNEL staining (green channel) and DAPI staining (blue channel). Single channel images were then analysed using FIJI. The “Local Auto Threshold” plugin was used to threshold background fluorescence and generate binary images. The use of a local threshold produces a binary image according to the local image characteristics within a radius of each pixel, rather than a global calculation of the image. The 'Phansalkar' Auto Local Threshold method was selected. The binary images were analysed using the “Analyse Particles” tool, which automates the detection and measurement acquisition of objects in a binary image. The number of cells was determined by the “count” output measure.

The number of apoptotic cells (determined from green channel image) and the total number of cells (determined from blue channel image) were used to quantify the number of apoptotic cells in the original multi-channel image. The number of apoptotic cells was represented as a percentage of the total number of cells in each image.

5.3.2.11.5.2 Quantification of fluorescent labelling

Images of sections of DRGs cultured in decellularised nerve, lyophilised decellularised nerve and collagen hydrogels labelled with NF-200 (n = 3 per time point), Sox2 and GS (n = 3 per time point) and MBP and NCAM-1 (n = 3 per time point) were analysed using FIJI software program to quantify fluorescent labelling.

Each fluorescent multi-channel image was separated into single channel images (red, green or blue channels). Single channel images were then analysed using FIJI as described in Section 1.3.2.11.4.1. The 'Phansalkar' Auto Local Threshold method was selected to threshold background fluorescence and generate binary images. The binary images were analysed using the “Analyse Particles” tool, and the “total area (µm^2)” output measure was used to quantify fluorescent labelling.

The total area (µm^2) of DAPI staining and the total area (µm^2) of fluorescent labelling determined from single-channel images were used to quantify fluorescent labelling in the original multi-channel image. Fluorescent labelling of NF-200, Sox2, GS, MBP and NCAM-1 was represented as a percentage of the total area of DAPI staining in each multi-channel image.

5.3.2.11.5.3 Quantification of maximum cell migration distance

Images of sections of DRGs cultured in decellularised nerve (n = 3 per time point), lyophilised decellularised nerve (n = 3 per time point), and collagen hydrogels (n = 3 per time point) labelled with NF-200 were analysed using FIJI software program to quantify the maximum cell migration distance in each image. With each image, the “Measure” tool was used to draw a line and determine the distance (µm) between x and y coordinates. The centre of the DRG explant was used as the x coordinate, and a migrating cell was used as the y-coordinate. A separate line was drawn for each migrating cell. The maximum cell migration distance (µm) for each image was determined.

5.3.2.12 ATPLite-M™ cell viability assay

Cell viability was determined using the ATP-lite M™ assay kit to quantify adenosine triphosphate (ATP) levels. The ATP present in the cells reacts with D-luciferin in the presence of luciferase to emit light proportional to ATP concentration.

5.3.2.12.1.1 ATP lite™ assay of DRG explants cultured in decellularised nerve, lyophilised decellularised nerve and collagen hydrogels

DRGs cultured with decellularised nerve segments (n = 3 per time point), DRGs cultured with lyophilised decellularised nerve segments (n = 3 per time point), and DRGs cultured in collagen gels (n = 3 per time point) were removed from culture, placed in individual wells of a 6-well tissue culture plate and macerated using a scalpel. Mammalian cell lysis solution (500 µL) was added to each sample, and incubated for 15 minutes with agitation at 700 rpm at room temperature. Following incubation, 50 µL from each sample was added to individual wells of a 96-well

Optiplate™ along with 50 µL substrate solution. The plate was covered in adhesive foil and incubated for 15 minutes with agitation at 700 rpm in the dark at room temperature. The luminescence of each well was then determined using a Top count scintillation counter, measured in counts per second (CPS).

5.4 Results

5.4.1 Lyophilisation of decellularised human femoral nerve

The effects of lyophilisation and rehydration on the histioarchitecture of decellularised human femoral nerve segments was assessed histologically using Sirius red/Miller's elastin staining. Picro-sirius red was used to stain collagen fibres within sections of native nerve, decellularised nerve and lyophilised decellularised nerve, whilst Miller's solution was used to stain elastin fibres (Figure 5.3). Visualisation under normal Kohler illumination showed that the histioarchitecture of lyophilised decellularised nerve was severely damaged in comparison to native and decellularised nerve (Figure 5.3 A, C & E). The collagen in the inter-fascicular epineurium and in the perineurial layers surrounding each fascicle appeared more disorganised and fragmented in comparison to native nerve, although the perineurium remained as a discrete band surrounding each fascicle. In comparison to native nerve, the endoneurium appeared more fragmented, and individual endoneurial tubes could no longer be identified. However, visualisation under circularly polarised light indicated a similar distribution of red, yellow and green collagen fibres between native and lyophilised decellularised nerve (Figure 5.3 B & F).

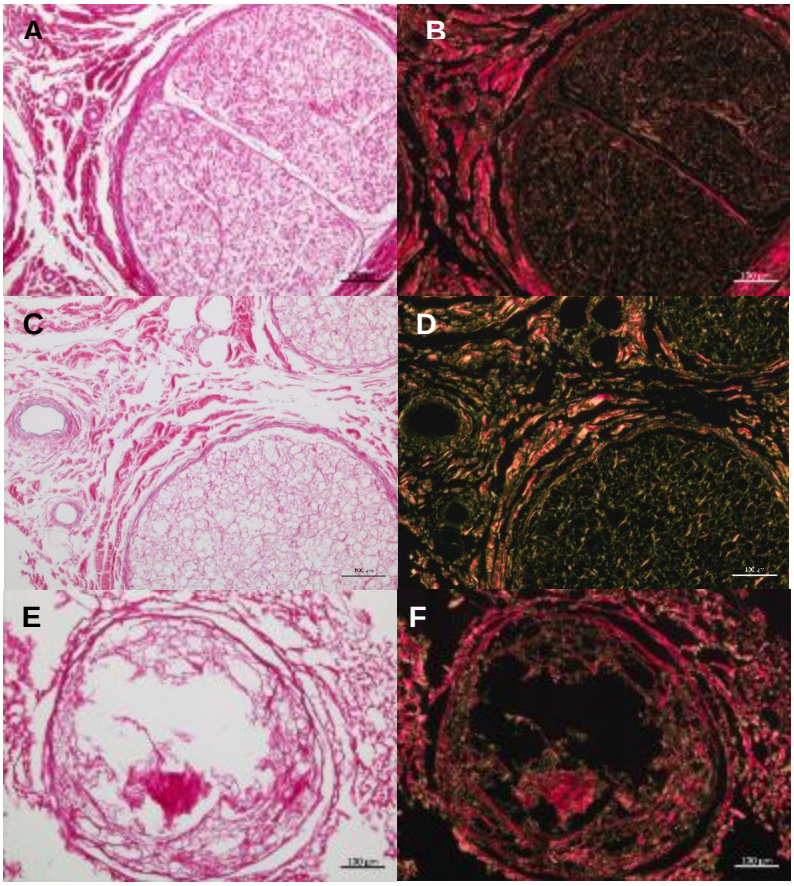

Figure 5.3 Images of sections of native, decellularised and lyophilised decellularised human femoral nerve stained with Sirius red / Miller's elastin. Representative images of native (A & B), decellularised (C & D) and lyophilised decellularised (E & F) human femoral nerve sections stained with Sirius red / Miller's elastin. Sirius red imaged using normal Köhler illumination (A & C) or circularly polarised light (B & D). Major structural alterations were observed in the endoneurium of freeze dried decellularised nerve in comparison to native nerve. Images taken using a x 10 objective. Scale bars 100 μm.

The effects of lyophilisation and rehydration on specific basement membrane components collagen type IV and laminin in decellularised human nerve were assessed using immunofluorescent labelling (Figures 5.4 and 5.5 respectively).

Sections of native nerve, decellularised nerve and lyophilised decellularised human femoral nerve were labelled with a primary monoclonal antibody against collagen type IV and a goat anti-mouse IgG secondary antibody (Figure 5.4). Collagen type IV was located in the endoneurium and perineurium of lyophilised decellularised nerve, although labelling intensity appeared slightly reduced in comparison to native nerve (Figure 5.4 C & E). Intense labelling was observed in the smooth muscle region of the human femoral artery positive control (Figure 5.4 A), and no labelling was observed in the isotype control (Figure 5.4 B).

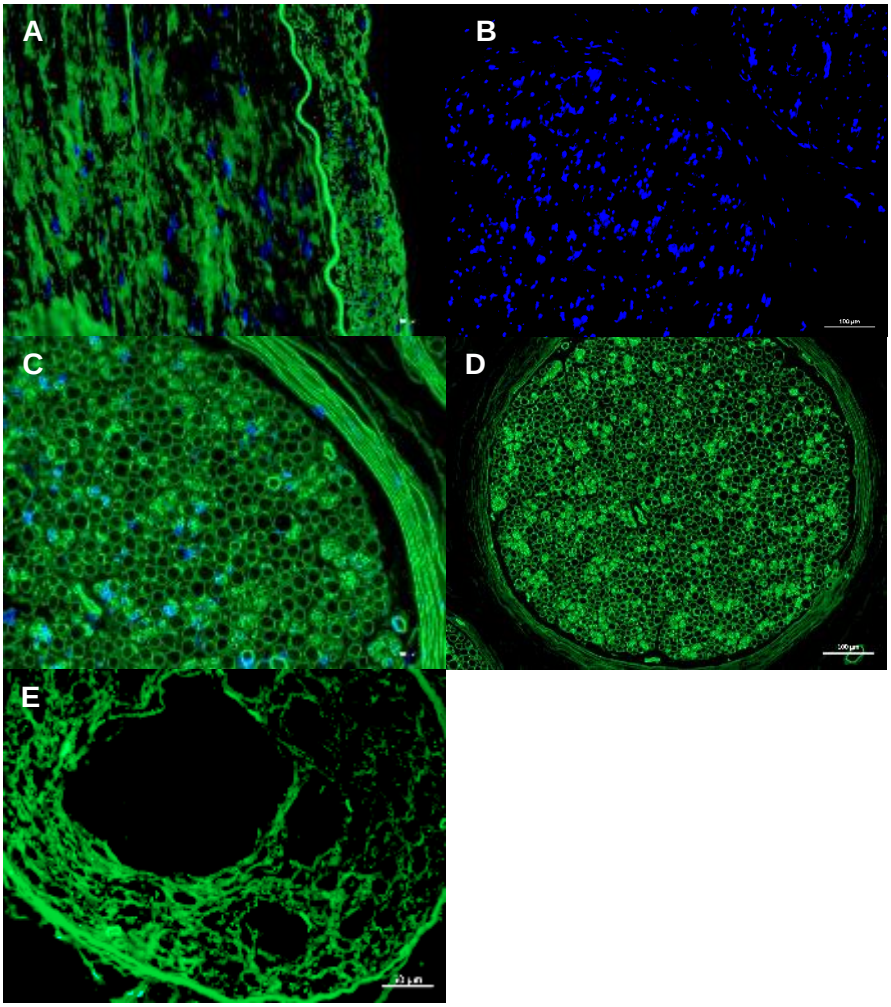

Figure 5.4 Images of immunofluorescent labelling of collagen type IV in sections of native, decellularised and lyophilised decellularised human femoral nerve. Representative images of sections of native human artery (A), native human femoral nerve incubated with an isotype control antibody (B), and native (C), decellularised (D) and lyophilised decellularised (E) human femoral nerve labelled with a primary monoclonal antibody against collagen type IV and counterstained with DAPI. Collagen type IV was present in freeze dried decellularised nerve, located in the endoneurium and perineurium. Images taken using a x 10 objective using DAPI and FITC filters. Scale bars 50 µm (A, C & D) and 100 µm (B).

Sections of native nerve, decellularised nerve and lyophilised decellularised human femoral nerve were also labelled with a primary monoclonal antibody against laminin and a goat anti-mouse IgG secondary antibody (Figure 5.5). Similarly to collagen type IV, laminin was located in the endoneurium and perineurium of lyophilised decellularised nerve, although labelling intensity appeared slightly reduced in comparison to native nerve (Figure 5.5 C & E). Laminin was observed in the smooth muscle and luminal regions of the human femoral artery positive control (Figure 5.5 A), and no labelling was observed in the isotype control (Figure 5.5 B)

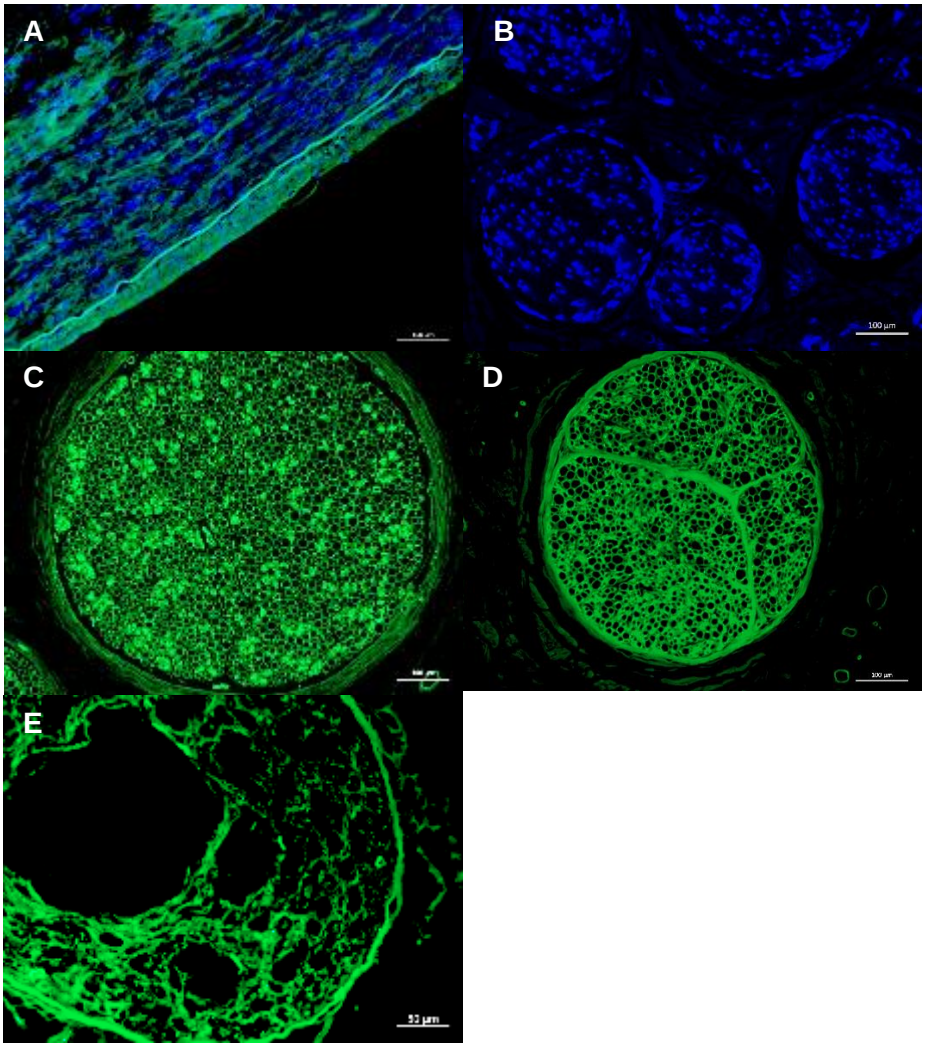

Figure 5.5 Images of immunofluorescent labelling of laminin in sections of native, decellularised and lyophilised decellularised human femoral nerve. Representative images of sections of native human artery (A), native human femoral nerve incubated with an isotype control antibody (B), and native (C), decellularised (D) and lyophilised decellularised (E) human femoral nerve labelled with a primary monoclonal antibody against laminin and counterstained with DAPI. Laminin was still present in freeze dried decellularised nerve, located in the endoneurium and perineurium. Images taken using a x 10 objective using DAPI and FITC filters. Scale bars 100 μm (A - C) and 50 μm (D).

5.4.2 Masson's Trichrome staining of DRGs cultured in decellularised nerve and lyophilised decellularised nerve

Sections of primary rat DRGs cultured in decellularised and lyophilised decellularised human femoral nerve segments at days 1, 7, 14, 21 and 28 in culture were assessed histologically using Masson's Trichrome staining (Figure 5.6). At day 1 in culture, visual observation of sections showed few migrating cells from the body of the DRG explants in DRGs cultured in decellularised nerve (Figure 5.6 A) and lyophilised decellularised nerve (Figure 5.6 F). However, from day 7 onwards, a greater number of cells migrating from the body of the DRG explants were observed in DRGs cultured in decellularised nerve (Figure 5.6 B – E) and lyophilised decellularised nerve (Figure 5.6 G – J). From day 7 onwards, cells migrating from the body of DRG explants cultured in decellularised nerve and lyophilised decellularised nerve appeared to be sporadically distributed (Figure 5.6 B – E & G – J).

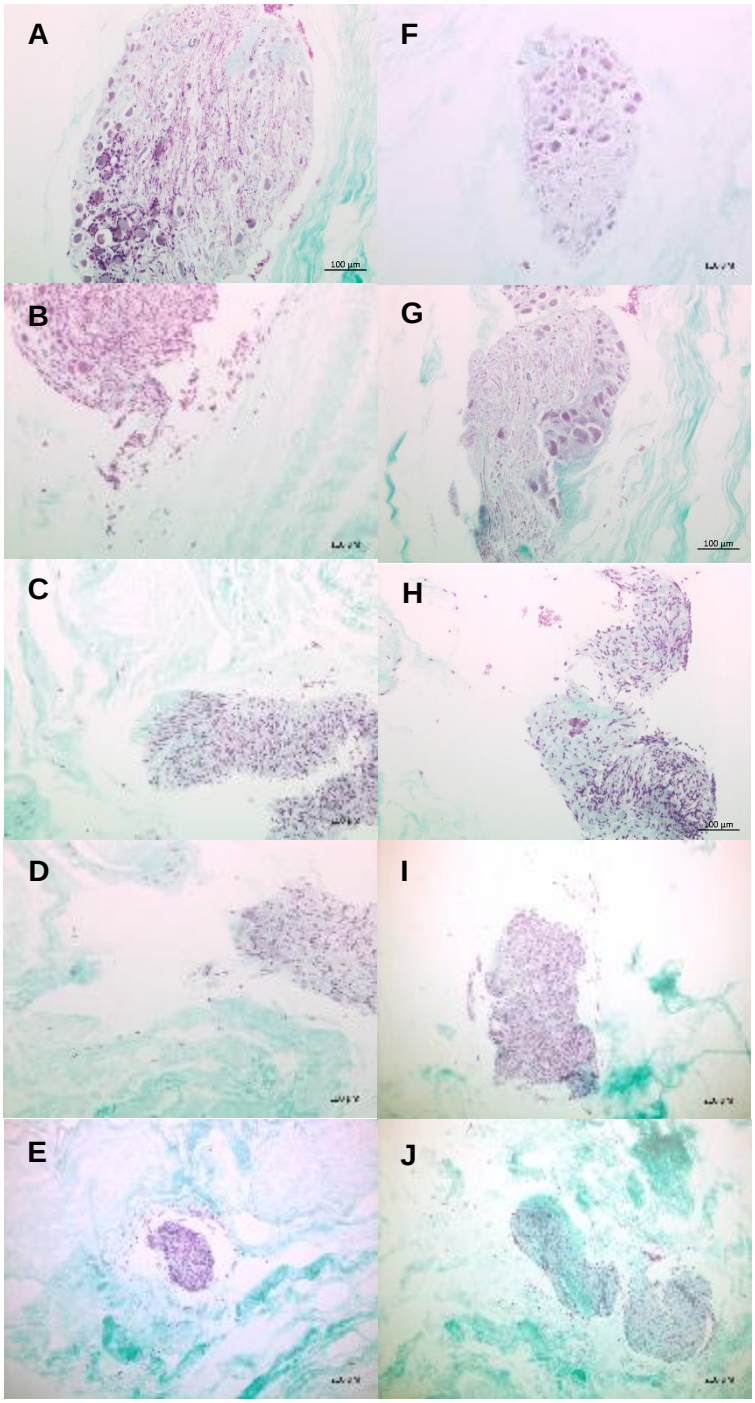

Figure 5.6 Masson's Trichrome staining of DRGs cultured in decellularised nerve and lyophilised decellularised nerve. Representative images of DRGs cultured in decellularised nerve (A-E), and lyophilised decellularised nerve (F-J) at time points day 1 (A & F), day 7 (B & G), day 14 (C & H), day 21 (D & I) and day 28 (E & J) stained with Masson's Trichrome. Sections imaged using normal Köhler illumination. Images taken using a x 10 objective and a x 4 objective. Scale bars 100 µm (A – C, F – H) and 200 µm (D, E, I & J).

5.4.3 Cell viability of DRGs cultured in decellularised and lyophilised decellularised human femoral nerve and collagen hydrogels

5.4.3.1 ATP content of DRG cultures over time

Cell viability of DRG explants cultured in decellularised nerve, lyophilised decellularised nerve and collagen hydrogels at days 1, 7, 14, 21 and 28 in culture was determined using ATP lite™ assay (Figure 5.7). DRG cells remained viable up to 28 days in culture for all conditions (Figure 5.7).

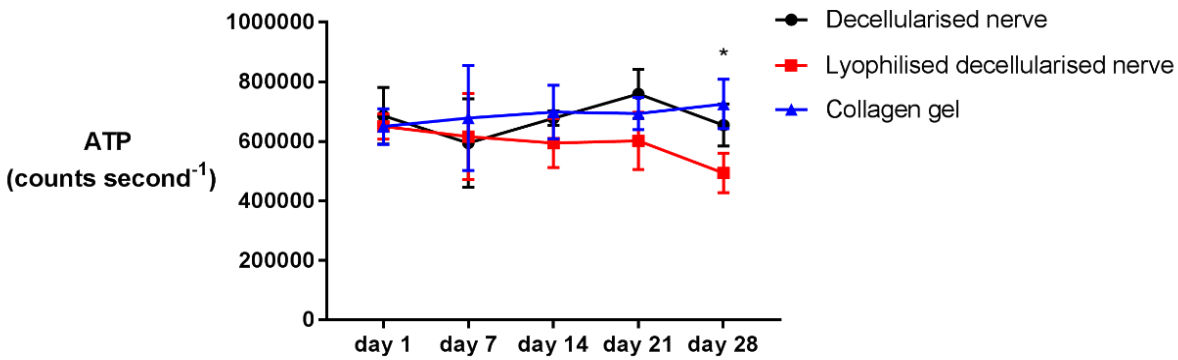

Figure 5.7 ATP content of primary rat DRGs cultured in decellularised and, lyophilised decellularised human femoral nerve and collagen hydrogels. ATP content of DRGs cultured in decellularised nerve, lyophilised decellularised nerve and collagen hydrogels at days 1, 7, 14, 21 and 28 in culture. Data is expressed as the mean counts per second (n = 3 per time point) ± 95 % confidence limits. Data was analysed by two-way ANOVA with Tukey's post hoc test ($p < 0.05$). The asterisk indicates a significant difference ($p < 0.05$) between the ATP content of DRGs cultured collagen hydrogels and decellularised nerve at day 28.

The data was analysed by two-way ANOVA (culture type vs time) with Tukey's post hoc test and this revealed no significant differences between the ATP content of DRGs cultured in decellularised nerve, lyophilised decellularised nerve or collagen hydrogels at days 1, 7, 14, or 21. At day 28 in culture, there was no significant difference between the ATP content of DRGs cultured in decellularised nerve and the ATP content of DRGs cultured in collagen hydrogels, and no significant difference between the ATP content of DRGs cultured in decellularised nerve and the ATP content of DRGs cultured in lyophilised decellularised nerve. However, at day 28 in culture the ATP content of DRGs cultured in lyophilised decellularised nerve were was significantly lower than the ATP content of DRGs cultured in collagen hydrogels ($p < 0.05$). Although there was an apparent decrease in the ATP content of DRGs cultured in decellularised nerve and lyophilised decellularised

nerve between day 21 and 28 in culture, this was not found to be significantly different (Figure 5.7).

5.4.3.2 Apoptotic cells in freshly isolated DRGs and DRGs cultured in decellularised nerve, lyophilised decellularised nerve and collagen hydrogels

Sections of freshly isolated primary rat DRGs were subject to a TUNEL assay to detect apoptotic cells (Figure 5.8). Relatively few apoptotic cells were observed in sections of freshly isolated DRGs, and these appeared to be mainly at the edges (Figure 5.8 A). A greater number of apoptotic cells were observed in benzonase treated DRGs, the positive control, and these were more evenly distributed across the tissue section (Figure 5.8 B). No apoptotic cells were detected in the negative control DRG section (Figure 5.8 C).

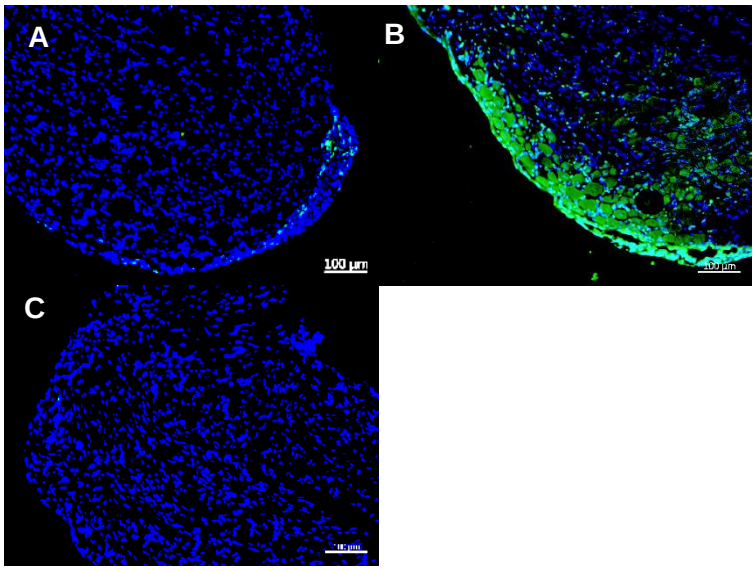

Figure 5.8 Apoptotic cells in freshly isolated primary rat DRGs.
Representative images of TUNEL assay of sections of freshly isolated DRGs (A), freshly isolated DRGs treated with benzonase (B) as positive controls, and freshly isolated DRGs treated as negative controls (C). Apoptotic cells shown as green. Images acquired using a x 10 objective and DAPI and fluorescein filters. Scale bars 100 µm.

Apoptotic cells within primary rat DRGs cultured in decellularised nerve, lyophilised decellularised nerve and collagen hydrogels at days 1, 7, 14, 21 and 28 in culture were detected using the TUNEL assay (Figure 5.9). Apoptotic cells were observed in sections of DRGs cultured in decellularised nerve, lyophilised decellularised nerve and collagen hydrogels at all time points in culture (Figure 5.9). At day 1 in culture, apoptotic cells were mainly located along the edges of the DRG, with few migrating apoptotic cells observed in DRGs cultured in decellularised nerve (Figure

5.9 A), lyophilised decellularised nerve (Figure 5.9 F), and collagen hydrogels (Figure 5.9 K). However, from day 7 onwards in culture, apoptotic cells appeared more evenly distributed within the DRG body, and a greater number of migrating apoptotic cells were observed in DRGs cultured in decellularised nerve, (Figure 5.9 B – E), lyophilised decellularised nerve (Figure 5.9 G - J) and collagen hydrogels (Figure 5.9 L – O).

The percent apoptotic cells (total number of apoptotic cells represented as a percentage of total cells) within primary rat DRGs cultured in decellularised nerve, lyophilised decellularised nerve and collagen hydrogels at days 1, 7, 14, 21 and 28 in culture are shown in Figure 5.10. The percent apoptotic cells in sections of DRGs cultured in collagen hydrogels increased slightly with prolonged culture time, from 6 % at day 1 to 11 % at day 28 in culture (Figure 5.10). There was little change in the percent apoptotic cells in sections of DRGs cultured in decellularised nerve between day 1 (9 %) and day 21 (10 %), however at day 28 the percent apoptotic cells had increased to 18 % (Figure 10). The percent apoptotic cells in DRGs cultured in lyophilised decellularised nerve increased from day 7 to day 28 in culture, and the percent apoptotic cells had increased to 31 % by day 28 (Figure 5.10).

No major differences were observed between the percent apoptotic cells in sections of DRGs cultured in decellularised nerve, lyophilised decellularised nerve and collagen hydrogels at day 1, 7, and 14 in culture (Figure 5.10). In addition, no major differences were observed between the percent apoptotic cells in sections of DRGs cultured in decellularised nerve and collagen hydrogels at day 21 or 28 in culture (Figure 5.10). However, the percent apoptotic cells in sections of DRGs cultured in lyophilised decellularised nerve was greater than the percent apoptotic cells in sections of DRGs cultured in decellularised nerve or collagen hydrogels at day 21 and 28 in culture (Figure 5.10).

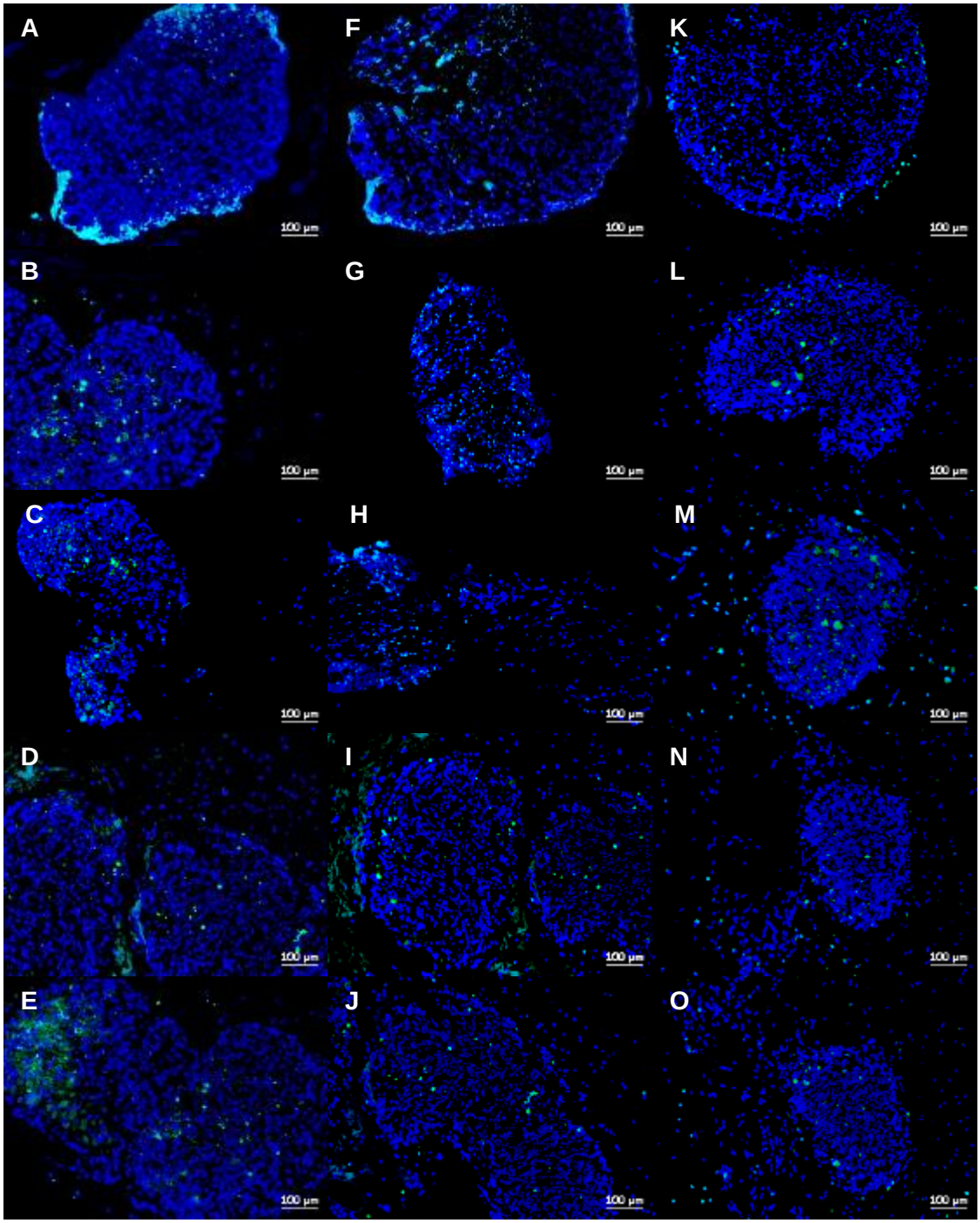

Figure 5.9 Apoptotic cells in sections of primary rat DRGs cultured in decellularised and lyophilised decellularised human femoral nerve segments and collagen hydrogels. Representative images of TUNEL assay of sections of DRGs cultured in decellularised nerve (A-E), lyophilised decellularised nerve (F-J) or collagen hydrogels (K-O). TUNEL assay was performed at time points day 1 (A, F & K), day 7 (B, G & L), day 14 (C, H & M), day 21 (D, I & N) and day 28 (E, J & O). Apoptotic cells shown as green. Images acquired using a x 10 objective and DAPI and fluorescein filters. Scale bars 100 µm.

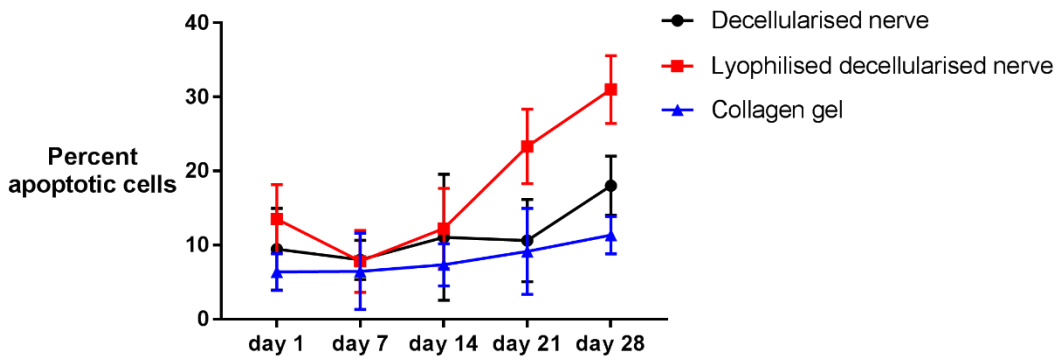

Figure 5.10 Quantification of apoptotic cells in primary rat DRGs cultured in decellularised and lyophilised decellularised human femoral nerve sections and collagen hydrogels. Percent apoptotic cells (number of apoptotic cells represented as a percentage of total number of cells) in sections of DRGs cultured in decellularised and lyophilised decellularised human femoral nerve segments and collagen hydrogels at days 1, 7, 14, 21 and 28 in culture. Number of cells calculated from images of TUNEL assay of sections of DRGs cultured in decellularised nerve, lyophilised decellularised nerve and or collagen hydrogels using Fiji software. Data represented as mean (n = 3 per time point) ± standard deviation.

5.4.4 Expression of NF-200 in DRGs cultured in decellularised nerve, lyophilised decellularised nerve and collagen hydrogels

Sections of native human femoral nerve and freshly isolated primary rat DRGs were labelled with a primary antibody against neurofilament-200 (NF-200) and a goat anti-rabbit IgG secondary antibody (Figure 5.11) to visualise neurofilaments. Neurofilament was observed within native human femoral nerve, confined to individual fascicles and appearing to form tightly aligned filaments corresponding with individual endoneurial tubes. However, labelling was fragmented and neurofilament did not appear to be ubiquitously expressed in the endoneurium (Figure 5.11 A). Neurofilament expression was observed within the freshly isolated DRGs, appearing as small, fragmented filaments tightly packed within the centre of the explanted tissue (Figure 5.11 B). No staining was observed in the isotype control sections (Figure 5.11 C).

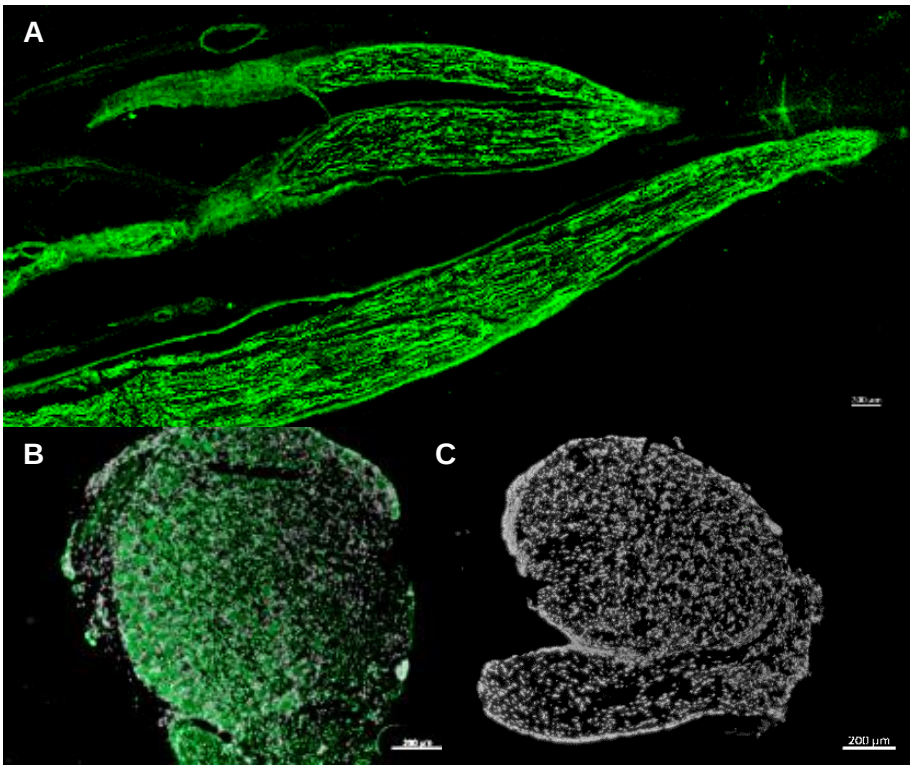

Figure 5.11 Immunofluorescent labelling of NF-200 in sections of native human femoral nerve and freshly isolated primary rat DRGs.
Representative images of sections of native human femoral nerve (A) and freshly isolated DRGs (B) labelled with a primary monoclonal antibody against NF-200 (green) and counterstained with DAPI (white), and freshly isolated DRGs incubated with an isotype control antibody (C). Images acquired using a x 10 objective and DAPI and FITC filters. Scale bars 200 µm.

Sections of primary rat DRGs cultured in decellularised and lyophilised decellularised human femoral nerve segments and collagen hydrogels at days 1, 7, 14, 21 and 28 in culture were labelled with a primary antibody against neurofilament-200 (NF-200) and a goat anti-rabbit IgG AF488 secondary antibody (Figure 5.12). The percent total area of neurofilament labelling (total area of neurofilament labelling (μm^2) represented as a percentage of the total area of DAPI staining (μm^2)) in sections of DRGs cultured in decellularised and lyophilised decellularised human femoral nerve segments and collagen hydrogels at days 1, 7, 14, 21 and 28 in culture is shown in Figure 5.13.

Sections of DRGs cultured in decellularised nerve showed that neurofilament expression appeared to gradually increase with prolonged culture time (Figure 5.12 A – E). Quantification of the percent total area of neurofilament labelling in DRGs cultured in decellularised nerve confirmed these observations, as the percent total area of neurofilament labelling increased over time from 20 % at day 1 to 40 % at day 28 (Figure 5.13). Sections of DRGs cultured in lyophilised decellularised nerve also showed that neurofilament expression appeared to gradually increase with prolonged culture time (Figure 5.12 F & G). Quantitative data corroborated these observations, as the percent total area of neurofilament labelling in DRGs cultured in lyophilised decellularised nerve increased from 12 % at day 1 to 20 % at day 28 (Figure 5.13). Neurofilament expression in sections of DRGs cultured in collagen hydrogels appeared to remain consistent, with no major differences observed at any time point (Figure 5.12 K – O). These observations were confirmed by quantification as the percent total area of neurofilament labelling in DRGs cultured in collagen hydrogels remained relatively consistent, from 42 % at day 1 to 45 % at day 28 (Figure 5.13).

Overall, the percent total area of neurofilament labelling in DRGs cultured in decellularised nerve was greater than in DRGs cultured in lyophilised decellularised nerve throughout the culture period (Figure 5.13). The percent total area of neurofilament labelling in DRGs cultured in collagen hydrogels was greater than in decellularised nerve and lyophilised decellularised nerve up to day 21 in culture. However, at day 28 no major differences were observed in the percent total area of neurofilament labelling in DRGs cultured in decellularised nerve (40 %) and collagen hydrogels (45 %) (Figure 5.13).

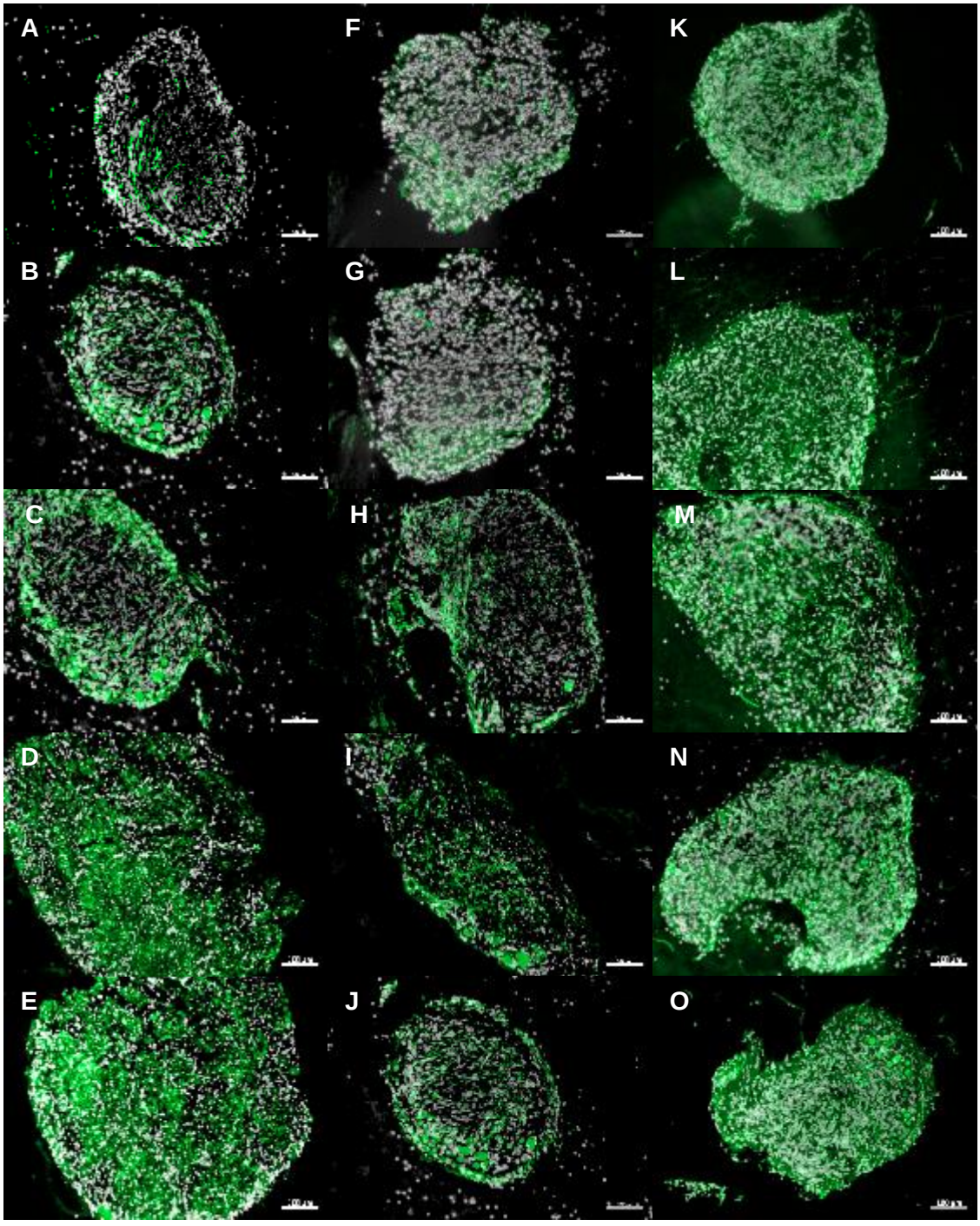

Figure 5.12 Immunofluorescent labelling of NF-200 in DRGs cultured in decellularised nerve, lyophilised decellularised nerve and collagen hydrogels. Representative images of DRGs cultured in decellularised nerve (A-E), lyophilised decellularised nerve (F-J) and collagen hydrogels (K-O) at time points points day 1 (A, F & K), day 7 (B, G & L), day 14 (C, H & M), day 21 (D, I & N) and day 28 (E, J & O) labelled with a primary monoclonal antibody against NF-200 (green) and counterstained with DAPI (white). Images taken using a x 10 objective using DAPI and FITC filters. Scale bars 100 μm.

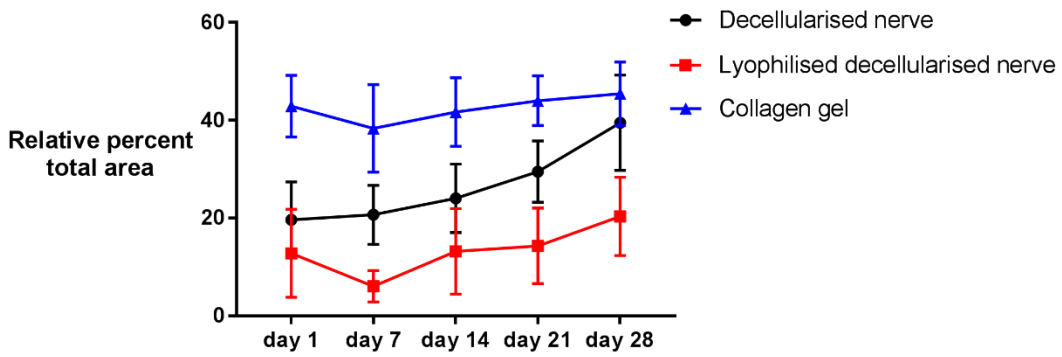

Figure 5.13 Quantification of immunofluorescent labelling of sections for NF-200 in primary rat DRGs cultured in decellularised and lyophilised decellularised human femoral nerve sections and collagen hydrogel.
Percent total area of neurofilament labelling (total area of neurofilament labelling (μm^2) represented as a relative percentage of the total area of DAPI staining (μm^2)) in sections of DRGs cultured in decellularised and lyophilised decellularised human femoral nerve segments and collagen hydrogels at days 1, 7, 14, 21 and 28 in culture. Total area (μm^2) of neurofilament labelling and DAPI staining calculated from images of sections of DRGs cultured in decellularised nerve, lyophilised decellularised nerve and collagen hydrogels labelled with NF-200 using Fiji software. Data represented as mean (n = 3 per time point) ± standard deviation.

Sections of DRGs cultured in decellularised and lyophilised decellularised human femoral nerve segments and collagen hydrogels at 28 days were also scanned and the scanned images tiled to present an overview of neurofilament expression and cell migration in the sections (Figure 5.14). Sections of DRGs cultured in decellularised nerve, lyophilised decellularised nerve and collagen hydrogels at 28 days showed neurofilament expression in cells migrating from the body of the DRG (Figure 5.14). Sections of DRGs cultured in collagen hydrogels showed neurofilament expression in migrating cells, although expression was sporadic, and neurofilament expression was mainly confined to the body of the DRG (Figure 5.14 A). However, sections of DRGs cultured in decellularised nerve showed neurofilament expression in migrating cells, and lower neuroflament expression in the body of the DRG (Figure 5.14 B). Furthermore, sections of DRGs cultured in lyophilised decellularised nerve also showed neurofilament expression in migrating cells, although overall neurofilament expression was lower than observed in DRGs cultured in collagen hydrogels or decellularised nerve (Figure 5.14 C).

Some differences were also observed in the orientation and distribution of migrating cells at day 28 (Figure 5.14). Sections of DRGs cultured in collagen hydrogels showed that cells were migrating from the body of the DRG, with no discernible alignment (Figure 5.14 A). However, sections of DRGs cultured in decellularised

nerve and lyophilised decellularised nerve showed aligned columns of migrating cells, although some sporadic migrating cells were observed (Figure 5.14 B & C).

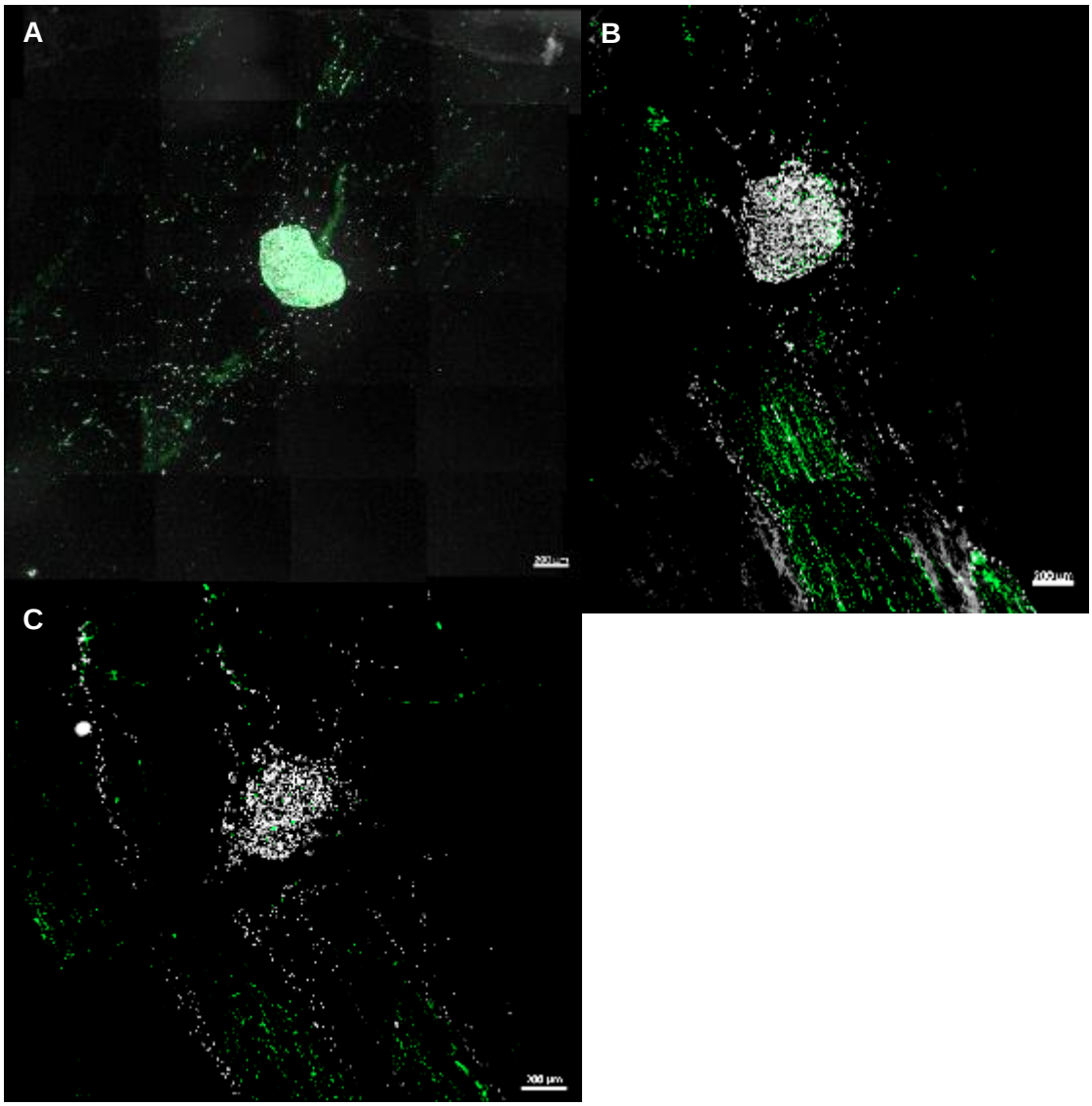

Figure 5.14 Images of immunofluorescent labelling of sections for NF-200 in primary rat DRGs cultured in decellularised and lyophilised decellularised human femoral nerve sections and collagen hydrogels at day 28 in culture. Representative images of tile scans of sections of DRGs cultured in collagen hydrogels (A), decellularised nerve (B) and lyophilised decellularised nerve (C) at time point day 28 labelled with a primary monoclonal antibody against NF-200 (green) and counterstained with DAPI (white). Images taken using a x 10 objective using DAPI and FITC filters. Tile scans were created by scanning whole sections and tiling images. Scale bars 500 µm.

5.4.5 Cell migration of DRGs cultured in decellularised nerve, lyophilised decellularised nerve and collagen hydrogels

Maximum cell migration distance was quantified by image analysis of sections of DRGs cultured in decellularised nerve, lyophilised decellularised nerve and collagen hydrogels at days 1, 7, 14, 21 and 28 in culture labelled with NF-200. The calculated maximum cell migration distances for each time point are shown in Figure 5.15. The data was analysed by two-way ANOVA with Tukey's post hoc test ($p<0.05$).

The maximum cell migration distance of DRGs cultured in collagen gels, decellularised nerve and lyophilised decellularised nerve increased with prolonged culture time, with increases observed at day 7, 14, 21 and 28 in culture (Figure 5.15). At day 1 in culture, there were no significant differences between the maximum cell migration distance of DRGs cultured in collagen hydrogels, decellularised nerve or lyophilised decellularised nerve (Figure 5.15). At day 7, 14, 21 and 28 in culture, the maximum cell migration distance of DRGs cultured in collagen hydrogels was significantly greater than the maximum cell migration distance for DRGs cultured in decellularised nerve (Figure 5.15). At day 7, 14, 21 and 28 in culture, the maximum cell migration distance of DRGs cultured in collagen hydrogels was also significantly greater than the maximum cell migration distance of DRGs cultured in lyophilised decellularised nerve (Figure 5.15). At day 7, 14 and 21 in culture, there were no significant differences between the maximum cell migration distance of DRGs cultured in decellularised nerve and lyophilised decellularised nerve (Figure 5.15). However, at day 28 in culture, the maximum cell migration distance for DRGs cultured in decellularised nerve was significantly greater than the maximum cell migration distance of DRGs cultured in lyophilised decellularised nerve (Figure 5.15).

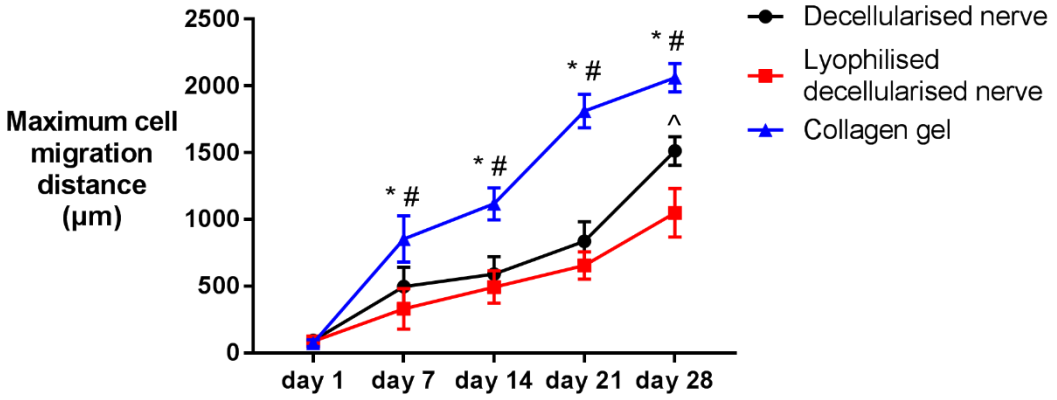

Figure 5.15 Maximum cell migration distance of primary rat DRGs cultured in decellularised and lyophilised decellularised human femoral nerve segments and collagen hydrogels. Maximum cell migration distance (µm) of DRGs cultured in decellularised nerve, lyophilised decellularised nerve and collagen hydrogels at days 1, 7, 14, 21 and 28 in culture. Cell migration distances (µm) calculated from images of sections of DRGs cultured in decellularised nerve, lyophilised decellularised nerve and collagen hydrogels labelled with NF-200 using ImageJ. Data represented as mean (n = 3 per time point) ± 95 % confidence limits. Statistical analysis was by two-way ANOVA with Tukey's post hoc test($p < 0.05$). Asterisks indicate a significant difference ($p< 0.05$) between the maximum cell migration distance of DRGs cultured in collagen hydrogels and decellularised nerve at day 7, day 14, day 21 and day 28. Hashtags indicate a significant difference ($p< 0.05$) between the maximum cell migration distance of DRGs cultured in collagen hydrogels and lyophilised decellularised nerve at day 7, day 14, day 21 and day 28. The caret indicates a significant difference between the maximum cell migration distance of DRGs cultured in decellularised nerve and lyophilised decellularised nerve at day 28.

5.4.6 Expression of satellite glial cell markers Sox2 and GS in primary rat DRGs cultured in decellularised and lyophilised decellularised human femoral nerve segments and collagen hydrogels

Sections of freshly isolated DRGs were labelled with primary antibodies against Sox2 and GS, a goat anti-mouse IgG AF647 secondary antibody and a goat anti-rabbit IgG AF488 secondary antibody (Figure 5.16). Sections of freshly isolated DRGs showed that a small number of Sox2 expressing cells were located sporadically in the body of the DRG (Figure 5.16 A). A greater number of GS expressing cells than Sox2 expressing cells were observed, and GS expressing cells appeared to form larger, circular structures in the body of the DRG (Figure 5.16 A). In addition, GS expressing cells appeared to form clusters of these circular structures (Figure 5.16 A). No labelling was observed in the native human nerve section labelled with an isotype control antibody (Figure 5.16 B).

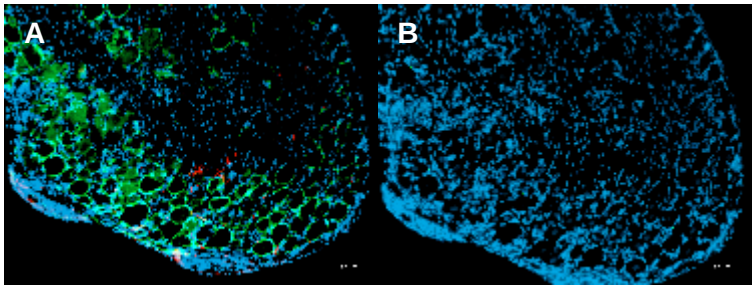

Figure 5.16 Immunofluorescent labelling of Sox2 and GS in sections of freshly isolated primary rat DRGs. Representative images of freshly isolated DRGs labelled with primary antibodies against Sox2 (red) and GS (green) (A) and freshly isolated DRGs incubated with isotype control antibodies (B) and counterstained with DAPI (blue). Images taken using a x 10 objective using DAPI and FITC filters. Scale bars 100 µm.

Sections of DRGs cultured in decellularised nerve, lyophilised decellularised nerve and collagen hydrogels at days 1, 7, 14, 21 and 28 in culture were also labelled with primary antibodies against Sox2 and GS, a goat anti-mouse IgG AF647 secondary antibody and a goat anti-rabbit IgG AF488 secondary antibody (Figure 5.17). The percent total area of Sox2 labelling (total area of Sox2 labelling (μm^2) represented as a percentage of the total area of DAPI staining (μm^2)) in sections of DRGs cultured in decellularised and lyophilised decellularised human femoral nerve segments and collagen hydrogels at days 1, 7, 14, 21 and 28 in culture is shown in

Figure 5.18. The percent total area of GS labelling (total area of GS labelling (μm^2) represented as a percentage of the total area of DAPI staining (μm^2)) in sections of DRGs cultured in decellularised and lyophilised decellularised human femoral nerve segments and collagen hydrogels at days 1, 7, 14, 21 and 28 in culture is shown in Figure 5.19.

Sox2 expression was observed in sections of DRGS cultured in decellularised nerve, lyophilised decellularised nerve and collagen hydrogels at all time points (Figure 5.17). Sox2 expressing cells were sporadically located, and the number of Sox2 expressing cells was low and highly variable (Figure 5.17). Quantification of Sox2 labelling showed that the percent total area of Sox2 labelling in DRGs cultured in decellularised and lyophilised decellularised nerve segments and collagen hydrogels varied between circa 1% and 8% at all time points in culture, and no major differences were observed over time in culture (Figure 5.18).

GS expression was also observed in sections of DRGs cultured in decellularised nerve, lyophilised decellularised nerve and collagen hydrogels at all time points (Figure 5.17). Sections of DRGS cultured in decellularised nerve, lyophilised decellularised nerve and collagen hydrogels showed that the expression pattern of GS changed with prolonged culture time. At day 1, GS expressing cells formed larger circular structures clustered together in the body of the DRG (Figure 5.17 A, F & K). At days 7, 14, 21, and 28 in culture these circular structures were absent, with sporadic cellular expression of GS, although some clustering of GS expressing cells was still observed (Figure 5.17 B-E, G-J & K-O).

Sections of DRGs cultured in collagen hydrogels showed that little change was observed in GS expression with prolonged culture time (Figure 5.17 K-O). The percent total area of GS labelling in DRGs cultured in collagen hydrogels decreased slightly from 48 % at day 1 to 37 % at day 28 in culture, however high variation was observed (Figure 5.19). Sections of DRGs cultured in decellularised nerve showed that GS expression appeared to decrease with increased time in culture (Figure 5.17 A-E). Quantification confirmed visual observations, as the percent total area of GS labelling in DRGs cultured in decellularised nerve changed from 46 % at day 1 to 9 % at day 28 (Figure 5.19). Sections of DRGs cultured in lyophilised decellularised nerve also showed that GS expression decreased with prolonged culture time, although not to the same extent as DRGs cultured in decellularised nerve (Figure 5. F-J). The percent total area of GS labelling in DRGs cultured in

lyophilised decellularised nerve decreased between day 1 (43 %) and day 28 (22 %) supporting visual observations (Figure 5.19).

Quantification of GS labelling showed no major differences between the percent total area of GS labelling in DRGs cultured in collagen hydrogels, decellularised nerve or lyophilised decellularised nerve at day 1 or day 7 (Figure 5.19). However, from day 7 onwards the percent total area of GS labelling in DRGs cultured in collagen hydrogels was greater than the percent total area of GS labelling in DRGs cultured in decellularised nerve or lyophilised decellularised nerve (Figure 5.19). From day 14 onwards, the percent total area of GS labelling in DRGs cultured in decellularised nerve was greater than the percent total area of GS labelling in DRGs cultured in lyophilised decellularised nerve (Figure 5.19).

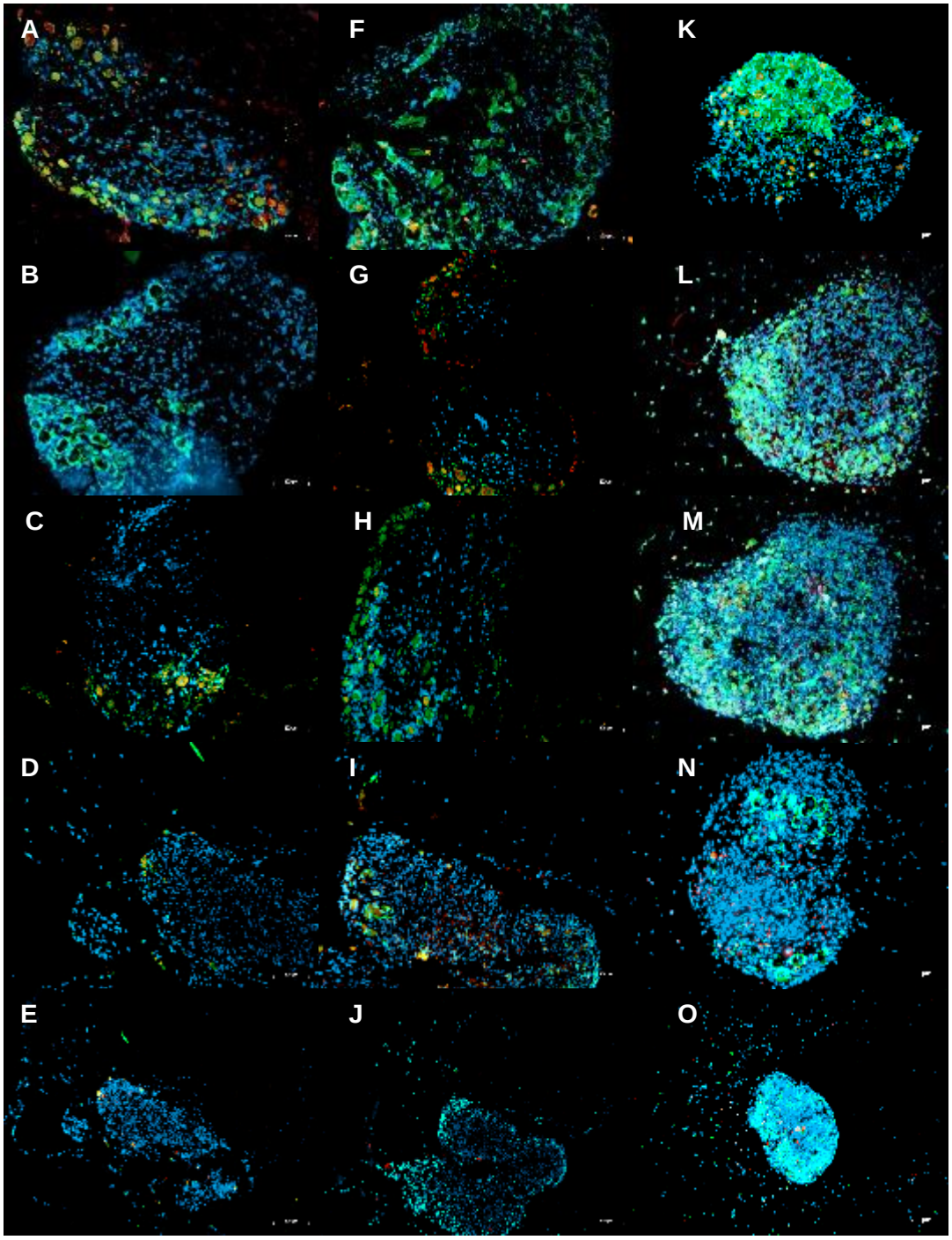

Figure 5.17 Immunofluorescent labelling of Sox2 and GS in sections of DRGs cultured in decellularised nerve, lyophilised decellularised nerve and collagen hydrogels. Representative images of sections of DRGs cultured in decellularised nerve (A-E), lyophilised decellularised nerve (F-J) and collagen hydrogels (K-O) at time points day 1 (A, F & K), day 7 (B, G & L), day 14 (C, H & M), day 21 (D, I & N) and day 28 (E, J & O) labelled with primary antibodies against Sox2 (red) and GS (green) and counterstained with DAPI (blue). Images taken using a x 10 objective using DAPI and FITC filters. Scale bars 100 μm.

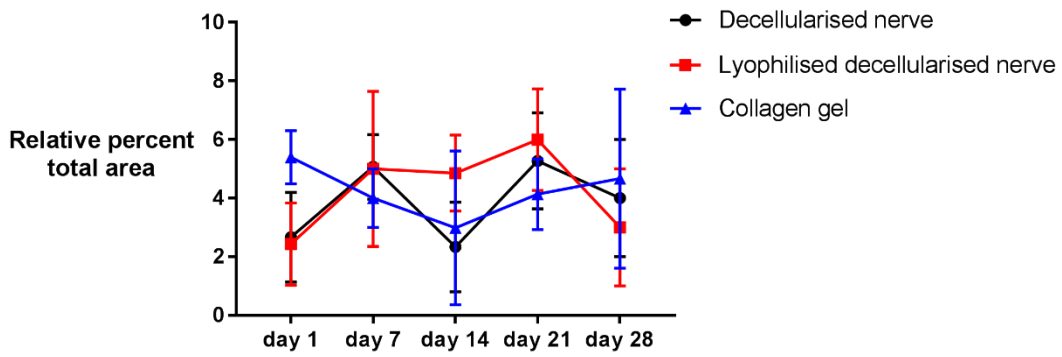

Figure 5.18 Quantification of immunofluorescent labelling of sections for Sox2 in primary rat DRGs cultured in decellularised and lyophilised decellularised human femoral nerve sections and collagen hydrogels. Percent total area of Sox2 labelling (total area of Sox2 labelling (μm^2) represented as a relative percentage of the total area of DAPI staining (μm^2)) in sections of DRGs cultured in decellularised and lyophilised decellularised human femoral nerve segments and collagen hydrogels at days 1, 7, 14, 21 and 28 in culture. Total area (μm^2) of Sox2 labelling and DAPI staining calculated from images of sections of DRGs cultured in decellularised nerve, lyophilised decellularised nerve and collagen hydrogels labelled with Sox2 using Fiji software. Data represented as mean (n = 3 per time point) ± standard deviation.

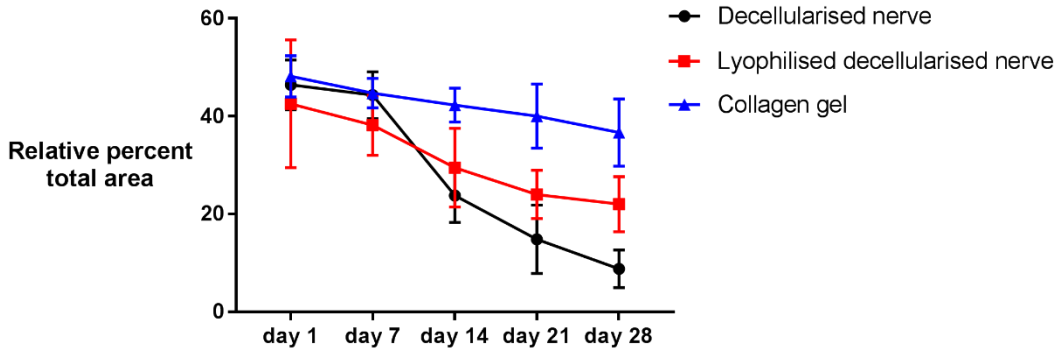

Figure 5.19 Quantification of immunofluorescent labelling of sections for GS in primary rat DRGs cultured in decellularised and lyophilised decellularised human femoral nerve sections and collagen hydrogels. Percent total area of GS labelling (total area of GS labelling (μm^2) represented as a percentage of the total area of DAPI staining (μm^2)) in sections of DRGs cultured in decellularised and lyophilised decellularised human femoral nerve segments and collagen hydrogels at days 1, 7, 14, 21 and 28 in culture. Total area (μm^2) of GS labelling and DAPI staining calculated from images of sections of DRGs cultured in decellularised nerve, lyophilised decellularised nerve and collagen hydrogels labelled with GS using Fiji software. Data represented as mean (n = 3 per time point) ± standard deviation.

5.4.7 Expression of Schwann cell markers MBP and NCAM-1 in DRGs cultured in decellularised nerve, lyophilised decellularised nerve and collagen hydrogels

Sections of freshly isolated DRGs were labelled with primary antibodies against MBP and NCAM-1, a goat anti-mouse IgG AF647 secondary antibody and a goat anti-rabbit IgG AF488 secondary antibody (Figure 5.20). Sections of freshly isolated DRGs showed that NCAM-1 expressing cells were mainly located along the edges of the body of the DRG, and the expression of NCAM-1 did not appear to co-localise with the expression of MBP (Figure 5.20 A). MBP expression was observed in sections of freshly isolated DRGs, and appeared to form clusters of elongated tubes in the centre of the DRG (Figure 5.20 A). No labelling was observed in the isotype control (Figure 5.20 B).

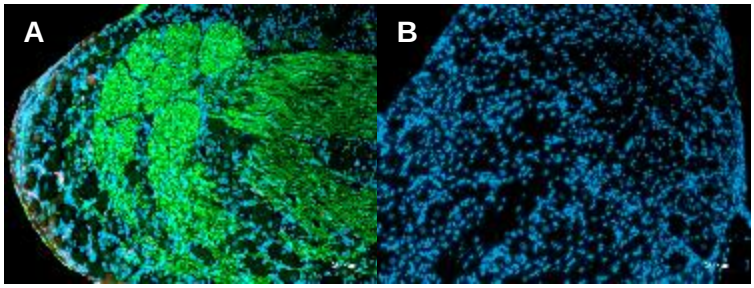

Figure 5.20 Immunofluorescent labelling of MBP and NCAM-1 in sections of freshly isolated DRGs. Representative images of sections of freshly isolated DRGs labelled with primary antibodies against MBP (green) and NCAM-1 (red) (A) and freshly isolated DRGs incubated with isotype control antibodies (B) and counterstained with DAPI (blue). Images taken using a x 10 objective using DAPI and FITC filters. Scale bars 100 µm.

Sections of DRGs cultured in decellularised nerve, lyophilised decellularised nerve and collagen hydrogels at days 1, 7, 14, 21 and 28 in culture were also labelled with primary antibodies against MBP and NCAM-1, a goat anti-mouse IgG AF647 secondary antibody and a goat anti-rabbit IgG AF488 secondary antibody (Figure 5.21). The percent total area of NCAM-1 labelling (total area of NCAM-1 labelling (μm^2) represented as a percentage of the total area of DAPI staining (μm^2)) in sections of DRGs cultured in decellularised and lyophilised decellularised human femoral nerve segments and collagen hydrogels at days 1, 7, 14, 21 and 28 in culture is shown in Figure 5.22. The percent total area of MBP labelling (total area of MBP labelling (μm^2) represented as a percentage of the total area of DAPI staining (μm^2)) in sections of DRGs cultured in decellularised and lyophilised decellularised human femoral nerve segments and collagen hydrogels at days 1, 7, 14, 21 and 28 in culture is shown in Figure 5.23.

Sections of DRGs cultured in cultured in decellularised nerve, lyophilised decellularised nerve and collagen hydrogels showed NCAM-1 expression at all time points in culture (Figure 5.21). However, at day 1 in culture NCAM-1 expression appeared to have increased in DRGs cultured in decellularised nerve, lyophilised decellularised nerve or collagen hydrogels (Figure 5.21 A, F & K) in comparison to freshly isolated DRGs (Figure 5.20 A).

No major differences in NCAM-1 expression were observed in sections of DRGs cultured in decellularised nerve, lyophilised decellularised nerve or collagen hydrogels between day 1 and day 7 in culture (Figure 5.21 A – B, F – G & K – L). From day 14 onwards, NCAM-1 expression appeared to decrease in sections of DRGs cultured in decellularised nerve, lyophilised decellularised nerve and collagen hydrogels (Figure 5.21 C – E, H – J, M – O). However, the percent total area of NCAM-1 labelling in DRGs cultured in collagen hydrogels gradually decreased from 25 % at day 1 to 5 % at day 28 (Figure 5.22). The percent total area of NCAM-1 labelling in DRGs cultured in decellularised nerve and lyophilised decellularised nerve also decreased between day 1 and day 28, although this decrease was not as great as in the collagen gels (Figure 5.22). The percent total area of NCAM-1 labelling in DRGs cultured in decellularised nerve decreased from 26 % at day 1 to 18 % at day 28, and the percent total area of NCAM-1 labelling in DRGs cultured in lyophilised decellularised nerve decreased from 27 % at day 1 to 19 % at day 28 (Figure 5.22).

At day 1 in culture, no major differences were observed in the percent total area of NCAM-1 labelling in DRGs cultured in decellularised nerve, lyophilised decellularised nerve or collagen hydrogels (Figure 5.22). However, the percent total area of NCAM-1 labelling in DRGs cultured in collagen hydrogels was lower than the percent total area of NCAM-1 labelling in DRGs cultured in decellularised nerve or lyophilised decellularised nerve from day 7 onwards (Figure 5.22). No major differences were observed in the percent total area of NCAM-1 labelling in DRGs cultured in decellularised nerve or lyophilised decellularised nerve at any time point in culture (Figure 5.22).

Sections of DRGS cultured in decellularised nerve, lyophilised decellularised nerve and collagen hydrogels showed that the expression pattern of MBP changed with prolonged culture time. At day 1 in culture, MBP appeared to form clusters of elongated tubes in the body of the DRG (Figure 5.21 A, F & K). However, from day 7 onwards, MBP expression appeared fragmented and distributed further away

from the centre of the DRG, with some sporadic cellular MBP expression also observed (Figure 5.21 B-E, G-J & L-O).

Sections of DRGs cultured in collagen hydrogels showed that MBP expression decreased with prolonged culture time, with almost no MBP expression observed by day 28 in culture (Figure 5.21 K-O). The percent total area of MBP labelling in DRGs cultured in collagen hydrogels also decreased with a prolonged culture time, although percent total area of MBP labelling remained relatively consistent from 38 % at day 1 to 36 % at day 7, and decreased from day 7 onwards to 7 % by day 28 (Figure 5.23). Sections of DRGs cultured in decellularised nerve and lyophilised decellularised nerve also showed that MBP expression decreased with prolonged culture time, although some MBP expression was still observed at day 28 (Figure 5.21 A – E & F - J). The percent total area of MBP labelling in DRGs cultured in decellularised nerve decreased from 51 % at day 1 to 38 % at day 14, and remained consistent from day 14 onwards to 37 % by day 28 (Figure 5.23). The percent total area of MBP labelling in DRGs cultured in lyophilised decellularised nerve decreased from day 39 % at day 1 to 20 % at day 28, with decreases observed at each time point (Figure 5.23).

The percent total area of MBP labelling in DRGs cultured in decellularised nerve was greater than in DRGs cultured in lyophilised decellularised nerve or collagen hydrogels throughout the culture period (Figure 5.23). From day 7 onwards, the percent total area of MBP labelling in DRGs cultured in lyophilised decellularised nerve was also greater than in DRGs cultured in collagen hydrogels (Figure 5.23).

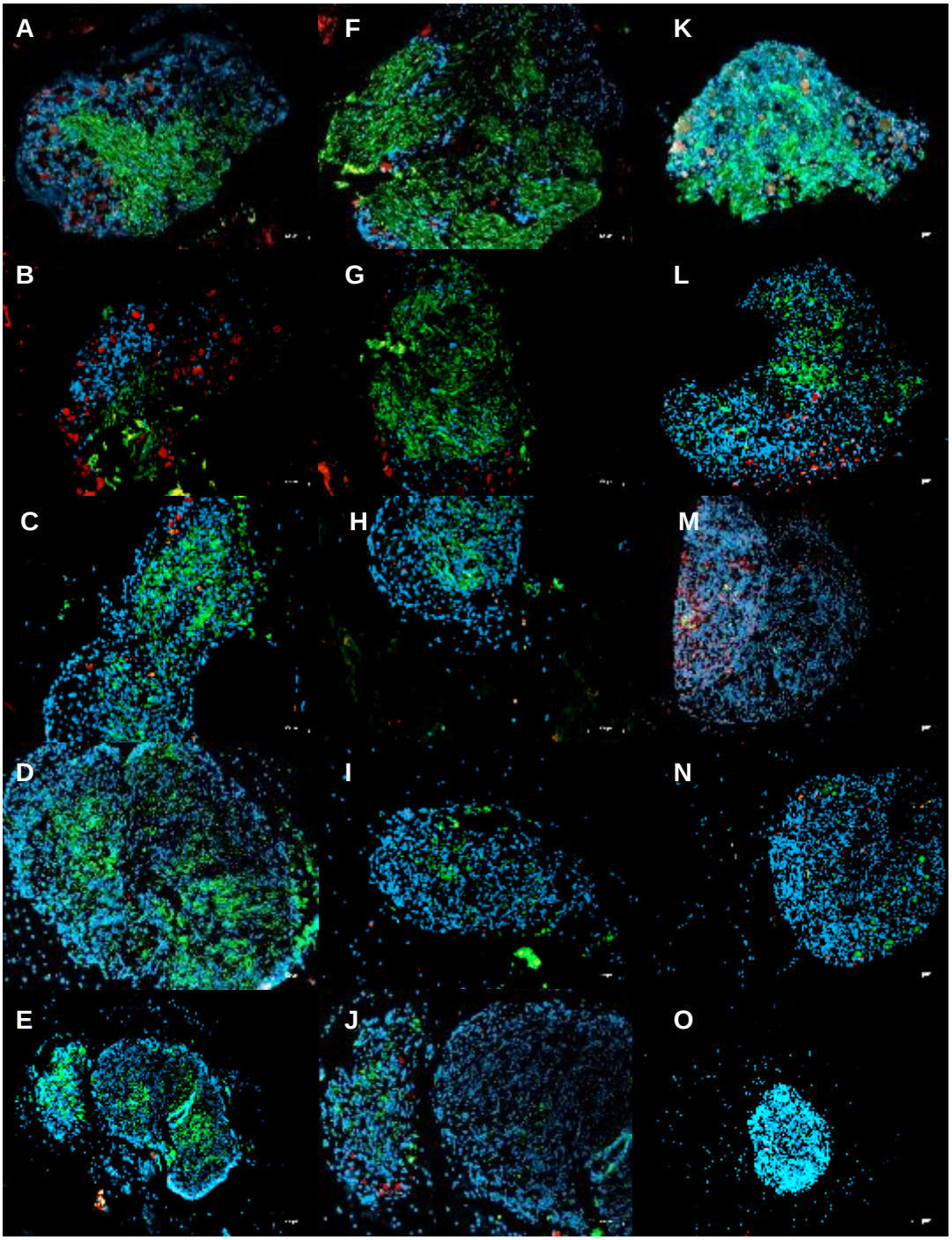

Figure 5.21 Immunofluorescent labelling of NCAM-1 and MBP in sections of DRGs cultured in decellularised nerve, lyophilised decellularised nerve and collagen hydrogels. Representative images of sections of DRGs cultured in decellularised nerve (A-E), lyophilised decellularised nerve (F-J) and collagen hydrogels (K-O) at time points points day 1 (A, F & K), day 7 (B, G & L), day 14 (C, H & M), day 21 (D, I & N) and day 28 (E, J & O) labelled with primary antibodies against NCAM-1 (red) and MBP (green) (A) and counterstained with DAPI (blue). Images taken using a x 10 objective using DAPI and FITC filters. Scale bars 100 μm.

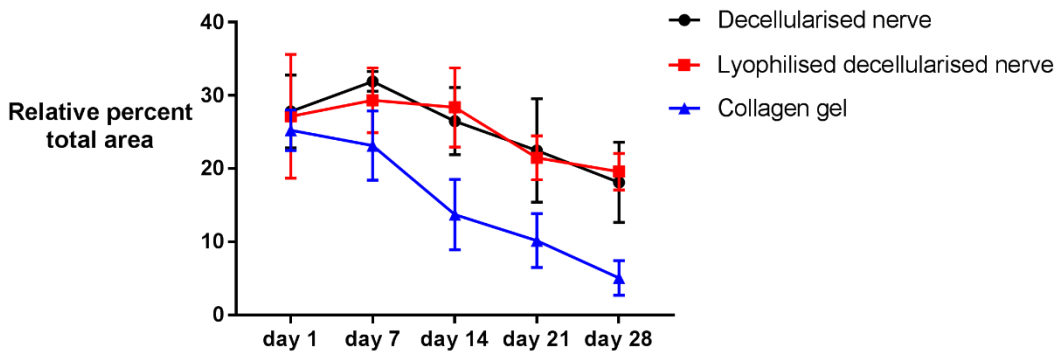

Figure 5.22 Quantification of immunofluorescent labelling of sections for NCAM-1 in primary rat DRGs cultured in decellularised and lyophilised decellularised human femoral nerve sections and collagen hydrogels. Percent total area of NCAM-1 labelling (total area of NCAM-1 labelling (μm^2) represented as a relative percentage of the total area of DAPI staining (μm^2)) in sections of DRGs cultured in decellularised and lyophilised decellularised human femoral nerve segments and collagen hydrogels at days 1, 7, 14, 21 and 28 in culture. Total area (μm^2) of NCAM-1 labelling and DAPI staining calculated from images of sections of DRGs cultured in decellularised nerve, lyophilised decellularised nerve and collagen hydrogels labelled with NCAM-1 using Fiji software. Data represented as mean (n = 3 per time point) ± standard deviation.

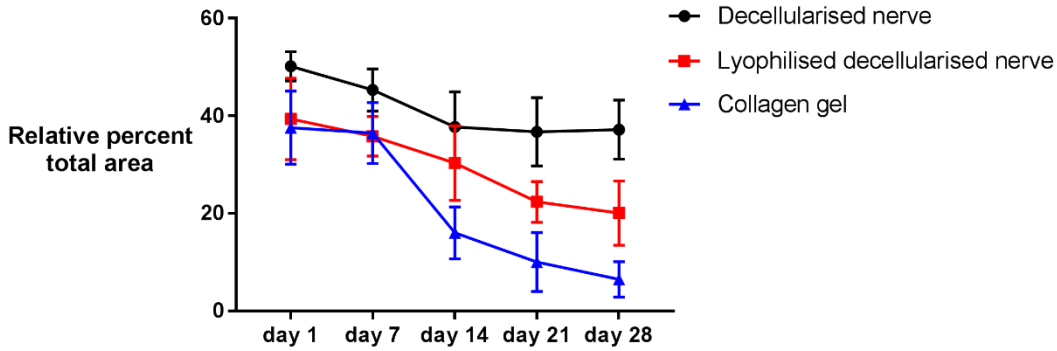

Figure 5.23 Quantification of immunofluorescent labelling of sections for MBP in primary rat DRGs cultured in decellularised and lyophilised decellularised human femoral nerve sections and collagen hydrogels. Percent total area of MBP labelling (total area of MBP labelling (μm^2) represented as a relative percentage of the total area of DAPI staining (μm^2)) in sections of DRGs cultured in decellularised and lyophilised decellularised human femoral nerve segments and collagen hydrogels at days 1, 7, 14, 21 and 28 in culture. Total area (μm^2) of MBP labelling and DAPI staining calculated from images of sections of DRGs cultured in decellularised nerve, lyophilised decellularised nerve and collagen hydrogels labelled with MBP using Fiji software. Data represented as mean (n = 3 per time point) ± standard deviation.

5.5 Discussion

Decellularised human femoral nerve segments were cultured with primary rat DRG explants *in vitro* for up to 28 days, in order to assess long-term biocompatibility and neurite outgrowth. Primary adult rat DRGs were chosen as they can be easily isolated and inserted into scaffolds, as discussed previously, and sprout neurites *in vitro*. The presence of a complex native ECM microenvironment, with intact endoneurial tubes, is believed to be the main advantage of decellularised nerve grafts in comparison to NGCs. In order to investigate the importance of a native ECM microenvironment, DRG explants were also cultured with rat tail type I collagen hydrogels, as a non-aligned control scaffold (Whitlock *et al.*, 2009; Khaing and Schmidt, 2012; Faroni *et al.*, 2015). Furthermore, it is hypothesised that inadequate preservation of the linear architecture of endoneurial tubes impairs axon regeneration and cellular infiltration in a decellularised nerve graft (Whitlock *et al.*, 2009). Lyophilised decellularised human nerve was identified as a potential variable scaffold in which the linear architecture of endoneurial tubes is disrupted. Histological analysis of lyophilised decellularised human nerve showed that the endoneurial architecture was severely damaged in comparison to native nerve, and individual endoneurial tubes could no longer be identified. However, basement membrane components laminin and collagen type IV were preserved. Therefore, lyophilisation was selected as a method to disrupt endoneurial architecture, and primary DRG explants were also cultured with lyophilised decellularised nerve as a disrupted variable to assess the importance of endoneurial architecture.

The *in vitro* culture experiments presented in this chapter were limited to a small number of replicates per time point. Three replicates was the maximum practicable number of replicates, due to limited availability of human femoral nerves, and the limited number of DRGs that could be isolated. Statistical analysis was only performed on parametric data, therefore quantitative image analysis data, of immunofluorescent labelling and TUNEL assay, was not statistically analysed.

It is essential for decellularised nerve grafts and NGCs to support the long-term adhesion and viability of Schwann cells to support axon regeneration, as axon regeneration has been reported to be slow (approximately 1 mm per day) and progressively fails over distance and time due to deterioration of the distal nerve stump and declining Schwann cell numbers (Ronchi and Raimondo, 2017; Wagstaff, 2018; López-Leal and Diaz, 2018). Collagen type I is commonly used for the fabrication of NGCs, as it is highly biocompatible and the smooth

microgeometry and transmural permeability (100, 000 D) enable nutrient diffusion through collagen type I matrices (Khaing and Schmidt, 2012; Kehoe *et al.*, 2012). Although decellularised human femoral nerve was shown to be biocompatible and retain a native ECM architecture, as discussed in Chapter 4, the architecture of native peripheral nerve ECM is less porous than homogenous collagen type I scaffolds, which may result in lower diffusion rates and adversely affect cell viability (Sun *et al.*, 2008; Zilic *et al.*, 2016). However, analysis of cell viability by ATPlite assay showed that there were no significant differences between the ATP content of DRGs cultured in collagen hydrogels and decellularised human femoral nerve up to day 28 in culture, indicating that decellularised human femoral nerve is also a suitable substrate for long-term cell viability. Furthermore, quantification of TUNEL staining supported these findings, as no major differences were observed between the percent apoptotic cells in DRGs cultured in decellularised nerve and collagen hydrogels at all time points in culture, although high variation was observed.

Analysis of cell viability by ATPlite assay showed that the ATP content of DRGs cultured in lyophilised decellularised nerve was significantly lower than the ATP content of DRGs cultured in decellularised nerve and collagen hydrogels at day 28 in culture, although no significant differences were found at earlier culture times. Quantification of TUNEL staining showed that there were no major differences between the percent apoptotic cells in DRGs cultured in decellularised nerve, lyophilised decellularised nerve and collagen hydrogels up to day 14 in culture, however, the percent apoptotic cells in DRGs cultured in lyophilised decellularised nerve was greater than the percent apoptotic cells in DRGs cultured in decellularised nerve and collagen hydrogels at both day 21 and day 28 in culture. These differences may be due to variability between DRGs, as high variation was observed in the data, but may also be due to an increase in the number of apoptosing cells producing ATP at day 21 in culture. Apoptosis, the process of programmed cell death, is a highly regulated, energy intensive cellular breakdown process, and is contingent upon the availability of intracellular ATP.

These results suggest that although initial cell viability is not affected, the disruption of endoneurial architecture adversely affects long-term cell viability in decellularised nerve. This may be due to impaired cell migration, or cell adhesion and the establishment of cell-matrix interactions required for long-term survival (Gilmore *et al.*, 2009). However, lyophilisation of decellularised nerve may also physically damage ECM proteins and collapse the delicate internal structure, which may have

contributed to this and also adversely affected long-term cellular adhesion and viability.

Collagen type 1 matrices, including hydrogels and aligned sponges, have previously been shown to support neurite outgrowth of primary rat DRG explants within 24 hours *in vitro* (Dalamagkas *et al.*, 2016; Geuna *et al.*, 2016; Neto *et al.*, 2017; Bozkurt *et al.*, 2007). Quantification of immunofluorescent labelling of NF-200 showed that the percent total area of NF-200 labelling in DRGs cultured in collagen hydrogels was greater than the percent total area of NF-200 labelling in decellularised nerve or lyophilised nerve up to day 21 in culture. Furthermore, neurofilament expression was observed at day 1 *in vitro*, and did not appear to significantly increase with prolonged culture time, suggesting that neurite outgrowth was rapidly established in DRGs cultured in collagen hydrogels. However, at day 28 in culture, no major differences were observed between the percent total area of NF-200 labelling in DRGs cultured in collagen hydrogels and decellularised nerve. One potential explanation for this could be that the homogenous, non-aligned permeable structure of collagen hydrogels enables rapid neurite outgrowth and permits neurite outgrowth and cell migration in all directions, whereas only endoneurial tubes of decellularised nerve ECM are permissive to neurite outgrowth and thus alignment with linear endoneurial tubes is required (Stang *et al.*, 2005; Whitlock *et al.*, 2009; Kehoe *et al.*, 2012). As discussed previously, it is hypothesised that inadequate preservation of endoneurial tubes impairs axon regeneration and cellular infiltration in a decellularised nerve graft (Whitlock *et al.*, 2009). The percent total area of NF-200 labelling was lower in DRGs cultured in lyophilised decellularised nerve than in DRGs cultured in decellularised nerve by day 28 in culture, supporting this hypothesis and suggesting that disruption to endoneurial architecture adversely affects neurite outgrowth in a decellularised nerve graft.

The non-aligned, homogenous structure of the collagen hydrogels may also explain the differences observed in cellular migration distance and orientation (Bozkurt *et al.*, 2007; Dalamagkas *et al.*, 2016). The maximum cell migration distance was significantly greater in DRGs cultured in collagen hydrogels than in DRGs cultured in decellularised nerve or lyophilised decellularised nerve from day 7 onwards in culture, however in collagen hydrogels cell migration was radial around the DRG, and no columnar alignment was observed. Collagen type I matrices are often manufactured as complex linear structures with highly aligned channels and parallel oriented pores to promote oriented axon regeneration, as discussed in Chapter 1

(Bozkurt *et al.*, 2007; Khaing and Schmidt, 2012). Various techniques have been used to form aligned scaffolds with a specific pore size, including electrospinning, cross-linking and unidirectional freezing (Stang *et al.*, 2005; Kehoe *et al.*, 2012). A study by Bozkurt *et al.* (2007) used unidirectional freezing followed by lyophilisation to produce a highly aligned collagen type I scaffold, and compared this scaffold to a non-aligned fibrin scaffold by culture with DRG explants for up to 21 days *in vitro*. The study reported random and irregular cellular migration in the non-aligned scaffold, as opposed to columnar oriented migrating cells in the aligned collagen scaffold, and found that neurite distance was significantly greater when associated with columnar oriented cells, including Schwann cells (Bozkurt *et al.*, 2007). Other studies have also reported random and irregular Schwann cell alignment and reduced neurite outgrowth of DRG explants when cultured with non-aligned scaffolds (Gnavi *et al.*, 2018; Khan *et al.*, 2002). Although the maximum cell migration distance was significantly lower in DRGs cultured in decellularised nerve or lyophilised decellularised nerve than in collagen hydrogels from day 7 onwards in culture, columnar oriented cell migration was observed in sections of DRGs cultured in decellularised nerve and lyophilised nerve. Therefore, these results suggest that the presence of a native ECM architecture promotes columnar oriented cell migration, which may be beneficial for promoting neurite outgrowth (Bozkurt *et al.*, 2007).

Although several studies of DRGs cultured with various scaffolds *in vitro* have reported columnar oriented cell migration in aligned scaffolds, as opposed to random cell migration in non-aligned scaffolds, only a small number of the migrating cells were found to be Schwann cells and changes in the expression of Schwann cell markers were not assessed (Bozkurt *et al.*, 2007; Gnavi *et al.*, 2018). Neural cell adhesion molecule-1 (NCAM-1) is a marker of non-myelinating Schwann cells, which closely associate with neurons and modulate neuron activity (Jessen *et al.*, 2015). NCAM-1 is involved in neuron-neuron adhesion, neurite fasciculation and the early stages of neurite development (Takeda *et al.*, 2001). Myelin basic protein (MBP) is produced by myelinating Schwann cells, which form the myelin sheath surrounding axons (Jessen *et al.*, 2015).

Quantification of immunofluorescent labelling of NCAM-1 showed that the percent total area of NCAM-1 labelling decreased in DRGs cultured in decellularised nerve, lyophilised decellularised nerve and collagen hydrogels over culture time, however the percent total area of NCAM-1 labelling decreased more in DRGs cultured in collagen hydrogels from day 7 onwards. This may be due to non-myelinating

Schwann cells responding to a loss of axonal contact or it may be due to neurite development, as NCAM-1 is expressed in the early stages (Takeda *et al.*, 2001). However, as discussed previously, no differences in neurofilament expression were observed between DRGs cultured in decellularised nerve and collagen hydrogels by day 28.

Quantification of immunofluorescent labelling of MBP showed that the percent total area of MBP labelling decreased with prolonged culture time in DRGs cultured in collagen hydrogels, decellularised nerve and lyophilised decellularised nerve. However, the percent total area of MBP labelling in DRGs cultured in collagen hydrogels was lower than the percent total area of MBP labelling in DRGs cultured in decellularised nerve or lyophilised decellularised nerve at all time points in culture. Therefore, stimuli from the native ECM of decellularised nerve, including topographical, ECM protein or basement membrane cues, may be influencing Schwann cell phenotype and function, or the interaction of migrating Schwann cells with developing neurites in endoneurial tubes maintained the stimuli for NCAM-1 and MBP expression (Roumazeilles *et al.*, 2018; Chernousov *et al.*, 2008; Spivey *et al.*, 2012). In addition, from day 7 onwards in culture, the percent total area of MBP labelling was greater in sections of DRGs cultured in decellularised nerve than in lyophilised decellularised nerve. This may be due to stimuli provided by intact endoneurial tubes, either influencing MBP expression directly, or indirectly due to the increased neurofilament expression observed in DRGs cultured in decellularised nerve (Allodi *et al.*, 2012; Spivey *et al.*, 2012; Chernousov *et al.*, 2008). However, MBP expression appeared greater in sections of freshly isolated DRG than in sections of DRGs cultured in decellularised nerve, lyophilised decellularised nerve and collagen hydrogels at any time point in culture, which may be due to reduced MBP expression in response to injury during the DRG isolation process, or due a lack of stimuli for MBP expression in the *in vitro* culture conditions.

Other studies of DRGs cultured with scaffolds have identified Schwann cells, but have not investigated other cell types in the DRG in detail (Bozkurt *et al.*, 2007; Neto *et al.*, 2017; Gnavi *et al.*, 2018). As discussed previously, DRGs also contain satellite glial cells (SGCs), which are capable of migrating out of the DRG explant and are thought to participate in peripheral nerve injury and repair (George *et al.*, 2018; Dubový *et al.*, 2019).

Quantification of immunofluorescent labelling of GS showed that the percent total area of GS labelling decreased in DRGs cultured in collagen hydrogels, decellularised nerve, and lyophilised decellularised nerve over 28 days in culture, consistent with the finding of other studies, which have reported a loss of GS expression when SGCs are cultured *in vitro* (Belzer *et al.*, 2010). The reduction in GS expression may be caused by a loss of axonal contact or reduced axonal signalling (Bak *et al.*, 2006; Huang *et al.*, 2013). However, from day 7 onwards, the percent total area of GS labelling in DRGs cultured in collagen hydrogels was greater than the percent total area of GS labelling in DRGs cultured in decellularised nerve or lyophilised decellularised nerve. This may be because SGCs retained a closer association with neurons in DRGs cultured in collagen hydrogels, or SGCs were responding to a loss of stimuli when DRGs were cultured in decellularised nerve or lyophilised decellularised nerve (Geuna *et al.*, 2016; Neto *et al.*, 2017).

SGCs are also thought to be multipotent cells, capable of differentiating into multiple cell types, including Schwann cell-like cells and oligodendrocytes (Svenningsen *et al.*, 2004; Hanani, 2005; Weider *et al.*, 2015). SGC nuclei have also been reported to express Sox2, a stem cell marker, although not all SGCs have been found to express Sox2 (Weider *et al.*, 2015; Koike *et al.*, 2015). Sox2 expression was observed sporadically in sections of DRGs cultured in collagen hydrogels, lyophilised nerve or decellularised nerve, although Sox2 expression did not appear to co-localise with GS expression, supporting the finding that not all SGCs express Sox2 (Koike *et al.*, 2015). However, quantification of immunofluorescent labelling of Sox2 showed that the percent total area of Sox2 labelling was highly variable and did not change with prolonged culture time, indicating a lack of differentiation which could be due to the absence of stimuli required (George *et al.*, 2018). Previous studies have shown SGCs only differentiate *in vitro* once cultured in isolation, and other studies have required elevated levels of Sox10 transcription factor to induce differentiation (Weider *et al.*, 2015; George *et al.*, 2018).

As discussed previously, one of the main limitations of the *in vitro* DRG culture experiments discussed in this chapter was the small number of repeats that could be included. Therefore, further investigations are required, including a repeat of the experiments discussed here, with a larger number of replicates in order to confirm the findings of this study.

5.6 Conclusions

The results presented in this chapter suggest that decellularised human femoral nerve is a suitable substrate to support cellular infiltration and axon regeneration. Decellularised human femoral nerve was shown to support long-term cell viability and migration, and the formation of aligned neurites when cultured with primary rat DRG explants for up to 28 days *in vitro*. These results also support the hypothesis that inadequate preservation of endoneurial tubes impairs cellular infiltration and axon regeneration, as lyophilisation of decellularised nerve adversely affected long-term cell viability, migration, and neurofilament expression of DRGs. Furthermore, decellularised nerve appeared to maintain the expression of MBP better than lyophilised decellularised nerve and collagen hydrogels, suggesting that intact endoneurial tubes may have a role in supporting Schwann cell phenotype and function.

Chapter 6: General Discussion

6.1 Introduction

Current interventions for peripheral nerve repair are limited, variable in efficacy, and are associated with a number of limitations which were discussed in Chapter 1. The motivation for this study was to develop a decellularised peripheral nerve allograft as an alternative surgical intervention for peripheral nerve repair. Decellularised nerve grafts offer considerable clinical potential, and there is existing clinical evidence to support the use of decellularised nerve grafts for peripheral nerve repair (Chapter 1). However, studies of the Avance® graft have not yet demonstrated consistently superior clinical outcomes to autografts, even for the repair of small defects (up to approximately 30 mm) (Karabekmez *et al.*, 2009; Whitlock *et al.*, 2009; Johnson *et al.*, 2011). It has been proposed that the currently available decellularised nerve graft has limited regenerative capacity in comparison to autografts, particularly for the repair of longer defects (greater than 30 mm), as a consequence of ECM disruption caused by the decellularisation process.

The overarching hypothesis of this study was that a biocompatible, decellularised peripheral nerve graft could be developed for future use in peripheral nerve repair, with the retention of overall ECM histioarchitecture and basement membrane. As discussed in Chapter 1, numerous decellularisation methods have been developed, and the effects of different decellularisation processes on the ECM are highly variable. The proprietary University of Leeds decellularisation process utilises low concentration SDS (0.1 %; w/v) plus proteinase inhibitors in combination with hypotonic and hypertonic buffers and nuclease treatment, and has been shown to remove cellular and nuclear material sufficiently from several tissues, with minimal alterations to the ECM (Booth *et al.*, 2002; Wilshaw *et al.*, 2012; Azhim *et al.*, 2014). Zilic *et al*. (2016) adapted the University of Leeds decellularisation process to develop a process for the decellularisation of porcine peripheral nerves, and the process was shown to achieve a sufficient reduction in DNA content. Histological results demonstrated the retention of basement membrane components, however structural changes were observed to the perineurium and endoneurial tubes, and changes were observed in the distribution of collagen fibrils, laminin and fibronectin (Zilic *et al.*, 2016).

In this study, the decellularisation process for porcine peripheral nerves described by Zilic *et al*. (2016) was further developed with the aim of minimising structural

changes whilst maintaining the efficacy of decellularisation (Chapter 3). Once an improved decellularisation process had been identified, the process was translated for the decellularisation of human femoral nerves (Chapter 4). Decellularised human femoral nerve segments were then cultured with primary adult rat DRG explants in order to investigate the ability of human decellularised nerve to support neurite outgrowth, cell viability and cell migration *in vitro* (Chapter 5).

6.2 Porcine vs human decellularised nerve grafts

Although the use of porcine tissue as a source material offers considerable clinical potential, the use of xenogeneic tissue for decellularised nerve grafts is associated with several limitations (Chapter 1). Preclinical and clinical evidence of axon regeneration only exists for the use of decellularised allografts, such as the Avance® graft, and there is little research comparing the use of decellularised allogeneic and xenogeneic nerve grafts *in vivo* (Wang et al., 2016). A study by Wood *et al.* (2014) compared human (xenograft) and rat (allograft) decellularised peripheral nerves in a rat sciatic nerve defect model in comparison to an autograft. Both the human and rat decellularised peripheral nerve grafts were prepared by AxoGen, using the same methods and quality testing as used for the commercial Avance® graft (Wood et al., 2014). The decellularised nerve grafts were evaluated 12 weeks post implantation, and it was shown that the myelinated axon count in the xenograft was significantly lower than in the allograft or autograft, and the authors concluded that the xenograft impaired regeneration. Wang *et al*. (2016), compared an autograft to decellularised rat and rabbit peripheral nerves in a rat sciatic defect model, and reported no significant differences between autograft, xenograft or allograft at 12 weeks post-implantation (Wang et al., 2016). Therefore, the importance of species specificity for the clinical use of decellularised nerve grafts for peripheral nerve repair and the potential effects of xenografts on axon regeneration remain unclear. In this study, a decellularised human femoral nerve graft was to developed to overcome the limitations associated with porcine tissue, and to provide a human decellularised nerve graft which could then be further developed and translated as a Class III medical device by NHSBT TES.

6.3 Development of improved decellularisation methods

An improved decellularisation process for porcine peripheral nerves was developed (Chapter 3). The major changes to the original process were to minimise chemical exposure and reduce the agitation speed during incubations, in order to minimise

damage to the ECM architecture and composition. Porcine peripheral nerves decellularised using the improved protocol were shown to have sufficient DNA content reduction and retain overall histioarchitecture. The improved decellularisation process for porcine peripheral nerves was then applied to segments of human femoral nerves (Chapter 4). The size of the nerve segments was increased from 30 mm (porcine) to 60 mm (human), which was considered more appropriate for clinical application. Initial results showed that the porcine peripheral nerve decellularisation protocol did not achieve sufficient DNA content reduction in human femoral nerves, which was likely due to the increase in the size of the nerve segments. Further development of the decellularisation process showed that the inclusion of an additional hypertonic buffer incubation achieved sufficient DNA content reduction in decellularised human femoral nerve. The inclusion of this additional hypertonic buffer incubation did not appear to adversely affect the ECM histioarchitecture, as human femoral nerves decellularised using the finalised protocol were shown to retain overall histioarchitecture.

The decellularisation process must result in a scaffold which is biocompatible. Prior to clinical application, decellularised nerve grafts must be shown to be biocompatible as a regulatory requirement, and International Organisation for Standardisation (ISO) standards must be adhered to. Part five of ISO standard 10993 (Biological evaluation of medical devices) includes guidelines for *in vitro* cytotoxicity testing, including contact and extract cytotoxicity testing. The results presented in this study demonstrated that decellularised porcine peripheral nerves (Chapter 3) and decellularised human femoral nerves (Chapter 4) were biocompatible. Contact cytotoxicity assays using BHK and L929 cells showed no changes in cell morphology and growth when cultured with the decellularised nerve. However, extract cytotoxicity testing should also be performed prior to clinical application.

It has been proposed that in addition to the criteria for successful decellularisation proposed by Crapo *et al*. (2011), discussed in Chapter 1, criteria should also include the removal of cell membrane debris (Kawecki *et al.*, 2018; Crapo *et al.*, 2011). In addition, a review of methods of quality control for decellularised nerve grafts by Philips *et al*. (2018) suggested that in addition to the previous criteria for decellularisation, quality control criteria for decellularised nerve grafts should include the removal of myelin, assessed by histological or immunohistochemical analyses (Philips *et al.*, 2018). The removal of myelin from a decellularised nerve graft is clinically important, as the presence of residual myelin debris has been

shown to inhibit axonal growth by prolonging the process of Wallerian degeneration (Chapter 1). As discussed in Chapter 3, several studies using other methods of decellularisation have shown incomplete removal of myelin from decellularised peripheral nerves (Gulati, 1988; Evans *et al.*, 1998; Wang *et al.*, 2016). Histological results presented in this study demonstrated the absence of myelin in decellularised porcine peripheral nerve (Chapter 3) and decellularised human femoral nerve (Chapter 4), indicating the decellularisation processes successfully removed myelin from the tissues.

6.4 Evaluation of biological components

Biochemical assays, including the quantification of collagen and GAG content using colourimetric assays, have been widely used to determine the effects of decellularisation processes on the biochemical composition of the ECM of various tissues, and to complement histological analysis (Kawecki *et al.*, 2018; Philips *et al.*, 2018). Interestingly, few studies of the development of decellularised xenogeneic or allogeneic peripheral nerve grafts have assessed the effects of decellularisation on biochemical composition (Philips *et al.*, 2018). Sridharan *et al.* (2015) decellularised rat sciatic nerves using a modified version of the decellularisation protocol described by Sondell *et al*. (1998), utilising a combination of 3 % (w/v) Triton X-100 and 2 % (w/v) sodium deoxycholate, and quantified the GAG and collagen content of native and decellularised rat sciatic nerves. Following decellularisation, the hydroxyproline content (a measure of collagen content) had decreased by more than 50 % and the GAG content had decreased by more than 90 %. The authors concluded this was likely due to ECM disruption caused by the detergents used (Sridharan *et al.*, 2015). In this study, biochemical analyses showed that there were no significant differences in the collagen and denatured collagen content of native and decellularised porcine peripheral nerves (Chapter 3) and between the collagen and denatured collagen content of native and decellularised human femoral nerve (Chapter 4). However, similar to the results reported by Sridharan *et al*. (2015), quantification of GAG content showed that there was a significant decrease in the GAG content of human femoral nerve following decellularisation (Chapter 4), although no significant difference was found between the GAG content of native and decellularised porcine peripheral nerve (Chapter 3). Glycosaminoglycans (GAGs) have various functions in peripheral nerve ECM, they are implicated in the maintenance of other ECM molecules, structural integrity and the regulation of cellular growth, and are located in the basement membrane (Krekoski *et al.*, 2001; Zuo *et al.*, 2002; Neubauer *et al.*, 2007). As discussed in Chapter 4, chondroitin

sulphate proteoglycans (CPSGs) are involved in the inhibition of axonal growth and have been shown to be inhibitory to axon regeneration (Krekoski *et al.*, 2001; Zuo *et al.*, 2002; Neubauer *et al.*, 2007). Therefore, the loss of GAGs in decellularised human femoral nerve may be clinically beneficial to promoting axonal regeneration.

One of the key advantages of decellularised nerve grafts in comparison to NGCs is the provision of specific basement membrane components (Burnett and Zager, 2004; de Ruiter *et al.*, 2009; Gaudet *et al.*, 2011). The basement membrane, located in the endoneurium and perineurium, facilitates cell-matrix interactions, enabling Schwann cell adhesion and promoting axon elongation and maturation in the endoneurium (Kerns, 2008). Many of the methods used to decellularise peripheral nerve been shown to significantly damage the basement membrane (Chapter 3) (Sondell *et al.*, 1998; Evans *et al.*, 1998; Krekoski *et al.*, 2001). In this study, decellularised porcine peripheral nerve, and decellularised human femoral nerve, were shown to retain laminin in comparison to native tissue. Furthermore, decellularised porcine peripheral nerve, and decellularised human femoral nerve, also retained basement membrane components collagen type IV and fibronectin, which have not been assessed by studies of the Avance® graft and may also be of clinical benefit (Yang *et al.*, 2011; Wood *et al.*, 2014).

6.5 Evaluation of the capacity of decellularised human femoral nerve to support primary cell populations *in vitro*

In order to promote axon regeneration, decellularised nerve grafts must be able to support the elongation of regenerating axons and viable populations of Schwann cells (Chapter 1). It was therefore important to determine whether decellularised human femoral nerve segments could support neurite outgrowth and viable populations of primary neural cells, including Schwann cells, *in vitro*. In this study, a novel method was developed for the culture of decellularised human femoral nerve segments with primary adult rat DRG explants in order to investigate the ability of human decellularised nerve to support neurite outgrowth, cell viability and cell migration *in vitro*. As discussed in Chapter 5, currently there is no *in vitro* model of peripheral nerve, and peripheral nerve regeneration cannot be replicated *in vitro* (Geuna *et al.*, 2016; Mobini *et al.*, 2017). DRG explant organotypic cultures are commonly used for *in vitro* studies of peripheral nerve regeneration, as they can be easily isolated and inserted into scaffolds, and enable quantification of neurite

outgrowth and cell migration from the body of the DRG explant (Geuna *et al.*, 2016; Neto *et al.*, 2017). However, there have been no previous studies of decellularised nerve grafts cultured with DRG explants *in vitro.* Therefore, the results presented in Chapter 5 represent a novel *in vitro* culture system for DRG explants with decellularised human nerve, which could be used for future *in vitro* culture studies of decellularised nerve.

The linear microarchitecture of endoneurial tubes is believed to be one of the key advantages of decellularised nerve grafts in comparison to NGCs (Khaing and Schmidt, 2012; Faroni *et al.*, 2015). In order to investigate the importance of endoneurial architecture in a decellularised nerve graft, DRG explants were also cultured in segments of lyophilised decellularised human nerve, in which endoneurial architecture was disrupted whilst basement membrane components laminin and collagen type IV were preserved (Chapter 5). The results presented in Chapter 5 represent a novel method for the disruption of endoneurial architecture whilst maintaining overall histioarchitecture and basement membrane components. Therefore, lyophilisation is a method which could be used for further studies of the effects of disruption to the endoneurial architecture on decellularised nerve both *in vitro* and *in vivo*. DRG explants were also cultured with rat tail type I collagen hydrogels, as a non-aligned control scaffold, to investigate the importance of a native ECM microenvironment and linear architecture (Whitlock *et al.*, 2009; Khaing and Schmidt, 2012; Faroni *et al.*, 2015)

Collagen hydrogels, decellularised nerve and lyophilised decellularised nerve cultured with DRGs were shown to support viable cells up to day 28 in culture. There were no differences in the ability of collagen hydrogels and decellularised nerve to support viable cells (Chapter 5), indicating that decellularised human femoral nerve is also a suitable substrate for supporting long-term cell viability. The results presented in Chapter 5 also suggest that disruption of endoneurial architecture in a decellularised nerve graft adversely affects long-term cell viability, and may be of clinical significance for the development of decellularised nerve grafts since sustained axon regeneration is dependent on the presence of viable populations of Schwann cells (Wagstaff, 2018; Jessen *et al.*, 2015). These results, however, may not necessarily be reflected upon implantation *in vivo*, and although lyophilisation was chosen as method to disrupt endoneurial architecture, this may not reflect damage to endoneurial architecture sustained during decellularisation.

The results presented in Chapter 5 also suggest that in comparison to DRGs cultured in collagen hydrogels, cell migration and the establishment of neurite outgrowth in DRGs cultured in decellularised nerve is delayed, although long-term neurite outgrowth may not be adversely affected as no differences were observed by day 28. It has been hypothesised that the homogenous, permeable structure of collagen hydrogels enables rapid and sustained neurite outgrowth and cell migration in all directions, whereas only the endoneurial tubes of decellularised nerve ECM are permissive to neurite outgrowth, and thus alignment with linear endoneurial tubes is required (Bozkurt *et al.*, 2007; Dalamagkas *et al.*, 2016). However, delayed neurite outgrowth could potentially impair the regenerative process, as axon regeneration progressively fails over distance and time if axon contact is not re-established, as discussed previously (Ronchi and Raimondo, 2017; Wagstaff, 2018; López-Leal and Diaz, 2018). The results presented in Chapter 5 also suggest that disruption to endoneurial architecture adversely affects long-term neurite outgrowth and cell migration in a decellularised nerve graft. However, columnar oriented cell migration was observed in DRGs cultured in decellularised nerve and lyophilised nerve, whereas cells migrating from the body of DRGs cultured in collagen hydrogels showed no discernible alignment. Therefore, these results suggest that the presence of a native ECM architecture promotes oriented cell migration, which may be beneficial for promoting oriented axon regeneration and increasing axon regeneration distance, as discussed in Chapter 5. Directional axon regeneration is required to re-establish axonal contact and prevent axon deviation, and NGCs, including collagen type I matrices, are often manufactured as complex linear structures with highly aligned channels and parallel oriented pores to replicate the native ECM architecture and promote oriented axon regeneration (Bozkurt *et al.*, 2007; Khaing and Schmidt, 2012; Allodi *et al.*, 2012)

Currently, it is thought that the efficacy of decellularised nerve grafts and NGCs is limited to shorter distances (up to 30 mm) due to insufficient host Schwann cell migration to sustain axon regeneration (Szynkaruk *et al.*, 2012; Gerth *et al.*, 2015; Busuttil *et al.*, 2017). Therefore, it is essential that decellularised peripheral nerve grafts are able to support Schwann cell infiltration and migration upon implantation (Szynkaruk *et al.*, 2012). However, the interaction of Schwann cells with decellularised nerve grafts has not been well characterised *in vitro*. Although several studies of DRGs cultured with various scaffolds *in vitro* investigated neurite outgrowth and cell migration, only a small number of the migrating cells were found to be Schwann cells, and changes in the expression of Schwann cell markers were not assessed (Bozkurt *et al.*, 2007; Gnavi *et al.*, 2018). In this study, the expression

of mature Schwann cell markers MBP and NCAM-1, and SGC markers GS and Sox2 in DRGs cultured in collagen hydrogels, decellularised and lyophilised decellularised nerve were assessed by immunofluorescent labelling (Chapter 5).

NCAM-1 and MBP expression were found to decrease more in DRGs cultured in collagen hydrogels than in decellularised or lyophilised decellularised nerve with prolonged culture time (Chapter 5). Therefore, these results suggest that stimuli from the native ECM of decellularised nerve, including topographical, ECM protein or basement membrane cues, may be influencing Schwann cell phenotype and function. Another potential explanation could be that close interaction of columnar-oriented migrating Schwann cells with developing neurites in endoneurial tubes maintained the stimuli for NCAM-1 and MBP expression (Roumazeilles *et al.*, 2018; Chernousov *et al.*, 2008; Spivey *et al.*, 2012). MBP expression was also found to decrease further in DRGs cultured in lyophilised decellularised nerve than in decellularised nerve (Chapter 5). This may be due to stimuli provided by intact endoneurial tubes, either influencing MBP expression directly, or indirectly due to the increased neurofilament expression observed in DRGs cultured in decellularised nerve (Allodi *et al.*, 2012; Spivey *et al.*, 2012; Chernousov *et al.*, 2008). These findings may be of clinical relevance for the future development of decellularised nerve grafts, and future studies investigating the supplementation of decellularised nerve grafts with Schwann cells. The results presented (Chapter 5) suggest that a native ECM microenvironment may have a role in influencing the phenotype and function of Schwann cells (Jessen and Mirsky, 2016; Chernousov *et al.*, 2008). Furthermore, in addition to the hypothesis that inadequate preservation of endoneurial architecture impairs axon regeneration and cellular infiltration in a decellularised nerve graft, it may also be that the preservation of endoneurial architecture is important for maintaining Schwann cell function and myelination (Whitlock *et al.*, 2009).

6.6 Future work

6.6.1 Future studies required for clinical translation

6.6.1.1 Scale up of production of decellularised human femoral nerves

Further studies are required to investigate how the decellularisation protocol could be adapted to produce large numbers of decellularised human femoral nerves for clinical use. The UK Human Tissue Act (2004) prevents tissues from individual donors coming into contact with tissues from other donors, therefore tissue from different donors must be decellularised separately. Increased sample numbers could be processed individually in parallel using closed loop systems, which have previously been used by NHSBT TES for the decellularisation of tissues. The use of a closed loop system for the introduction and removal of decellularisation solutions would also enable processing in a lower-grade aseptic cleanroom, as the closed system remains sterile and reduces the risk of contamination. It is also possible that the decellularisation process could be shortened for use in a commercial setting. Furthermore, future automation of solution changes would reduce personnel burden and decrease solution change-over times.

Good Manufacturing Practice (GMP) production must also adhered to meet regulatory requirements for the production of decellularised human tissue for clinical use and maintain consistency between batches. In this study, Cambridge antibiotic solution was used as part of the decellularisation process for human femoral nerves (Chapter 4), since this is used by NHSBT TES for human tissue decellularisation for clinical use. In order to meet GMP requirements, all other solutions used in the decellularisation process would need to be quality assured and obtained from approved suppliers.

6.6.1.2 Sterilisation of decellularised human femoral nerves

Prior to clinical application, a sterilisation method for decellularised human femoral nerves must be identified. Medical devices, including decellularised nerve grafts derived from allogeneic and xenogeneic sources, must be sterilised prior to implantation. The accepted sterility assurance level (SAL) for medical devices, defined in ISO standard 14937, is 10^{-6} whereby less than 1 in 1,000,000 devices sterilised by a given method within a defined set of parameters will contain a surviving viable microorganism (ISO, 2009).

There are several potential sterilisation methods which could be applied to decellularised human femoral nerves, including ethylene oxide, electron beam (E-beam), γ-irradiation, peracetic acid (PAA), supercritical CO_2 and hydrogen peroxide (in isolation or in combination with copper (II) chloride) (Delgado *et al.*, 2014; Leow-Dyke *et al.*, 2016). Terminal sterilisation methods, including γ-irradiation, ethylene oxide and E-beam, would enable the decellularised tissue to be sterilised after packaging, and are therefore preferable for commercial production as aseptic packaging is not required and the risk of contamination post sterilisation is eliminated.

Each sterilisation method presents several advantages and limitations, and sterilisation processes can significantly alter the histoarchitecture and biomechanical properties of ECM-based scaffolds (Badylak *et al.*, 2009; Hodde *et al.*, 2007a). Radiation-based sterilisation methods, such as γ-irradiation and E-beam, have been shown to damage the collagen chains within the ECM, and chemical sterilants (e.g. oxidising agents, including peracetic acid, and alkylating agents, including ethylene oxide) may also disrupt ECM proteins (Grant *et al.*, 1973; Hodde *et al.*, 2007b). For example, the standard accepted dosage for medical device sterilisation using γ-irradiation is 25 kilograys (kGy), as determined by ISO 11137. However, this dose of γ-irradiation has previously been shown to damage the collagen within ECM of decellularised tissues through the generation of free radicals, and alter the biomechanical properties of decellularised tissues (Smith and Kearney, 1996; Edwards *et al.*, 2017). In this study, lyophilisation of decellularised human femoral nerve was shown to damage the internal histioarchitecture (Chapter 5). Therefore, sterilisation strategies requiring lyophilisation, e.g. γ-irradiation, may not be suitable for decellularised human femoral nerve, and would require further investigation.

6.6.1.3 Biomechanical evaluation

Peripheral nerves are exposed to an array of mechanical forces associated with body movement, including tensile, compressive and shear forces (Chapter 1). Peripheral nerves are able to withstand mechanical forces because of the viscoelastic properties of the ECM, which enables the nerve to elongate in response to longitudinal stress during body movements (Topp and Boyd, 2012). Therefore, for clinical application, it is essential that decellularised peripheral nerve grafts retain the biomechanical properties of native nerve, as any alterations to biomechanical properties may adversely affect axon regeneration *in vivo*.

The use of chemical detergent decellularisation methods is known to disrupt the structure and composition of ECM molecules, and can alter the biomechanical properties of the ECM (Chapter 1). As discussed previously, Zilic *et al*. (2016) developed a decellularisation process for porcine peripheral nerve. The study investigated the biomechanical properties of native and decellularised nerves using uniaxial tensile testing, and assessed the Young's modulus, ultimate tensile strength (UTS) and strain at UTS (Zilic *et al.*, 2016). The study showed no significant difference in the Young's modulus of native and decellularised porcine peripheral nerve, however there was a significant increase in the UTS and strain at UTS of decellularised nerve in comparison to native nerve. The authors hypothesised that these changes in decellularised nerve were due to uncrimping or relaxation of collagen fibres caused by cell removal during the decellularisation process, which has previously been associated with increased stiffness in soft tissues (Williams *et al.*, 2009; Zilic *et al.*, 2016). The results were comparable to other studies of decellularised tissues, including porcine meniscus, which have reported similar alterations to biomechanical properties (Stapleton *et al.*, 2008; Abdelgaied *et al.*, 2015). However, the clinical implications of alterations to the biomechanical properties of decellularised nerve grafts remain unclear.

In this study, the decellularisation process described by Zilic *et al.* (2016) was modified, and was also applied to human femoral nerves. Therefore, the biomechanical properties of the decellularised porcine peripheral nerves and decellularised human femoral nerves developed in this study should be evaluated by uniaxial tensile testing methods. In addition, biomechanical evaluation could also include suture retention tensile testing, as for clinical use decellularised peripheral nerve grafts must be able to retain sutures upon implantation, and compression testing.

6.6.1.4 Biological evaluation

Further biological evaluation of decellularised human femoral nerves is required prior to clinical application. Once a sterilisation method has been identified, the effects of sterilisation on ECM architecture, biochemical composition and the retention of basement membrane components would also need to be determined, using the analysis methods described in Chapters 3 and 4.

Further analyses could include immunohistochemical assessment of different types of collagen, including collagen type I, II and III, which have been discussed in Chapter 1. Scanning electron microscopy (SEM) or transmission electron

microscopy (TEM) could also be used to further investigate the preservation of ECM ultrastructure, and the preservation of key basement membrane components. Further biological evaluation could also include the assessment of residual cellular debris and membrane components following decellularisation. As discussed in Chapter 1, MHC class I molecules remaining in decellularised tissues could illicit a specific host immune response upon implantation. Immunohistochemical analyses could be therefore be used to assess the removal of MHC Class I and Class II molecules from the decellularised nerve.

6.6.1.5 *In vivo* biocompatibility

Preclinical *in vivo* studies are necessary prior to clinical translation of decellularised nerve grafts or NGCs, in order to ensure biocompatibility and assess the occurrence of adverse events, and evaluate the efficacy of axon regeneration (Szynkaruk *et al.*, 2012). Therefore, future work should include evaluating the decellularised human femoral nerve graft developed in this study *in vivo*.

The most commonly used *in vivo* model for peripheral nerve regeneration is a rat sciatic nerve defect model, however various different defect lengths have been used, typically ranging from 10 – 30 mm (Mobini *et al.*, 2017). Decellularised peripheral nerve grafts and an array of NGCs have been evaluated *in vivo* using rat sciatic nerve defect models, as discussed in Chapter 1 (Pedrini *et al.*, 2018; Lovati *et al.*, 2018). Autografts, the gold standard intervention for peripheral nerve repair are often used as a control, and outcome measures used to assess regeneration include behavioural, electrophysiological and histological analyses. A recent review of the use of decellularised nerve grafts for peripheral nerve repair assessed the various outcome measures that can be used for peripheral nerve regeneration, and reported on the most widely used behavioural, electrophysiological and histological analyses (Pedrini *et al.*, 2018). The study reported that common histological analyses included assessment of infiltration by cells of the immune system and Schwann cells, and assessment of axon count, diameter, myelination and axon regeneration distance. Common behavioural analyses were walking-track analysis and toe-spreading reflex, and response to surface stimulation, measured using electromyography, was the most common electrophysiological analysis. However as outcome measures were found to differ between studies, comparing the efficacy of different NGCs or decellularised nerve grafts is problematic (Pedrini *et al.*, 2018).

The decellularised human femoral nerve graft developed in this study should be evaluated *in vivo*, using a rat sciatic nerve defect model. Autografts should be used

as a control, and widely used behavioural, electrophysiological and histological analyses (as above) should be used to ensure comparison with the findings of other studies of decellularised nerve grafts. A number of studies have reported a limited efficacy of decellularised nerve grafts over longer distances, typically exceeding 20 - 30 mm, as discussed in Chapter 1 (Szynkaruk *et al.*, 2012; Karabekmez *et al.*, 2009). Therefore, a number of different defect lengths could also be used, ranging from 10 - 40 mm, in order to assess the efficacy of the decellularised human femoral nerve graft over increasing distances and compare with the findings of other studies. Lyophilised decellularised human nerve could also be evaluated *in vivo* in a rat sciatic nerve defect model, in order to investigate the importance of endoneurial architecture.

6.6.2 Future studies to support the clinical use of decellularised nerve

6.6.2.1 Repopulation with primary Schwann cells

It has been hypothesised that the efficacy of decellularised nerve grafts is limited to shorter distances due to insufficient host Schwann cell migration to sustain axon regeneration (Szynkaruk *et al.*, 2012; Gerth *et al.*, 2015; Busuttil *et al.*, 2017). Therefore, it is thought that the development of a decellularised nerve graft repopulated with Schwann cells may offer considerable clinical potential as an Advanced Therapy Medicinal Product (ATMP). Although recent experimental strategies for enhancing peripheral nerve regeneration have included the repopulation of decellularised nerve grafts with exogenous autologous Schwann cells (Chapter 1), there is currently no clinically viable source of minimally manipulated exogenous autologous Schwann cells (Faroni *et al.*, 2015; Mobini *et al.*, 2017; Lackington *et al.*, 2017). ASCs and BMSCs have, however, demonstrated promising experimental results for peripheral nerve repair, and are currently the only potential source of exogenous autologous Schwann cells.

A number of studies have focused on the repopulation of decellularised human nerve grafts with primary rat Schwann cells, and have assessed axon regeneration *in vivo* in rat sciatic nerve defect models (Pedrini *et al.*, 2018). However, few studies have investigated the long-term interaction of primary Schwann cells with decellularised nerve grafts *in vitro*, and there is currently no established method for the introduction of primary Schwann cells into a decellularised nerve graft (Szynkaruk *et al.*, 2012; Pedrini *et al.*, 2018).

Future work could therefore include establishing a method for the introduction of primary Schwann cells into a decellularised nerve graft, using primary rat Schwann cells as an accessible source of a large number of Schwann cells for method development. A purified population of primary Schwann cells could be isolated from rat sciatic nerves, using a previously established method (Kaewkhaw *et al.*, 2012). Direct injection of cell suspension is the most commonly used method to introduce Schwann cells into decellularised nerve grafts (Fan *et al.*, 2014; Mobini *et al.*, 2017). A method for the introduction of Schwann cells into decellularised human femoral nerve could be established using primary rat Schwann cells, including identifying the number of cells to be injected, volume of cell suspension to be injected and the method of injection i.e. location and number of injection points within the decellularised nerve. In addition, several studies of repopulating NGCs with primary Schwann cells have investigated the use of perfusion bioreactors for introducing cells to the conduit. A study by Sun *et al*. (2008) established a simple closed loop perfusion bioreactor to introduce primary Schwann cells on a scaffold manufactured from longitudinally aligned microfibers of viscose rayon and polystyrene. The study reported that a perfusion rate of 0.8 $mL.h^{-1}$ increased the total cell number within the scaffold 2.5 fold in comparison to static culture, and that cells were distributed more uniformly (Sun *et al.*, 2008). Therefore, the use of a simple closed loop perfusion bioreactor for the introduction of primary Schwann cells to decellularised human femoral nerve could be investigated and assessed using DNA quantification, to determine the number of cells introduced to the conduit, and histological analysis to assess cell distribution.

Following the establishment of a method to introduce Schwann cells, future work could also include long-term *in vitro* culture of primary Schwann cells with decellularised human nerve, in order to investigate the ability of decellularised human femoral nerve to support viable primary Schwann cell populations in isolation. A long-term *in vitro* culture system of up 28 days would be established, and cell viability and migration could be assessed *in vitro* using the analyses described in Chapter 5 at various time points in culture. Changes in the expression of various Schwann cell markers, including those used in Chapter 5, would also be evaluated. The results presented in this study (Chapter 5) suggested that disruption to endoneurial architecture adversely affects long term cell viability and migration. Therefore, primary human rat Schwann cells could also be cultured with lyophilised decellularised human femoral nerve and assessed using the same analyses, in order to investigate the importance of endoneurial architecture on cell viability, migration and distribution, and the effects on Schwann cell phenotype.

Future *in vivo* studies could also include evaluating a decellularised human nerve graft repopulated with primary Schwann cells using a rat sciatic nerve defect model, as described above. The results of this study could be compared to the use of a decellularised nerve graft in isolation to repair a rat sciatic nerve defect, in order to investigate the effects of incorporating Schwann cells on axon regeneration. Future studies could also include repopulating a lyophilised decellularised nerve graft with Schwann cells, in order to assess the effects of disruption to endoneurial architecture on implanted Schwann cells and axon regeneration *in vivo*.

6.6.3 Development of a decellularised human nerve ECM hydrogel

Hydrogels, including collagen type I hydrogels, are common materials used for NGC fabrication (Chapter 1). Recent developments in NGC fabrication have focused on replicating the native ECM microenvironment, with the incorporation of basement membrane components, adhesion motifs, and altering the biochemical composition (Gu *et al.*, 2014). Decellularised ECM hydrogels offer considerable clinical potential for tissue repair, as the biochemical composition and basement membrane components of the native ECM are preserved, and the hydrogels can be developed with highly tuneable properties including stiffness and porosity, and can be moulded or injectable for less invasive repair (Saldin *et al.*, 2017). Decellularised ECM hydrogels have been developed from a variety of porcine source tissues including spinal cord, urinary bladder, small intestinal submucosa and cardiac tissues such as myocardium, and have demonstrated promising results both *in vitro* and *in vivo* in comparison to other hydrogels, including collagen type I hydrogels and Matrigel™ (Saldin *et al.*, 2017). Decellularised ECM hydrogels also offer potential for the future development of cellular therapies and pharmacotherapies for peripheral nerve repair (Faroni *et al.*, 2015; Fathi and Zaminy, 2017). Autologous Schwann cells, ASCs or BMSCs could easily be suspended in the hydrogel, and growth factors or other small molecules could also be incorporated into the hydrogel prior to implantation (Faroni *et al.*, 2015; Houschyar *et al.*, 2016; Jiang *et al.*, 2017).

Decellularised ECM hydrogels have previously been developed from porcine peripheral nerves, and have been evaluated both *in vitro* and *in vivo* (Zou *et al.*, 2018; Lin *et al.*, 2018). Zou *et al.* (2018) developed an ECM hydrogel derived from decellularised porcine peripheral nerves, and evaluated the hydrogel in comparison to Matrigel™ and a collagen type I hydrogel, using an *in vitro* co-culture system with primary rat DRGs and Schwann cells. The study reported increased neurite

outgrowth, and increased re-myelination of DRGs cultured in the decellularised ECM hydrogel in comparison to DRGs cultured in Matrigel™ or the collagen hydrogel (Zou *et al.*, 2018). Lin *et al.* (2018) also developed a decellularised porcine peripheral nerve ECM hydrogel, and found that the hydrogel supported primary rat Schwann cell proliferation and preserved Schwann cell phenotype when cultured *in vitro*. In addition, the ECM hydrogel was combined with electrospun PLA fibres and used to repair a 15 mm rat sciatic nerve defect *in vivo*, and compared to both an empty PLA conduit and a decellularised porcine peripheral nerve graft. The study reported morphological, electrophysiological and functional outcomes, and found that the ECM hydrogel achieved superior axon regeneration in comparison to the empty conduit, and similar outcomes to the autograft control (Lin *et al.*, 2018).

Future work could include the development of a decellularised human nerve ECM hydrogel, which could be translated for clinical application as a Class III medical device. Human femoral nerves would be decellularised using the decellularisation process described in Chapter 4. A method for the preparation of a decellularised nerve ECM hydrogel would be developed using previously established methods for producing decellularised ECM hydrogels, including enzymatic digestion and acid hydrolysis (Saldin *et al.*, 2017). The ECM hydrogel would be characterised using histological and biochemical analyses (including collagen, fat and glycosaminoglycan (GAG) quantification) to ensure retention of ECM components, spectrophotometry to study gelation kinetics, and SEM to determine fibril diameter and orientation. Gel stiffness and compressive strength would also be determined using rheology and biomechanical analyses. The developed ECM hydrogel could then be cultured *in vitro* with primary rat DRG explants. Cell viability, migration and neurite outgrowth could be assessed as described in Chapter 5, using viability assays and immunofluorescent labelling.

In addition, a decellularised human nerve ECM hydrogel incorporating Schwann cells could be developed by resuspending cells within the hydrogel (Faroni *et al.*, 2015; Houschyar *et al.*, 2016). A repopulated ECM hydrogel could then be evaluated *in vitro*, using the analyses described above, and *in vivo* using a rat sciatic nerve defect model as described previously.

6.7 Conclusion

Current surgical interventions for peripheral nerve repair are associated with a number of limitations (Burnett and Zager, 2004). Autografts require the sacrifice of a functional nerve and often provide insufficient material for major reconstruction, and cadaveric fresh-frozen allografts present significant risks associated with potential immunogenicity and patient immunosuppression (Lee and Wolfe, 2000; Schmidt and Leach, 2003). A small number of NGCs are clinically available, however clinical trials have reported that the efficacy of NGCs is restricted to the repair of small defects, up to 20 mm in length (Gu *et al.*, 2011; De Luca *et al.*, 2014). Decellularised peripheral nerve grafts offer considerable clinical potential, and there is existing clinical evidence to support their use for peripheral nerve repair (Moore *et al.*, 2011; Gerth *et al.*, 2015). However, clinical trials have not yet demonstrated consistently superior outcomes to autografts, and it is hypothesised that the decellularised nerve graft has diminished regenerative capacity as a consequence of ECM disruption caused by the decellularisation process (Whitlock *et al.*, 2009; Karabekmez *et al.*, 2009). In this study, a novel decellularised human femoral nerve graft of clinical utility was developed. Decellularised human femoral nerves were shown to retain a native ECM histioarchitecture and biochemical composition, and were shown to be biocompatible and support the viability, migration and phenotype of primary DRG cells for up to 28 days *in vitro*. However, further investigations are required to evaluate clinical potential for use in peripheral nerve repair. A sterilisation process must be developed and evaluated for the decellularised nerve graft. Decellularised and sterilised human femoral nerves must be biomechanically evaluated to ensure the retention of native biomechanical properties. In addition, although results of the *in vitro* experiments presented in this study are promising, the efficacy of a sterilised decellularised human femoral nerve graft for peripheral nerve repair must be evaluated *in vivo* prior to clinical translation.

Chapter 7: References

AAMODT, J. M. & GRAINGER, D. W. 2016. Extracellular matrix-based biomaterial scaffolds and the host response. *Biomaterials,* 86**,** 68-82.

ABDELGAIED, A., STANLEY, M., GALFE, M., BERRY, H., INGHAM, E. & FISHER, J. 2015. Comparison of the biomechanical tensile and compressive properties of decellularised and natural porcine meniscus. *Journal of biomechanics,* 48**,** 1389-1396.

AHMED, M. R. & JAYAKUMAR, R. 2003. Peripheral nerve regeneration in RGD peptide incorporated collagen tubes. *Brain research,* 993**,** 208-216.

AHMED, Z., UNDERWOOD, S. & BROWN, R. 2003. Nerve guide material made from fibronectin: assessment of in vitro properties. *Tissue engineering,* 9**,** 219-231.

ALLODI, I., GUZMÁN-LENIS, M.-S., HERNÀNDEZ, J., NAVARRO, X. & UDINA, E. 2011. In vitro comparison of motor and sensory neuron outgrowth in a 3D collagen matrix. *Journal of neuroscience methods,* 198**,** 53-61.

ALLODI, I., UDINA, E. & NAVARRO, X. 2012. Specificity of peripheral nerve regeneration: interactions at the axon level. *Progress in neurobiology,* 98**,** 16-37.

ANSSELIN, A. D., FINK, T. & DAVEY, D. F. 1997. Peripheral nerve regeneration through nerve guides seeded with adult Schwann cells. *Neuropathol Appl Neurobiol,* 23**,** 387-98.

ARCHIBALD, S. J., KRARUP, C., SHEFNER, J., LI, S. T. & MADISON, R. D. 1991. A collagen-based nerve guide conduit for peripheral nerve repair: an electrophysiological study of nerve regeneration in rodents and nonhuman primates. *J Comp Neurol,* 306**,** 685-96.

AYALA-GARCÍA, M., GONZÁLEZ YEBRA, B., FLORES, A. & GUANÍ GUERRA, E. 2012. *The Major Histocompatibility Complex in Transplantation*.

AZHIM, A., SYAZWANI, N., MORIMOTO, Y., FURUKAWA, K. & USHIDA, T. 2014. The use of sonication treatment to decellularize aortic tissues for preparation of bioscaffolds. *Journal of biomaterials applications,* 29**,** 130-141.

BADYLAK, S. F. 2004. Xenogeneic extracellular matrix as a scaffold for tissue reconstruction. *Transplant immunology,* 12**,** 367-377.

BADYLAK, S. F. 2014. Decellularized allogeneic and xenogeneic tissue as a bioscaffold for regenerative medicine: factors that influence the host response. *Annals of biomedical engineering,* 42**,** 1517-1527.

BADYLAK, S. F., FREYTES, D. O. & GILBERT, T. W. 2009. Extracellular matrix as a biological scaffold material: structure and function. *Acta biomaterialia,* 5**,** 1-13.

BAK, L. K., SCHOUSBOE, A. & WAAGEPETERSEN, H. S. 2006. The glutamate/GABA-glutamine cycle: aspects of transport, neurotransmitter homeostasis and ammonia transfer. *Journal of neurochemistry,* 98**,** 641-653.

BATTISTON, B., TOS, P., CONFORTI, L. & GEUNA, S. 2007. Alternative techniques for peripheral nerve repair: conduits and end-to-side neurorrhaphy. *How To Improve the Results of Peripheral Nerve Surgery.* Springer.

BAYRAK, A., TYRALLA, M., LADHOFF, J., SCHLEICHER, M., STOCK, U. A., VOLK, H.-D. & SEIFERT, M. 2010. Human immune responses to porcine xenogeneic matrices and their extracellular matrix constituents in vitro. *Biomaterials,* 31**,** 3793-3803.

BELKAS, J. S., SHOICHET, M. S. & MIDHA, R. 2004. Peripheral nerve regeneration through guidance tubes. *Neurological research,* 26**,** 151-160.

BELL, J. H. & HAYCOCK, J. W. 2011. Next generation nerve guides: materials, fabrication, growth factors, and cell delivery. *Tissue Engineering Part B: Reviews,* 18**,** 116-128.

BELLAMKONDA, R. V. 2006. Peripheral nerve regeneration: an opinion on channels, scaffolds and anisotropy. *Biomaterials,* 27**,** 3515-3518.

BELZER, V., SHRAER, N. & HANANI, M. 2010. Phenotypic changes in satellite glial cells in cultured trigeminal ganglia. *Neuron glia biology,* 6**,** 237-243.

BERTLEFF, M. J., MEEK, M. F. & NICOLAI, J.-P. A. 2005. A prospective clinical evaluation of biodegradable neurolac nerve guides for sensory nerve repair in the hand. *The Journal of hand surgery,* 30**,** 513-518.

BHUYAN, A. K. 2010. On the mechanism of SDS-induced protein denaturation. *Biopolymers,* 93**,** 186-99.

BIERNASKIE, J. A., MCKENZIE, I. A., TOMA, J. G. & MILLER, F. D. 2006. Isolation of skin-derived precursors (SKPs) and differentiation and enrichment of their Schwann cell progeny. *Nat Protoc,* 1**,** 2803-12.

BILBAO, J. M. & SCHMIDT, R. E. 2015. Normal Anatomy of the Peripheral (Sural) Nerve. *Biopsy Diagnosis of Peripheral Neuropathy.* Springer.

BOCCAFOSCHI, F., RAMELLA, M., FUSARO, L., CATOIRA, M. C. & CASELLA, F. 2019. Biological Grafts: Surgical Use and Vascular Tissue Engineering Options for Peripheral Vascular Implants.

BONENFANT, N. R., SOKOCEVIC, D., WAGNER, D. E., BORG, Z. D., LATHROP, M. J., LAM, Y. W., DENG, B., DESARNO, M. J., ASHIKAGA, T., LOI, R. & WEISS, D. J. 2013. The effects of storage and sterilization on de-cellularized and re-cellularized whole lung. *Biomaterials,* 34**,** 3231-45.

BOOTH, C., KOROSSIS, S., WILCOX, H., WATTERSON, K., KEARNEY, J., FISHER, J. & INGHAM, E. 2002. Tissue engineering of cardiac valve prostheses I: development and histological characterization of an acellular porcine scaffold. *The Journal of heart valve disease,* 11**,** 457-462.

BOYD, J. G. & GORDON, T. 2002. A dose-dependent facilitation and inhibition of peripheral nerve regeneration by brain-derived neurotrophic factor. *Eur J Neurosci,* 15**,** 613-26.

BOZKURT, A., BROOK, G. A., MOELLERS, S., LASSNER, F., SELLHAUS, B., WEIS, J., WOELTJE, M., TANK, J., BECKMANN, C. & FUCHS, P. 2007. In vitro assessment of axonal growth using dorsal root ganglia explants in a novel three-dimensional collagen matrix. *Tissue engineering,* 13**,** 2971-2979.

BRAUNEWELL, K. H., PESHEVA, P., MCCARTHY, J. B., FURCHT, L. T., SCHMITZ, B. & SCHACHNER, M. 1995. Functional Involvement of Sciatic Nerve-derived Versicanand Decorin-like Molecules and other Chondroitin Sulphate Proteoglycans in ECM-mediated Cell Adhesion and Neurite Outgrowth. *European Journal of Neuroscience,* 7**,** 805-814.

BROOKS, D. N., WEBER, R. V., CHAO, J. D., RINKER, B. D., ZOLDOS, J., ROBICHAUX, M. R., RUGGERI, S. B., ANDERSON, K. A., BONATZ, E. E. & WISOTSKY, S. M. 2012. Processed nerve allografts for peripheral nerve

reconstruction: a multicenter study of utilization and outcomes in sensory, mixed, and motor nerve reconstructions. *Microsurgery,* 32**,** 1-14.

BURNETT, M. G. & ZAGER, E. L. 2004. Pathophysiology of peripheral nerve injury: a brief review. *Neurosurgical focus,* 16**,** 1-7.

BUSHNELL, B. D., MCWILLIAMS, A. D., WHITENER, G. B. & MESSER, T. M. 2008. Early clinical experience with collagen nerve tubes in digital nerve repair. *The Journal of hand surgery,* 33**,** 1081-1087.

BUSUTTIL, F., RAHIM, A. A. & PHILLIPS, J. B. 2017. Combining gene and stem cell therapy for peripheral nerve tissue engineering. *Stem cells and development,* 26**,** 231-238.

CAI, J., PENG, X., NELSON, K. D., EBERHART, R. & SMITH, G. M. 2005. Permeable guidance channels containing microfilament scaffolds enhance axon growth and maturation. *Journal of Biomedical Materials Research Part A,* 75**,** 374-386.

CAO, J., SUN, C., ZHAO, H., XIAO, Z., CHEN, B., GAO, J., ZHENG, T., WU, W., WU, S. & WANG, J. 2011. The use of laminin modified linear ordered collagen scaffolds loaded with laminin-binding ciliary neurotrophic factor for sciatic nerve regeneration in rats. *Biomaterials,* 32**,** 3939-3948.

CASELLA, G. T., BUNGE, R. P. & WOOD, P. M. 1996. Improved method for harvesting human Schwann cells from mature peripheral nerve and expansion in vitro. *Glia,* 17**,** 327-338.

CHANG, C. J., HSU, S. H., YEN, H. J., CHANG, H. & HSU, S. K. 2007. Effects of unidirectional permeability in asymmetric poly(DL-lactic acid-co-glycolic acid) conduits on peripheral nerve regeneration: an in vitro and in vivo study. *J Biomed Mater Res B Appl Biomater,* 83**,** 206-15.

CHEN, C.-J., OU, Y.-C., LIAO, S.-L., CHEN, W.-Y., CHEN, S.-Y., WU, C.-W., WANG, C.-C., WANG, W.-Y., HUANG, Y.-S. & HSU, S.-H. 2007. Transplantation of bone marrow stromal cells for peripheral nerve repair. *Experimental neurology,* 204**,** 443-453.

CHEN, F.-M. & LIU, X. 2016. Advancing biomaterials of human origin for tissue engineering. *Progress in polymer science,* 53**,** 86-168.

CHEN, Y.-S., HSIEH, C.-L., TSAI, C.-C., CHEN, T.-H., CHENG, W.-C., HU, C.-L. & YAO, C.-H. 2000. Peripheral nerve regeneration using silicone rubber chambers filled with collagen, laminin and fibronectin. *Biomaterials,* 21**,** 1541-1547.

CHERNOUSOV, M. A., YU, W. M., CHEN, Z. L., CAREY, D. J. & STRICKLAND, S. 2008. Regulation of Schwann cell function by the extracellular matrix. *Glia,* 56**,** 1498-1507.

COLEN, K. L., CHOI, M. & CHIU, D. T. 2009. Nerve grafts and conduits. *Plastic and reconstructive surgery,* 124**,** e386-e394.

COSTA, F. A. L. & MOREIRA NETO, F. L. 2015. Satellite glial cells in sensory ganglia: its role in pain. *Revista brasileira de anestesiologia,* 65**,** 73-81.

CRAPO, P. M., GILBERT, T. W. & BADYLAK, S. F. 2011. An overview of tissue and whole organ decellularization processes. *Biomaterials,* 32**,** 3233-3243.

CUI, L., JIANG, J., WEI, L., ZHOU, X., FRASER, J. L., SNIDER, B. J. & YU, S. P. 2008. Transplantation of embryonic stem cells improves nerve repair and functional recovery after severe sciatic nerve axotomy in rats. *Stem Cells,* 26**,** 1356-65.

DAHL, S. L., KOH, J., PRABHAKAR, V. & NIKLASON, L. E. 2003. Decellularized native and engineered arterial scaffolds for transplantation. *Cell transplantation,* 12**,** 659-666.

DAHLIN, L., BRANDT, J., NILSSON, A., LUNDBORG, G. & KANJE, M. 2007. *Schwann cells, acutely dissociated from a predegenerated nerve trunk, can be applied into a matrix used to bridge nerve defects in rats*, Springer.

DAHLIN, L. B., ANAGNOSTAKI, L. & LUNDBORG, G. 2001. Tissue response to silicone tubes used to repair human median and ulnar nerves. *Scand J Plast Reconstr Surg Hand Surg,* 35**,** 29-34.

DAI, Z., RONHOLM, J., TIAN, Y., SETHI, B. & CAO, X. 2016. Sterilization techniques for biodegradable scaffolds in tissue engineering applications. *Journal of Tissue Engineering,* 7**,** 2041731416648810.

DALAMAGKAS, K., TSINTOU, M. & SEIFALIAN, A. 2016. Advances in peripheral nervous system regenerative therapeutic strategies: a biomaterials approach. *Materials Science and Engineering: C,* 65**,** 425-432.

DALTON, P. D. & MEY, J. 2009. Neural interactions with materials. *Front Biosci,* 14**,** 769-795.

DALY, K. A., STEWART-AKERS, A. M., HARA, H., EZZELARAB, M., LONG, C., CORDERO, K., JOHNSON, S. A., AYARES, D., COOPER, D. K. & BADYLAK, S. F. 2009. Effect of the αGal epitope on the response to small intestinal submucosa extracellular matrix in a nonhuman primate model. *Tissue engineering Part A,* 15**,** 3877-3888.

DALY, W., YAO, L., ZEUGOLIS, D., WINDEBANK, A. & PANDIT, A. 2012. A biomaterials approach to peripheral nerve regeneration: bridging the peripheral nerve gap and enhancing functional recovery. *Journal of the Royal Society Interface,* 9**,** 202-221.

DE LUCA, A. C., FARONI, A. & REID, A. J. 2015. Dorsal root ganglia neurons and differentiated adipose-derived stem cells: an in vitro co-culture model to study peripheral nerve regeneration. *Journal of visualized experiments: JoVE*.

DE LUCA, A. C., LACOUR, S. P., RAFFOUL, W. & DI SUMMA, P. G. 2014. Extracellular matrix components in peripheral nerve repair: how to affect neural cellular response and nerve regeneration? *Neural regeneration research,* 9**,** 1943.

DE RUITER, G. C., MALESSY, M. J., YASZEMSKI, M. J., WINDEBANK, A. J. & SPINNER, R. J. 2009. Designing ideal conduits for peripheral nerve repair. *Neurosurgical focus,* 26**,** E5.

DE RUITER, G. C., SPINNER, R. J., VERHAAGEN, J. & MALESSY, M. J. 2014. Misdirection and guidance of regenerating axons after experimental nerve injury and repair: a review. *Journal of neurosurgery,* 120**,** 493-501.

DELGADO, L. M., PANDIT, A. & ZEUGOLIS, D. I. 2014. Influence of sterilisation methods on collagen-based devices stability and properties. *Expert review of medical devices,* 11**,** 305-314.

DODLA, M. C. & BELLAMKONDA, R. V. 2008. Differences between the effect of anisotropic and isotropic laminin and nerve growth factor presenting scaffolds on nerve regeneration across long peripheral nerve gaps. *Biomaterials,* 29**,** 33-46.

DONOGHOE, N., ROSSON, G. D. & DELLON, A. L. 2007. Reconstruction of the human median nerve in the forearm with the Neurotube™. *Microsurgery: Official*

Journal of the International Microsurgical Society and the European Federation of Societies for Microsurgery, 27**,** 595-600.

DU, J., CHEN, H., QING, L., YANG, X. & JIA, X. 2018. Biomimetic neural scaffolds: a crucial step towards optimal peripheral nerve regeneration. *Biomaterials science,* 6**,** 1299-1311.

DUBOVÝ, P., KLUSÁKOVÁ, I., HRADILOVÁ-SVÍŽENSKÁ, I., BRÁZDA, V., KOHOUTKOVÁ, M. & JOUKAL, M. 2019. A conditioning sciatic nerve lesion triggers a pro-regenerative state in primary sensory neurons also of dorsal root ganglia non-associated with the damaged nerve. *Frontiers in Cellular Neuroscience,* 13**,** 11.

EDWARDS, J. H., HERBERT, A., JONES, G. L., MANFIELD, I. W., FISHER, J. & INGHAM, E. 2017. The effects of irradiation on the biological and biomechanical properties of an acellular porcine superflexor tendon graft for cruciate ligament repair. *Journal of Biomedical Materials Research Part B: Applied Biomaterials,* 105**,** 2477-2486.

EMIN ÖNGER, M., DELIBAŞ, B., PıNAR TÜRKMEN, A., ERENER, E., ALTUNKAYNAK, B. & KAPLAN, S. 2016. *The role of growth factors in nerve regeneration*.

ERBA, P., MANTOVANI, C., KALBERMATTEN, D. F., PIERER, G., TERENGHI, G. & KINGHAM, P. J. 2010. Regeneration potential and survival of transplanted undifferentiated adipose tissue-derived stem cells in peripheral nerve conduits. *J Plast Reconstr Aesthet Surg,* 63**,** e811-7.

ERDAG, G. & MORGAN, J. R. 2004. Allogeneic versus xenogeneic immune reaction to bioengineered skin grafts. *Cell transplantation,* 13**,** 701-712.

EVANS, P. J., MACKINNON, S. E., LEVI, A., WADE, J. A., HUNTER, D. A., NAKAO, Y. & MIDHA, R. 1998. Cold preserved nerve allografts: changes in basement membrane, viability, immunogenicity, and regeneration. *Muscle & nerve,* 21**,** 1507-1522.

FAN, L., YU, Z., LI, J., DANG, X. & WANG, K. 2014. Schwann-like cells seeded in acellular nerve grafts improve nerve regeneration. *BMC Musculoskelet Disord,* 15**,** 165.

FAROLE, A. & JAMAL, B. T. 2008. A bioabsorbable collagen nerve cuff (NeuraGen) for repair of lingual and inferior alveolar nerve injuries: a case series. *Journal of Oral and Maxillofacial Surgery,* 66**,** 2058-2062.

FARONI, A. & MAGNAGHI, V. 2011. The neurosteroid allopregnanolone modulates specific functions in central and peripheral glial cells. *Front Endocrinol (Lausanne),* 2**,** 103.

FARONI, A., MOBASSERI, S. A., KINGHAM, P. J. & REID, A. J. 2015. Peripheral nerve regeneration: experimental strategies and future perspectives. *Advanced drug delivery reviews,* 82**,** 160-167.

FARONI, A., SMITH, R. J. & REID, A. J. 2014. Adipose derived stem cells and nerve regeneration. *Neural Regen Res,* 9**,** 1341-6.

FATHI, S. S. & ZAMINY, A. 2017. Stem cell therapy for nerve injury. *World journal of stem cells,* 9**,** 144.

FAULK, D. M., CARRUTHERS, C. A., WARNER, H. J., KRAMER, C. R., REING, J. E., ZHANG, L., D'AMORE, A. & BADYLAK, S. F. 2014a. The effect of detergents on the basement membrane complex of a biologic scaffold material. *Acta Biomater,* 10**,** 183-93.

FAULK, D. M., CARRUTHERS, C. A., WARNER, H. J., KRAMER, C. R., REING, J. E., ZHANG, L., D'AMORE, A. & BADYLAK, S. F. 2014b. The Effect of Detergents on the Basement Membrane Complex of a Biologic Scaffold Material. *Acta biomaterialia,* 10**,** 10.1016/j.actbio.2013.09.006.

FERCANA, G., BOWSER, D., PORTILLA, M., LANGAN, E. M., CARSTEN, C. G., CULL, D. L., SIERAD, L. N. & SIMIONESCU, D. T. 2014. Platform technologies for decellularization, tunic-specific cell seeding, and in vitro conditioning of extended length, small diameter vascular grafts. *Tissue Engineering Part C: Methods,* 20**,** 1016-1027.

FERNG, A. S., CONNELL, A. M., MARSH, K. M., QU, N., MEDINA, A. O., BAJAJ, N., PALOMARES, D., IWANSKI, J., TRAN, P. L. & LOTUN, K. 2017. Acellular porcine heart matrices: whole organ decellularization with 3D-bioscaffold & vascular preservation. *J Clin Trans Res,* 3**,** 260-70.

FINE, E. G., DECOSTERD, I., PAPALOIZOS, M., ZURN, A. D. & AEBISCHER, P. 2002. GDNF and NGF released by synthetic guidance channels support sciatic nerve regeneration across a long gap. *Eur J Neurosci,* 15**,** 589-601.

FORNARO, M., LEE, J., RAIMONDO, S., NICOLINO, S., GEUNA, S. & GIACOBINI-ROBECCHI, M. 2008. Neuronal intermediate filament expression in rat dorsal root ganglia sensory neurons: an in vivo and in vitro study. *Neuroscience,* 153**,** 1153-1163.

FRANCO LAMBERT, A. P., FRAGA ZANDONAI, A., BONATTO, D., CANTARELLI MACHADO, D. & PEGAS HENRIQUES, J. A. 2009. Differentiation of human adipose-derived adult stem cells into neuronal tissue: does it work? *Differentiation,* 77**,** 221-8.

FRERICHS, O., FANSA, H., SCHICHT, C., WOLF, G., SCHNEIDER, W. & KEILHOFF, G. 2002. Reconstruction of peripheral nerves using acellular nerve grafts with implanted cultured Schwann cells. *Microsurgery,* 22**,** 311-315.

GABELLA, G. 2012. *Structure of the autonomic nervous system*, Springer Science & Business Media.

GALILI, U., CLARK, M. R., SHOHET, S. B., BUEHLER, J. & MACHER, B. A. 1987. Evolutionary relationship between the natural anti-Gal antibody and the Gal alpha 1----3Gal epitope in primates. *Proceedings of the National Academy of Sciences,* 84**,** 1369-1373.

GANDHI, N. S. & MANCERA, R. L. 2008. The structure of glycosaminoglycans and their interactions with proteins. *Chemical biology & drug design,* 72**,** 455-482.

GAO, X., WANG, Y., CHEN, J. & PENG, J. 2013. The role of peripheral nerve ECM components in the tissue engineering nerve construction. *Reviews in the Neurosciences,* 24**,** 443-453.

GARBAY, B., HEAPE, A., SARGUEIL, F. & CASSAGNE, C. 2000. Myelin synthesis in the peripheral nervous system. *Progress in neurobiology,* 61**,** 267-304.

GARDINER, N. J. 2011. Integrins and the extracellular matrix: key mediators of development and regeneration of the sensory nervous system. *Developmental neurobiology,* 71**,** 1054-1072.

GARDINER, N. J., MOFFATT, S., FERNYHOUGH, P., HUMPHRIES, M. J., STREULI, C. H. & TOMLINSON, D. R. 2007. Preconditioning injury-induced neurite outgrowth of adult rat sensory neurons on fibronectin is mediated by mobilisation of axonal α5 integrin. *Molecular and Cellular Neuroscience,* 35**,** 249-260.

GAUDET, A. D., POPOVICH, P. G. & RAMER, M. S. 2011. Wallerian degeneration: gaining perspective on inflammatory events after peripheral nerve injury. *J Neuroinflammation,* 8**,** 110.

GEORGE, D., AHRENS, P. & LAMBERT, S. 2018. S atellite glial cells represent a population of developmentally arrested S chwann cells. *Glia,* 66**,** 1496-1506.

GEORGIOU, M., BUNTING, S. C., DAVIES, H. A., LOUGHLIN, A. J., GOLDING, J. P. & PHILLIPS, J. B. 2013. Engineered neural tissue for peripheral nerve repair. *Biomaterials,* 34**,** 7335-7343.

GERTH, D. J., TASHIRO, J. & THALLER, S. R. 2015. Clinical outcomes for Conduits and Scaffolds in peripheral nerve repair. *World Journal of Clinical Cases: WJCC,* 3**,** 141.

GEUNA, S., RAIMONDO, S., FREGNAN, F., HAASTERT-TALINI, K. & GROTHE, C. 2016. In vitro models for peripheral nerve regeneration. *European Journal of Neuroscience,* 43**,** 287-296.

GEUNA, S., RAIMONDO, S., RONCHI, G., DI SCIPIO, F., TOS, P., CZAJA, K. & FORNARO, M. 2009. Histology of the peripheral nerve and changes occurring during nerve regeneration. *International review of neurobiology,* 87**,** 27-46.

GILBERT, T. W., FREUND, J. M. & BADYLAK, S. F. 2009. Quantification of DNA in biologic scaffold materials. *Journal of Surgical Research,* 152**,** 135-139.

GILBERT, T. W., SELLARO, T. L. & BADYLAK, S. F. 2006. Decellularization of tissues and organs. *Biomaterials,* 27**,** 3675-3683.

GILMORE, A. P., OWENS, T. W., FOSTER, F. M. & LINDSAY, J. 2009. How adhesion signals reach a mitochondrial conclusion—ECM regulation of apoptosis. *Current opinion in cell biology,* 21**,** 654-661.

GILPIN, A. & YANG, Y. 2017. Decellularization strategies for regenerative medicine: from processing techniques to applications. *BioMed research international,* 2017.

GINGRAS, M., BERGERON, J., DÉRY, J., DURHAM, H. D. & BERTHOD, F. 2003. In vitro development of a tissue-engineered model of peripheral nerve regeneration to study neurite growth. *The FASEB journal,* 17**,** 2124-2126.

GNAVI, S., FORNASARI, B., TONDA-TURO, C., LAURANO, R., ZANETTI, M., CIARDELLI, G. & GEUNA, S. 2018. In vitro evaluation of gelatin and chitosan electrospun fibres as an artificial guide in peripheral nerve repair: a comparative study. *Journal of tissue engineering and regenerative medicine,* 12**,** e679-e694.

GRANT, R. A., COX, R. W. & KENT, C. M. 1973. The effects of gamma irradiation on the structure and reactivity of native and cross-linked collagen fibres. *J Anat,* 115**,** 29-43.

GRATCHEV, A., GUILLOT, P., HAKIY, N., POLITZ, O., ORFANOS, C., SCHLEDZEWSKI, K. & GOERDT, S. 2001. Alternatively Activated Macrophages Differentially Express Fibronectin and Its Splice Variants and the Extracellular Matrix Protein βIG-H3. *Scandinavian journal of immunology,* 53**,** 386-392.

GRAUSS, R., HAZEKAMP, M., VAN VLIET, S., GITTENBERGER-DE GROOT, A. & DERUITER, M. 2003. Decellularization of rat aortic valve allografts reduces leaflet destruction and extracellular matrix remodeling. *The Journal of thoracic and cardiovascular surgery,* 126.

GRINSELL, D. & KEATING, C. 2014. Peripheral nerve reconstruction after injury: a review of clinical and experimental therapies. *BioMed research international,* 2014.

GROTHE, C. & NIKKHAH, G. 2001. The role of basic fibroblast growth factor in peripheral nerve regeneration. *Anatomy and embryology,* 204**,** 171-177.

GU, X., DING, F. & WILLIAMS, D. F. 2014. Neural tissue engineering options for peripheral nerve regeneration. *Biomaterials,* 35**,** 6143-6156.

GU, X., DING, F., YANG, Y. & LIU, J. 2011. Construction of tissue engineered nerve grafts and their application in peripheral nerve regeneration. *Progress in neurobiology,* 93**,** 204-230.

GUENARD, V., KLEITMAN, N., MORRISSEY, T., BUNGE, R. & AEBISCHER, P. 1992. Syngeneic Schwann cells derived from adult nerves seeded in semipermeable guidance channels enhance peripheral nerve regeneration. *The Journal of Neuroscience,* 12**,** 3310-3320.

GULATI, A. K. 1988. Evaluation of acellular and cellular nerve grafts in repair of rat peripheral nerve. *Journal of neurosurgery,* 68**,** 117-123.

HAASTERT, K., LIPOKATIC, E., FISCHER, M., TIMMER, M. & GROTHE, C. 2006. Differentially promoted peripheral nerve regeneration by grafted Schwann cells over-expressing different FGF-2 isoforms. *Neurobiology of disease,* 21**,** 138-153.

HAN, H., AO, Q., CHEN, G., WANG, S. & ZUO, H. 2010. A novel basic fibroblast growth factor delivery system fabricated with heparin-incorporated fibrin–fibronectin matrices for repairing rat sciatic nerve disruptions. *Biotechnology letters,* 32**,** 585-591.

HANANI, M. 2005. Satellite glial cells in sensory ganglia: from form to function. *Brain research reviews,* 48**,** 457-476.

HAUGH, M. G., MURPHY, C. M. & O'BRIEN, F. J. 2010. Novel freeze-drying methods to produce a range of collagen-glycosaminoglycan scaffolds with tailored mean pore sizes. *Tissue Eng Part C Methods,* 16**,** 887-94.

HE, Z. & JIN, Y. 2016. Intrinsic control of axon regeneration. *Neuron,* 90**,** 437-451.

HEINO, J. 2007. The collagen family members as cell adhesion proteins. *Bioessays,* 29**,** 1001-10.

HELLIWELL, J. A., THOMAS, D. S., PAPATHANASIOU, V., HOMER-VANNIASINKAM, S., DESAI, A., JENNINGS, L. M., ROONEY, P., KEARNEY, J. N. & INGHAM, E. 2017. Development and characterisation of a low-concentration sodium dodecyl sulphate decellularised porcine dermis. *Journal of tissue engineering,* 8**,** 2041731417724011.

HERSEL, U., DAHMEN, C. & KESSLER, H. 2003. RGD modified polymers: biomaterials for stimulated cell adhesion and beyond. *Biomaterials,* 24**,** 4385-4415.

HICKS, C., STEVANATO, L., STROEMER, R. P., TANG, E., RICHARDSON, S. & SINDEN, J. D. 2013. In vivo and in vitro characterization of the angiogenic effect of CTX0E03 human neural stem cells. *Cell transplantation,* 22**,** 1541-1552.

HILES, R. W. 1972. Freeze dried irradiated nerve homograft: a preliminary report. *The Hand,* 4**,** 79-84.

HIROSE, T., TANI, T., SHIMADA, T., ISHIZAWA, K., SHIMADA, S. & SANO, T. 2003. Immunohistochemical demonstration of EMA/Glut1-positive perineurial cells and CD34-positive fibroblastic cells in peripheral nerve sheath tumors. *Modern pathology,* 16**,** 293-298.

HODDE, J., JANIS, A., ERNST, D., ZOPF, D., SHERMAN, D. & JOHNSON, C. 2007a. Effects of sterilization on an extracellular matrix scaffold: part I. Composition and matrix architecture. *J Mater Sci Mater Med,* 18**,** 537-43.

HODDE, J., JANIS, A. & HILES, M. 2007b. Effects of sterilization on an extracellular matrix scaffold: part II. Bioactivity and matrix interaction. *J Mater Sci Mater Med,* 18**,** 545-50.

HOUSCHYAR, K., MOMENI, A., PYLES, M., CHA, J., MAAN, Z., DUSCHER, D., JEW, O., SIEMERS, F. & SCHOONHOVEN, J. V. 2016. The role of current techniques and concepts in peripheral nerve repair. *Plastic surgery international,* 2016.

HU, X., HUANG, J., YE, Z., XIA, L., LI, M., LV, B., SHEN, X. & LUO, Z. 2009. A novel scaffold with longitudinally oriented microchannels promotes peripheral nerve regeneration. *Tissue Engineering Part A,* 15**,** 3297-3308.

HUANG, L. Y. M., GU, Y. & CHEN, Y. 2013. Communication between neuronal somata and satellite glial cells in sensory ganglia. *Glia,* 61**,** 1571-1581.

HUDSON, T. W., LIU, S. Y. & SCHMIDT, C. E. 2004a. Engineering an improved acellular nerve graft via optimized chemical processing. *Tissue engineering,* 10**,** 1346-1358.

HUDSON, T. W., ZAWKO, S., DEISTER, C., LUNDY, S., HU, C. Y., LEE, K. & SCHMIDT, C. E. 2004b. Optimized acellular nerve graft is immunologically tolerated and supports regeneration. *Tissue engineering,* 10**,** 1641-1651.

HURWITZ, Z. M., IGNOTZ, R., LALIKOS, J. F. & GALILI, U. 2012. Accelerated porcine wound healing after treatment with α-gal nanoparticles. *Plastic and reconstructive surgery,* 129**,** 242e-251e.

IDE, C., TOHYAMA, K., TAJIMA, K., ENDOH, K., SANO, K., TAMURA, M., MIZOGUCHI, A., KITADA, M., MORIHARA, T. & SHIRASU, M. 1998. Long acellular nerve transplants for allogeneic grafting and the effects of basic fibroblast growth

factor on the growth of regenerating axons in dogs: a preliminary report. *Experimental neurology,* 154**,** 99-112.

IKEDA, M., UEMURA, T., TAKAMATSU, K., OKADA, M., KAZUKI, K., TABATA, Y., IKADA, Y. & NAKAMURA, H. 2014. Acceleration of peripheral nerve regeneration using nerve conduits in combination with induced pluripotent stem cell technology and a basic fibroblast growth factor drug delivery system. *J Biomed Mater Res A,* 102**,** 1370-8.

INC, A. 2013. Avance: Process Matters.

ISHIBE, K., TAMATSU, Y., MIURA, M. & SHIMADA, K. 2011. Morphological study of the vasa nervorum in the peripheral branch of human facial nerve. *Okajimas folia anatomica Japonica,* 88**,** 111-119.

ISO 2009. ISO 14937: Sterilization of health care products-general requirements for characterization of a sterilizing agent and the development, validation and routine control of a sterilization process for medical devices.: ISO.

JACQUES, L. & KLINE, D. 2000. Response of the peripheral nerve to physical injury, Crockard a, Hayward R, Hoff Jt (eds): Neurosurgery: the Scientific Basis of Clinical Practice. *London: Blackwell,* 1**,** 516-525.

JENKINS, P. M., LAUGHTER, M. R., LEE, D. J., LEE, Y. M., FREED, C. R. & PARK, D. 2015. A nerve guidance conduit with topographical and biochemical cues: potential application using human neural stem cells. *Nanoscale Res Lett,* 10**,** 972.

JESSEN, K. & MIRSKY, R. 2016. The repair Schwann cell and its function in regenerating nerves. *The Journal of physiology,* 594**,** 3521-3531.

JESSEN, K. R., MIRSKY, R. & LLOYD, A. C. 2015. Schwann cells: development and role in nerve repair. *Cold Spring Harbor perspectives in biology***,** a020487.

JESURAJ, N. J., SANTOSA, K. B., NEWTON, P., LIU, Z., HUNTER, D. A., MACKINNON, S. E., SAKIYAMA-ELBERT, S. E. & JOHNSON, P. J. 2011. A systematic evaluation of Schwann cell injection into acellular cold-preserved nerve grafts. *Journal of neuroscience methods,* 197**,** 209-215.

JIANG, L., JONES, S. & JIA, X. 2017. Stem cell transplantation for peripheral nerve regeneration: Current options and opportunities. *International journal of molecular sciences,* 18**,** 94.

JIANG, X., LIM, S. H., MAO, H.-Q. & CHEW, S. Y. 2010. Current applications and future perspectives of artificial nerve conduits. *Experimental neurology,* 223**,** 86-101.

JOHNSON, P. J., NEWTON, P., HUNTER, D. A. & MACKINNON, S. E. 2011. Nerve endoneurial microstructure facilitates uniform distribution of regenerative fibers: a post hoc comparison of midgraft nerve fiber densities. *Journal of reconstructive microsurgery,* 27**,** 083-090.

JONES, G., HERBERT, A., BERRY, H., EDWARDS, J. H., FISHER, J. & INGHAM, E. 2017. Decellularization and characterization of porcine superflexor tendon: a potential anterior cruciate ligament replacement. *Tissue Engineering Part A,* 23**,** 124-134.

JØNSSON, K. L., LAUSTSEN, A., KRAPP, C., SKIPPER, K. A., THAVACHELVAM, K., HOTTER, D., EGEDAL, J. H., KJOLBY, M., MOHAMMADI, P., PRABAKARAN, T., SØRENSEN, L. K., SUN, C., JENSEN, S. B., HOLM, C. K., LEBBINK, R. J., JOHANNSEN, M., NYEGAARD, M., MIKKELSEN, J. G., KIRCHHOFF, F., PALUDAN, S. R. & JAKOBSEN, M. R. 2017. IFI16 is required for DNA sensing in human macrophages by promoting production and function of cGAMP. *Nature Communications,* 8**,** 14391.

JUNQUEIRA, L. C. U., BIGNOLAS, G. & BRENTANI, R. 1979. Picrosirius staining plus polarization microscopy, a specific method for collagen detection in tissue sections. *The Histochemical journal,* 11**,** 447-455.

KAEWKHAW, R., SCUTT, A. M. & HAYCOCK, J. W. 2012. Integrated culture and purification of rat Schwann cells from freshly isolated adult tissue. *Nature protocols,* 7**,** 1996-2004.

KARABEKMEZ, F. E., DUYMAZ, A. & MORAN, S. L. 2009. Early clinical outcomes with the use of decellularized nerve allograft for repair of sensory defects within the hand. *Hand,* 4**,** 245-249.

KASIMIR, M. T., RIEDER, E., SEEBACHER, G., SILBERHUMER, G., WOLNER, E., WEIGEL, G. & SIMON, P. 2003. Comparison of different decellularization procedures of porcine heart valves. *Int J Artif Organs,* 26**,** 421-7.

KASTRITI, M. E. & ADAMEYKO, I. 2017. Specification, plasticity and evolutionary origin of peripheral glial cells. *Current opinion in neurobiology,* 47**,** 196-202.

KAWECKI, M., ŁABUŚ, W., KLAMA-BARYLA, A., KITALA, D., KRAUT, M., GLIK, J., MISIUGA, M., NOWAK, M., BIELECKI, T. & KASPERCZYK, A. 2018. A review of decellurization methods caused by an urgent need for quality control of cell-free extracellular matrix'scaffolds and their role in regenerative medicine. *Journal of Biomedical Materials Research Part B: Applied Biomaterials,* 106**,** 909-923.

KEANE, T. J., SWINEHART, I. T. & BADYLAK, S. F. 2015. Methods of tissue decellularization used for preparation of biologic scaffolds and in vivo relevance. *Methods,* 84**,** 25-34.

KEHOE, S., ZHANG, X. & BOYD, D. 2012. FDA approved guidance conduits and wraps for peripheral nerve injury: a review of materials and efficacy. *Injury,* 43**,** 553-572.

KERNS, J. M. 2008. The microstructure of peripheral nerves. *Techniques in Regional Anesthesia and Pain Management,* 12**,** 127-133.

KHAING, Z. Z. & SCHMIDT, C. E. 2012. Advances in natural biomaterials for nerve tissue repair. *Neuroscience letters,* 519**,** 103-114.

KHAN, Z., FERRARI, G., KASPER, M., TONGE, D., STEINER, J., HAMILTON, G. & GORDON-WEEKS, P. 2002. The non-immunosuppressive immunophilin ligand GPI-1046 potently stimulates regenerating axon growth from adult mouse dorsal root ganglia cultured in Matrigel. *Neuroscience,* 114**,** 601-609.

KHEIR, E., STAPLETON, T., SHAW, D., JIN, Z., FISHER, J. & INGHAM, E. 2011. Development and characterization of an acellular porcine cartilage bone matrix for use in tissue engineering. *Journal of Biomedical Materials Research Part A,* 99**,** 283-294.

KIERNAN, J. & RAJAKUMAR, R. 2013. *Barr's the human nervous system: an anatomical viewpoint*, Lippincott Williams & Wilkins.

KIM, H. A., MINDOS, T. & PARKINSON, D. B. 2013. Plastic fantastic: Schwann cells and repair of the peripheral nervous system. *Stem cells translational medicine***,** sctm. 2013-0011.

KINGHAM, P. J., KALBERMATTEN, D. F., MAHAY, D., ARMSTRONG, S. J., WIBERG, M. & TERENGHI, G. 2007. Adipose-derived stem cells differentiate into a Schwann cell phenotype and promote neurite outgrowth in vitro. *Experimental neurology,* 207**,** 267-274.

KITADA, M., MURAKAMI, T., WAKAO, S., LI, G. & DEZAWA, M. 2019. Direct conversion of adult human skin fibroblasts into functional Schwann cells that achieve robust recovery of the severed peripheral nerve in rats. *Glia*.

KOCH, D., ROSOFF, W. J., JIANG, J., GELLER, H. M. & URBACH, J. S. 2012. Strength in the periphery: growth cone biomechanics and substrate rigidity response in peripheral and central nervous system neurons. *Biophysical journal,* 102**,** 452-460.

KOCH, H., HAMMER, N., OSSMANN, S., SCHIERLE, K., SACK, U., HOFMANN, J., WECKS, M. & BOLDT, A. 2015. Tissue engineering of ureteral grafts: preparation of biocompatible crosslinked ureteral scaffolds of porcine origin. *Frontiers in bioengineering and biotechnology,* 3**,** 89.

KOENIG, H. L. 2012. Localization of Protein Metabolism in Neurons". *Protein Metabolism of the Nervous System***,** 93.

KOIKE, T., WAKABAYASHI, T., MORI, T., HIRAHARA, Y. & YAMADA, H. 2015. Sox2 promotes survival of satellite glial cells in vitro. *Biochemical and biophysical research communications,* 464**,** 269-274.

KOMIYAMA, T., NAKAO, Y., TOYAMA, Y., ASOU, H., VACANTI, C. A. & VACANTI, M. P. 2003. A novel technique to isolate adult Schwann cells for an artificial nerve conduit. *Journal of neuroscience methods,* 122**,** 195-200.

KOOPMANS, G., HASSE, B. & SINIS, N. 2009. The role of collagen in peripheral nerve repair. *International review of neurobiology,* 87**,** 363-379.

KREKOSKI, C. A., NEUBAUER, D., ZUO, J. & MUIR, D. 2001. Axonal regeneration into acellular nerve grafts is enhanced by degradation of chondroitin sulfate proteoglycan. *The Journal of Neuroscience,* 21**,** 6206-6213.

LACKINGTON, W. A., RYAN, A. J. & O'BRIEN, F. J. 2017. Advances in nerve guidance conduit-based therapeutics for peripheral nerve repair. *ACS Biomaterials Science & Engineering,* 3**,** 1221-1235.

LAKKIS, F. G. & LECHLER, R. I. 2013. Origin and biology of the allogeneic response. *Cold Spring Harb Perspect Med,* 3.

LEE, J. Y., GIUSTI, G., FRIEDRICH, P. F., ARCHIBALD, S. J., KEMNITZER, J. E., PATEL, J., DESAI, N., BISHOP, A. T. & SHIN, A. Y. 2012. The effect of collagen nerve conduits filled with collagen-glycosaminoglycan matrix on peripheral motor nerve regeneration in a rat model. *J Bone Joint Surg Am,* 94**,** 2084-91.

LEE, S. K. & WOLFE, S. W. 2000. Peripheral nerve injury and repair. *Journal of the American Academy of Orthopaedic Surgeons,* 8**,** 243-252.

LEOW-DYKE, S. F., ROONEY, P. & KEARNEY, J. N. 2016. Evaluation of Copper and Hydrogen Peroxide Treatments on the Biology, Biomechanics, and Cytotoxicity of Decellularized Dermal Allografts. *Tissue Eng Part C Methods,* 22**,** 290-300.

LEWIN, S. L., UTLEY, D. S., CHENG, E. T., VERITY, A. N. & TERRIS, D. J. 1997. Simultaneous treatment with BDNF and CNTF after peripheral nerve transection and repair enhances rate of functional recovery compared with BDNF treatment alone. *Laryngoscope,* 107**,** 992-9.

LI, Z., PENG, J., WANG, G., YANG, Q., YU, H., GUO, Q., WANG, A., ZHAO, B. & LU, S. 2008. Effects of local release of hepatocyte growth factor on peripheral nerve regeneration in acellular nerve grafts. *Exp Neurol,* 214**,** 47-54.

LIAO, J., JOYCE, E. M. & SACKS, M. S. 2008. Effects of decellularization on the mechanical and structural properties of the porcine aortic valve leaflet. *Biomaterials,* 29**,** 1065-1074.

LIN, T., LIU, S., CHEN, S., QIU, S., RAO, Z., LIU, J., ZHU, S., YAN, L., MAO, H., ZHU, Q., QUAN, D. & LIU, X. 2018. Hydrogel derived from porcine decellularized nerve tissue as a promising biomaterial for repairing peripheral nerve defects. *Acta Biomater,* 73**,** 326-338.

LIN, Y. L., JEN, J. C., HSU, S. H. & CHIU, I. M. 2008. Sciatic nerve repair by microgrooved nerve conduits made of chitosan-gold nanocomposites. *Surg Neurol,* 70 Suppl 1**,** S1:9-18.

LOHMEYER, J. A., SIEMERS, F., MACHENS, H. G. & MAILANDER, P. 2009. The clinical use of artificial nerve conduits for digital nerve repair: a prospective cohort study and literature review. *J Reconstr Microsurg,* 25**,** 55-61.

LONDONO, R., DZIKI, J. L., HALJASMAA, E., TURNER, N. J., LEIFER, C. A. & BADYLAK, S. F. 2017. The effect of cell debris within biologic scaffolds upon the macrophage response. *Journal of biomedical materials research Part A,* 105**,** 2109-2118.

LÓPEZ-LEAL, R. & DIAZ, P. 2018. In Vitro Analysis of the Role of Schwann Cells on Axonal Degeneration and Regeneration Using Sensory Neurons from Dorsal Root Ganglia. *Schwann Cells.* Springer.

LOVATI, A. B., D'ARRIGO, D., ODELLA, S., TOS, P., GEUNA, S. & RAIMONDO, S. 2018. Nerve repair using decellularized nerve grafts in rat models. A review of the literature. *Frontiers in cellular neuroscience,* 12**,** 427.

LUO, J., KOROSSIS, S. A., WILSHAW, S.-P., JENNINGS, L. M., FISHER, J. & INGHAM, E. 2014. Development and characterization of acellular porcine pulmonary valve scaffolds for tissue engineering. *Tissue Engineering Part A,* 20**,** 2963-2974.

MACKINNON, S. E. 1988. Surgery of the peripheral nerve. *Carpal tunnel syndrome***,** 146-169.

MACKINNON, S. E. & DELLON, A. L. 1990. Clinical nerve reconstruction with a bioabsorbable polyglycolic acid tube. *Plastic and reconstructive surgery,* 85**,** 419-424.

MADURA, T. 2012. *Pathophysiology of Peripheral Nerve Injury*, INTECH Open Access Publisher.

MAGNAGHI, V., PROCACCI, P. & TATA, A. M. 2009. Chapter 15: Novel pharmacological approaches to Schwann cells as neuroprotective agents for peripheral nerve regeneration. *Int Rev Neurobiol,* 87**,** 295-315.

MAI, J. K. & PAXINOS, G. 2011. *The human nervous system*, Academic Press.

MANOUKIAN, O. S., ARUL, M. R., RUDRAIAH, S., KALAJZIC, I. & KUMBAR, S. G. 2019. Aligned microchannel polymer-nanotube composites for peripheral nerve regeneration: Small molecule drug delivery. *Journal of Controlled Release*.

MASAND, S. N., PERRON, I. J., SCHACHNER, M. & SHREIBER, D. I. 2012. Neural cell type-specific responses to glycomimetic functionalized collagen. *Biomaterials,* 33**,** 790-797.

MASON, S. & PHILLIPS, J. B. 2011. An ultrastructural and biochemical analysis of collagen in rat peripheral nerves: the relationship between fibril diameter and mechanical properties. *Journal of the Peripheral Nervous System,* 16**,** 261-269.

MATSUMOTO, K., OHNISHI, K., KIYOTANI, T., SEKINE, T., UEDA, H., NAKAMURA, T., ENDO, K. & SHIMIZU, Y. 2000. Peripheral nerve regeneration across an 80-mm gap bridged by a polyglycolic acid (PGA)–collagen tube filled with laminin-coated collagen fibers: a histological and electrophysiological evaluation of regenerated nerves. *Brain research,* 868**,** 315-328.

MCKENZIE, I. A., BIERNASKIE, J., TOMA, J. G., MIDHA, R. & MILLER, F. D. 2006. Skin-derived precursors generate myelinating Schwann cells for the injured and dysmyelinated nervous system. *J Neurosci,* 26**,** 6651-60.

MCPHERSON, T., LIANG, H., RECORD, R. & BADYLAK, S. 2000. Galα (1, 3) Gal epitope in porcine small intestinal submucosa. *Tissue engineering,* 6**,** 233-239.

MEEK, M. F., NICOLAI, J.-P. A. & ROBINSON, P. H. 2006. Secondary digital nerve repair in the foot with resorbable p (DLLA-ε-CL) nerve conduits. *Journal of reconstructive microsurgery,* 22**,** 149-152.

MELCANGI, R. C., CAVARRETTA, I. T., BALLABIO, M., LEONELLI, E., SCHENONE, A., AZCOITIA, I., MIGUEL GARCIA-SEGURA, L. & MAGNAGHI, V. 2005. Peripheral nerves: a target for the action of neuroactive steroids. *Brain Res Brain Res Rev,* 48**,** 328-38.

MOBINI, S., SPEARMAN, B. S., LACKO, C. S. & SCHMIDT, C. E. 2017. Recent advances in strategies for peripheral nerve tissue engineering. *Current Opinion in Biomedical Engineering,* 4**,** 134-142.

MONTOYA, C. V. & MCFETRIDGE, P. S. 2009a. Preparation of ex vivo-based biomaterials using convective flow decellularization. *Tissue Eng Part C Methods,* 15**,** 191-200.

MONTOYA, C. V. & MCFETRIDGE, P. S. 2009b. Preparation of ex vivo–based biomaterials using convective flow decellularization. *Tissue Engineering Part C: Methods,* 15**,** 191-200.

MOORE, A. M., MACEWAN, M., SANTOSA, K. B., CHENARD, K. E., RAY, W. Z., HUNTER, D. A., MACKINNON, S. E. & JOHNSON, P. J. 2011. Acellular nerve allografts in peripheral nerve regeneration: a comparative study. *Muscle & nerve,* 44**,** 221-234.

MOORE, A. M., RAY, W. Z., CHENARD, K. E., TUNG, T. & MACKINNON, S. E. 2009. Nerve allotransplantation as it pertains to composite tissue transplantation. *Hand,* 4**,** 239-244.

MORANO, M., WROBEL, S., FREGNAN, F., ZIV-POLAT, O., SHAHAR, A., RATZKA, A., GROTHE, C., GEUNA, S. & HAASTERT-TALINI, K. 2014. Nanotechnology versus stem cell engineering: in vitro comparison of neurite inductive potentials. *International journal of nanomedicine,* 9**,** 5289.

MORRIS, A. H., STAMER, D. & KYRIAKIDES, T. The host response to naturally-derived extracellular matrix biomaterials. Seminars in immunology, 2017. Elsevier, 72-91.

MOSAHEBI, A., WIBERG, M. & TERENGHI, G. 2003. Addition of fibronectin to alginate matrix improves peripheral nerve regeneration in tissue-engineered conduits. *Tissue engineering,* 9**,** 209-218.

MUHEREMU, A. & AO, Q. 2015. Past, Present, and Future of Nerve Conduits in the Treatment of Peripheral Nerve Injury. *BioMed research international,* 2015.

MURAKAMI, T., FUJIMOTO, Y., YASUNAGA, Y., ISHIDA, O., TANAKA, N., IKUTA, Y. & OCHI, M. 2003. Transplanted neuronal progenitor cells in a peripheral nerve gap promote nerve repair. *Brain Res,* 974**,** 17-24.

NAGATA, S., HANAYAMA, R. & KAWANE, K. 2010. Autoimmunity and the clearance of dead cells. *Cell,* 140**,** 619-630.

NARYAN, S. K., ARUMUGAM, M. & CHITTORIA, R. 2018. Outcome of human peripheral nerve repair interventions using conduits: a systematic review. *Journal of the neurological sciences*.

NETO, E., ALVES, C. J., LEITÃO, L., SOUSA, D. M., ALENCASTRE, I. S., CONCEIÇÃO, F. & LAMGHARI, M. 2017. Axonal outgrowth, neuropeptides expression and receptors tyrosine kinase phosphorylation in 3D organotypic cultures of adult dorsal root ganglia. *PloS one,* 12**,** e0181612.

NEUBAUER, D., GRAHAM, J. B. & MUIR, D. 2007. Chondroitinase treatment increases the effective length of acellular nerve grafts. *Experimental neurology,* 207**,** 163-170.

NEUBAUER, D., GRAHAM, J. B. & MUIR, D. 2010. Nerve grafts with various sensory and motor fiber compositions are equally effective for the repair of a mixed nerve defect. *Experimental neurology,* 223**,** 203-206.

NIEUWENHUIS, B., HAENZI, B., ANDREWS, M. R., VERHAAGEN, J. & FAWCETT, J. W. 2018. Integrins promote axonal regeneration after injury of the nervous system. *Biological Reviews,* 93**,** 1339-1362.

O'NEILL, J. D., ANFANG, R., ANANDAPPA, A., COSTA, J., JAVIDFAR, J., WOBMA, H. M., SINGH, G., FREYTES, D. O., BACCHETTA, M. D., SONETT, J. R. & VUNJAK-NOVAKOVIC, G. 2013. Decellularization of human and porcine lung tissues for pulmonary tissue engineering. *Ann Thorac Surg,* 96**,** 1046-55; discussion 1055-6.

O'ROURKE, C., DAY, A., MURRAY-DUNNING, C., THANABALASUNDARAM, L., COWAN, J., STEVANATO, L., GRACE, N., CAMERON, G., DRAKE, R. & SINDEN, J. 2018. An allogeneic 'off the shelf'therapeutic strategy for peripheral nerve tissue engineering using clinical grade human neural stem cells. *Scientific reports,* 8**,** 2951.

OLIVEIRA, J. T., ALMEIDA, F. M., BIANCALANA, A., BAPTISTA, A. F., TOMAZ, M. A., MELO, P. A. & MARTINEZ, A. M. 2010. Mesenchymal stem cells in a polycaprolactone conduit enhance median-nerve regeneration, prevent decrease of creatine phosphokinase levels in muscle, and improve functional recovery in mice. *Neuroscience,* 170**,** 1295-303.

ORBAY, H., UYSAL, A. C., HYAKUSOKU, H. & MIZUNO, H. 2012. Differentiated and undifferentiated adipose-derived stem cells improve function in rats with peripheral nerve gaps. *Journal of Plastic, Reconstructive & Aesthetic Surgery,* 65**,** 657-664.

PALUDAN, S. R. & BOWIE, A. G. 2013. Immune sensing of DNA. *Immunity,* 38**,** 870-80.

PANIAGUA GUTIERREZ, J. R., BERRY, H., KOROSSIS, S., MIRSADRAEE, S., LOPES, S. V., DA COSTA, F., KEARNEY, J., WATTERSON, K., FISHER, J. &

INGHAM, E. 2014. Regenerative potential of low-concentration SDS-decellularized porcine aortic valved conduits in vivo. *Tissue Engineering Part A,* 21**,** 332-342.

PARMAKSIZ, M., DOGAN, A., ODABAS, S., ELCIN, A. E. & ELCIN, Y. M. 2016. Clinical applications of decellularized extracellular matrices for tissue engineering and regenerative medicine. *Biomedical Materials,* 11**,** 022003.

PEDRINI, F. A., BORIANI, F., BOLOGNESI, F., FAZIO, N., MARCHETTI, C. & BALDINI, N. 2018. Cell-Enhanced Acellular Nerve Allografts for Peripheral Nerve Reconstruction: A Systematic Review and a Meta-Analysis of the Literature. *Neurosurgery*.

PELTONEN, S., ALANNE, M. & PELTONEN, J. 2013. Barriers of the peripheral nerve. *Tissue Barriers,* 1**,** e24956.

PEREIRA, J. A., LEBRUN-JULIEN, F. & SUTER, U. 2012. Molecular mechanisms regulating myelination in the peripheral nervous system. *Trends in neurosciences,* 35**,** 123-134.

PHILIPS, C., CORNELISSEN, M. & CARRIEL, V. 2018. Evaluation methods as quality control in the generation of decellularized peripheral nerve allografts. *Journal of neural engineering,* 15**,** 021003.

PHILLIPS, J. B., SMIT, X., ZOYSA, N. D., AFOKE, A. & BROWN, R. A. 2004. Peripheral nerves in the rat exhibit localized heterogeneity of tensile properties during limb movement. *The Journal of physiology,* 557**,** 879-887.

PODUSLO, J. F. & CURRAN, G. L. 1996. Permeability at the blood-brain and blood-nerve barriers of the neurotrophic factors: NGF, CNTF, NT-3, BDNF. *Brain Res Mol Brain Res,* 36**,** 280-6.

POLLARD, J. & FITZPATRICK, L. 1973. A comparison of the effects of irradiation and immunosuppressive agents on regeneration through peripheral nerve allografts: an ultrastructural study. *Acta neuropathologica,* 23**,** 166-180.

POORNEJAD, N., FROST, T. S., SCOTT, D. R., ELTON, B. B., REYNOLDS, P. R., ROEDER, B. L. & COOK, A. D. 2015. Freezing/Thawing without Cryoprotectant Damages Native but not Decellularized Porcine Renal Tissue. *Organogenesis,* 11**,** 30-45.

POPLAWSKI, G., ISHIKAWA, T., BRIFAULT, C., LEE-KUBLI, C., REGESTAM, R., HENRY, K. W., SHIGA, Y., KWON, H., OHTORI, S. & GONIAS, S. L. 2018. Schwann cells regulate sensory neuron gene expression before and after peripheral nerve injury. *Glia*.

POPPLER, L. H., EE, X., SCHELLHARDT, L., HOBEN, G. M., PAN, D., HUNTER, D. A., YAN, Y., MOORE, A. M., SNYDER-WARWICK, A. K. & STEWART, S. A. 2016. Axonal growth arrests after an increased accumulation of Schwann cells expressing senescence markers and stromal cells in acellular nerve allografts. *Tissue engineering Part A,* 22**,** 949-961.

RAEDER, R. H., BADYLAK, S. F., SHEEHAN, C., KALLAKURY, B. & METZGER, D. W. 2002. Natural anti-galactose α1, 3 galactose antibodies delay, but do not prevent the acceptance of extracellular matrix xenografts. *Transplant immunology,* 10**,** 15-24.

RAHMAN, S., GRIFFIN, M., NAIK, A., SZARKO, M. & BUTLER, P. E. M. 2018. Optimising the decellularization of human elastic cartilage with trypsin for future use in ear reconstruction. *Scientific Reports,* 8**,** 3097.

RAJPUT, K., REDDY, S. & SHANKAR, H. 2012. Painful neuromas. *The Clinical journal of pain,* 28**,** 639-645.

RANA, D., ZREIQAT, H., BENKIRANE-JESSEL, N., RAMAKRISHNA, S. & RAMALINGAM, M. 2017. Development of decellularized scaffolds for stem cell-driven tissue engineering. *J Tissue Eng Regen Med,* 11**,** 942-965.

RAO, S. S. & WINTER, J. O. 2009. Adhesion molecule-modified biomaterials for neural tissue engineering. *Front Neuroeng,* 2**,** 6.

RIEDER, E., KASIMIR, M.-T., SILBERHUMER, G., SEEBACHER, G., WOLNER, E., SIMON, P. & WEIGEL, G. 2004. Decellularization protocols of porcine heart valves differ importantly in efficiency of cell removal and susceptibility of the matrix to recellularization with human vascular cells. *The Journal of thoracic and cardiovascular surgery,* 127**,** 399-405.

RODRíGUEZ, F. J., VERDÚ, E., CEBALLOS, D. & NAVARRO, X. 2000. Nerve guides seeded with autologous Schwann cells improve nerve regeneration. *Experimental neurology,* 161**,** 571-584.

RONCHI, G. & RAIMONDO, S. 2017. Chronically denervated distal nerve stump inhibits peripheral nerve regeneration. *Neural regeneration research,* 12**,** 739.

ROSARIO, D. J., REILLY, G. C., ALI SALAH, E., GLOVER, M., BULLOCK, A. J. & MACNEIL, S. 2008. Decellularization and sterilization of porcine urinary bladder matrix for tissue engineering in the lower urinary tract. *Regen Med,* 3**,** 145-56.

ROUMAZEILLES, L., DOKALIS, N., KAULICH, E. & LELIEVRE, V. 2018. It is all about the support—The role of the extracellular matrix in regenerating axon guidance. *Cell adhesion & migration,* 12**,** 87-92.

ROVAK, J. M., MUNGARA, A. K., AYDIN, M. A. & CEDERNA, P. S. 2004. Effects of vascular endothelial growth factor on nerve regeneration in acellular nerve grafts. *J Reconstr Microsurg,* 20**,** 53-8.

RUIJS, A. C., JAQUET, J.-B., KALMIJN, S., GIELE, H. & HOVIUS, S. E. 2005. Median and ulnar nerve injuries: a meta-analysis of predictors of motor and sensory recovery after modern microsurgical nerve repair. *Plastic and reconstructive surgery,* 116**,** 484-494.

SAFFORD, K. M., SAFFORD, S. D., GIMBLE, J. M., SHETTY, A. K. & RICE, H. E. 2004. Characterization of neuronal/glial differentiation of murine adipose-derived adult stromal cells. *Exp Neurol,* 187**,** 319-28.

SAHENK, Z., SEHARASEYON, J. & MENDELL, J. R. 1994. CNTF potentiates peripheral nerve regeneration. *Brain Res,* 655**,** 246-50.

SALDIN, L. T., CRAMER, M. C., VELANKAR, S. S., WHITE, L. J. & BADYLAK, S. F. 2017. Extracellular matrix hydrogels from decellularized tissues: structure and function. *Acta biomaterialia,* 49**,** 1-15.

SALZER, J. L. 2012. Axonal regulation of Schwann cell ensheathment and myelination. *Journal of the Peripheral Nervous System,* 17**,** 14-19.

SALZER, J. L. 2015. Schwann cell myelination. *Cold Spring Harbor perspectives in biology,* 7**,** a020529.

SANTIAGO, L. Y., CLAVIJO-ALVAREZ, J., BRAYFIELD, C., RUBIN, J. P. & MARRA, K. G. 2009. Delivery of adipose-derived precursor cells for peripheral nerve repair. *Cell Transplant,* 18**,** 145-58.

SCHMIDT, C. E. & LEACH, J. B. 2003. Neural tissue engineering: strategies for repair and regeneration. *Annual review of biomedical engineering,* 5**,** 293-347.

SEDDON, A. M., CURNOW, P. & BOOTH, P. J. 2004. Membrane proteins, lipids and detergents: not just a soap opera. *Biochimica et Biophysica Acta (BBA)-Biomembranes,* 1666**,** 105-117.

SEDDON, H. 1943. Three types of nerve injury. *Brain,* 66**,** 237-288.

SHENG, Z.-H. & CAI, Q. 2012. Mitochondrial transport in neurons: impact on synaptic homeostasis and neurodegeneration. *Nature Reviews Neuroscience,* 13**,** 77-93.

SIEMIONOW, M., BOZKURT, M. & ZOR, F. 2010. Regeneration and repair of peripheral nerves with different biomaterials: review. *Microsurgery,* 30**,** 574-588.

SIEMIONOW, M. & BRZEZICKI, G. 2009. Current techniques and concepts in peripheral nerve repair. *International review of neurobiology,* 87**,** 141-172.

SILL, T. J. & VON RECUM, H. A. 2008. Electrospinning: applications in drug delivery and tissue engineering. *Biomaterials,* 29**,** 1989-2006.

SILVA, J. B., MARCHESE, G., CAUDURO, C. & DEBIASI, M. 2017. Nerve conduits for treating peripheral nerve injuries: A systematic literature review. *Hand Surgery and Rehabilitation,* 36**,** 71-85.

SMITH, C. & KEARNEY, J. 1996. The effects of irradiation and hydration upon the mechanical properties of tendon. *Journal of Materials Science: Materials in Medicine,* 7**,** 645-650.

SONDELL, M., LUNDBORG, G. & KANJE, M. 1998. Regeneration of the rat sciatic nerve into allografts made acellular through chemical extraction. *Brain research,* 795**,** 44-54.

SOWA, Y., KISHIDA, T., IMURA, T., NUMAJIRI, T., NISHINO, K., TABATA, Y. & MAZDA, O. 2016. Adipose-Derived Stem Cells Promote Peripheral Nerve Regeneration In Vivo without Differentiation into Schwann-Like Lineage. *Plast Reconstr Surg,* 137**,** 318e-330e.

SPIVEY, E. C., KHAING, Z. Z., SHEAR, J. B. & SCHMIDT, C. E. 2012. The fundamental role of subcellular topography in peripheral nerve repair therapies. *Biomaterials,* 33**,** 4264-4276.

SRIDHARAN, R., REILLY, R. B. & BUCKLEY, C. T. 2015. Decellularized grafts with axially aligned channels for peripheral nerve regeneration. *Journal of the mechanical behavior of biomedical materials,* 41**,** 124-135.

STANG, F., FANSA, H., WOLF, G. & KEILHOFF, G. 2004. Collagen nerve conduits--assessment of biocompatibility and axonal regeneration. *Bio-medical materials and engineering,* 15**,** 3-12.

STANG, F., FANSA, H., WOLF, G., REPPIN, M. & KEILHOFF, G. 2005. Structural parameters of collagen nerve grafts influence peripheral nerve regeneration. *Biomaterials,* 26**,** 3083-3091.

STANG, F., KEILHOFF, G. & FANSA, H. 2009. Biocompatibility of different nerve tubes. *Materials,* 2**,** 1480-1507.

STAPLETON, T. W., INGRAM, J., KATTA, J., KNIGHT, R., KOROSSIS, S., FISHER, J. & INGHAM, E. 2008. Development and characterization of an acellular porcine medial meniscus for use in tissue engineering. *Tissue Engineering Part A,* 14**,** 505-518.

SUN, A. X., PREST, T. A., FOWLER, J. R., BRICK, R. M., GLOSS, K. M., LI, X., DEHART, M., SHEN, H., YANG, G. & BROWN, B. N. 2019. Conduits harnessing spatially controlled cell-secreted neurotrophic factors improve peripheral nerve regeneration. *Biomaterials*.

SUN, T., NORTON, D., VICKERS, N., L MCARTHUR, S., NEIL, S. M., RYAN, A. J. & HAYCOCK, J. W. 2008. Development of a bioreactor for evaluating novel nerve conduits. *Biotechnology and bioengineering,* 99**,** 1250-1260.

SUN, W., SUN, C., ZHAO, H., LIN, H., HAN, Q., WANG, J., MA, H., CHEN, B., XIAO, Z. & DAI, J. 2009. Improvement of sciatic nerve regeneration using laminin-binding human NGF-beta. *PLoS One,* 4**,** e6180.

SUNDERLAND, S. 1951. A classification of peripheral nerve injuries producing loss of function. *Brain,* 74**,** 491-516.

SUNDERLAND, S. S. 1990. The anatomy and physiology of nerve injury. *Muscle & nerve,* 13**,** 771-784.

SURI, S. & SCHMIDT, C. E. 2010. Cell-laden hydrogel constructs of hyaluronic acid, collagen, and laminin for neural tissue engineering. *Tissue Engineering Part A,* 16**,** 1703-1716.

SVENNINGSEN, Å. F., COLMAN, D. R. & PEDRAZA, L. 2004. Satellite cells of dorsal root ganglia are multipotential glial precursors. *Neuron glia biology,* 1**,** 85-93.

SYED, O., WALTERS, N. J., DAY, R. M., KIM, H. W. & KNOWLES, J. C. 2014. Evaluation of decellularization protocols for production of tubular small intestine submucosa scaffolds for use in oesophageal tissue engineering. *Acta Biomater,* 10**,** 5043-5054.

SZYNKARUK, M., KEMP, S. W., WOOD, M. D., GORDON, T. & BORSCHEL, G. H. 2012. Experimental and clinical evidence for use of decellularized nerve allografts in peripheral nerve gap reconstruction. *Tissue Engineering Part B: Reviews,* 19**,** 83-96.

TAKEDA, Y., MURAKAMI, Y., ASOU, H. & UYEMURA, K. 2001. The roles of cell adhesion molecules on the formation of peripheral myelin. *The Keio journal of medicine,* 50**,** 240-248.

TASSLER, P., DELLON, A. & CANOUN, C. 1994. Identification of elastic fibres in the peripheral nerve. *Journal of Hand Surgery (British and European Volume),* 19**,** 48-54.

TOPP, K. S. & BOYD, B. S. 2012. Peripheral nerve: from the microscopic functional unit of the axon to the biomechanically loaded macroscopic structure. *Journal of Hand Therapy,* 25**,** 142-152.

VAFAEE, T., THOMAS, D., DESAI, A., JENNINGS, L. M., BERRY, H., ROONEY, P., KEARNEY, J., FISHER, J. & INGHAM, E. 2018. Decellularization of human donor aortic and pulmonary valved conduits using low concentration sodium dodecyl sulfate. *Journal of tissue engineering and regenerative medicine,* 12**,** e841-e853.

VENKATASUBRAMANIAN, R. T., GRASSL, E. D., BAROCAS, V. H., LAFONTAINE, D. & BISCHOF, J. C. 2006. Effects of freezing and cryopreservation on the mechanical properties of arteries. *Ann Biomed Eng,* 34**,** 823-32.

VERHEIJEN, M. H., CHRAST, R., BURROLA, P. & LEMKE, G. 2003. Local regulation of fat metabolism in peripheral nerves. *Genes & development,* 17**,** 2450-2464.

WAGSTAFF, L. J. 2018. *The role of Schwann cell c-Jun in restoring axon regeneration deficits in the peripheral nervous system.* UCL (University College London).

WAKIMURA, Y., WANG, W., ITOH, S., OKAZAKI, M. & TAKAKUDA, K. 2015. An experimental study to bridge a nerve gap with a decellularized allogeneic nerve. *Plastic and reconstructive surgery,* 136**,** 319e-327e.

WALSH, S., BIERNASKIE, J., KEMP, S. & MIDHA, R. 2009. Supplementation of acellular nerve grafts with skin derived precursor cells promotes peripheral nerve regeneration. *Neuroscience,* 164**,** 1097-1107.

WANG, J., DING, F., GU, Y., LIU, J. & GU, X. 2009. Bone marrow mesenchymal stem cells promote cell proliferation and neurotrophic function of Schwann cells in vitro and in vivo. *Brain research,* 1262**,** 7-15.

WANG, S. & CAI, L. 2010. Polymers for fabricating nerve conduits. *International Journal of Polymer Science,* 2010.

WANG, W., ITOH, S. & TAKAKUDA, K. 2016. Comparative study of the efficacy of decellularization treatment of allogenic and xenogeneic nerves as nerve conduits. *Journal of Biomedical Materials Research Part A,* 104**,** 445-454.

WANG, Y., JIA, H., LI, W.-Y., TONG, X.-J., LIU, G.-B. & KANG, S.-W. 2012. Synergistic effects of bone mesenchymal stem cells and chondroitinase ABC on nerve regeneration after acellular nerve allograft in rats. *Cellular and molecular neurobiology,* 32**,** 361-371.

WANG, Z., HAN, N., WANG, J., ZHENG, H., PENG, J., KOU, Y., XU, C., AN, S., YIN, X., ZHANG, P. & JIANG, B. 2014. Improved peripheral nerve regeneration with sustained release nerve growth factor microspheres in small gap tubulization. *Am J Transl Res,* 6**,** 413-21.

WEI, Y., TIAN, W., YU, X., CUI, F., HOU, S., XU, Q. & LEE, I.-S. 2007. Hyaluronic acid hydrogels with IKVAV peptides for tissue repair and axonal regeneration in an injured rat brain. *Biomedical Materials,* 2**,** S142.

WEIDER, M., WEGENER, A., SCHMITT, C., KÜSPERT, M., HILLGÄRTNER, S., BÖSL, M. R., HERMANS-BORGMEYER, I., NAIT-OUMESMAR, B. & WEGNER, M. 2015. Elevated in vivo levels of a single transcription factor directly convert satellite glia into oligodendrocyte-like cells. *PLoS genetics,* 11**,** e1005008.

WENGER, M. P., BOZEC, L., HORTON, M. A. & MESQUIDA, P. 2007. Mechanical properties of collagen fibrils. *Biophysical journal,* 93**,** 1255-1263.

WHITE, L. J., TAYLOR, A. J., FAULK, D. M., KEANE, T. J., SALDIN, L. T., REING, J. E., SWINEHART, I. T., TURNER, N. J., RATNER, B. D. & BADYLAK, S. F. 2017. The impact of detergents on the tissue decellularization process: a ToF-SIMS study. *Acta biomaterialia,* 50**,** 207-219.

WHITLOCK, E. L., TUFFAHA, S. H., LUCIANO, J. P., YAN, Y., HUNTER, D. A., MAGILL, C. K., MOORE, A. M., TONG, A. Y., MACKINNON, S. E. & BORSCHEL, G. H. 2009. Processed allografts and type I collagen conduits for repair of peripheral nerve gaps. *Muscle & nerve,* 39**,** 787-799.

WIGGLESWORTH, K. M., RACKI, W. J., MISHRA, R., SZOMOLANYI-TSUDA, E., GREINER, D. L. & GALILI, U. 2011. Rapid recruitment and activation of macrophages by anti-Gal/α-Gal liposome interaction accelerates wound healing. *The Journal of Immunology,* 186**,** 4422-4432.

WILLIAMS, C., LIAO, J., JOYCE, E., WANG, B., LEACH, J., SACKS, M. & WONG, J. 2009. Altered structural and mechanical properties in decellularized rabbit carotid arteries. *Acta biomaterialia,* 5**,** 993-1005.

WILSHAW, S., ROONEY, P., BERRY, H., KEARNEY, J., HOMER-VANNIASINKAM, S., FISHER, J. & INGHAM, E. 2012. Development and characterization of acellular allogeneic arterial matrices. *Tissue Eng Part A,* 18**,** 471-483.

WOLFORD, L. M. & RODRIGUES, D. B. 2011. Autogenous grafts/allografts/conduits for bridging peripheral trigeminal nerve gaps. *Atlas of the oral and maxillofacial surgery clinics of North America,* 19**,** 91-107.

WONG, K. M., BABETTO, E. & BEIROWSKI, B. 2017. Axon degeneration: make the Schwann cell great again. *Neural regeneration research,* 12**,** 518.

WONG, M. L. & GRIFFITHS, L. G. 2014. Immunogenicity in xenogeneic scaffold generation: antigen removal vs. decellularization. *Acta biomaterialia,* 10**,** 1806-1816.

WOOD, M. D., KEMP, S. W., LIU, E. H., SZYNKARUK, M., GORDON, T. & BORSCHEL, G. H. 2014. Rat-derived processed nerve allografts support more axon regeneration in rat than human-derived processed nerve xenografts. *Journal of biomedical materials research Part A,* 102**,** 1085-1091.

XIE, F., LI, Q. F., GU, B., LIU, K. & SHEN, G. X. 2008. In vitro and in vivo evaluation of a biodegradable chitosan–PLA composite peripheral nerve guide conduit material. *Microsurgery,* 28**,** 471-479.

YAMNIUK, A. P. & VOGEL, H. J. 2005. Calcium- and magnesium-dependent interactions between calcium- and integrin-binding protein and the integrin alphaIIb cytoplasmic domain. *Protein Sci,* 14**,** 1429-37.

YANG, L. M., LIU, X. L., ZHU, Q. T., ZHANG, Y., XI, T. F., HU, J., HE, C. F. & JIANG, L. 2011. Human peripheral nerve-derived scaffold for tissue-engineered nerve grafts: Histology and biocompatibility analysis. *Journal of Biomedical Materials Research Part B: Applied Biomaterials,* 96**,** 25-33.

YUAN, A., RAO, M. V. & NIXON, R. A. 2012. Neurofilaments at a glance. *Journal of cell science,* 125**,** 3257-3263.

YURCHENCO, P. D. 2011. Basement membranes: cell scaffoldings and signaling platforms. *Cold Spring Harbor perspectives in biology,* 3**,** a004911.

YURCHENCO, P. D., SMIRNOV, S. & MATHUS, T. 2002. Analysis of basement membrane self-assembly and cellular interactions with native and recombinant glycoproteins. *Methods in cell biology***,** 111-144.

ZACK-WILLIAMS, S. D., BUTLER, P. E. & KALASKAR, D. M. 2015. Current progress in use of adipose derived stem cells in peripheral nerve regeneration. *World journal of stem cells,* 7**,** 51.

ZALEWSKI, A. A. & GULATI, A. K. 1982. Evaluation of histocompatibility as a factor in the repair of nerve with a frozen nerve allograft. *Journal of neurosurgery,* 56**,** 550-554.

ZIEGLER, L., GRIGORYAN, S., YANG, I. H., THAKOR, N. V. & GOLDSTEIN, R. S. 2011. Efficient generation of schwann cells from human embryonic stem cell-derived neurospheres. *Stem Cell Rev,* 7**,** 394-403.

ZILIC, L., GARNER, P. E., YU, T., ROMAN, S., HAYCOCK, J. W. & WILSHAW, S. P. 2015. An anatomical study of porcine peripheral nerve and its potential use in nerve tissue engineering. *Journal of anatomy,* 227**,** 302-314.

ZILIC, L., WILSHAW, S. P. & HAYCOCK, J. W. 2016. Decellularisation and histological characterisation of porcine peripheral nerves. *Biotechnology and bioengineering*.

ZOU, J.-L., LIU, S., SUN, J.-H., YANG, W.-H., XU, Y.-W., RAO, Z.-L., JIANG, B., ZHU, Q.-T., LIU, X.-L., WU, J.-L., CHANG, C., MAO, H.-Q., LING, E.-A., QUAN, D.-P. & ZENG, Y.-S. 2018. Peripheral Nerve-Derived Matrix Hydrogel Promotes Remyelination and Inhibits Synapse Formation. *Advanced Functional Materials,* 28**,** 1705739.

ZOU, Y. & ZHANG, Y. 2012. Mechanical evaluation of decellularized porcine thoracic aorta. *J Surg Res,* 175**,** 359-68.

ZUO, J., NEUBAUER, D., GRAHAM, J., KREKOSKI, C. A., FERGUSON, T. A. & MUIR, D. 2002. Regeneration of axons after nerve transection repair is enhanced by degradation of chondroitin sulfate proteoglycan. *Experimental neurology,* 176**,** 221-228.

Appendix A: Materials

Table I Equipment used throughout the study

Equipment	Reference code	Supplier
Automatic pipettes	Various	Gilson / Finnpipette
Balance	GR200	A&D Instruments Ltd
Bench top Eppendorf Centrifuge	5415R	Hyland Scientific
Class I laminar flow cabinet	-	Howarth Airtech Ltd
Class II safety cabinet	HERASafeKS	Heraeus
Centrifuge	Harrier 15/80	Sanyo Biomedical
Confocal microscope	LSM800	Carl Zeiss Ltd
Cryotome	CM1850	Leica
Dissection equipment	Various	Fine Scientific Tools Ltd
Freeze Drier	ModulyoD-230	Thermo Savant
Freezer (-20 °C)	Electrolux 3000	Jencons Plc
Freezer (-80 °C)	Various	Sanyo Biomedical
Fridge	ER8817C	Jencons Plc
Fluorescent microscope	AXIO Imager M2	Carl Zeiss Ltd
Haemocytometer (22 x 47 mm)	Neubauer	VWR International
Histology moulds	E10.8/4161	Raymond A Lamb
Histology water bath	MH8515	Barnstead Electrothermal
Hotplate stirrer	CB162	Stuart Scientific
Hotplate	E18/1	Raymond A Lamb
Hot wax oven	E18/31	Raymond A Lamb
Incubator (inCu safe 37 °C)	-	Sanyo Biomedical
Inverted microscope	CK40	Olympus
Liquid Nitrogen Dewar	BIO65	Jencons Plc
Magnetic stirrer	Stuart SB161	Scientific Laboratory Supplies Ltd
Microtome	RM2255	Leica

Microplate spectrophotometer	Multiscan Spectrum 1500	Thermo Scientific Ltd
NanoDrop spectrophotometer	ND-1000	Labtech
Oven (hot air)	-	Genlab Ltd
pH meter	Jenway 3510	VWR International
Pipette boy	Various	Integra Biosciences
Plate shaker	Vari-shaker	Dynatech Ltd
Slide holders	E102	Raymond A Lamb
Staining troughs	E105	Raymond A Lamb
Stainless steel spatulas	Various	Fisher Scientific
Stainless steel pins (11 x 3 mm)	Various	Fisher Scientific
Table shaker	KS130	IKA
Table shaker	PSU 10i	Grant
Tissue processor	TP1020	Leica
Topcount luminescence plate reader	-	Packard Bioscience
Wax dispenser	E66	Raymond A Lamb
Vortex	Topmix FB15024	Fisher Scientific

Table II Consumables used throughout the study

Consumable	Reference code	Supplier
Automatic pipettes	Various	Gilson / Finnpipette
Autoclave plain closure bags	-	Westfield Medical Ltd
Bijoux tubes (5 mL)	SLS7522	Scientific Laboratory Supplies Ltd
Black-walled 96 well plate	G655076	Scientific Laboratory Supplies Ltd
Coverslips (22 x 64 mm)	MIC3228	Scientific Laboratory Supplies Ltd
Cryovials, 1mL	Various	Nunc International
Histology cassettes	EMB-130-020R	Fisher Scientific
Filter pipette tips	Various	Starlab
Flat bottomed clear 96-well plate	269620	Scientific Laboratory Supplies Ltd
Microtube, 1.5 mL loop cap	212-9573	VWR International
Microtome blades	SD3050835	Fisher Scientific
Optiplate (96 well plate)	165305	Fisher Scientific
Parafilm	-	Bemis
Pasteur pipettes (3 mL)	pmk-500-070w	Fisher Scientific
Petri dishes	82.1473.001	Sarstedt
Scalpel blades	Various	Fisher Scientific
Serological pipettes (5, 10, 25 mL)	Various	Sigma Aldrich
Specimen pots (150 mL, 250 mL)	Various	Scientific Laboratory Supplies Ltd
Superfrost Plus slides	J1800-AMNZ	Thermo Scientific Ltd
Syringes (1 mL, 10 mL)	Various	Terumo
Syringe (hypodermic) needle 23 G	NN2332R	Terumo
Syringe filter (0.22 µm pore size)	10268401	Millex Merck Millipore
Tissue Culture flasks (T75, T175)	Various	Thermo Scientific Ltd
Tissue Culture plates (6-well)	140675-6	Thermo Scientific Ltd
Universal tubes (25 mL)	CON9000	Scientific Laboratory Supplies Ltd

Table III Chemicals and reagents used throughout the study

Chemical / reagent	Reference code	Supplier
1,9 dimethylene blue	34-1088	Sigma-Aldrich
Acetic acid, glacial	10001CU	VWR International
Acetone	20065.362	Fisher Scientific
Agarose	A9539	Sigma Aldrich
Aprotinin (50 mL; 10,000 KIU.mL-1)	AP020	Nordic Pharma
ATPLiteM® assay kit	6016947	Perkin Elmer Ltd
Bovine Serum Albumin	A7030	Sigma Aldrich
Benzonase nuclease hc, purity > 99 % (250 U.µL-1)	70664	Merck
Calcium chloride	C7902	Sigma Aldrich
Calf thymus DNA	D4522	Sigma
Cambridge antibiotic solution	04-301	Resource Bioscience
Carbon dioxide (CO2) in air (5% (v/v))	-	British Oxygen Company Ltd
Chloramine T	C9887	Sigma Aldrich
Chondroitin sulphate B	C3788	Sigma Aldrich
Citric acid	20276.292	VWR International
Collagen (rat tail) type 1 2 mg·mL1, in 0.6% (v/v) acetic acid (60-30-810)	60-30-810	First Link Ltd
Cyanoacrylate contact adhesive	-	Scotch® Super Glue Liquid
DAPI (4',6-diamidino-2-phenylindole dihydrochloride)	D9564	Sigma Aldrich
DeadEnd™ Fluorometric TUNEL system	G3250	Promega
Dimethyl sulfoxide (DMSO)	D9564	Sigma
disodium hydrogen orthophosphate (anhydrous)	1.06586.0500	Merck Millipore
DNeasy blood and tissue kit	69504	Qiagen

Dulbecco's minimal essential medium	D6546	Sigma
DPBS (without Ca/Mg)	D8537	Sigma
DPBS (with Ca/Mg)	D8662	Sigma
DPX mountant	RRSP29	Atom Scientific
EDTA (disodium ethylenediaminetetraacetic acid)	E/P140/53	Thermo Fisher Scientific Ltd
Eosin Y	1.09844.1000	Merck Millipore
Ethanol (100 % v/v)	E/0650DF	Fisher Scientific
Fluorescence mounting medium	S3023	Dako
Foetal bovine serum	EU-000	Sera Lab
Formic acid	F-4166	Sigma Aldrich
Goat serum	5425S	New England Biolabs
Giemsa stain	352603R	VWR International
Gentamycin sulphate	345814	Sigma Aldrich
Glasgow's minimal essential medium	G5154	Sigma
Hams F12 nutrient mixture (+ L-glutamine)	N4888	Sigma
Haematoxylin (Mayer's)	RRSP60	Atom Scientific
Haematoxylin (Weigert's) A/B	RRSP72-D/RRSP73-D	Atom Scientific
Hanks Balanced Salt Solution (HBSS)	H9269	Sigma
Hydroxylamine hydrochloride	159417	Sigma Aldrich
Hydrochloric acid (6 M)	H/1200/PB17	Fisher Scientific
Iron (III) chloride (hexahydrate)	F2877	Sigma Aldrich
Lard	-	Tesco
L-cystine hydrochloride	C1276	Sigma Aldrich
L-glutamine (200 mM)	G7513	Sigma
Luxol Fast Blue	212171000	Acros Organics
Lithium carbonate	203629	Sigma

Magnesium chloride hexahydrate	25108.26	Thermo Fisher Scientific Ltd
Methanol-free formaldehyde (16 %; w/v)	28906	Thermo Fisher Scientific Ltd
Miller's stain	LAMB/080-D	Raymond A Lamb
Nerve Growth factor	N8133	Sigma
Neutracon	-	Deacon Laboratories Ltd
Neutral Buffered Formalin (10 % v/v)	RRFFD4000-G	Fisher Scientific
Nuclease free water	436912C	VWR International
OCT compound	361606E	VWR International
Oxalic acid	1017440	Thermo Fisher Scientific Ltd
Papain	A3814.0100	Applichem
Parrafin wax	W2	Raymond A Lamb
PBS tablets	BR0014G	Oxoid
p-dimethylaminobenzaldehyde	S647861	Sigma Aldrich
Penicillin (5000 U.mL-1)/Streptomycin (5 mg.mL-1)	P4458	Sigma
Perchloric acid (60 % vv/v)	294583P	Sigma Aldrich
pH standards (4, 7, 10)	-	Scientific Laboratory Supplies Ltd
PicoGreen™ detection kit	P7589	Invitrogen Life Technologies
Picric acid	36011	Sigma Aldrich
Polymyxin B sulphate	5291	Merck Chemicals
Potassium permanganate	P/6520/53	Thermo Fisher Scientific Ltd
Propan-1-ol	20861.363	VWR International
Proteinase K solution	S3020	Dako
Scott's tap water	RRSP/190	Atom Scientific
Sirius Red	F3B	Raymond A Lamb
Sodium acetate (trihydrate)	S/2040/53	Thermo Fisher Scientific Ltd
Sodium azide solution (1 % w/v)	786-229	G Biosciences
Sodium chloride	S/3160/33	Thermo Fisher Scientific Ltd

sodium di-hydrogen orthophosphate	102454R	VWR International
sodium hydroxide	S8045	Thermo Fisher Scientific Ltd
SteriSrips	R1540C	Medisave
Sucrose	S9378-500G	Sigma
Trans-4-hydroxy-L-proline	H7279	Sigma Aldrich
Trichloroacetic acid (99% w/v)	152130010	Acros Organics
Trigene	CLE1230	Scientific Laboratory Supplies Ltd
Tris (trizma base)	T1503	Sigma Aldrich
Triton X-100	X100-500ML	Sigma
Trypan blue solution (0.4 % v/v)	T8154	Sigma
Trypsin-EDTA solution (0.5 %; w/v)	T3924	Sigma
Tryptone phosphate broth (TPB)	T8782	Sigma
Tween-20	P1379	Sigma Aldrich
UltraPure™ 10 % (w/v) sodium dodecyl sulphate solution	24730-020	Invitrogen Life Technologies
Vancomycin hydrochloride	861987-1G	Merck Chemicals
Virkon®	CLE1554	DuPont
Xylene	GPS1001-G	Atom Scientific
α chymotrypsin	C4129-10	Sigma Aldrich

Appendix B: Conference presentations and awards

- Georgina Webster, Richard M Hall, Paul Rooney and Stacy-Paul Wilshaw (July 2015), Development of acellular allogeneic nerve grafts, EPSRC Centre of Doctoral Training Joint Conference, University of Leeds, UK. (Poster presentation)

- Georgina Webster, Richard M Hall, Paul Rooney and Stacy-Paul Wilshaw (July 2016), Development and characterisation of an acellular allogeneic nerve graft, Annual Tissue and Cell Engineering Society meeting (TCES), London, UK. (Poster presentation)

- Georgina Webster, Richard M Hall, Paul Rooney and Stacy-Paul Wilshaw (December 2016), Development and characterisation of a decellularised allogeneic nerve graft for peripheral nerve repair, Annual White Rose Work in Progress Meeting; Biomaterials and Tissue Engineering Group (BiTEG), York, UK. (Poster presentation)

- Georgina Webster, Richard M Hall, Paul Rooney and Stacy-Paul Wilshaw (June 2017), Development and characterisation of a decellularised allogeneic nerve graft for peripheral nerve repair, Tissue Engineering and Regenerative Medicine International Society (TERMIS) EU Meeting, Davos, Switzerland. (Poster presentation)

- Georgina Webster, Richard M Hall, Paul Rooney and Stacy-Paul Wilshaw (July 2017), Development and characterisation of a decellularised allogeneic nerve graft, Annual Tissue and Cell Engineering Society meeting (TCES), Manchester, UK. (Poster presentation)

- Georgina Webster, Richard M Hall, Paul Rooney and Stacy-Paul Wilshaw (July 2017), Development and characterisation of a decellularised allogeneic nerve graft for peripheral nerve repair, EPSRC Centre of Doctoral Training Symposium, University of Leeds, UK. (Oral presentation). **Second prize: Best oral presentation**

- Georgina Webster, Richard M Hall, Paul Rooney and Stacy-Paul Wilshaw (October 2017), Development and characterisation of a decellularised allogeneic nerve graft for peripheral nerve repair, EPSRC Centre of Doctoral Training Joint Conference, Leeds, UK. (Oral presentation)

- Georgina Webster, Richard M Hall, Paul Rooney and Stacy-Paul Wilshaw (December 2017), Development and characterisation of a decellularised human femoral nerve graft, Annual White Rose Work in Progress Meeting; Biomaterials and Tissue Engineering Group (BiTEG), Leeds, UK. (Poster presentation)

- Georgina Webster, Richard M Hall, Paul Rooney and Stacy-Paul Wilshaw (September 2018), Development and characterisation of a decellularised allogeneic nerve graft for peripheral nerve reconstruction, Tissue Engineering and Regenerative Medicine International Society (TERMIS) Wold Congress, Kyoto, Japan. (Poster presentation)